

Mathematical Modelling of Oxygen - Plankton System Under the Climate Change

*Thesis submitted for the degree of
Doctor of Philosophy
at the
University of Leicester*

by

Yadigar Sekerci Firat

Department of Mathematics

University of Leicester

March 2016

Abstract

Oxygen production due to phytoplankton photosynthesis is an important phenomenon keeping in mind the underlying dynamics of marine ecosystems. However, despite its crucial importance, not only for marine but also for terrestrial ecosystems, the coupled oxygen-plankton dynamics have been overlooked.

This dissertation aims to provide insight into an oxygen-plankton system using mathematical modelling. We firstly develop a ‘baseline’ oxygen-phytoplankton model which is then further developed through the addition of biologically relevant factors such as plankton respiration and the predator effect of zooplankton. The properties of the model have been studied both in the nonspatial case, which corresponds to a well mixed system with a spatially uniform distribution of species, and in the spatially explicit extension, by taking into account the transport of oxygen and movement of plankton by turbulent diffusion.

Since the purpose of this work is to reveal the oxygen dynamics, the effect of global warming is considered taken into consideration and modelled by various oxygen production rates and phytoplankton growth functions in Chapters 5 and 6. It is shown that sustainable oxygen production is only possible in an intermediate range of the production rate. If the oxygen production rate becomes sufficiently low or high, in the course of time, the system’s dynamics shows abrupt changes resulting in plankton extinction and oxygen depletion. We show that the spatial system’s sustainability range is larger than that of the corresponding nonspatial system. We show that oxygen production by phytoplankton can stop suddenly if the water temperature exceeds a certain critical threshold. Correspondingly, this dissertation reveals the scenarios of extinction which can potentially lead to an ecological disaster.

Acknowledgements

This PhD thesis would not have been possible without the help and support from many people and I would like to take the opportunity to acknowledge some.

Firstly, I would like to express my sincere gratitude to my supervisor, Professor Sergei Petrovskii, for his patience, encouragement and support during my studies. His valuable guidance has helped me at all the stages of this thesis. His advice on both research as well as on my career has been invaluable. I would never have had received his wealth of experience and knowledge anywhere else.

I would like to thank all the honourable staff members of the mathematics department for their help and making so many things easier. I extend my appreciation to the fellow research students in Michael Atiyah offices. A special thanks goes to Masha for being a great friend.

Importantly, my deepest thanks goes to my husband, Ishak, who was always with me from the initial stages to the end of my PhD journey. Thank you for always believing in me, for your unconditional support, strength and love. This thesis would not have been possible without you. I would like to show my gratitude to my family. They deserve a tremendous amount of credit for this accomplishment as they have always been a source of inspiration and support throughout my life.

I would like to thank Professor Horst Malchow (Osnabrück University) and Professor Ruslan Davidchack (University of Leicester) for very helpful comments to improve the quality of the thesis.

Finally, I would like to thank Turkish Ministry of National Education for financial support to carry out this research.

Contents

Abstract	ii
Acknowledgements	iii
List of Figures	vii
List of Tables	xi
1 Introduction	1
1.1 General features of plankton community	1
1.2 Mathematical approach	6
1.3 Thesis outline	11
2 Baseline Model	13
2.1 Introduction	13
2.2 Model Formulation	14
2.2.1 Examining the steady states and existence	17
2.2.2 Stability analysis	23
2.2.3 Numerical simulations	25
2.3 Discussion and Concluding Remarks	31
3 Zooplankton Predation Effect on Oxygen Dynamics	33
3.1 Introduction	33
3.2 The ‘advanced’ three-component model and results	34
3.2.1 Equilibrium existence and analysis	36
3.2.2 Stability analysis	37
3.3 Numerical Simulations	44
3.3.1 Temporal dynamics	44
3.3.2 Spatial dynamics	50
3.4 Discussion and Concluding remarks	60
4 Plankton Respiration Effect on Oxygen Dynamics	62
4.1 Introduction	62
4.2 Model formulation	63

4.2.1	Equilibria analysis and steady states	67
4.2.2	Stability analysis	70
4.3	Numerical Simulations	77
4.3.1	Temporal dynamics	77
4.3.2	Spatial pattern in 1D	83
4.3.3	System spatial dependence to the chosen initial conditions	84
4.3.4	Pattern formation in 2D	91
4.4	Discussion and Concluding remarks	103
5	The Effect of Temperature	105
5.1	Introduction	105
5.2	Numerical Simulations	
	Temporal Dynamics	106
5.2.1	Effect of decreasing A	108
5.2.2	Effect of increasing A	113
5.2.3	Effect of decreasing c_1	116
5.2.4	Spatial dynamics	120
5.3	Ecology catastrophe and paths to extinction	123
5.4	Discussion and Concluding remarks	130
6	Temperature Effect, Long-living Transient	132
6.1	Introduction	132
6.2	Parametrization of “A” and “ c_1 ” functions	133
6.3	Numerical Simulations	135
6.3.1	Temporal dynamics	135
6.3.2	Spatial dynamics	140
6.4	Extinction, early warning signals and intermittency	143
6.5	Discussion and Concluding remarks	148
7	Conclusions	150
A	Simplifying a Model System	155
B	Dimensionless Form	159
C	Linearized System Matrix	161
C.0.1	Baseline model linearized system	161
C.0.2	Linearized system for predation effect model	162
C.0.3	Linearized system for respiration effect model	169
D	Numerical Method: Finite Differences	177
E	Different Parametrizations of Oxygen-Phytoplankton Model	180

Bibliography

186

List of Figures

1.1	Phase plane trajectories	9
1.2	Plankton distribution in the Barrent Sea	10
1.3	Spatial distribution of plankton in 2D, numerical approach	10
2.1	Flow chart for basic model formulation	15
2.2	Baseline model isoclines	18
2.3	Steady state values of oxygen and phytoplankton vs. B and c_1	21
2.4	Steady state values of oxygen and phytoplankton vs. A and c_1	22
2.5	Steady state values of oxygen and phytoplankton vs. B and A	22
2.6	Eigenvalues vs. A and c_1	24
2.7	Eigenvalues vs. varying A for fixed c_1	25
2.8	Bifurcation diagram for oxygen-phytoplankton model	25
2.9	Spatial distribution of oxygen-phytoplankton	27
2.10	Spatial distribution of oxygen-phytoplankton for different time	28
2.11	Spatial system succession for different B values	29
2.12	Oxygen-phytoplankton spatial distributions for different time	29
2.13	Oxygen-phytoplankton spatial distribution for $A(x) = \exp(\frac{\varepsilon}{x})$	30
2.14	Oxygen-phytoplankton spatial distribution for $A(x) = \frac{1}{((0.01+10^{-4}*x)+\varepsilon)}$	30
3.1	Flow chart for predation effect model formulation	35
3.2	Steady states of zooplankton-free states	39
3.3	Eigenvalues vs. A and c_1 for zooplankton-free state	40
3.4	Eigenvalues vs. A for zooplankton-free state	40
3.5	Coexistence steady state	41
3.6	Coexistence state eigenvalues real part vs. A and c_1	42
3.7	Coexistence state eigenvalues imaginary part vs. A and c_1	43
3.8	Eigenvalues vs. A for the coexistence state	43
3.9	Bifurcation diagram for oxygen-phytoplankton-zooplankton system	44
3.10	Temporal dynamics for changing parameter c_1 for fixed $A = 0.4$	45
3.11	Temporal dynamics for changing parameter c_1 for fixed $A = 0.8$	45
3.12	Effect of changes in parameter A and for fixed $c_1 = 0.8$	46
3.13	Temporal variations of system components for $A = 1$ and $c_1 = 0.1$	46
3.14	Effect of changes in parameter A and for fixed $c_1 = 0.7$	47
3.15	Effect of changes in parameter A and for fixed $c_1 = 0.2$	48
3.16	Effect of changes in parameter A and for fixed $c_1 = 0.4$	49
3.17	Temporal dynamics for $A = 1, c_1 = 0.01$	52
3.18	Distribution of system components vs. time for different time	52

3.19	Phase plane of population densities	53
3.20	Spatial distribution of system components for different time	53
3.21	Snapshots of system components for $c_1 = 0.6$	54
3.22	Snapshots of system components for $c_1 = 0.9$	54
3.23	Snapshots of system components for large time limit	55
3.24	Travelling front for different time moments	56
3.25	Snapshots of the density distribution over space	56
3.26	The effect on spatial system for changes in parameter c_1	57
3.27	Spatial distribution of system components for $A = 0.4, c_1 = 0.4$	58
3.28	Spatial distribution of system components for $A = 0.6, c_1 = 0.4$	58
3.29	Spatial distribution of system components for $A = 0.7, c_1 = 0.4$	59
4.1	Flow chart for respiration effect model formulation	63
4.2	System isoclines for oxygen-phytoplankton system	68
4.3	Lower positive steady state, $E_2^{(1)}$	71
4.4	The eigenvalues for $E_2^{(1)} = (\check{c}_1, \check{u}_1, 0)$	72
4.5	Eigenvalues vs. A for $c_1 = 0.4, c_1 = 0.7$	73
4.6	Upper positive steady state, $E_2^{(2)}$	73
4.7	Eigenvalues of the $E_2^{(2)} = (\check{c}_2, \check{u}_2, 0)$	74
4.8	Eigenvalues vs. A for $E_2^{(2)}$ for $c_1 = 0.4$, and $c_1 = 0.7$	74
4.9	Steady state values of oxygen, phytoplankton and zooplankton	75
4.10	The eigenvalues real parts for $E_3 = (\check{c}, \check{u}, \check{v})$	75
4.11	The eigenvalues imaginary parts for $E_3 = (\check{c}, \check{u}, \check{v})$	76
4.12	Eigenvalues vs. A for E_3 for $c_1 = 0.4$, and $c_1 = 0.7$	76
4.13	Bifurcation diagram for coexistence state in small & large scale	77
4.14	Temporal dynamics of changes in parameter A for $c_1 = 0.659$	78
4.15	Phase space trajectory for fixed $c_1 = 0.659$	78
4.16	Temporal dynamics of changes in parameter c_1 for $A = 2$	79
4.17	Phase space trajectory for fixed $A = 2$	80
4.18	Temporal dynamics of changes in parameter A and $c_1 = 0.7$	80
4.19	Phase space trajectory for fixed $c_1 = 0.7$	81
4.20	Temporal dynamics of changes in parameter A and $c_1 = 0.7$	82
4.21	Phase space trajectory for changes in A	83
4.22	System spatial response to chosen initials I	85
4.23	System spatial response to chosen initials II	86
4.24	System spatial response to chosen initials III	86
4.25	System spatial response to chosen initials IV	87
4.26	System components initial distributions for $A = 2.05$	88
4.27	System components initial distributions for $A = 2.2$	88
4.28	System components initial distributions for $A = 2$	89
4.29	Effect of changes in parameter A for different time	89
4.30	Effect of changes in parameter A for fixed $c_1 = 0.7$	90
4.31	Spatial distribution of oxygen in 2D for $A = 2.01$	93
4.32	Spatial distribution of oxygen in 2D for $A = 2.02$	94
4.33	Spatial distribution of oxygen in 2D for $A = 2.05$	95

4.34	Spatial distribution of oxygen in 2D for $A = 2.09$	96
4.35	Spatial distribution of oxygen in 2D for $A = 2.3$	97
4.36	Spatial distribution of oxygen in 2D for $A = 2.4$	98
4.37	Spatial distribution of oxygen in 2D for $A = 2.7$	99
4.38	Spatial distribution of oxygen in 2D for $A = 2.02$	100
4.39	Spatial distribution of oxygen in 2D for $A = 2.06$	101
4.40	Spatial distribution of oxygen in 2D for $A = 2.4$	101
4.41	Spatial distribution of oxygen in 2D for $A = 2.7$	102
4.42	Spatial distribution of oxygen in 2D for $A = 2.4$	102
5.1	Sketch of the continuously decreasing A function	109
5.2	Effect of decrease in parameter A and fixed $c_1 = 0.7$	110
5.3	Phase space structure for different A_0 and fixed $c_1 = 0.7$	111
5.4	Effect of decrease in parameter A and fixed $c_1 = 0.7$	111
5.5	Phase space structure for different A_0 and fixed $c_1 = 0.7$	112
5.6	Effect of changes in slope, ω	112
5.7	Phase space structure for different ω and fixed $c_1 = 0.7$	112
5.8	Sketch of the continuously increasing A function	113
5.9	Effect of changes in parameter A and for fixed $c_1 = 0.7$	114
5.10	Phase space structure for different A_0 and for fixed $c_1 = 0.7$	114
5.11	Effect of changes in parameter A_0 and for fixed $c_1 = 0.7$	115
5.12	Phase space structure for different A_0 and $c_1 = 0.7$	115
5.13	Effect of changes in slope, parameter ω	116
5.14	Sketch of the continuously decreasing c_1 function	117
5.15	Effect of changes in parameter c_0 and for fixed $A = 2.01$	118
5.16	Phase space structure for varying c_0 and fixed $A = 2.01$	118
5.17	Effect of changes in parameter A and fixed $c_0 = 0.7$	119
5.18	Phase space structure for varying c_0 and fixed $A = 2.01$	119
5.19	Effect of changes in slope, ω	119
5.20	Spatial response to the changes in parameter A_0 and fixed $c_1 = 0.7$	121
5.21	Spatial response to the changes in parameter A_0 and fixed $c_1 = 0.7$	121
5.22	The effect of changing parameter ω , for $A_0 = 2$	122
5.23	The effect of changing parameter c_1 , for $c_0 = 0.7$	122
5.24	The effect of changing parameter ω , for $A = 2.05$ and $c_0 = 0.71$	123
5.25	Max-min values of oxygen concentration and its average concentration	125
5.26	Spatial distributions of system components for $A_0 = 2.02$, $\omega = 10^{-3}$	126
5.27	Spatial distributions of system components for $A_0 = 2.05$, $\omega = 10^{-4}$	127
5.28	Ecology catastrophe and paths to extinction	128
5.29	Sketch for paths to extinction for different initials	129
6.1	Sketch of A and c_1 functions vs. time	135
6.2	Effect of changes in parameter A_0	136
6.3	3D Phase space structure for changes in parameter A_0	137
6.4	Effect of changes in parameter A_1	137
6.5	3D Phase space structure for changes in parameter A_1	138
6.6	Effect of changes in parameter $c_1^{(2)}$	138

6.7	Phase space structure for changes in parameter $c_1^{(2)}$	139
6.8	Effect of changes in parameter $c_1^{(1)}$	140
6.9	3D Phase space structure for changes in parameter $c_1^{(1)}$	140
6.10	Effect of changes in parameter A_0	142
6.11	Effect of changes in parameter A_1	142
6.12	Effect of changes in parameter A_1	143
6.13	Effect of changes in parameter $c_1^{(2)}$	143
6.14	Effect of changes in parameter $c_1^{(1)}$	144
6.15	Effect of changes in parameter A_1 on spatial distribution	145
6.16	Maximum-minimum values, intermittency and power-spectrum . . .	146
6.17	Patchy, extinction, early warning signals	147
6.18	Extinction level analysis for different A_0	147
E.1	The (null)-isoclines of the oxygen-phytoplankton system, Model 1 .	181
E.2	The (null)-isoclines of the oxygen-phytoplankton system, Model 2 .	182
E.3	The (null)-isoclines of the oxygen-phytoplankton system, Model 3 .	182
E.4	The (null)-isoclines of the oxygen-phytoplankton system, Model 4 .	183
E.5	The (null)-isoclines of the oxygen-phytoplankton system, Model 5 .	184
E.6	The (null)-isoclines of the oxygen-phytoplankton system, Model 6 .	185
E.7	The (null)-isoclines of the oxygen-phytoplankton system, Model 7 .	185

List of Tables

C.1	Eigenvalues for (\tilde{c}, \tilde{u})	163
C.2	Eigenvalues for $(\tilde{c}, \tilde{u}, 0)$	167
C.3	Eigenvalues for $(\bar{c}, \bar{u}, \bar{v})$	168
C.4	Eigenvalues for $(\dot{c}, \dot{u}, 0)^{(1)}$ in large scale	171
C.5	Eigenvalues for $(\dot{c}, \dot{u}, 0)^{(2)}$ in large scale	172
C.6	Eigenvalues for $(\ddot{c}, \ddot{u}, \ddot{v})$ in large scale	173
C.7	Eigenvalues for $(\dot{c}, \dot{u}, 0)^{(1)}$ in small scale	174
C.8	Eigenvalues for $(\dot{c}, \dot{u}, 0)^{(2)}$ in small scale	175
C.9	Eigenvalues for $(\ddot{c}, \ddot{u}, \ddot{v})$ in small scale	176

To my husband

Chapter 1

Introduction

1.1 General features of plankton community

The word phytoplankton originates from the Greek words phyto (plant) and plankton (wandering). The discovery of phytoplankton dates back to the 1600s and early 1700s with the pioneering work of Anton van Leeuwenhoek on the use of high quality lenses to examine pond water [83]. In the latter half of the 19th century, Victor Hensen [96, 263], who was concerned about the functional role of plankton, introduced the term plankton which was subsequently used in several other works [108, 218], and in current times plankton history is reviewed in [235].

Plankton are floating organisms of many different phyla¹ living in the pelagic zone of inland waters, i.e. they cannot swim or move against currents, hence their motions depend on water movement [13, 57]. Their functional classification is based on trophic level, size, and distribution. Autotrophs, i.e. primary producers, constitute phytoplankton, whereas heterotrophs, i.e. consumers, include bacterioplankton and zooplankton [156]. Phytoplankton can be classified according to the scaling in size and they are of microscopic size, usually single-celled organisms [12, 208, 212, 232]².

The color of phytoplankton is determined by the pigments that are dominant in their cells. Most of them appear green coloured due to the high concentration of chlorophyll (a green pigment responsible for the absorption of light for photosynthesis) and red or orange due to the high level of carotene pigment [3]. Therefore, phytoplankton take up carbon dioxide using sun light and other chemical nutrients and release oxygen [91, 129, 186]. Due to containing chlorophyll pigments, these photosynthesising organisms constitute the base of the food

¹Phylum: A group that has a generic relationship or common origin.

²Parts of this paragraph were taken from [227]

chain [30]. Hence, they are responsible for 70% of oxygen production [15, 57]. Furthermore, phytoplankton are estimated to be responsible for at least one half of the total photosynthetic activity on Earth, thereby accounting considerably for production of the atmospheric oxygen [91, 169].

More than half of the earth's atmospheric oxygen is produced as a result of phytoplankton photosynthesis [233]. Oxygen, a waste product of the photosynthetic process, is essential for living beings and the existence of aquatic life [233]. Photosynthetic processes occur in the biologically active layer (upper layer) of ocean. Produced oxygen is then released into the atmosphere or is transferred to the deep ocean [169, 201]. Oxygen transfer from surface layer to the subsurface layers (by respiration and sinking) is affected by oceanic processes, such as circulation, convection, nutrient concentration, temperature and salinity [118]. Oceanographers have focussed on the question of the limiting factors of this process [61]. It is thought that oxygen productivity rapidly increases with increasing light intensity [62].

Production of organic compounds from carbon dioxide to maintain aquatic food chains makes phytoplankton an important agent for primary production [91]. Besides, a prominent feature of phytoplankton is in regulating the oceans' and atmosphere carbon dioxide by fixing it into the organic compounds through photosynthesis [38, 91, 115, 169]. The fact that about 70% of the earth's surface is covered by aquatic ecosystems emphasizes the great significance of plankton for living beings [38].

Prior to modern concerns about accelerated climate change, research has focused on the functional activity of phytoplankton due to its importance on global climate by regulating global carbon cycle and by regulating oceanic temperatures [47, 197]. The amount of dissolved oxygen³ in water body is important due to its effect on atmospheric carbon dioxide concentration, because it determines physical and biogeochemical cycles, such as the flux of oxygen from sea to air [91, 118]. Air-sea oxygen flux is a consequence of the difference between pressure of the gas in the surface layer and air pressure and this process is affected by water surface temperature [119]. Setting this aside, phytoplankton are not only responsible for the regulation of oxygen and carbon dioxide circulation, they are also responsible for the circulation of other chemical substances in a water body, such as phosphorus, nitrogen and sulphur [10, 91, 212, 216]. Therefore, phytoplankton also play a crucial role on global climate [for more details see [29, 47, 268] and references therein].

³The dissolved oxygen is oxygen that is dissolved in a solution

Phytoplankton are important for being a major food source for their marine consumers [197, 212]. Herbivorous marine animals graze on phytoplankton, whilst in turn carnivores graze on herbivores and so on up the food chain to the top predators. There is a large body of literature concerned with herbivorous groups, i.e. zooplankton [79, 107, 209]. Some external factors affect the abundance of phytoplankton in water body too, i.e. temperature, salinity, wind intensity, sunlight, predation etc. [34, 208, 238]. In particular, predation is one of the most common controlling measures of phytoplankton abundance and predator existence depends on the presence of its prey [56]. The underlying interactions between phytoplankton and zooplankton are of prey-predator kind [139, 262]. Zooplankton predation is also well documented in many laboratory experiments to further understand their feeding behavior on phytoplankton [114, 131, 266].

The interaction between phytoplankton and zooplankton is affected by some external factors. Namely, higher temperatures decrease predator density and in turn this leads to an increase in prey density [111]. Further research into the effect of temperature on marine organisms is carried out in terms of two different biological aspects: direct and indirect. The former is related to organisms' temperature tolerance and the latter stems from changing surrounding environment condition, i.e. surrounding water temperature [19]. We will not go into details about the direct effect, but it is known that maximal performance of living cells occurs when temperatures are between 25°C and 40°C [16, 211]. This performance rate is generally modelled by a non-linear exponential function [211]. Another interesting effect of temperature on marine organisms is its effect on body function, i.e. temperature affects many cellular metabolic processes by altering enzyme-mediated biochemical processes. The structural integrity of enzymes decays at high temperatures which leads to an adverse effect on enzymatic structure [75, 78]. Warmer water leads to faster metabolism and increased respiration due to increased cell division influenced by increasing temperature [4, 59, 117, 203].

The photosynthetic rate is also sensitive to temperature [211]. A quick increase in photosynthetic rate is observed when temperatures are between 10°C and 20°C [219]. Photosynthetic rate is measured either as CO_2 assimilation or the O_2 production rate and it is observed that for temperatures below 13°C , the CO_2 compensation point is proportional to O_2 concentration [116]. Specifically, extinction of the marine biota occurs when temperatures exceed 30°C [267]. Glime [78], worked on the temperature effect on photosynthetic rate and observed that at 23°C the optimum photosynthetic rate occurs, whereas organisms die at 33°C .

This work provides a useful framework to reveal the change in oxygen concentration under the influence of temperature. Ku and Edwards [126, 57] stated that an increase in oxygen inhibition of photosynthesis is observed with temperatures varying between 5°C and 40°C [126]. They added that present O_2 levels affect the optimum photosynthetic rate, e.g. the optimum rate of photosynthesis occurs at 21% of the O_2 level. In [126] and [172], water temperature has been investigated to understand the production and consumption rate of oxygen by making some experiments on two sea grass communities. It has been shown that temperature has a prominent effect on marine ecosystem dynamics to a large extent, thus its changes are of considerable interest.

Marine systems are not only affected by changing temperatures, but also affect the heat balance of Earth. Oceans have a crucial impact on changing atmospheric temperature and account for roughly 84% of the total increase of the Earth's temperature from 1955 to 1998 [133]. It stems from its role in the transfer of heat and balance of CO_2 , thereby oceans have the capability of slowing down climate change due to their massive presence and its storage and transport capability of heat [102, 134].

Recent studies on the Earth's climate show a trend of continuously increasing temperature [103, 148, 149, 264]. By the end of 21st century, average water temperatures could rise between 2°C and 6°C [157]. In light of these records, ocean temperature has elevated since 1950s and will continue to increase [102]. The average global temperature is expected to have increase by 1.8°C - 4°C during the 21st century [188]. The warming process can be explained as some of the heat energy is trapped by greenhouse gases and promoted to warm up the planet. The increasing greenhouse gas concentrations have resulted in an increase in temperature on the sea surface and atmosphere in the past century by 0.4°C - 0.8°C [1]. Intense warming of 0.03 - $0.04^{\circ}\text{C yr}^{-1}$ has been observed through the water column from 1974 to 2001 in the Catalan Sea [258]. Consequently, temperature changes of the Earth's surface leads to the warming up of deep waters. Deep ocean water warming leads to detrimental consequences by affecting the Antarctic system and the air-sea heat flux [71, 152].

Marine systems' relevance to climate change has grasped researchers' attention which has been reflected in substantial research and publications on climate change effects on marine system, which has increased considerably since 1993 [89]. Aquatic systems' response to climate change is studied both in oceans [89, 181] and river ecosystems [187]. The link between climate change and marine systems comes from temperature changes of water body resulting in changes to water body

circulation, nutrient export and decomposition process [154]. As a consequence, water body dissolved oxygen is reduced [247].

So far, it has been emphasized that climate change effects on marine systems can be observed by measuring either CO_2 assimilation or O_2 production. However, there is another way to quantify climate change effects on marine systems and that are annually recurring life cycle events called phenology. Phenology is the simplest approach to observe the species' response to climate change [264]. Some phenological events, such as changing migration time, seasonal activities, changing larva stage can give insight into current climate change. Phytoplankton are sensitive to any changes in the surrounding environment. Hence any changes in the climate impact the common behavior of the population, e.g. unpredictable spring weather results in mismatching of larval release with spring phytoplankton bloom [57, 248]. In addition, any changes in climate affect marine systems, such as phytoplankton productivity and abundance of phytoplankton communities [104]. Even if there is no certain effect on species distribution in marine ecosystems, the interactions of species are affected by climate change [223].

There are some severe ecological consequences in response to the changing environmental conditions. They are known as hypoxia and anoxia and occur as a result of oxygen depletion in water body. Hypoxia takes place when the dissolved oxygen concentration $\leq 2 \text{ mg } l^{-1}$, whilst anoxia arises when the dissolved oxygen concentration decreases to $0 \text{ mg } l^{-1}$. The duration and severity of hypoxic and anoxic events affect growth and reproduction of aquatic organisms and in some cases can lead to mortality of these organisms [51, 158, 257]. Although there is a certain threshold for the existence of anoxia, the threshold of hypoxia is not exact. Hypoxia thresholds vary between species due to the various responses of oxygen depletion for various marine fauna. Nonetheless, the increase incidence of hypoxia is one of the crucial ecological results of climate change [174]. Depletion of oxygen in deep water and its influence on marine systems has been studied intensively over the past decades, as the declines in dissolved oxygen in bottom water strongly affect features of marine fauna, such as feeding ability, reproduction, abundance and even existence [52, 63, 204, 205]. It has been observed that excess sedimentation affects both marine flora and fauna and leads to hypoxia and a decrease in marine systems' population [37, 80, 100, 255]. In the same manner, oceanic anoxic events affect inhabited marine organisms in these region [128]. It should be emphasized that this decline in oxygen in water body is higher than in the past [77].

1.2 Mathematical approach

Awareness of the importance of mathematical modelling has been growing in recent decades. It provides a framework of the underlying complexity of natural phenomena in many fields, such as engineering, physics, chemistry [198]. In particular, mathematical modelling is a powerful research tool in biology and ecology to understand the real underlying population dynamics and communities [155, 172, 180, 198, 229]. Modelling marine ecosystems poses a very complex problem due to the vast number of interacting species and sub-communities [58, 155, 177]. In some cases field observations and experiments become impossible or expensive, therefore mathematical modelling takes its place to reduce these problems and contributes to providing further insights into the ecological problems with the assistance of computer simulations [137, 197].

The earliest plankton studies started as a part of fisheries. Separation of plankton studies as a field for itself had been originated in the 1940-1950s [189]. At the end of the 19th century, marine biological laboratories and societies prompted interest in plankton research in many countries [189]. From then on, there has been a growing number of publications building on mathematical modelling of plankton communities [53, 68, 112, 182, 213]. One of the common models of plankton productivity was given by [15]. Phytoplankton bloom control by zooplankton via an ordinary differential equation was given by [68]. Spring phytoplankton bloom due to temperature change was described by a mathematical model in [249]. For prey-predator interactions between phytoplankton and zooplankton, Lotka-Volterra equations are used in [54, 132, 159, 224]. Food uptake and growth empirical relationships among zooplankton and fish have been considered in [55, 109].

Being tiny and growing quickly are features that make phytoplankton very suitable organisms for both field and laboratory works. Because phenological events happen rapidly, studying these communities becomes convenient in terms of data collection and modelling [91, 197]. Plankton dynamics are extensively studied through field and laboratory experiments. In addition, theoretical studies of modelling population dynamics are of particular interest as models have the ability to show the relation between population dynamics and climate change [33, 250]. In experimental works, field data on phytoplankton temporal and spatial distribution were detailed with the help of the plankton recorder invention [88]. These were further improved by phytoplankton photosynthetic measurements [178]. Moreover, scuba diving observations and remote camera control systems have contributed to

deeper understanding of marine systems [87, 98]. The advance of satellite oceanography substantially contributed to visualisation of plankton communities and its spatial distribution [9]. For further historical information on ocean studies see [189].

As it is mentioned above, marine systems are complex. But here, the purpose of this study is to make an insight into some basic features of relevant ecosystems, i.e. to reveal the properties of model dynamics. In this case, the simplest model can be determined as a starting point. In this simplest form under the assumption of spatial homogeneity, population density is only a function of time, but not space. Population models are described by ordinary differential equations (ODE) [171, 253]. Single species population dynamics can be described by [195]:

$$\frac{dx(t)}{dt} = xf(x), \quad (1.1)$$

where x is the population density at time t , with per capita growth rate $f(x)$. Depending on the number of interacting species, the single species population model can be extended, e.g. multi-species model. One of the simplest models of two interacting species takes the form of two coupled ODEs:

$$\frac{dx(t)}{dt} = f(x, y), \quad (1.2)$$

$$\frac{dy(t)}{dt} = g(x, y), \quad (1.3)$$

where f and g are continuous functions, x and y are the population densities at time t and functions f and g represent the population change due to reproduction and mortality. For such autonomous systems, we can construct a phase plane for each value of t and each point (x, y) is assigned a unique vector $(f(x, y), g(x, y))$. Solutions of the system are assigned to *trajectories* in the phase plane. So, the solution curve passing through (x, y) must be tangent to these vectors. The pair $x(t), y(t)$ is assigned a unique point in the *phase plane* (x, y) . Locations of points where either $f(x, y)$ or $g(x, y)$ is zero has a special meaning. If $f(x, y) = 0$, it means that there is no change on x and the direction vector is parallel to y axis. Similarly, if $g(x, y) = 0$, so y does not change and the direction vector is parallel to the x axis. The point which satisfy one of these conditions is called an *isocline*. Steady states of system (1.2-1.3) do not appear to undergo any change. Note that, system steady states are the intersections of the systems' x isocline and y isocline. Here f and g are nonlinear functions and \bar{x} and \bar{y} are *steady-state* solutions of the

following system:

$$f(\bar{x}, \bar{y}) = 0, \quad g(\bar{x}, \bar{y}) = 0.$$

The linearised system corresponding to (1.2-1.3) is given as:

$$\frac{dX(t)}{dt} = a_{11}X + a_{12}Y, \quad (1.4)$$

$$\frac{dY(t)}{dt} = a_{21}X + a_{22}Y, \quad (1.5)$$

where $X(t) = x(t) - \bar{x}$, $Y(t) = y(t) - \bar{y}$ and the community matrix with f_x , f_y , g_x and g_y denoting first order partial derivatives with respect to (x, y) , is given by

$$A = \begin{pmatrix} a_{11} & a_{12} \\ a_{21} & a_{22} \end{pmatrix} = \begin{pmatrix} f_x & f_y \\ g_x & g_y \end{pmatrix}_{(\bar{x}, \bar{y})} \quad (1.6)$$

The eigenvalues λ of the matrix A are given as a solution of the following equation:

$$\det(A - \lambda I) = 0$$

where I is the unit matrix.

By the principle of linear superposition, the general solution of (1.4-1.5) is a linear combination of $e^{\lambda_1 t}$ and $e^{\lambda_2 t}$. In the case of real eigenvalues, the steady state is called a *node* (see Figs. 1.1a-b); if at least one of them is of opposite sign, the steady state (\bar{x}, \bar{y}) is called a *saddle* (see Fig. 1.1c); if all are positive, the steady state is *unstable*; if all eigenvalues are negative, the steady state is *stable*. Furthermore, in the case of complex eigenvalues, the steady state is called a *focus* (see Figs. 1.1d-e) [56, 198]. For a graphical illustration of the behavior of system trajectories near an equilibrium point, see Fig. 1.1.

In reality, densities of populations change both in time and in space. This leads to the inclusion of space into models resulting in partial differential equations (PDEs); works on PDEs date back to the work of Fisher [67] with the application of PDEs to the spatial spread of diseases and genes. In 1950s, Turing [254], focussed on pattern formation under diffusion and Skellam [234], applied the diffusion equation of random dispersal modelling to population dynamics.

The simplest form of the reaction-diffusion equations is as follows:

$$\frac{\partial x}{\partial t} = D\Delta x + f, \quad (1.7)$$

$$\frac{\partial y}{\partial t} = D\Delta y + g, \quad (1.8)$$

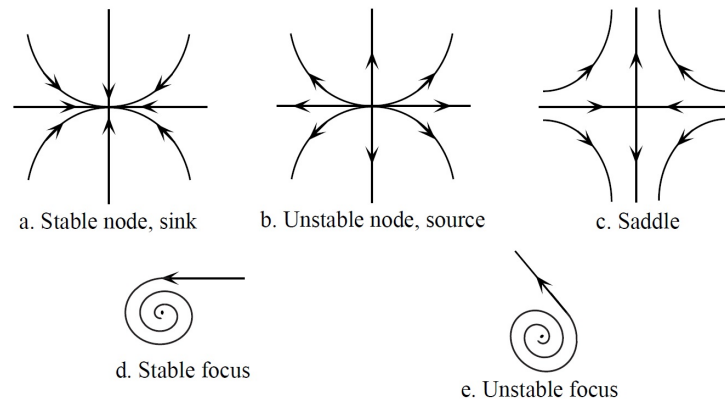


FIGURE 1.1: Phase trajectories in the neighborhood of the following types of points. Image is taken from <http://www.maths.lth.se/matematiklth/courses/FMAN15/media/material/lin2d.pdf>.

where D is the diffusion coefficient, f and g are the corresponding functions for population densities at a given time and location and Δ is the Laplace operator. Reaction-diffusion equations have been applied to marine systems, and are assumed to be an appropriate model based on the effect of water movement on species distribution [24, 120, 229].

Population distributions are usually heterogeneous in their environments, and this distribution is often patchy [185]. The patchiness is observed in many field observations [2, 49, 64, 81, 143, 245]. In particular, plankton patchiness in water body have been focused on in [27, 90, 94, 156, 184, 202, 239, 241, 244, 251]. The image of phytoplankton patchy distribution in north of Norway is given in Fig. 1.2. Similar dynamics of plankton patchy distribution have been observed in reaction diffusion systems: for instance, zooplankton distribution in the two-dimensional case is given for different time moments in Fig. 1.3 for an appropriate choice of functions f and g [147]. Here, phytoplankton distribution is qualitatively similar with the zooplankton distribution, thereby only predator distribution is given for the sake of brevity. The irregular patterns in Fig. 1.3d show a qualitatively similar distribution which is observed in real ecological plankton systems in the ocean; see Fig. 1.2. In general, patchy distributions have been often observed in prey-predator system [168, 199].

There exists some research on plankton population dynamics to reveal its dynamics under the effect of interacting group/groups. One of the interactions focused on are fish and zooplankton interactions [40, 82, 110, 240]. Indeed, the prey-predator interaction is the most common interaction among species. But the ecological relation between these groups cannot be restricted only as a prey-predator (cf. the classical work by Lotka [139] and Volterra [262]) interaction.



FIGURE 1.2: Patchy distribution of phytoplankton north of Norway in the Barents Sea in July 2004. Different densities of phytoplankton are given different shades of blue and green. The pale blue waters contain extremely high concentrations of the phytoplankton. Image is taken from [http : rsta.royalsocietypublishing.org/content/363/1837/2873/F1](http://rsta.royalsocietypublishing.org/content/363/1837/2873/F1) of MODIS Rapid Response Project at NASA/GSFC.

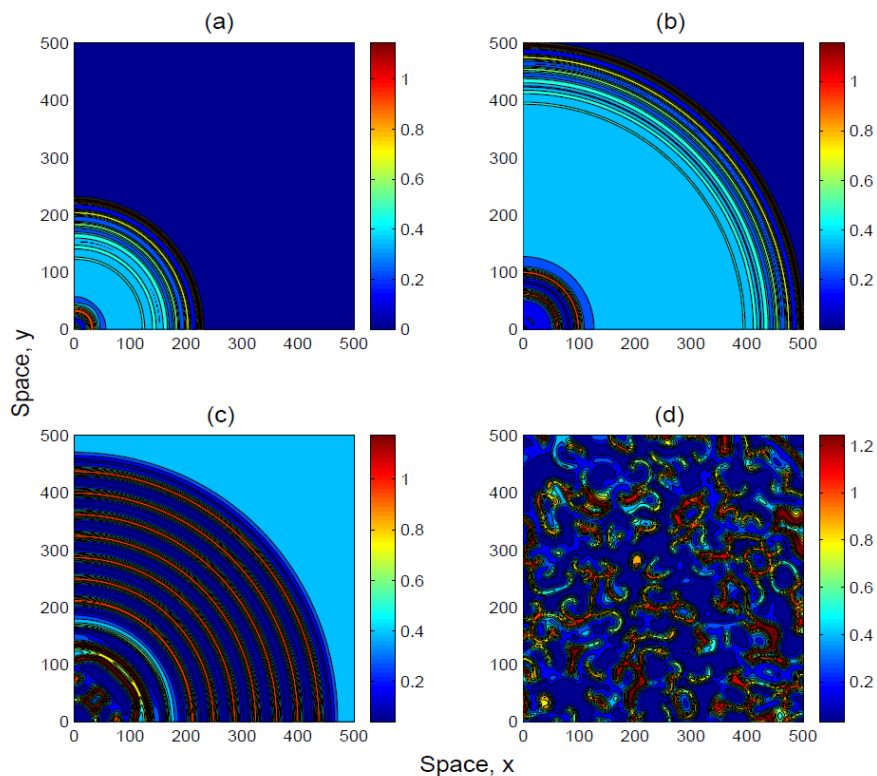


FIGURE 1.3: Zooplankton density spatial distribution in two-dimensions for different time moments (a) $t = 125$, (b) $t = 275$, (c) $t = 1000$, (d) $t = 3500$. Phytoplankton density shows qualitatively similar behavior. With permission from Malchow et al. [147].

Another relation is observed as nutrient-plankton interaction, with a simple diffusion model, since the pioneer work of Riley et al. [214]. Moreover, other approach on the plankton system, which we attempt to build our model on, are resource-consumer type interactions, when the interacting agents are not biological species, considered by Feltham and Chaplin [66]. They have focussed on diffused resource consumed by its consumer. In our case, oxygen (resource) diffuses through the water body and is consumed by the phytoplankton, which is also its producer.

1.3 Thesis outline

This work intends to study the oxygen dynamics in a plankton system within the introduced framework of ordinary and reaction-diffusion systems. A special remark should be made on the observation of the model system. We begin with analysing both analytically and numerically a system comprising of oxygen-phytoplankton and then analyse the addition of zooplankton.

This dissertation is organized as follows. Chapter 1 gives a general background on relevant oxygen and plankton issues in marine ecosystems.

Chapter 2 deals with spatial and nonspatial dynamical behavior of our basic oxygen-phytoplankton model system.

Chapter 3 gives ecologically more realistic results with the addition of the zooplankton to our basic resource-consumer model. Therefore, predation effects on oxygen concentration is taken into account in this chapter. It should be emphasized here that the improved oxygen-plankton models' behavior is quite similar to the prey-predator model dynamical response in [147]. Then the systems' nonspatial and corresponding spatial dynamics are given in the one-dimensional case.

In Chapter 4, we have introduced plankton respiration terms and include them into the improved model system. The results presented include the non-spatial and spatial case in one-dimension. Contrary to the general structure of this dissertations' each chapter, here we give the spatial distribution of oxygen concentration in water body in two-dimensions by keeping in mind the phytoplankton spatial distribution in two dimensional case is qualitatively similar with the distribution of oxygen concentration.

Chapter 5 focuses on the system's dynamical response to the changing environmental condition. Specifically, we consider the effect of a continuously increasing temperature function with time as a consequence of the global climate change. The system's nonspatial and its corresponding spatial case to the changing surrounding water temperature are given. We will show that a sufficiently large

increase or decrease in the relevant controlling parameters can result in a sudden decline in oxygen production and plankton extinction.

Chapter 6 continues the study of changing environmental condition. But in this case, we focus on the system's response to the stopping the increase of temperature with time. Therefore, we choose a piecewise linear temperature function and try to observe the system's nonspatial and spatial response to this hypothetical change of environmental condition.

In Chapter 7, I conclude with a summary of results and present new directions in order to encourage possible future work in hope that subsequent research will fill the gaps and improve the understanding of underlying properties of marine ecosystem responses to global climate change.

Chapter 2

Baseline Model

2.1 Introduction

Dynamics of oxygen production due to phytoplankton photosynthetic activity has long been a focus of research, both in field measurements and in laboratory settings. Oxygen concentration is measured by the level of oxygen production resulting from photosynthetic activities. The earliest measurement of oxygen production (dating back to almost 90 years ago) was made by determining changes in oxygen concentration in bottles submerged in the water by using Winkler techniques [72]. In his classical book, Harris [91] considered the connection between the growth rate of oxygen production and photosynthesis, as photosynthesis constitutes the main source of energy accessible to the cells. Paasche [186] showed that the concentration of oxygen in the ocean is due to the photosynthetic activity of phytoplankton, which are mainly responsible for the photosynthetic process in oceans. Phytoplankton, therefore, play an essential role in maintaining life on Earth in terms of oxygen production [169]¹.

Phytoplankton are greatly responsible for photosynthetic process as in the ocean making them important agents of aquatic system for primary production [91, 186]. More than one half of the total photosynthetic activity on Earth is carried out by them, thereby they account for the majority of the oxygen release to the Earth's atmosphere [169]. Therefore, oceanic system are responsible for regulating the atmospheric oxygen budget. This produced oxygen is then utilized by some marine animals, for organic matter oxidation and the rest is released to the atmosphere [91].

There is a large body of literature concerned with various aspects of spatiotemporal dynamics of plankton [5, 57, 105, 106, 150, 160, 163]. In particular,

¹The majority of this chapter has been published in [227]

an oxygen-plankton system model combined with nutrient and zooplankton components is examined by Mocenni [163]. Based on this model accounting for the interplay between the physical and chemical processes in coastal ecosystems it does not address the main relation between plankton populations and oxygen concentration. Another plankton-oxygen model has been proposed and analyzed by Misra [160] including the effect of some ‘exogenous’ factors (such as light, wind intensity, temperature, phosphorus, eutrophication, etc.), hence leaving the internal plankton-oxygen dynamics out of the focus.

The intricate structure of marine systems lies in the wide variety of species and their inter-intra species interactions [58, 155, 177]. Therefore, field studies are not applicable due to their inability to discern the contribution of all existing constituents. Hence, a ‘realistic’ ecosystem model can include many equations [65, 125]. As with all modelling approaches, we aim to simplify the system’s complexity through the choice of key factors. Numerous controlling factors affecting oxygen production by phytoplankton include temperature, salinity, predation, nutrient availability, depth of water, light etc. [34, 208, 238]. Here, we focus on a reduced model incorporating the conceptual model based on the relationship between oxygen itself and phytoplankton as its producer.

In this chapter, we introduce a ‘baseline’ model which neglects some external factors to further our understanding of the main interactions (related to oxygen production in photosynthesis and its consumption) between oxygen and phytoplankton. Hence, in subsection 2.2, we introduce our oxygen-phytoplankton model. In subsections 2.2.1 and 2.2.2, steady states and their existence conditions are examined. In subsection 2.2.3, our two-component system is studied through extensive numerical simulations both in nonspatial and spatial case to reveal the properties of the model.

2.2 Model Formulation

The structure of our baseline model describing the interactions between oxygen and phytoplankton is illustrated by a flow chart (see Fig. 2.1). Flows of matter through the system are indicated by arrows.

We begin with a simple conceptual model that only takes into account the temporal dynamics of the oxygen itself and the phytoplankton as its main

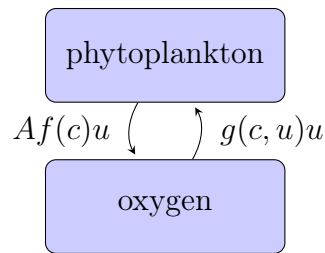


FIGURE 2.1: Interactions between oxygen & phytoplankton. Arrows show the flows of matter through the system, and the parametrizations of the rates are as labelled. Phytoplankton produces oxygen through photosynthesis during the day-time depending on existence of sunlight and consumes it during the night [36].

producer.

$$\frac{dc(t)}{dt} = Af(c)u - mc, \quad (2.1)$$

$$\frac{du(t)}{dt} = g(c, u)u. \quad (2.2)$$

Here c and u denote the concentration of the dissolved oxygen and the phytoplankton density, respectively, at time t , $f(c)$ is the amount of oxygen produced per unit time and per unit phytoplankton mass, $g(c, u)$ is the per capita phytoplankton growth rate, A describes the effect of the environmental factors on the rate of oxygen production, and the term mc takes into account oxygen losses due to natural depletion, e.g. its diffusion to the atmosphere, consumption of marine organisms, etc. Note that Eq. (2.1) is linear with respect to u , and indeed we are not aware of any evidence that the photosynthesis rate can depend on phytoplankton density. On the contrary, Eq. (2.2) should normally be nonlinear with respect to u (hence the dependence of g on u) as the high phytoplankton density is known to damp on its own growth, e.g. due to self shading and/or nutrient depletion. Moreover, it is known that world's oxygen output decline can be explained by the decline in phytoplankton density [259].

In order to understand what can be the properties of functions f and g , we have to look more closely at the oxygen production and consumption. We consider $f(c)$ first. Oxygen is produced inside phytoplankton cells through photosynthesis and then diffuses through the cell membrane into the surrounding water. The diffusion flux is always directed from areas with higher concentration of the diffusing substance to the areas with lower ones, and this more prominent with the increasing difference between concentrations (cf. Fick's law [39]). Therefore, for the same rate of photosynthesis, the amount of oxygen that gets through the cell

membrane will be larger the lower the oxygen concentration is in the surrounding water. Therefore, f should be a monotonously decreasing function of c . We further assume that the oxygen flux through the cell membrane tends to zero when the oxygen concentration in the water is very large, i.e. in physical terms, is close to its saturating value for $c \rightarrow \infty$. The above features are qualitatively taken into account by the following parametrization:

$$f(c) = 1 - \frac{c}{c + c_0}, \quad (2.3)$$

where c_0 is the half-saturation constant.

Considering phytoplankton multiplication, we assume that $g(c, u) = \alpha(c) - \gamma u$ where the first term describes the phytoplankton linear growth and the second term accounts for intraspecific competition for resources. Eq. (2.2) for the phytoplankton growth is therefore essentially the logistic growth equation where $1/\gamma$ plays the role of the carrying capacity, which we assume does not depend on c . However, the linear growth rate α should depend on c , which can be seen from the following argument. Phytoplankton produce oxygen by photosynthesis during the daytime, but they need oxygen for their metabolic processes (e.g. breathing) during the night; therefore, low oxygen concentration is unfavorable for phytoplankton and is likely to depress its reproduction [36]. On the other hand, a phytoplankton cell cannot take more oxygen than it needs. Hence, α should be a monotonously increasing function of c tending to a constant value for $c \rightarrow \infty$. The simplest parametrization for α is then given by the Monod function, so that for $g(c, u)$ we obtain:

$$g(c, u) = \frac{Bc}{c + c_1} - \gamma u, \quad (2.4)$$

where c_1 is the half-saturation constant and B is the phytoplankton maximum per capita growth rate.

With (2.3–2.4), Eqs. (2.1–2.2) take the following form:

$$\frac{dc}{dt} = A \left(1 - \frac{c}{c + c_0} \right) u - mc, \quad (2.5)$$

$$\frac{du}{dt} = \left(\frac{Bc}{c + c_1} - \gamma u \right) u. \quad (2.6)$$

The system (2.5–2.6) contains six parameters; however, their number can be reduced by choosing dimensionless variables as follows:

$$t' = tm, \quad c' = \frac{c}{c_0}, \quad u' = \frac{\gamma u}{m},$$

and renaming new parameters accordingly as

$$\hat{B} = \frac{B}{m}, \quad \hat{A} = \frac{A}{c_0\gamma} \quad \text{and} \quad \hat{c} = \frac{c_1}{c_0}.$$

For convenience, we now simplify the notations by omitting the primes and hats, i.e. by changing $t' \rightarrow t$, $c' \rightarrow c$, $u' \rightarrow u$, $\hat{A} \rightarrow A$ and $\hat{B} \rightarrow B$ and $\hat{c} \rightarrow c_1$. Eqs. (2.5–2.6) then take the following form:

$$\frac{dc}{dt} = A \left(1 - \frac{c}{c+1} \right) u - c \equiv f(c, u), \quad (2.7)$$

$$\frac{du}{dt} = \left(\frac{Bc}{c+c_1} - u \right) u \equiv g(c, u), \quad (2.8)$$

where all variables and parameters are now dimensionless. For detailed analytical work on obtaining the dimensionless form; see Appendix B. The analysis of the model properties will be done in terms of dimensionless parameters and variables. A brief discussion of possible parameter values in real ecosystems will be done in Section 5.3

2.2.1 Examining the steady states and existence

The next step is to reveal the existence of the equilibria (steady states), (\tilde{c}, \tilde{u}) as given by the non-negative solutions of the following system:

$$f(\tilde{c}, \tilde{u}) = 0, \quad g(\tilde{c}, \tilde{u}) = 0.$$

Biologically meaningful system equilibria are non-negative intersection points of the oxygen zero-growth isocline and the phytoplankton zero-growth isocline. The shape of these (null-)isoclines is shown in Fig. 2.2. The first isocline (i.e. for oxygen increase) is given by the curve $\tilde{u} = \frac{\tilde{c}}{A}(\tilde{c}+1)$ and the second isocline (i.e. for phytoplankton growth) is given by $\tilde{u} = 0$ and $\tilde{c} = \frac{\tilde{u}c_1}{B-\tilde{u}}$. Correspondingly, Eqs. (2.7–2.8) have at most two non-negative solutions. One is the extinction state $(0, 0)$ and the other is the coexistence state (\tilde{c}, \tilde{u}) . The extinction state exists for all parameter values. The coexistence state exists only under certain conditions.

Parameter B takes values with the range $\{1, 1.4, 2, 2.4, 3, 3.4, 4, 4.4, 5, 5.4\}$. In Fig. 2.2, \tilde{c} and \tilde{u} correspond to the steady state of oxygen and phytoplankton, respectively. From the model system (2.7–2.8), the coexistence steady state is given by the intersection of the isoclines shown, with a circle, as \tilde{c} and \tilde{u} which is readily seen on Fig. 2.2. The steady state values \tilde{c} and \tilde{u} are the solutions of the

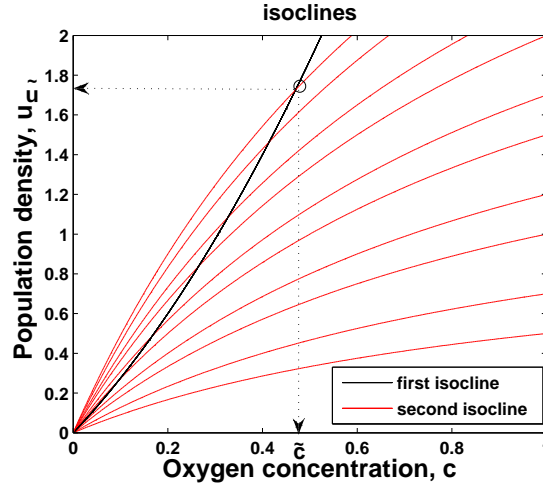


FIGURE 2.2: The (null-)isoclines of the oxygen-phytoplankton system (2.7–2.8). Black curve shows the oxygen isocline for $A = 0.4$ and $c_1 = 1$; red curves show the phytoplankton isocline for B changes from 1 to 5.4 for the range is given in the text from bottom to top.

following system:

$$A \left(1 - \frac{\tilde{c}}{\tilde{c} + 1} \right) \tilde{u} - \tilde{c} = 0, \quad (2.9)$$

$$\left(\frac{B\tilde{c}}{\tilde{c} + c_1} - \tilde{u} \right) \tilde{u} = 0, \quad (2.10)$$

from which the equations for the isoclines can be obtained, respectively, as

$$\tilde{u} = \frac{\tilde{c}}{A}(\tilde{c} + 1) \quad (2.11)$$

and

$$\tilde{u} = \frac{B\tilde{c}}{\tilde{c} + c_1}. \quad (2.12)$$

The corresponding curves are shown in Fig. 2.2.

Note that Eq. (2.12) can be rearranged in terms of \tilde{c} as follows:

$$\tilde{c} = \frac{\tilde{u}c_1}{B - \tilde{u}}. \quad (2.13)$$

Substituting (2.13) into Eq. (2.11), the following quadratic equation is obtained for \tilde{u} :

$$A\tilde{u}^2 + (-2AB - c_1^2 + c_1)\tilde{u} + AB^2 - c_1B = 0, \quad (2.14)$$

so that its solution is given by

$$\tilde{u} = \frac{-\sigma \pm \sqrt{\sigma^2 - 4A\kappa}}{2A} \quad \text{and} \quad \tilde{c} = \frac{\tilde{u}c_1}{B - \tilde{u}}, \quad (2.15)$$

where

$$\sigma = -2AB - c_1^2 + c_1 \quad \text{and} \quad \kappa = AB^2 - c_1B. \quad (2.16)$$

It is readily seen that a unique positive root exists if the following conditions are satisfied. Consider

$$\tilde{u} = \frac{-\sigma - \sqrt{\sigma^2 - 4A\kappa}}{2A} > 0, \quad (2.17)$$

then

$$\sigma^2 - 4A\kappa \geq 0, \quad \sigma < 0, \quad (2.18)$$

and

$$-\sigma - \sqrt{\sigma^2 - 4A\kappa} > 0,$$

so that

$$0 > -4A\kappa \implies \kappa > 0 \implies AB > c_1. \quad (2.19)$$

On the other hand

$$\tilde{u} = \frac{-\sigma + \sqrt{\sigma^2 - 4A\kappa}}{2A} > 0, \quad (2.20)$$

then

$$-\sigma + \sqrt{\sigma^2 - 4A\kappa} > 0,$$

so that

$$0 < -4A\kappa \implies \kappa < 0 \implies AB < c_1. \quad (2.21)$$

Therefore, the unique positive root exists for

$$\tilde{u} = \frac{-\sigma - \sqrt{\sigma^2 - 4A\kappa}}{2A} > 0 \quad \text{for} \quad AB > c_1. \quad (2.22)$$

Thus, using the expression (2.17) for \tilde{u} , we have arrived at condition given by Eq. (2.22). Note that the choice of the other root (see (2.20)) instead of (2.17) results in $\tilde{u} < 0$ and hence it is ecologically meaningless.

The shape of the second isocline, as given by Eq. (2.12) or (2.13), depends on parameter B , and taking sufficiently small values of B eventually results in the disappearance of the positive steady state (see the succession of red curves in Fig. 2.2) so that the only remaining equilibrium is extinction. From the geometric argument, it is readily seen that the positive steady state exists if and only if the slope of the oxygen isocline at the origin is less than the slope of the phytoplankton isocline. Let us define the first (oxygen) isocline's tangent line and its angle with the x-axis as α . Similarly, we define the second isocline's tangent line and its angle

with the x-axis as β . Then the following holds:

$$\tilde{u} = \frac{1}{A}\tilde{c}(\tilde{c} + 1), \quad (2.23)$$

$$\frac{d\tilde{u}}{d\tilde{c}} = \frac{1}{A}(2\tilde{c} + 1)|_{\tilde{c}=0} = \frac{1}{A}, \quad (2.24)$$

$$tg_{\alpha} = \frac{1}{A}. \quad (2.25)$$

$$\tilde{u} = \frac{B\tilde{c}}{\tilde{c} + c_1}, \quad (2.26)$$

$$\frac{d\tilde{u}}{d\tilde{c}} = \frac{Bc_1}{(\tilde{c} + c_1)^2}|_{\tilde{c}=0} = \frac{B}{c_1} \quad (2.27)$$

$$tg_{\beta} = \frac{B}{c_1}. \quad (2.28)$$

$$\alpha < \beta \Rightarrow \frac{1}{A} < \frac{B}{c_1} \quad (2.29)$$

$$c_1 < AB \quad (2.30)$$

and similarly,

$$c_1 > AB \quad \text{for} \quad \alpha > \beta. \quad (2.31)$$

From Eqs. (2.11) and (2.12), we obtain that the isoclines' slopes are $1/A$ and B/c_1 , respectively. Correspondingly, the condition of their intersection is

$$\frac{1}{A} < \frac{B}{c_1}, \quad \text{so that} \quad AB > c_1, \quad (2.32)$$

which obviously coincides with (2.22). We mention here that condition $AB > c_1$ has a clear biological interpretation. Recall that A quantifies the rate of oxygen production. Therefore, condition (2.32) (or (2.22)) means that, since oxygen is a vital resource, its production must be high enough in order to support the phytoplankton existence.

Now, our concern is to ensure that the steady states are always positive under the assumption of condition given by Eq. (2.22). All results are presented in dimensionless variables introduced in Section 2.2. In our numerical simulations we fix one of parameters A , B or c_1 and the remaining parameters take fixed hypothetical values from a meaningful range to ensure a positive steady state.

The steady state results of oxygen-phytoplankton are shown in Fig. 2.3 for the equilibrium point (\tilde{c}, \tilde{u}) . We fix $A = 0.2$ and consider B to vary between 10 to 20 and the range of c_1 is 1 to 2. P , ($P = \sigma^2 - 4A\kappa$), is a function of

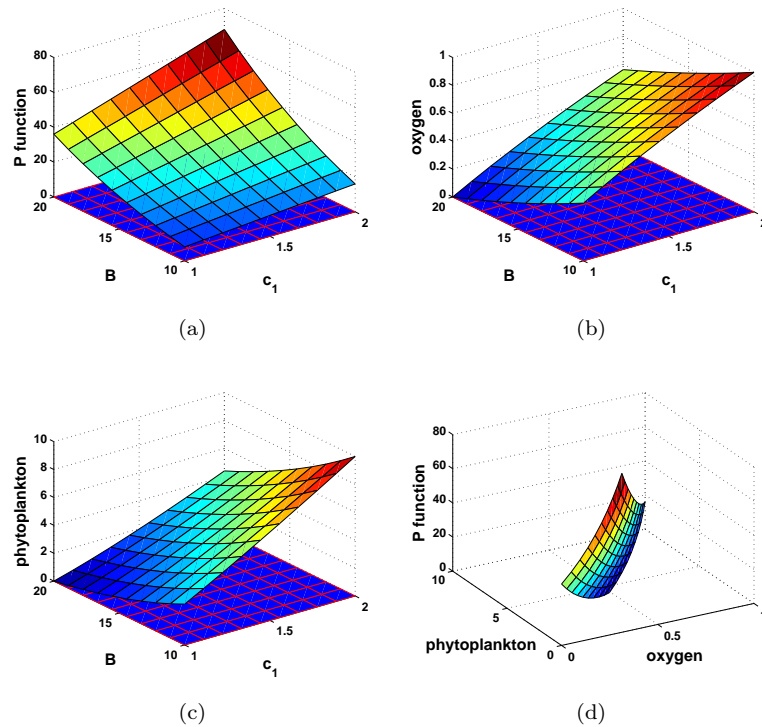


FIGURE 2.3: Steady state values of oxygen and phytoplankton vs. given range of B and c_1 and for $A = 0.2$. Blue surface with red edge color is given to show the separation of negative and positive part.

δ , κ (see Eq. (2.16)) and should satisfy the condition $P \geq 0$ for the meaningful solution of \tilde{u} (see Eq. (2.22)). P versus oxygen and phytoplankton is shown in Fig. 2.3d. Under the above set of parameters, we note that condition Eq. (2.22) is satisfied. The blue planes with red coloured edges that lie the zero surface act as a visual aid to separate the positive and negative parts ignored to make our system biologically reasonable; see in Figs. 2.3a-c. System steady states under the controlling parameters A and c_1 for fixed B_1 value and the function of P are shown in Fig. 2.4. In the same sense, system steady states on the controlling parameters B and A for a fixed c_1 value and the function of P are shown in Fig. 2.5.

This subsection 2.2.1 forms the basis of the fundamental analytical part of our work. The following sections on spatial and nonspatial system dynamics build on these key concepts. As both components (oxygen and phytoplankton) satisfy positive existence states our theoretical model agrees with the observed biological reality; see Figs. 2.3-2.5. Hence, the following subsection 2.2.2 should satisfy the conditions given by the Eqs. (2.19), (2.32) or (2.22).

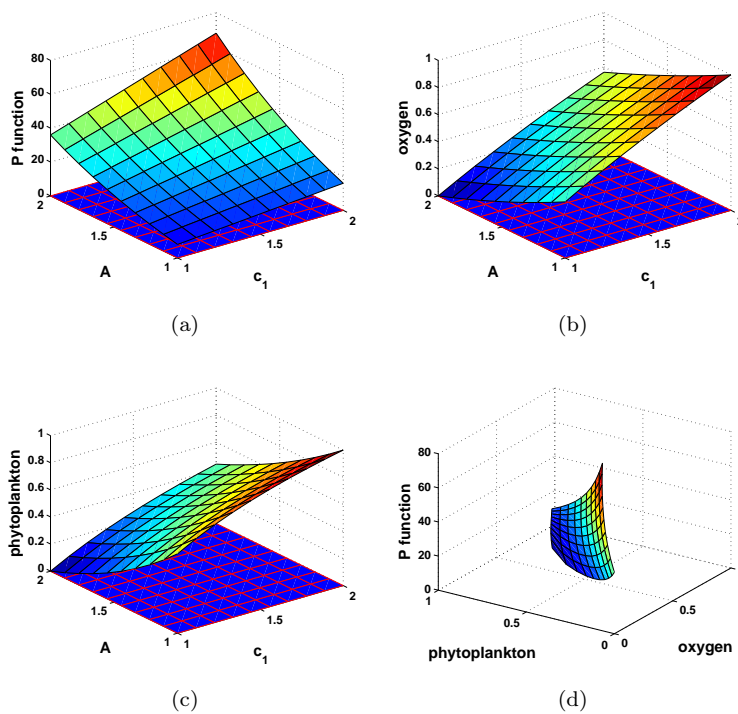


FIGURE 2.4: Steady state values of oxygen and phytoplankton vs. given range of A and c_1 for $B = 2$.

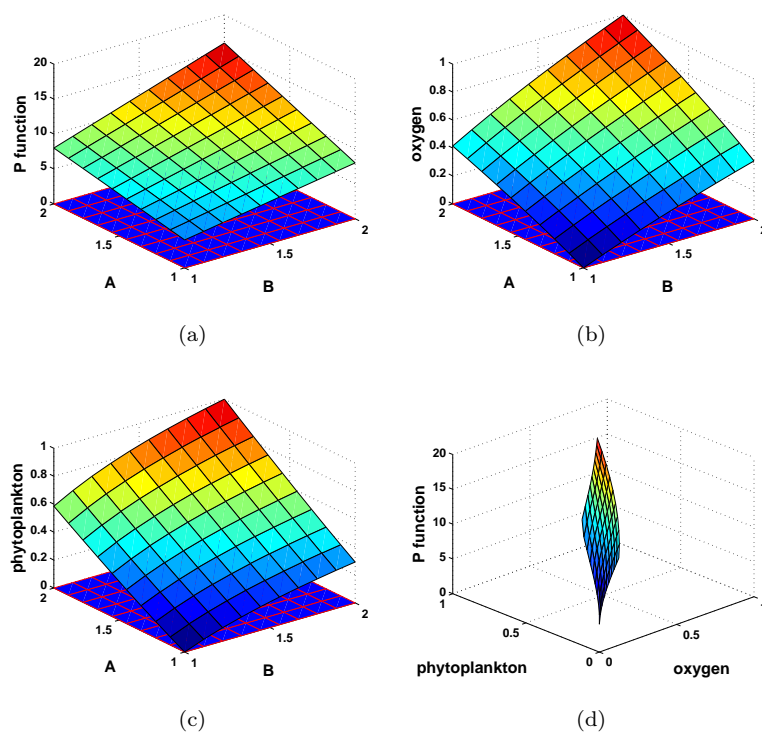


FIGURE 2.5: Steady state values of system components vs. given range of A and B for $c_1 = 1$.

2.2.2 Stability analysis

The nonspatial two-component system (2.7–2.8) has two equilibria with the first one being the extinction state $(0, 0)$ and the second being the coexistence state (\tilde{c}, \tilde{u}) ; see Section 2.2.1.

The Jacobian matrix of the system given by Eqs. (2.9–2.10) is:

$$A = \begin{pmatrix} -\frac{Au}{(1+c)^2} - 1 & A\left(1 - \frac{c}{1+c}\right) \\ \frac{Bc_1u}{(c+c_1)^2} & \frac{Bc}{c+c_1} - 2u \end{pmatrix}. \quad (2.33)$$

For each of the steady states, the eigenvalues are the solutions of the characteristic equation:

$$\det(A_i - \lambda I) = 0, \quad (2.34)$$

where I is the unit matrix and A_i is the matrix (2.33) with the elements calculated at the steady state E_i , $i = 1, 2$. Below we give a brief summary of the results, details of the calculations can be found in Appendix C.

- Extinction state E_1

The eigenvalues of matrix A_1 are -1 and 0 . The fact that one of the eigenvalues is zero means that linear stability analysis is not informative. Generally speaking, in this case, one has to perform a higher order stability analysis to determine the stability of the equilibrium, e.g. by applying the Center Manifold Theory² [26, 130]. Alternatively, in order to avoid tedious analytical calculations, we can check the stability by numerical simulations.

- Oxygen-phytoplankton (coexistence) state E_2

The eigenvalues of matrix A_2 are the solutions of the following characteristic equation:

$$\left(-\frac{A\tilde{u}}{(1+\tilde{c})^2} - 1 - \lambda\right) \left(\frac{B\tilde{c}}{\tilde{c}+c_1} - 2\tilde{u} - \lambda\right) - \frac{A}{1+\tilde{c}} \frac{Bc_1\tilde{u}}{(\tilde{c}+c_1)^2} = 0, \quad (2.35)$$

where \tilde{c} and \tilde{u} are given by Eqs. (2.13) and (2.11).

Instead, in Fig. 2.6, we show λ for each of the eigenvalues λ_1, λ_2 (Figs. 2.6a-b), accordingly as a function on the controlling parameters A and c_1 .

²One of the main methods of simplifying the study of dynamical systems is to reduce the dimensions of the system. Center Manifold Theory is a rigorous mathematical technique to carry out this reduction near equilibria and provides information on the stability of equilibria [26, 130].

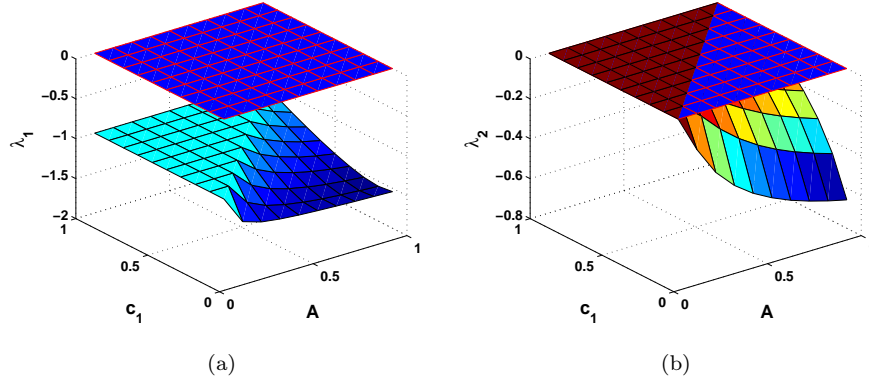


FIGURE 2.6: The eigenvalues of the system (2.5-2.6) linearized in the vicinity of the E_2 shown as functions of parameters A and c_1 . E_2 does not exist on the left hand side of the plots.

All of the system's eigenvalues for matrix A_2 are real and the stability of the coexistence steady state (\tilde{c}, \tilde{u}) is shown by numerical simulations. Note that Fig. 2.6 is conducted under the condition given by Eq. (2.22). For a given set of parameter values of A and c_1 , the eigenvalues are given for steady state (\tilde{c}, \tilde{u}) in Fig. (2.6). It is seen that this steady state is always stable when $\lambda_2 \neq 0$. Namely, as for the stability of the steady states, it is straightforward to see (e.g. by considering the direction of the flow in different regions of the phase plane) that the coexistence state (\tilde{c}, \tilde{u}) is stable for all parameter values when it is feasible, i.e. is situated in the first quarter of the plane (see Fig. 2.6b). In that case, the extinction state $(0, 0)$ is unstable and hence (\tilde{c}, \tilde{u}) is a global attractor. When the coexistence state is not feasible, then the extinction state is stable and acts as a global attractor. Note that Fig. 2.6 effectively plays the role of a bifurcation diagram. However, standard bifurcation diagrams can be shown by choosing hypothetical values of c_1 for given a range of A .

We mention here that the standard bifurcation diagram would not be sufficiently informative here as we are interested in possible changes in the steady state stability as a response to the changes in two parameters rather than only one. Fig. 2.7 shows each of the eigenvalues λ_1 and λ_2 as a function of the controlling parameter A for two hypothetical values c_1 . It is readily seen that the equilibrium (\tilde{c}, \tilde{u}) is always stable for $\lambda_2 \neq 0$. The case of $\lambda_2 = 0$ and the stability of the coexistence state (\tilde{c}, \tilde{u}) will be discussed in subsection 2.2.3 (As it is observed in subsection 2.2.3, this steady state is always stable when $\lambda_2 = 0$).

Figure 2.8 shows the results of the steady states analysis as a map in parameter plane (A, c_1) . Here, c_1 is chosen as a second controlling parameter due to its effect on phytoplankton growth. The curve between Domain 1-2 indicates

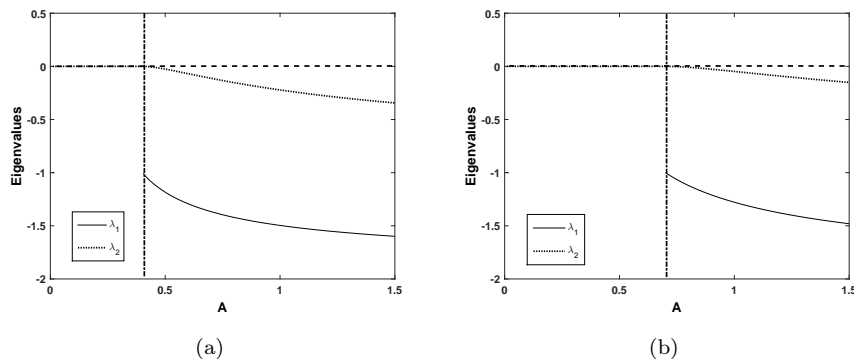


FIGURE 2.7: Eigenvalues vs A , oxygen-phytoplankton state for (a) $c_1 = 0.4$, (b) $c_1 = 0.7$. The vertical line shows the feasibility condition, for the values of A on the left of the line coexistence state does not exist.

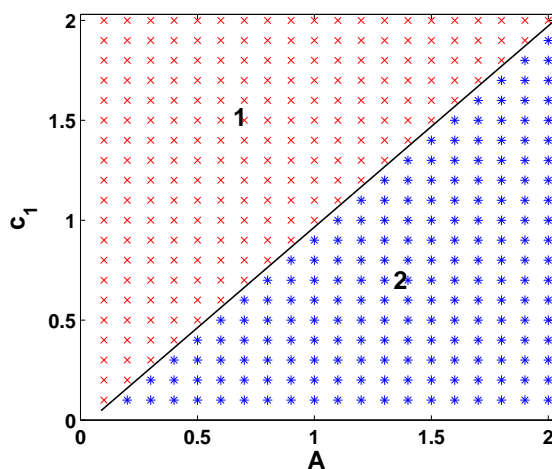


FIGURE 2.8: A map in the parameter plane (A, c_1) for $B = 1$ where different domains correspond to stability and its feasibility of (\tilde{c}, \tilde{u}) ; see details in the text. Since the map is obtained in numerical simulations, the positions of the domains boundary is approximate.

where the eigenvalues are equal to zero. Hence, Domain 1 corresponds to the range where system has no positive equilibrium, while Domain 2 is always stable for (\tilde{c}, \tilde{u}) . Red crosses represent zero eigenvalues, while the blue stars indicate negative eigenvalues; see detailed eigenvalue table Appendix C in Table C.1, hence stability of steady state.

2.2.3 Numerical simulations

In previous sections, properties of the nonspatial system were examined. In this section we broaden our study of the oxygen-phytoplankton system by incorporating a spatial dependence. We consider a spatially explicit extension of the model

(2.7– 2.8), defined by the following system of reaction-diffusion equations:

$$\frac{\partial c}{\partial t} = D_T \frac{\partial^2 c}{\partial x^2} + A \left(1 - \frac{c}{c+1} \right) u - c, \quad (2.36)$$

$$\frac{\partial u}{\partial t} = D_T \frac{\partial^2 u}{\partial x^2} + \left(\frac{Bc}{c+c_1} - u \right) u. \quad (2.37)$$

As before $c = c(x, t)$ denotes the concentration of oxygen and $u = u(x, t)$ is the density of phytoplankton at time t and position x (where x could be depth (i.e. vertical) or a horizontal coordinate), and D_T is the coefficient of the turbulent diffusion [165, 183].

We mention here that, in reality, the transport of oxygen in the sea water takes place due to the combined action of molecular³ and turbulent diffusion⁴, so that the coefficient in Eq. (2.36) should actually be $D_T + D_0$ rather than just D_T , where D_0 is the molecular diffusion coefficient. However, on the spatial scales relevant to plankton dynamics (i.e. 10^{-1} to 10^5 meters) the rate of molecular diffusion is known to be several orders of magnitude smaller than that of turbulent diffusion. Hence, $D_0 \ll D_T$ and $D_T + D_0 \approx D_T$.

We also mention here that, having considered appropriate scaling of the spatial coordinates as $x \rightarrow x' = x\sqrt{m/D_T}$, cf. the lines after Eqs. (2.5–2.6), the coefficient D_T will disappear from the equations. Correspondingly, below we consider Eqs. (2.36–2.37) to be dimensionless by setting $D_T = 1$. Also, for the following numerical simulations, we fix values of two parameters of A , c_1 , B at their hypothetical value and focus on the effect of variations of the remaining one. Equations (2.36–2.37) are considered on a finite domain $0 < x < L$ where parameter L is the domain length. At the domain boundaries, the Neumann (zero-flux) boundary conditions are imposed to describe an environment surrounded by dispersal barriers.

The choice of initial conditions is a subtle issue as different initial conditions may result in very different spatiotemporal dynamics [147]. In this chapter, we consider the initial species distribution describing a phytoplankton patch in a space with uniformly distributed oxygen:

$$c(x, 0) = p, \quad (2.38)$$

$$u(x, 0) = 0.5 \quad \text{for } |x_i| < \epsilon, \quad \text{otherwise } v(x, 0) = 0, \quad (2.39)$$

³Molecular diffusion is related with random molecular motion that constitutes heat [183].

⁴The diffusion is called as turbulent due to turbulence of environmental fluids [183].

where p and ε are dimensionless variables; for our numerical examples $p = 0.2$ (initial distribution of oxygen) and $\varepsilon = 100$ (patch diameter). Equations (2.36–2.37) are solved numerically using the forward finite difference method. Mesh step values for space, Δx , and time, Δt have been selected to be sufficiently small in order to ensure accurate approximation and agreement of ecological reality. The mesh steps are chosen as $\Delta t = 0.01$ and $\Delta x = 0.5$ and it was checked that these values are sufficiently small to avoid any significant numerical artifacts.

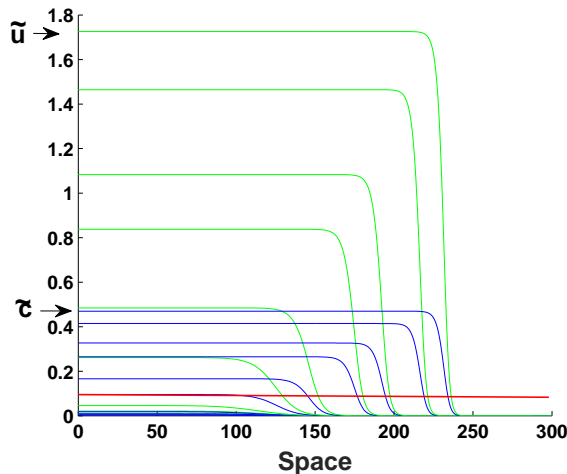


FIGURE 2.9: The density of oxygen (blue) and phytoplankton (green) over space (i.e. horizontal) with given parameter values, $t = 200$, $A = 0.4$, $c_1 = 1$ and B changes from 1 to 5.4 for curves from bottom to top, respectively (see Fig. 2.2 for corresponding nonspatial system). Below red line the system do not satisfy the necessary condition given by Eq. (2.22).

Increasing the value of B results in increase in steady state of components for both oxygen and phytoplankton (see Fig. 2.9). In Fig. 2.9, existence of the positive steady state depends on parameter B and for sufficiently small values of B the positive steady state disappears leaving the remaining equilibrium to be the extinction state. It should be emphasized that the curves below the red line do not satisfy the necessary condition given by Eq. (2.22). Similar succession (only extinction state remaining) is valid for a specific choice of parameter values for A and c_1 .

Fig. 2.2 and Fig. 2.9, show the coexistence steady state for the nonspatial and spatial system. The dynamics observed in the nonspatial system corresponds to the dynamics in its spatial counterparts. This illustration is a remarkable example to show the correspondence between obtained spatial and nonspatial system for a given set of parameters. The distribution of oxygen and phytoplankton forms a plateau where these quantities are exactly at their steady state values (\tilde{c} , \tilde{u}) in Fig. 2.9.

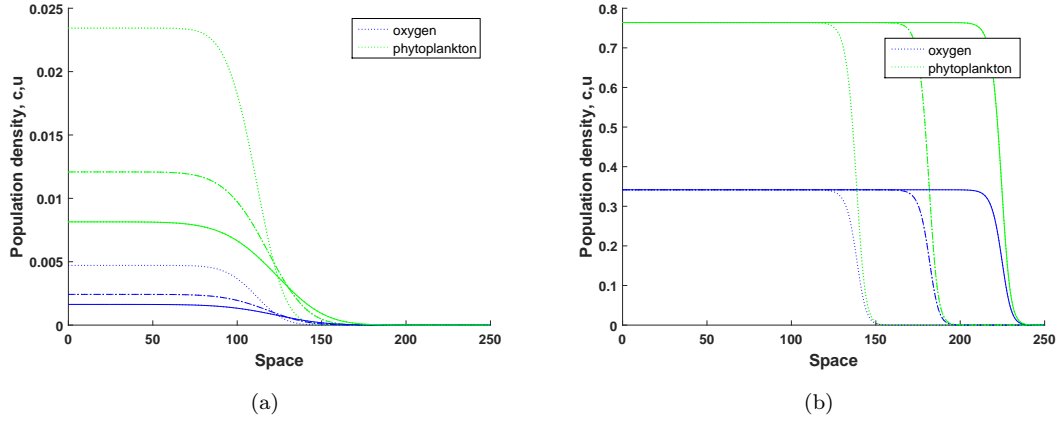


FIGURE 2.10: Phytoplankton density and oxygen concentration versus space (i.e. horizontal) shown at $t = 100$ (dotted line), $t = 200$ (dashed-dotted line) and $t = 300$ (solid line) obtained for (a) $A = 0.2$, (b) $A = 0.6$ and other parameters are $B = 3$, $c_1 = 1$ with given initial distribution Eqs. (2.38–2.39).

In Fig. 2.10a, a sketch of oxygen concentration and phytoplankton distribution is given at different moments in time and it is observed that oxygen and phytoplankton go extinct a large time limit. However, an interesting situation is observed for an increase in A the species persist through the propagation of travelling fronts where these quantities are exactly on their steady state values Fig. 2.10b. Note that the emerging pattern moves right with constant speed (see Eq. (3.25)) without changing its shape. We want to emphasize that the nonspatial system steady states fully coincide with the steady states of its spatial counterparts Fig. 2.10b.

We assume A proportional to temperature. The succession of dynamical scenarios for different values of B and given an exponential function corresponding A is shown in Fig. 2.11. With an increase in B , oxygen concentration and phytoplankton density are increased; see Figs. 2.11a-d. Fig. 2.12 shows oxygen and phytoplankton dynamics for the given exponential temperature function at different time moments depicted by different colors. As an example, Fig. 2.12 (right) shows the temperature decrease from water surface to the deep. Contrary to Fig. 2.12, Fig. 2.13 shows oxygen and phytoplankton dynamics for the same exponential function for small value of B . We have also explored the possibility of a different functional form for A , $A(x) = \frac{1}{((0.01+10^{-4}*x)+\varepsilon)}$. For a larger time limit there is an abrupt decay of the system's components as indicated by the black curve in Figs. 2.14a-b. It may be explained that if temperature is not at its optimum value, extinction becomes inevitable for both oxygen and phytoplankton. As an example of chosen parameter values it can be said that in contrast to large

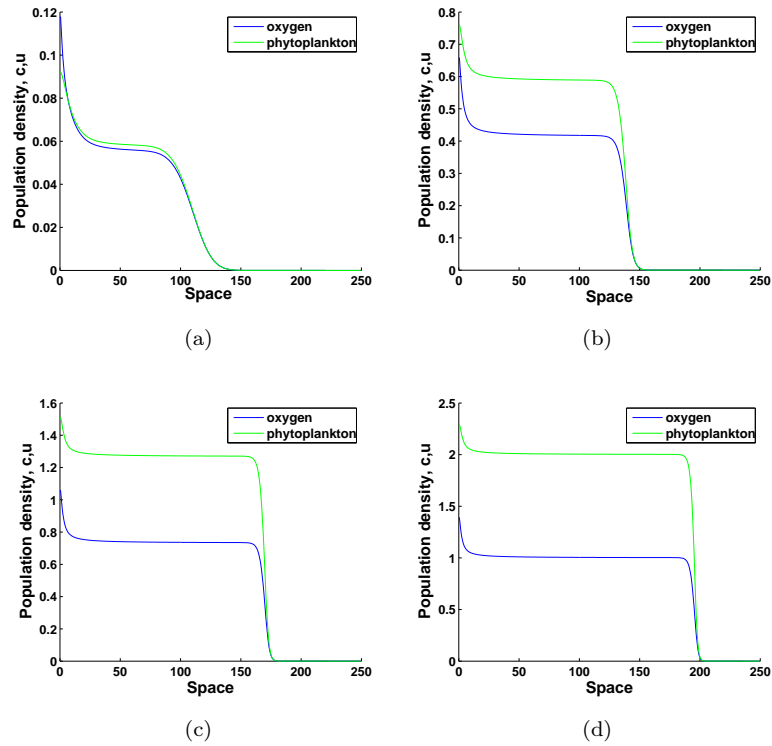


FIGURE 2.11: Phytoplankton density and oxygen concentration over space (i.e. vertical) for different B values 1, 2, 3 and 4 left to right, top to bottom, respectively, for given parameter values $A(x) = \exp(\frac{\varepsilon}{x+\delta})$, $\delta \ll \varepsilon$, $\delta = 0.01$, $\varepsilon = 1$, $c_1 = 1$ and $t = 100$ with given initial distributions (see Eqs. (2.38–2.39)).

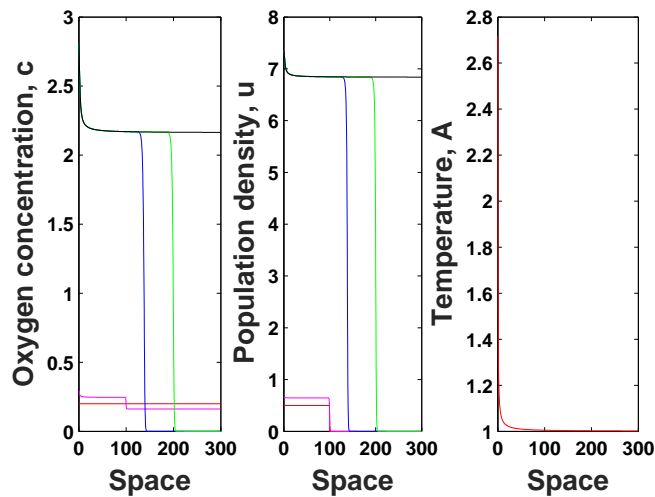


FIGURE 2.12: Oxygen-phytoplankton distributions and temperature function $A(x) = \exp(\frac{\varepsilon}{x+\delta})$, $\delta \ll \varepsilon$ vs. space (i.e. vertical) are obtained for given parameter values $\delta = 0.01$, $B = 10$, $\varepsilon = 1$, $c_1 = 1$ with given initials (see Eqs. (2.38–2.39)) for different time values $t = 0.1$ (magenta), $t = 20$ (blue), $t = 50$ (green), $t = 500$ (black) and red lines are given for initial condition for oxygen and phytoplankton.

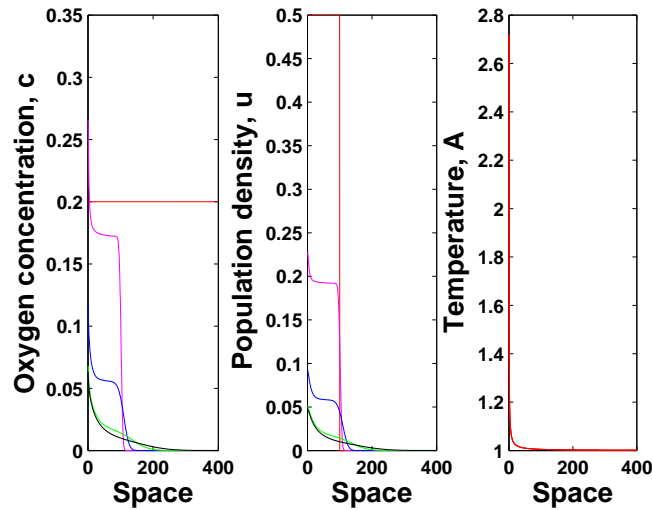


FIGURE 2.13: Oxygen-phytoplankton distribution and temperature function $A(x) = \exp(\frac{\varepsilon}{x+\delta})$, $\delta \ll \varepsilon$ versus space (i.e. vertical) for given parameter values $B = 1$, $\varepsilon = 1$, $c_1 = 1$ with given initial conditions (see Eqs. (2.38–2.39)) for different time values $t = 0.1$ (magenta), $t = 100$ (blue), $t = 1000$ (green), $t = 3000$ (black) and red line is shown for initial condition of both oxygen and phytoplankton.

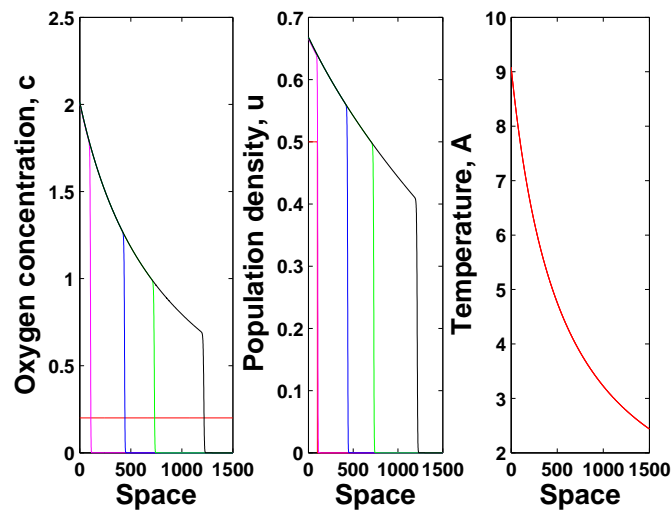


FIGURE 2.14: Oxygen-phytoplankton distribution and temperature function A , $A(x) = \frac{1}{((0.01+10^{-4}*x)+\varepsilon)}$, versus space (i.e. vertical) from left to right for given parameter values $B = 1$, $\varepsilon = 0.1$, $c_1 = 1$ with given initial conditions (see Eqs. (2.38–2.39)) for different time values $t = 10$ (magenta), $t = 500$ (blue), $t = 1000$ (green), $t = 2000$ (black) from left to right. Red line is shown for initial condition of both oxygen and phytoplankton.

values of B (when $B = 10$; in Fig. 2.12), small values of B drive (when $B = 1$; in Figs. 2.14) the system components to extinction at different time moments.

2.3 Discussion and Concluding Remarks

Oxygen production and consumption is a topic gaining significant importance as an upcoming environmental problem related to global warming [1, 174, 175, 220]. Our aim is to describe this important environmental issue with a mathematical model by using diffusion-reaction equations and try to understand the underlying dynamics. For this reason, this chapter focusses on the basic interaction between oxygen production and phytoplankton growth. Understanding the basic relation between oxygen and phytoplankton systems can provide useful information to many scientific areas in bettering our understanding of global warming (see [29, 268] for further and detailed research on this subject).

In this chapter, we attempt to build a new approach to model the existing plankton system by using resource-consumer interaction. For specific parameter set it can be shown that Mocenni's model [163] is reduced to ours; see Appendix A for the reduction of a model system to our model system.

We first considered the nonspatial version of the model in Sections 2.2.1–2.2.2 corresponding to a well-mixed system with a spatially uniform distribution of species. The properties of this model have been studied both analytically and numerically. In particular, we found analytical conditions for the existence of a (unique) positive equilibrium corresponding to the coexistence of two components. In ecological terms, parameter values corresponding to the existence of the positive equilibrium ensure oxygen existence, whilst the disappearance of this steady state should be regarded as an ecological disaster resulting in mass extinction of the plankton species.

In Section 2.2.3, we then considered a spatially explicit extension of our model which takes into account the transport of plankton and oxygen by turbulent diffusion. The model is described by a system of two partial differential equations of reaction-diffusion type. The properties of the system were studied by extensive numerical simulations due to its underlying complex analytical solution. From the spatial system, it is readily seen that there are two steady states which are the extinction and coexistence state (see Figs. 2.9–2.11). We gained knowledge how the nonspatial system appears to provide us with an outline of properties of the spatial system's dynamics.

The purpose of this chapter is to demonstrate oxygen production by phytoplankton through photosynthesis, which has a contribution to the oxygen production and to show the temperature effect on our model system (2.5–2.6). Different types of temperature functions are considered in numerical simulations such as

$A(x) = \frac{\varepsilon}{x+\delta}$, $A(x) = \exp(\frac{\varepsilon}{x+\delta})$ and $A(x) = \frac{1}{((0.01+0.0001*x)+\varepsilon)}$ in order to reveal the system dynamics dependence on varying A . Note that, the chosen hypothetical functions are decreasing to obtain the system sensitivity in the case of decreasing oxygen production (see Chapter 5 and Chapter 6) for further detail on system dynamics dependence to the changing environmental conditions). For Figs. 2.11–2.13, we choose A to be an exponential function $A(x) = \exp(\frac{\varepsilon}{x+\delta})$. However, $A(x) = \frac{1}{((0.01+0.0001*x)+\varepsilon)}$ is used for Fig. 2.14. The obtained results show that temperature affects the dynamical response of oxygen-phytoplankton system, e.g. it affects oxygen and phytoplankton density (see Figs. 2.11–2.13), it leads to abrupt decay (see Fig. 2.14). It is known that the water temperature affects phytoplankton growth and abundance [7, 60, 207]. For this reason this issue will become a focus of the following chapters (Chapter 5 and Chapter 6). The similar succession of the system properties is observed for $A(x) = \frac{\varepsilon}{x+\delta}$, hence the results obtained for this function are not presented here for the brevity.

Perhaps the most interesting property of our model is that phytoplankton are predicted to survive only if the rate of oxygen production is above a certain critical value; see condition given by Eq. (2.22). Since the rate of oxygen production may be expected to depend on the properties of the environment, it makes our model a convenient and relevant theoretical tool that can be used for the purposes of nature conservation and marine ecosystems management. This will become a focus of our following chapters.

Chapter 3

Zooplankton Predation Effect on Oxygen Dynamics

3.1 Introduction

In this chapter, we introduce an improved model by building upon our basic oxygen-phytoplankton system, taking into account the predation effect on oxygen dynamics. Phytoplankton play an important role in oxygen production [169], and on the other hand it is grazed upon by its predator. Therefore, predation affects water body oxygen concentration by reducing the abundance of phytoplankton communities, thereby zooplankton density is affected, in turn due to its sensitivity to any changes in algal growth [86, 246]. On the other hand predation response of zooplankton community is affected by the decrease in dissolved oxygen concentration in the water body [21, 45, 175, 176]. In field observations, low dissolved oxygen concentration affects predation, escape behaviour of prey, feeding and swimming movements of predator. Therefore, zooplankton density decreases with decreasing oxygen concentration as a result of the inability to escape from their feeders [21]¹.

There is considerable literature concerned with various aspects of spatiotemporal plankton dynamics (in space and time). Conceptual prey-predator-type models to describe the phytoplankton and zooplankton interactions in marine ecosystems were considered in much detail in [146, 147, 197] but with no attention to oxygen production. In another mathematical study, Edwards and Brindley [57] investigated the dynamics of a coupled plankton-nutrient system, but did not pay any attention to their possible relation to dissolved oxygen. There are relatively few papers where oxygen production is considered explicitly

¹The majority of this chapter has been published in [227]

[5, 150, 160, 161, 162, 163] but these papers leave out of the scope some important features of plankton dynamics such as, for instance, the pronounced heterogeneity of its spatial distribution (known as plankton patchiness). In particular, Marchettini et al. [150] studied the trophic dynamics by developing a mathematical model of biochemical processes in a lagoon ecosystem. The dissolved oxygen concentration in a multi-component system is considered by them. In another modelling study, Allegretto et al. [5] showed the existence of periodic solutions in modelling Italian coastal lagoons.

In spite of the vast literature concerning marine ecosystem modelling, the dynamics of the dissolved oxygen concentration as an essential component of plankton systems has not been studied in sufficient detail. Nevertheless, this issue is obviously of significant practical and theoretical importance. Correspondingly, the aim of this chapter is to consider the effect of phytoplankton-zooplankton (prey-predator) interactions on the dynamics of the dissolved oxygen. In turn, this requires a good understanding of the properties of the baseline two-components oxygen-phytoplankton system as given in Chapter 2.

In view of the above, this chapter is structured as follows. In the next section, a new mathematical model of oxygen-plankton dynamics is proposed and analyzed. In Section 3.2, we extend our model to include zooplankton. In Sections 3.3.1 and 3.3.2, the properties of the three-component system are studied by extensive numerical simulations first for the nonspatial system then extended to include a spatial component, revealing rich spatiotemporal dynamics including chaos and travelling fronts of extinction. In Section 3.4, the ecological relevance and potential importance of our findings is discussed.

3.2 The ‘advanced’ three-component model and results

The baseline oxygen-phytoplankton model focused on in Chapter 2 can be made biologically more realistic by taking into account zooplankton. Indeed, zooplankton is the main consumer of phytoplankton and it is well known that its effect can change the system’s properties significantly, usually making the dynamics more complex, cf. [57, 64, 144]. In the model below, we assume that the phyto-zooplankton trophic interaction is described by the standard prey-predator model with the functional response of Holling type II.

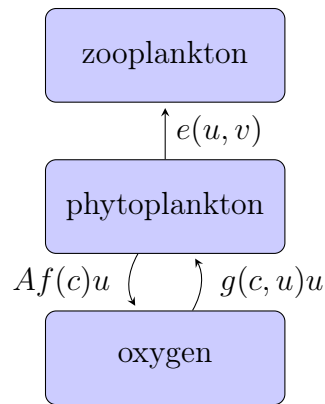


FIGURE 3.1: Interactions between oxygen & phytoplankton & zooplankton. Arrows show the flows of matter through the system, and the parametrizations of the rates are as labelled.

The interaction between oxygen, phytoplankton and zooplankton is given by a flow chart in Fig. 3.1. Flows of matter through the system are indicated by arrows.

Therefore, the corresponding temporal dynamic's are described by the following system of three coupled ordinary differential equations:

$$\frac{dc(t)}{dt} = Af(c)u - c, \quad (3.1)$$

$$\frac{du(t)}{dt} = g(c, u)u - e(u, v), \quad (3.2)$$

$$\frac{dv(t)}{dt} = \beta e(u, v) - \mu v, \quad (3.3)$$

where all notations are the same as in Chapter 2. Additionally, here v is the zooplankton density at time t , and e is the per capita zooplankton growth rate due to predation. The function of $e(u, v)$ describes growth of the predator population where β is the (dimensionless) maximum per capita growth rate, whilst μ is the predator mortality rate. In the model above, we assume that the phytoplankton-zooplankton interaction is described by the standard prey-predator model with functional response of Holling type II [166, 167, 195, 198]. The second negative term of Eq. (3.2) corresponds to the grazing of zooplankton on phytoplankton, hence this predation contributes to predator (zooplankton) growth term $\beta e(u, v)$. The term μv stands for natural mortality of zooplankton.

We consider a Holling type II predator response and use the following parametrization for predation:

$$e(u, v) = \frac{uv}{u + h}, \quad (3.4)$$

where h is the half-saturation constant. With (3.4), cf. Chapter 2 to Eqs. (2.7–2.8), then Eqs. (3.5–3.7) take the following form:

$$\frac{dc}{dt} = A\left(1 - \frac{c}{c+1}\right)u - c, \quad (3.5)$$

$$\frac{du}{dt} = \left(\frac{Bc}{c+c_1} - u\right)\gamma u - \frac{uv}{u+h}, \quad (3.6)$$

$$\frac{dv}{dt} = \frac{\beta uv}{u+h} - \mu v. \quad (3.7)$$

Here, dissolved oxygen depends mainly on the oxygen production by phytoplankton photosynthetic activity, while phytoplankton is grazed upon by its predator zooplankton. The model system (3.5–3.7) is built to reveal the underlying dynamics of the predation effect on water body oxygen concentration by neglecting oxygen consumption due to zooplankton, assuming that zooplankton density is not very high.

3.2.1 Equilibrium existence and analysis

The nonspatial three-component system (3.5–3.7) has at most three equilibria.

1. The trivial equilibrium $E_1 = (0, 0, 0)$ corresponding to extinction. It is readily seen that this equilibrium exists always, regardless what the parameter values are.
2. The semi-trivial equilibrium $E_2 = (\tilde{c}, \tilde{u}, 0)$. Once $v = 0$, the system (3.5–3.7) is reduced to the oxygen-phytoplankton system (2.7–2.8); therefore, the results obtained in Section 2.2 apply. In particular, the steady state values \tilde{c} and \tilde{u} are given by Eqs. (2.11–2.13), and the condition of the equilibrium existence is given by the related condition (2.22).
3. The positive (coexistence) equilibrium $E_3 = (\bar{c}, \bar{u}, \bar{v})$. This equilibrium exists under certain conditions that are obtained below.

The steady state values \bar{c} , \bar{u} and \bar{v} are the solutions of the following system:

$$A\left(1 - \frac{c}{c+1}\right)u - c = 0, \quad (3.8)$$

$$\left(\frac{Bc}{c+c_1} - u\right)\gamma u - \frac{uv}{u+h} = 0, \quad (3.9)$$

$$\frac{\beta uv}{u+h} - \mu v = 0, \quad (3.10)$$

that can be solved semi-explicitly as follows:

$$\bar{u} = \frac{\mu h}{\beta - \mu}, \quad \bar{c} = \frac{-1 + \sqrt{1 + 4A\bar{u}}}{2}, \quad \bar{v} = \gamma(\bar{u} + h) \left(\frac{B\bar{c}}{\bar{c} + c_1} - \bar{u} \right), \quad (3.11)$$

(where we have omitted the second root for \bar{c} because it is always negative and hence biologically meaningless).

It is then readily seen that all the steady state values (3.11) are positive under the following conditions:

$$\beta > \mu, \quad \sqrt{1 + 4A\bar{u}} > 1 \quad \text{and} \quad \frac{B\bar{c}}{\bar{c} + c_1} - \bar{u} > 0, \quad (3.12)$$

which thus gives the conditions of E_3 existence. Since all the parameters in (3.12) are positive due to their biological meaning, the second condition in (3.12) holds identically; however, the first and third ones impose nontrivial restrictions on the range of biologically meaningful parameter values.

3.2.2 Stability analysis

In the following, we are going to discuss the stability of the steady states E_1 , E_2 and E_3 . For this reason we calculate the Jacobian matrix of the system (3.8–3.10):

$$B = \begin{pmatrix} -\frac{Au}{(1+c)^2} - 1 & A\left(1 - \frac{c}{1+c}\right) & 0 \\ \frac{Bc_1\gamma u}{(c+c_1)^2} & \frac{Bc\gamma}{c+c_1} - 2\gamma u - \frac{vh}{(u+h)^2} & -\frac{u}{u+h} \\ 0 & \frac{\beta vh}{(u+h)^2} & \frac{\beta u}{u+h} - \mu \end{pmatrix}. \quad (3.13)$$

For each of the steady states, the eigenvalues are the solutions of the characteristic equation:

$$\det(B_i - \lambda I) = 0, \quad (3.14)$$

where I is the unit matrix and B_i is the matrix (3.13) with the elements calculated at the steady state E_i , $i = 1, 2, 3$. Below, we give a brief summary of the results, whilst detailed calculations can be found in Appendix C.

Our system's equilibrium points are the solutions of $\frac{dc}{dt} = 0$, $\frac{du}{dt} = 0$ and $\frac{dv}{dt} = 0$, which are all taken to be positive to make our system ecologically meaningful. It means that intersections of these three equilibrium points are the isocline's of the system components describing oxygen constant concentration isocline, phytoplankton zero growth isocline and zooplankton zero growth isocline [11].

It is readily seen that the steady state position of \bar{u} is fixed. It is obvious that \bar{u} from Eq. (3.10) is determined by the half saturation constant, the mortality

rate of zooplankton and β is the maximum per capita growth rate of zooplankton. In addition, shape and the position of \bar{c} and \bar{v} are characterized by the above conditions (3.12). These conditions ensure that non-negative steady states are used for our numerical simulations.

- Extinction state E_1

The eigenvalues of matrix B_1 are $-\mu$, -1 and 0 . The fact that one of the eigenvalues is zero tells us that the linear stability analysis is not informative. Therefore, the same numerical approach to determine the stability of the model system is considered as in Chapter 2. On the other hand, a theoretical approach can be used with the application of the Center Manifold Theory [26, 130]. In this way, we avoid the tedious analytical calculations.

- Zooplankton-free, oxygen-phytoplankton state E_2

The eigenvalues of matrix B_2 are the solutions of the following characteristic equation:

$$\left[\left(-\frac{A\tilde{u}}{(1+\tilde{c})^2} - 1 - \lambda \right) \left(\frac{B\tilde{c}}{\tilde{c}+c_1} - 2\tilde{u} - \lambda \right) - \frac{A}{1+\tilde{c}} \frac{Bc_1\tilde{u}}{(\tilde{c}+c_1)^2} \right] \left(\frac{\beta\tilde{u}}{\tilde{u}+h} - \mu - \lambda \right) = 0, \quad (3.15)$$

where \tilde{c} and \tilde{u} are given by Eqs. (2.13) and (2.11). The analytical solution of Eq. (3.15) is bulky and hence we do not show it here for the sake of brevity (but see Appendix C for more details).

The goal of the presentation of steady states Figs. 3.2 and 3.5 is to show that our temporal and spatio-temporal dynamics simulations are based on the case that the system's whole components lie in an ecologically reasonable area. In order to prove validation of the above condition given by Eq. (3.12) is obtained analytically from Eq.(3.11), the steady state results of oxygen-phytoplankton-zooplankton are shown in Fig. 3.2. We fix parameter values at some hypothetical values: $B = 1$, $\gamma = 1$, $\beta = 1$, $\mu = 0.5$, $h = 0.1$ and consider A and c_1 changing between 0.1 to 1. Here $\gamma = 1$ is to provide the correspondence with the oxygen-phytoplankton model in Chapter 2.

Figures 3.2a-b show the oxygen and phytoplankton positive steady state areas, respectively. In this case, it is seen that the relevant condition given by Eq. (2.22) hold (see Section 2.2.1). In Fig. 3.2, there is a straight line separating the zero $A-c_1$ surface and the positive oxygen area in which condition given by

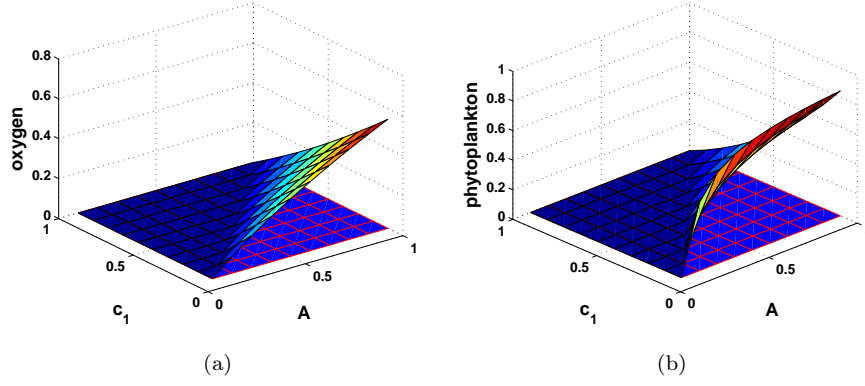


FIGURE 3.2: Steady state values of oxygen and phytoplankton vs. A and c_1 for $(c, u, 0)$. A and c_1 change from 0.1 to 1 and the other parameters are given in the text.

Eq. (2.22) holds. Therefore, the area to the left side of this line, which lies on the zero surface, represents the negative part of oxygen and phytoplankton steady state. To the right side of this line lies the area of our main concern in simulations (to obtain positive steady state).

Figure 3.3 shows that the three component system steady states and their eigenvalues completely coincide with our baseline model system when zooplankton is absent (see in subsection 2.2.2 from Fig. 2.6). It should be emphasized that all of the eigenvalues are real for E_2 , while the eigenvalues become complex conjugates for E_3 , excluding zero eigenvalues (see Table C.2 and see Table C.3). It can be predicted that there is no oscillation for temporal dynamics of zooplankton zero growth system. Figure 3.4 shows each of the eigenvalues λ_1 , λ_2 and λ_3 as a function of the controlling parameter A for two hypothetical values of c_1 . It is readily seen that equilibrium E_2 can be either stable or unstable. For example, for $c_1 = 0.4$, E_2 is stable for $A = 0.42$ but it is a saddle point for $A = 0.5$ (see Table C.2 for more details on the system eigenvalues for given set of system parameters).

- Oxygen, phytoplankton and zooplankton coexistence state E_3

For this equilibrium, the eigenvalues of the corresponding matrix B_3 are the solutions of the following characteristic equation:

$$\left[\left(-\frac{A\bar{u}}{(1+\bar{c})^2} - 1 - \lambda \right) \left(\frac{B\bar{c}}{\bar{c}+c_1} - 2\bar{u} - \frac{\bar{v}h}{(\bar{u}+h)^2} - \lambda \right) - \frac{A}{1+\bar{c}} \left(\frac{Bc_1\bar{u}}{(\bar{c}+c_1)^2} \right) \right] \left(\frac{\beta\bar{u}}{\bar{u}+h} - \mu - \lambda \right) - \frac{\beta\bar{u}\bar{v}h}{(\bar{u}+h)^3} \left(\frac{A\bar{u}}{(1+\bar{c})^2} + 1 + \lambda \right) = 0. \quad (3.16)$$

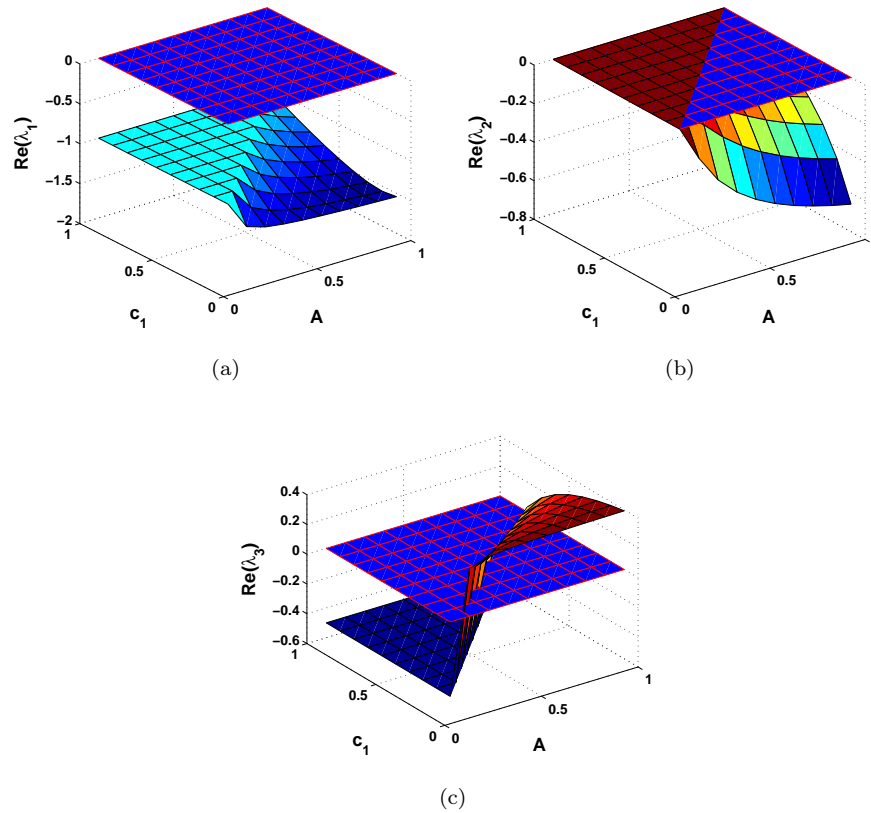


FIGURE 3.3: The eigenvalues of the system (3.5–3.7) linearized in the vicinity of the $(c, u, 0)$ steady state vs. A and c_1 . Other parameters are given in the text.

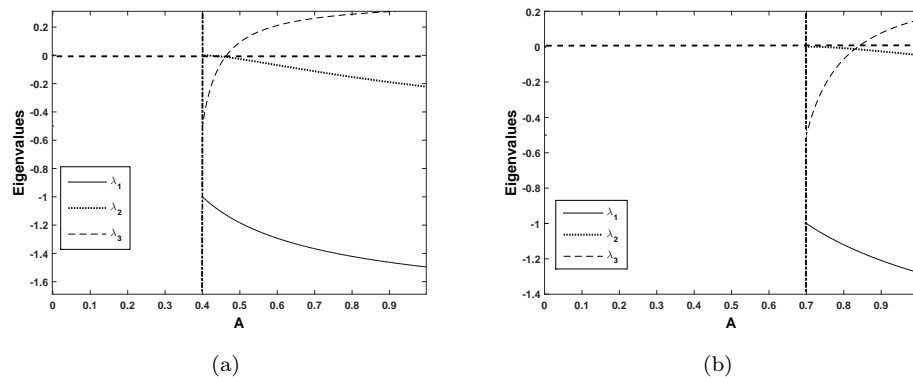


FIGURE 3.4: Eigenvalues vs. A for zooplankton-free state E_2 for (a) $c_1 = 0.4$, (b) $c_1 = 0.7$. The vertical line shows the feasibility condition, for the values of A on the left of the line E_2 does not exist.

The analytical solution of Eq. (3.16) is obtained as it is cumbersome; (see Appendix C for details). Figure 3.5 shows the steady states of Eq. (3.11) under condition (3.12). Figs. 3.5a-c show the position of oxygen, phytoplankton and zooplankton positive steady state area over the range of same parameter values considered in Fig. 3.2. The phytoplankton steady state is just a plane for given

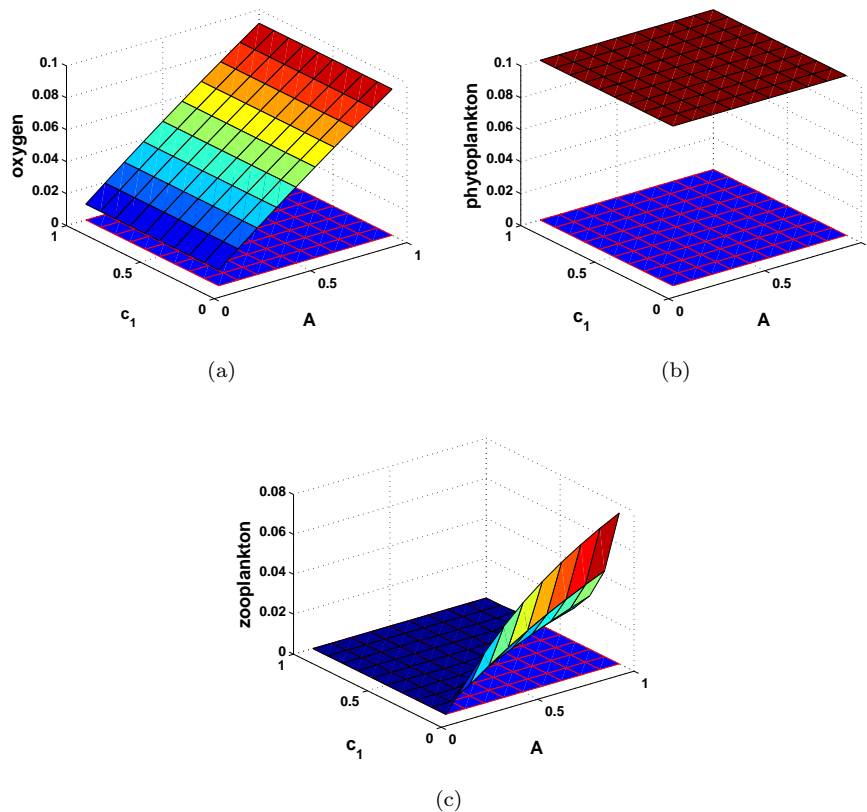


FIGURE 3.5: Steady state values of oxygen, phytoplankton and zooplankton vs. A and c_1 (as given by the system (3.5–3.7)) with other given parameter values as in the text for given range of A and c_1 .

range of parameters because there is no dependence on oxygen and zooplankton concentration. It means that phytoplankton steady state is formed by fixed parameters seen on Eq. (3.11).

Figure 3.6 shows the real part of eigenvalues for $(\bar{c}, \bar{u}, \bar{v})$ as given in Eq. (3.11). Depending on the choice of values for A and c_1 , we obtain instability or stability. For some values of the pair A and c_1 , solutions are oscillatory and the amplitudes of these oscillations rely upon the real part of the related eigenvalues. Also, the frequency of this oscillatory behavior depends on the amplitude of the related imaginary part (Section 4.8 in [56]). It is easily recognised that small changes in system parameters such as A and/or c_1 result in significant changes of stability or oscillatory behavior (see Table C.3).

The imaginary part of eigenvalues for the steady state $(\bar{c}, \bar{u}, \bar{v})$ given by Eq. (3.11) is presented in Fig. 3.7. As it is seen from Fig. 3.7, one of the eigenvalues is real and the others are complex. We have a conjugate pair of eigenvalues as solutions to the quadratic characteristic equation. Complex conjugate pairs of eigenvalues are presented in Fig. 3.7. Simulations results provide support for our

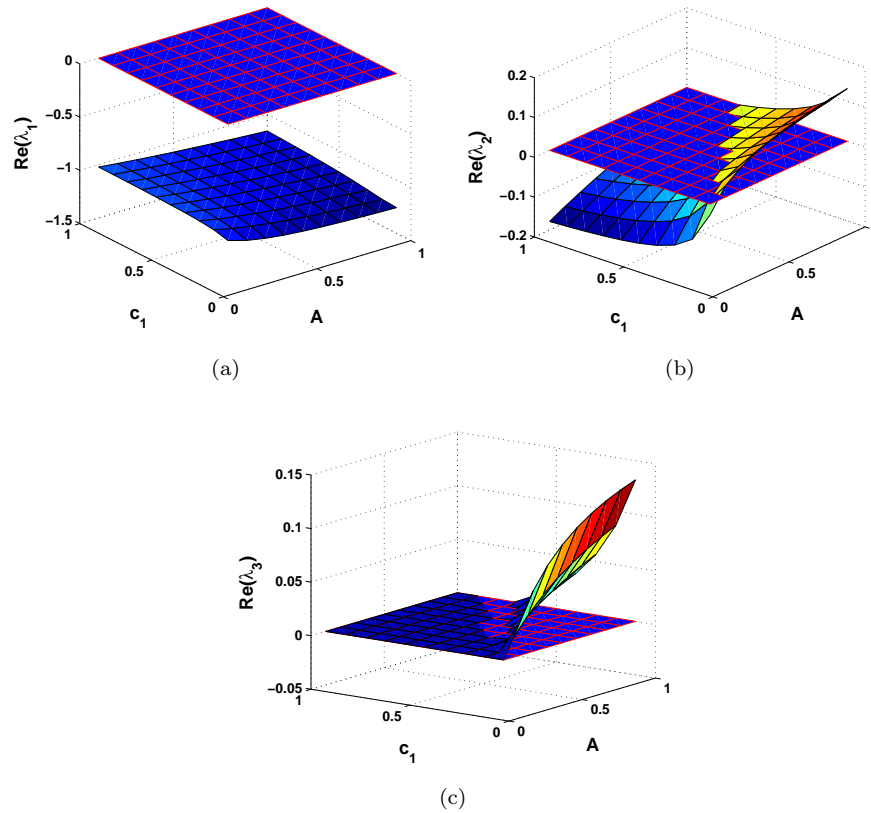


FIGURE 3.6: The eigenvalues real parts of the system (3.5–3.7) linearized in the vicinity of the $(\bar{c}, \bar{u}, \bar{v})$ steady state vs. A and c_1 with other given parameter values. A and c_1 changes from 0.1 to 1.

analytical findings.

Figure 3.8 shows $\text{Re}(\lambda)$ for each of the eigenvalues λ_1 , λ_2 and λ_3 as a function of the controlling parameter A for two hypothetical values c_1 . Note that in this case two of the eigenvalues appear to be complex-conjugate, so that $\text{Re}\lambda_2 = \text{Re}\lambda_3$. Of the two different real parts, λ_1 is distinctly negative (see solid curve in Fig. 3.8) whilst $\text{Re}(\lambda_2) = \text{Re}(\lambda_3)$ is very small (for the given parameter set), positive for $c_1 = 0.4$ Fig. 3.8a and negative for $c_1 = 0.7$ Fig. 3.8b.

Figure 3.9 shows a sketch of the bifurcation diagram in the parameter plane (A, c_1) for other hypothetical values of parameters, as given in the text. Here, red crosses dominating Domain 1 show the region for E_2 is not feasible, Domain 1 and Domain 2 show the region for E_3 is not feasible (see Table C.2), while the blue stars, i.e. Domain 2 and Domain 3 show the stable region for E_2 and E_3 , respectively. Therefore, Domain 3 and Domain 4 are the saddle regions for E_2 . Domain 2 corresponds to zero eigenvalues for E_3 . The black circle region, i.e. Domain 4 is always a saddle for both E_2 and E_3 . It should be emphasized that Domain 3 and Domain 4 correspond to E_2 being an unstable node, while Domain

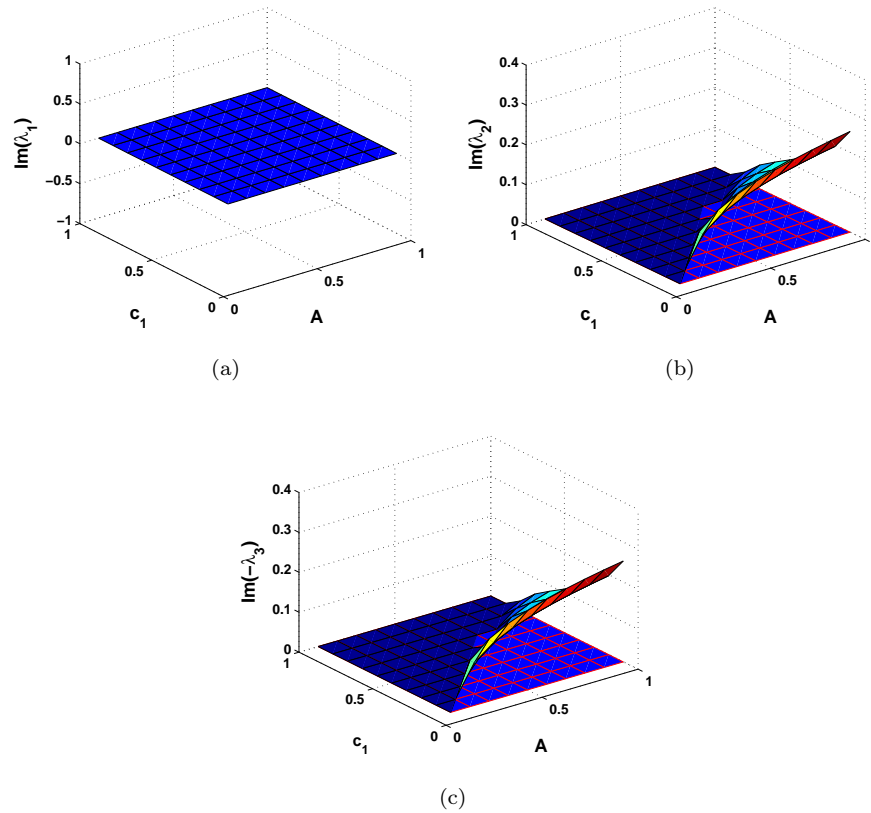


FIGURE 3.7: The eigenvalues imaginary parts of the system (3.5–3.7) linearised in the vicinity of the $(\bar{c}, \bar{u}, \bar{v})$ steady state vs. A and c_1 with other given parameter values as in the text. A and c_1 changes from 0.1 to 1 for curves from bottom to top.

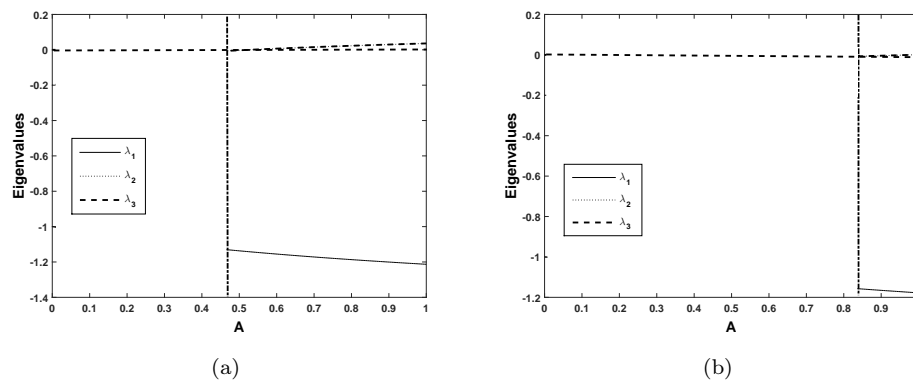


FIGURE 3.8: Eigenvalues vs. A oxygen, phytoplankton and zooplankton coexistence state E_3 for (a) $c_1 = 0.4$, (b) $c_1 = 0.7$. The vertical line shows the feasibility condition, for the values of A on the left of the line E_3 does not exist.

4 corresponds to E_3 being an unstable focus (see Tables C.2–C.3).

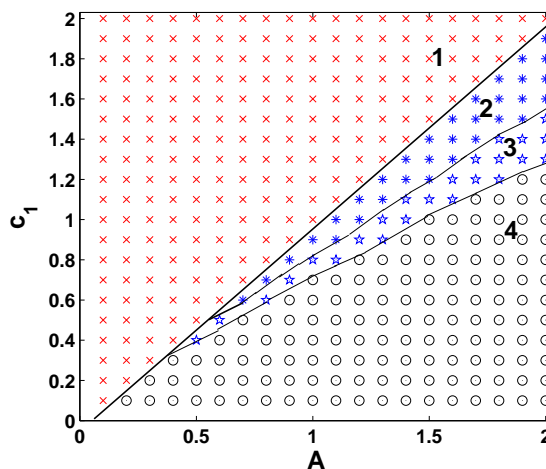


FIGURE 3.9: Bifurcation diagram for oxygen-phyto-zooplankton system in parameter plane (A, c_1) where red crosses dominating Domain 1 show the region for E_2 is not feasible; see comments in text. The other parameters are given in the text.

3.3 Numerical Simulations

3.3.1 Temporal dynamics

In this section, we perform numerical simulations of oxygen-phytoplankton-zooplankton nonspatial system (3.5–3.7). Understanding of the temporal dynamics creates a convenient framework for the understanding of the complex dynamics of the spatio-temporal system. In all our numerical simulations shown in this section, we fix parameters at some hypothetical values as $B = 1.8$, $\beta = 1$, $\mu = 0.5$, $\gamma = 1$ and $h = 0.1$, and vary A and c_1 in a certain range. Our particular interest is to understand the effect of changes in parameter A as it may, in terms of the real-world plankton system, account for the effect of environmental changes.

Initial values for all of the numerical simulations are defined under the relevant figures. It is important to emphasise here that initial values of system components are fixed for each pair of figures to understand the effect of changes in the parameter values in A and c_1 .

Oxygen-phytoplankton-zooplankton densities converge qualitatively to steady state values in Fig. 3.10a. Figure 3.10a shows the approaches to the extinction state, whilst Fig.3.10b shows periodic oscillations. This change in stability of the same steady state is a result of slight changes of system parameter c_1 . The reasoning behind Fig.3.10a is that when zooplankton concentration is zero (see Table C.3) system's steady state is stable. When we have all system components already somehow distributed across the whole domain, the population growth in any given

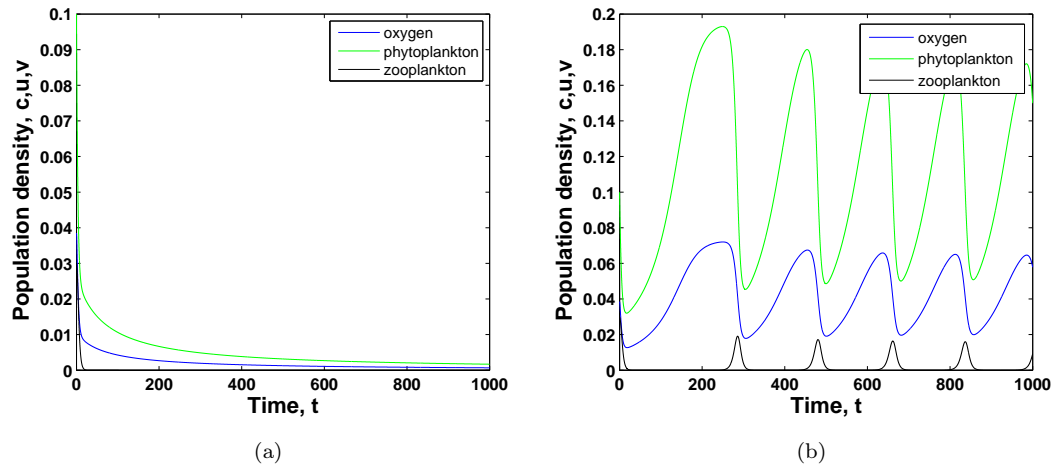


FIGURE 3.10: Effect of changes in parameter c_1 . The densities of oxygen, phytoplankton and zooplankton versus time obtained for parameter values (a) $A = 0.4, c_1 = 0.9$, (b) $A = 0.4, c_1 = 0.3$ and the initials are $c_0 = 0.0385, u_0 = 0.1, v_0 = 0.03$. Other parameters are given in the text.

location can happen because of two things, either local population growth or recolonization due to diffusion. Comparison of the snapshots at different times show that in our system the growth from small densities happens because of recolonizations. Therefore, the so called atto-fox problem is not related here [104].

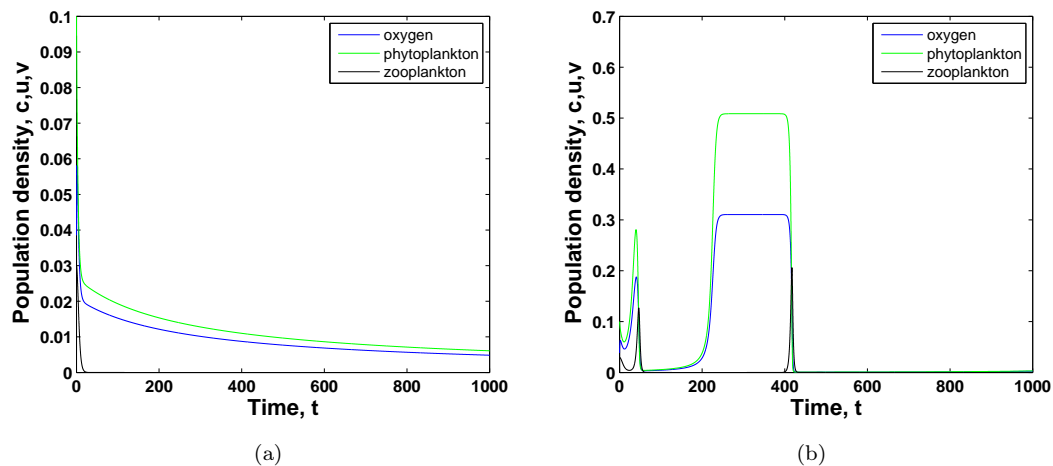


FIGURE 3.11: The effect of changes in parameter c_1 . The densities of oxygen, phytoplankton and zooplankton against time obtained for other given parameter values (a) $A = 0.8, c_1 = 0.9$, (b) $A = 0.8, c_1 = 0.3$ and the initials are $c_0 = 0.0385, u_0 = 0.1, v_0 = 0.03$. Other parameters are given in the text.

Figure 3.11 illustrates the changes on c_1 from $c_1 = 0.9$ (Fig. 3.11a) to (Fig. 3.11b) $c_1 = 0.3$ for same parameter value $A = 0.8$. All of the values of related eigenvalues are easily seen in Table C.3. Fig. 3.11a shows qualitatively the

same result as in Fig. 3.10a. The absence of zooplankton is represented by the stable steady state.

In Fig. 3.11b, the system's trajectories first approach the saddle point and stay in its vicinity for considerable time but finally then converge to the system's stable point. However, in Fig. 3.11a the population densities immediately converge to their steady state. In Fig. 3.11b, following an initial oscillation, both oxygen and phytoplankton densities reach a certain level remaining constant.

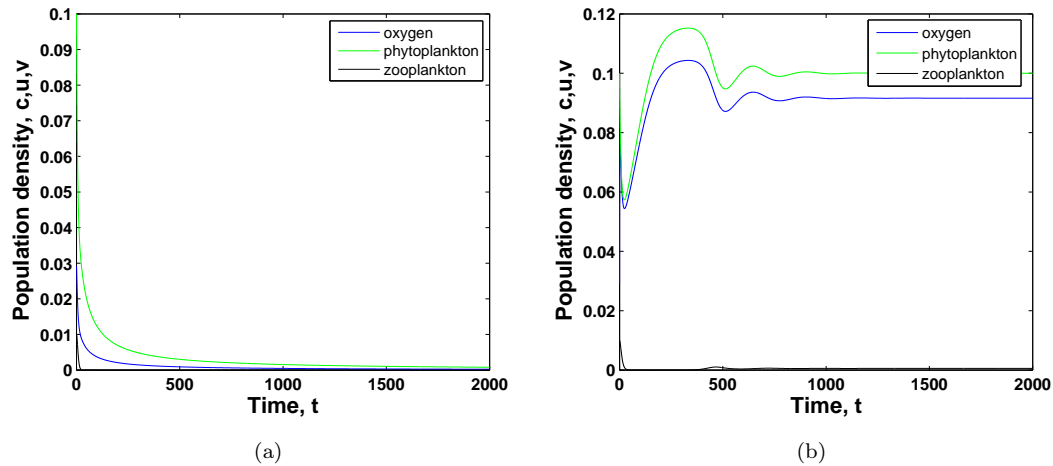


FIGURE 3.12: Effect of changes in parameter A . The density of oxygen, phytoplankton and zooplankton against time obtained for parameter values (a) $A = 0.3$, $c_1 = 0.8$, (b) $A = 1$, $c_1 = 0.8$. The initial conditions are $c_0 = 0.0292$, $u_0 = 0.1$, $v_0 = 0.01$. Other parameters are given in the text.

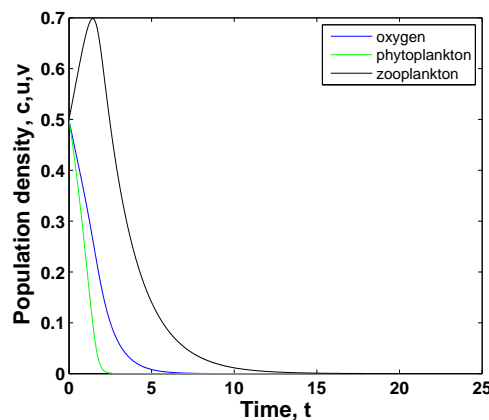


FIGURE 3.13: Oxygen, phyto-zooplankton densities over time simulated for parameters $A = 1$ and $c_1 = 0.1$, other parameters are the same as in the previous figure. The initial conditions are $c_0 = 0.5$, $u_0 = 0.5$ and $v_0 = 0.5$.

Fig. 3.12 shows the oxygen concentration and the phytoplankton and zooplankton densities versus time obtained for $c_1 = 0.8$ and two different values of A .

In the case of $A = 0.3$ (Fig. 3.12a), all components go extinct in the large-time limit. This is not surprising as, for these parameter values, the conditions (2.32) and (3.12) do not hold and hence only the extinction steady state exists. However, for $A = 1$ (Fig. 3.12b), conditions (3.12) for the coexistence state existence hold (but the conditions (2.32) do not) so that, in the large-time limit, the densities converge to some positive steady state values (although \bar{v} appears to be quite small in this case).

These simple results have an underlying biological explanation. Once the oxygen production rate (as quantified by parameter A) becomes low, e.g. as a result of environmental changes, the available amount of oxygen may not be sufficient to support life of the plankton community, which results in plankton extinction.

On a more technical note, we mention here not only the extinction/persistence issue, but also that the rate of convergence can differ greatly for different parameter values. Figure 3.13 shows the simulation results obtained for $A = 1$ and $c_1 = 0.1$. Obviously, all the system's components go extinct in the course of time. However, we notice that, whilst for the parameters of Fig. 3.12 the convergence occurs over the time scale of 10^3 , for the parameters of Fig. 3.13 the convergence occurs 100 times faster.

Apart from the existence/extinction change in the system's behavior, the effect of changes in parameter A may have a somewhat more subtle effect on the stability of the system. Fig. 3.14 shows the oxygen concentration and the phyto-zooplankton densities versus time obtained for the same value of $c_1 = 0.7$ and two

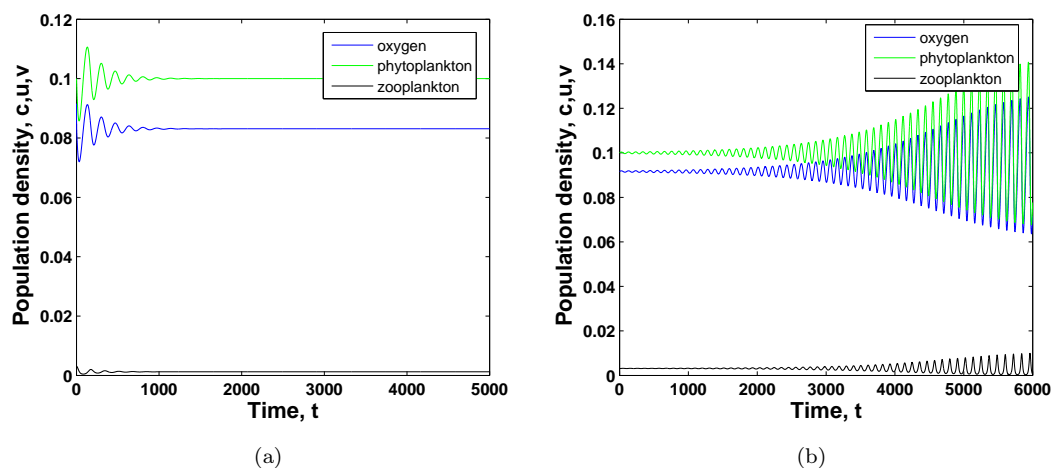


FIGURE 3.14: Effect of changes in parameter A . The density of oxygen, phytoplankton and zooplankton versus time obtained for (a) $A = 0.9$, $c_1 = 0.7$, (b) $A = 1$, $c_1 = 0.7$. In both cases, the initial conditions are $c_0 = 0.0916$, $u_0 = 0.1$ and $v_0 = 0.0031$. Other parameters are given in the text.

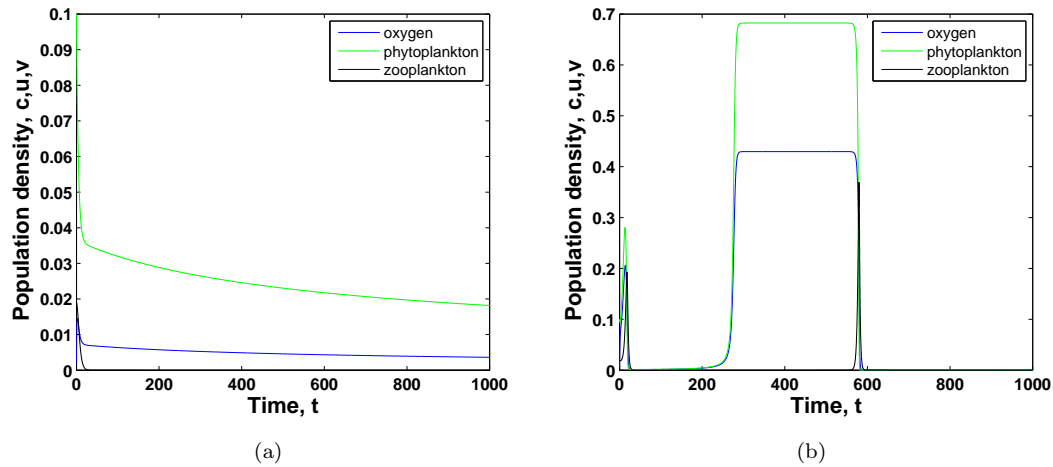


FIGURE 3.15: Effect of changes in parameter A . The density of oxygen, phytoplankton and zooplankton versus time obtained for other given parameter values (a) $A = 0.2$, $c_1 = 0.2$, (b) $A = 0.9$, $c_1 = 0.2$ the initial conditions are $c_0 = 0.02$, $u_0 = 0.1$, $v_0 = 0.019$.

different values of A . For $A = 0.9$ (Fig. 3.14a), the densities eventually converge to the steady state values after a sequence of damping oscillations, which obviously corresponds to E_3 being a stable focus. However, the situation is different for $A = 1$ (Fig. 3.14b) where the system eventually develops periodic oscillations. This change in the system's properties is in full agreement with our analysis of the steady state stability undertaken in Section 3.2.1 (see also Appendix); indeed, the Hopf bifurcation occurs when A changes from 0.9 to 1.

Contrary to Fig. 3.11 (obtained as a response of varying c_1), varying A illustrates almost same dynamical response (see Fig. 3.15). The emerging patterns immediately converge to its steady state for Fig. 3.15a. It is seen that system trajectories first approach the saddle point and then they converge to the limit cycle of large period that lays close to both saddle points, i.e. $(\tilde{c}, \tilde{u}, 0)$ and $(0, 0, 0)$ in Fig. 3.15b.

An interesting succession of dynamical regimes observed for a sequence of increasing values of A is shown in Fig. 3.16. Figure 3.16a obtained for $A = 0.41$ shows that oxygen and plankton densities converge to the zooplankton-free steady state E_2 . Note that the initial zooplankton density drops very fast (so that the corresponding curve in Fig. 3.16a at this resolution almost coincides with the vertical axis).

For $A = 0.5$ (Fig. 3.16b), the system dynamics follows a long-living transient. Over the first stage of the dynamics (up to $t \approx 1000$), the densities apparently converge to the zooplankton-free steady state. However, this state is a saddle

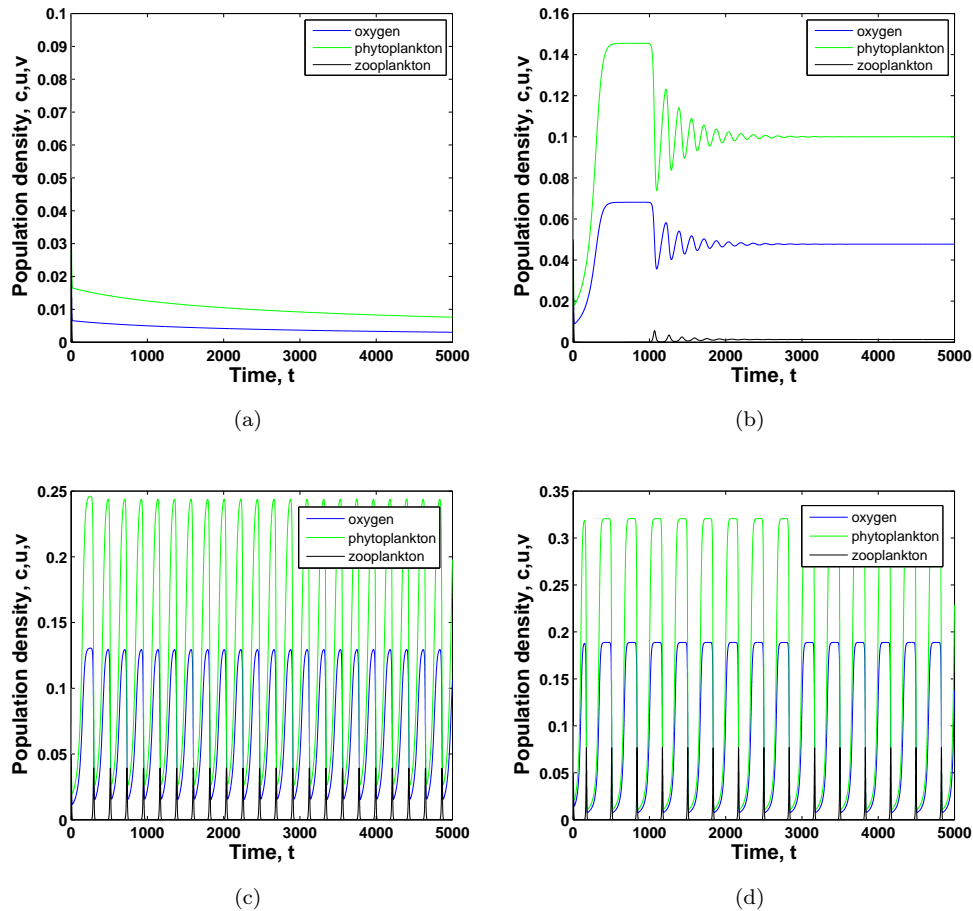


FIGURE 3.16: Effect of changes in parameter A . The density of oxygen, phytoplankton and zooplankton versus time obtained for (a) $A = 0.41$, (b) $A = 0.5$, (c) $A = 0.6$ and (d) $A = 0.7$. In all cases $c_1 = 0.4$, other parameters are the same as in the previous figures. The initial conditions are $c_0 = 0.06, u_0 = 0.1, v_0 = 0.05$.

rather than a stable equilibrium. After staying in its vicinity for a considerable time (roughly, between $t = 400$ and $t = 1000$), the trajectory then shoots away to the vicinity of E_3 (which, for these parameter values, is a stable focus) so that the densities eventually converge to their steady state values \bar{c} , \bar{u} and \bar{v} .

The Hopf bifurcation occurs between $A = 0.5$ and $A = 0.6$, so that for $A = 0.6$ (Fig. 3.16c) the system dynamics is periodical with the densities obviously following the stable limit cycle. A further increase in A leads to an increase in the size of the limit cycle and to an increase in the period of oscillations; see Fig. 3.16d obtained for $A = 0.7$.

In conclusion to this section, we mention that the system exhibits a similar succession of dynamical regimes in response to a change in parameter c_1 ; in particular, an increase in c_1 may result in the loss of stability of the coexistence state E_3 and the emergence of periodical oscillations. We do not show these simulations

results here for the sake of brevity.

3.3.2 Spatial dynamics

Now we are going to consider the properties of the oxygen-plankton system in space. For this purpose, we consider a spatially explicit extension of the model (3.5–3.7) which is described by the following system of reaction-diffusion equations:

$$\frac{\partial c}{\partial t} = D_T \frac{\partial^2 c}{\partial x^2} + A \left(1 - \frac{c}{c+1} \right) u - c, \quad (3.17)$$

$$\frac{\partial u}{\partial t} = D_T \frac{\partial^2 u}{\partial x^2} + \left(\frac{Bc}{c+c_1} - u \right) \gamma u - \frac{uv}{u+h}, \quad (3.18)$$

$$\frac{\partial v}{\partial t} = D_T \frac{\partial^2 v}{\partial x^2} + \left(\frac{\beta uv}{u+h} \right) - \mu v. \quad (3.19)$$

Here all of the system components keep their usual meaning as in Chapter 2, i.e. $c = c(x, t)$ is the concentration of oxygen and $u = u(x, t)$ and $v = v(x, t)$ are the densities of phytoplankton and zooplankton at time t and position x , and D_T is the coefficient of the turbulent diffusion [165, 183].

Systems' diffusional and transport tendency is exactly same as in the previous chapter (see Chapter 2 for more details). Similarly, the transport of zooplankton results from the interplay between the turbulent diffusion and the self-movement of the zooplankton organisms. However, the mixing due to the self-movement of zooplankton (which we assume to be random in space and described by the biodiffusion coefficient D_v) appears to be much smaller compared to the turbulent mixing [183], i.e. $D_v \ll D_T$, so that $D_T + D_v \approx D_T$.

Eqs. (3.17–3.19) to be dimensionless by setting $D_T = 1$. Also, we fix some of parameters as $\beta = 1$, $\gamma = 1$, $\mu = 0.5$ and $h = 0.1$ and focus on the effect of variations in A and c_1 . Equations (3.17–3.19) are considered in a finite domain $0 < x < L$ where parameter L is the domain length (i.e. horizontal). At the domain boundaries, the zero-flux boundary condition is imposed.

The choice of the different initial conditions may result in very different spatiotemporal dynamics [147]. In this chapter, we consider the initial species distribution describing a zooplankton patch in a space with uniformly distributed oxygen and phytoplankton:

$$c(x, 0) = c_0, \quad (3.20)$$

$$u(x, 0) = u_0, \quad (3.21)$$

$$v(x, 0) = v_0 \quad \text{for } |x| < \epsilon, \quad \text{otherwise } v(x, 0) = 0, \quad (3.22)$$

where c_0 , u_0 and v_0 are thus the initial densities and ϵ is the patch diameter. The results shown below are obtained for $v_0 = 0.5$ and $\epsilon = 100$.

Equations (3.17–3.19) are solved numerically using the forward finite difference method (see in Appendix D). The mesh steps are chosen as $\Delta t = 0.01$ and $\Delta x = 0.5$ and it was checked that these values are sufficiently small to avoid any numerical artifacts.

Note that the insight into the properties of the nonspatial system that we made in Sections 2.2 and 3.2 creates a useful framework for the understanding of the properties of the spatiotemporal system (3.17–3.19). In particular, as we have observed in our numerical simulations (not shown here for the sake of brevity), if the conditions (3.12) for the existence of the positive steady state E_3 do not hold but the condition (2.32) for the existence of the zooplankton-free equilibrium E_2 holds, zooplankton eventually goes extinct over the whole space and the phytoplankton density u and the oxygen concentration c converge, in the course of time, to the spatially uniform distribution $c(x, t) \equiv \tilde{c}$ and $u(x, t) \equiv \tilde{u}$. In case the condition given by Eq. (2.32) does not hold either, then all three components eventually converge to zero everywhere in space.

The following series of Figs. 3.17–3.19 are given as an example of our system's correspondence with the prey-predator model in [147]. For this set of figures, contrary to previous simulations, we consider a different set of parameters, whereby the particular choice of system parameters is explicitly stated in figure captions. Therefore, Fig. 3.17 shows oxygen concentration and plankton densities versus time obtained for two different time moments. In this case, the succession of periodic oscillations is the same for different time moments. Oxygen concentration and plankton densities versus time are shown for different time moments for fixed positions in space in Fig. 3.18. Remarkably, for some parameter values chosen from [147], the system behaves like a prey-predator system (see Chapter 10 in [147]). The population densities approach the steady state through damped oscillations only for a sequence of oscillations increasing in amplitude to form leading to irregular oscillations. For longer times (see Fig. 3.18b), the irregularity of the oscillations are seen clearly. The phase plane of local population densities obtained in Fig. 3.19. Parameters are the same as in Fig. 3.18b.

Figures 3.20a–b present the simulation results in the spatial system (3.17–3.19) obtained for parameters corresponding to nonspatial system simulation results (Figs. 3.17a–b), respectively. In the wake of population fronts chaotic oscillations emerge followed by a plateau corresponding to the system components steady state. This plateau is short lived and succeeded by oscillations increasing in

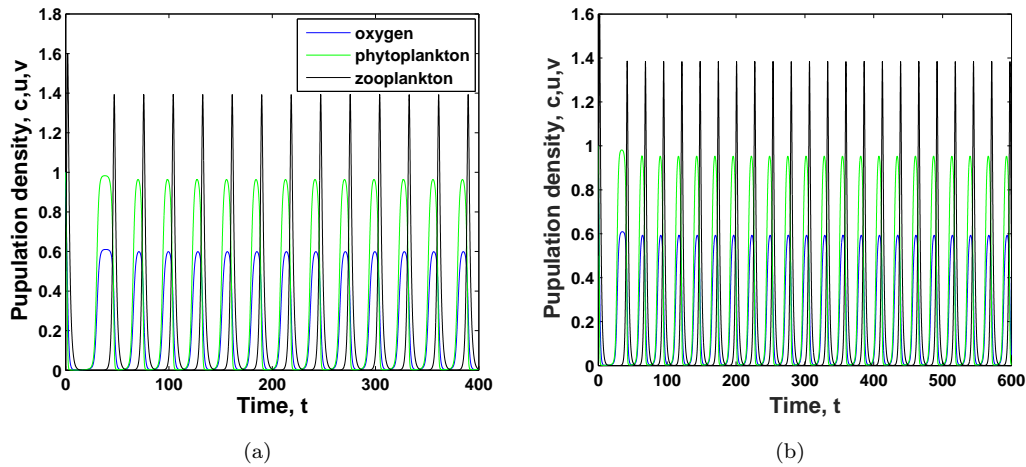


FIGURE 3.17: Oxygen, phytoplankton and zooplankton distribution over space ($L = 1000$) for system (3.5–3.7) for different moments (a) $t = 400$, (b) $t = 600$ and for given parameters as $B = 1$, $\gamma = 1$, $\beta = 2$, $\mu = 0.6$, $h = 0.35$, $A = 1$, $c_1 = 0.01$. The initial conditions are $c_0 = 1$, $u_0 = 1$, $v_0 = 0.5$.

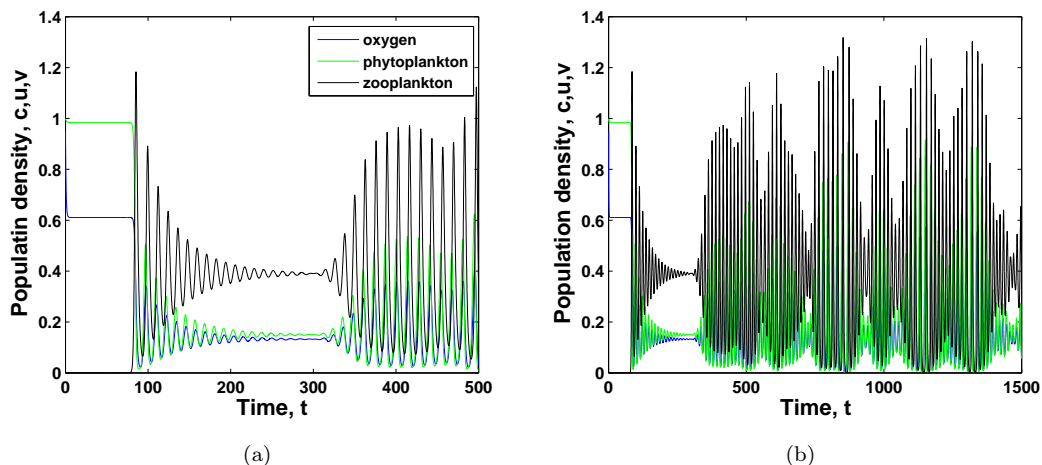


FIGURE 3.18: Oxygen, phytoplankton and zooplankton time evolution space $x = 500$ for different time moments (a) $t = 500$, (b) $t = 1500$ and the system other parameters are given as $B = 1$, $c_1 = 0.01$, $\gamma = 1$, $\beta = 2$, $\mu = 0.6$, $h = 0.35$ and $A = 1$. The initial conditions are $c_0 = 1$, $u_0 = 1$, $v_0 = 0.5$.

amplitude with a tendency to a travelling front. With increasing time the amplitude of chaotic oscillations in the wake of population fronts increase. Eventually, the domain is dominated by the irregular pattern, after the travelling wave leaves the domain for $t = 1500$. The large time simulation is not shown here for the sake of brevity. Remarkably, for these parameter values (a closer look for parameter choice [147] from Fig. 10.5 in Chapter 10), our oxygen-plankton model system almost corresponds to the prey-predator system.

Formation of oxygen and phytoplankton fronts is followed by the growth

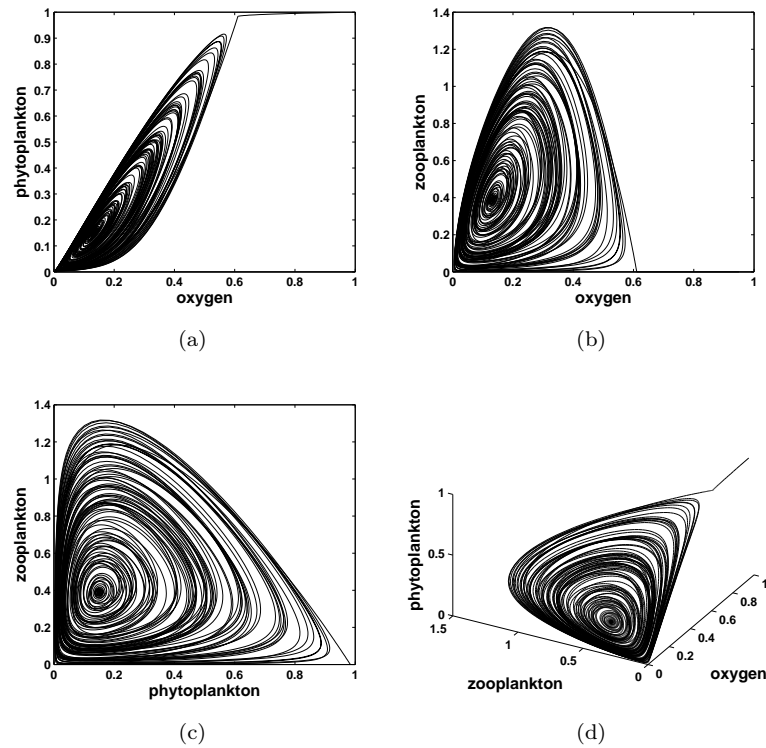


FIGURE 3.19: Phase plane structure of oxygen-phyto-zooplankton distributions at a fixed point in space $x = 500$ vs. time for given parameter values $t = 1500$, $A = 1$, $B = 1$, $c_1 = 0.01$, $\gamma = 1$, $\beta = 2$, $\mu = 0.6$, $h = 0.35$, for initials $c_0 = 1, u_0 = 1, v_0 = 0.5$.

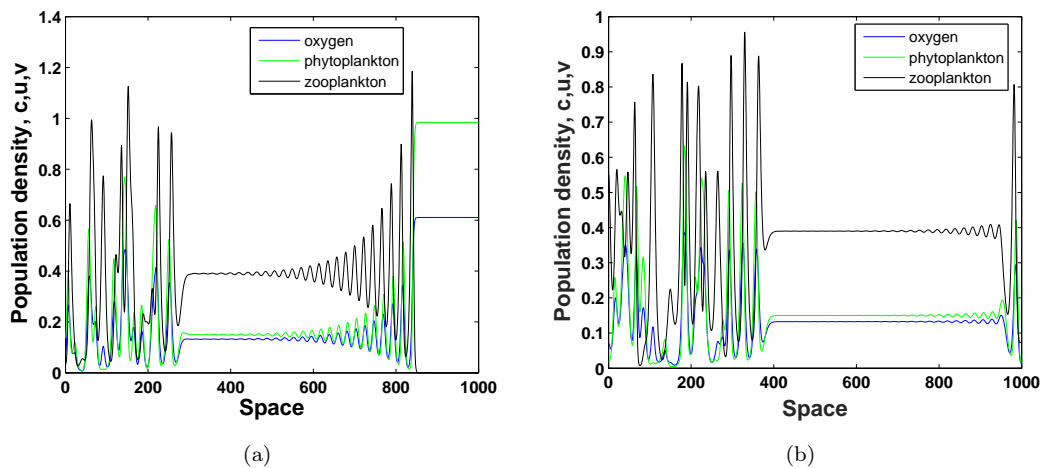


FIGURE 3.20: Oxygen, phytoplankton and zooplankton distribution over space ($L = 1000$) (a) $t = 400$, (b) $t = 600$. Parameter values are as given in Fig. 3.17. The initial conditions are $c_0 = u_0 = 1, v_0$ as in Eq. (3.22).

of irregular spatial distributions for $t = 100$ and $t = 200$ in Fig. 3.21. Eventually, the waves propagating with given speed as in Eq. (3.25) are connecting the steady states $(\tilde{c}, \tilde{u}, 0)$. However, in the case $\mu = 0.4$, $h = 0.1$ (see Fig. 3.22), formation

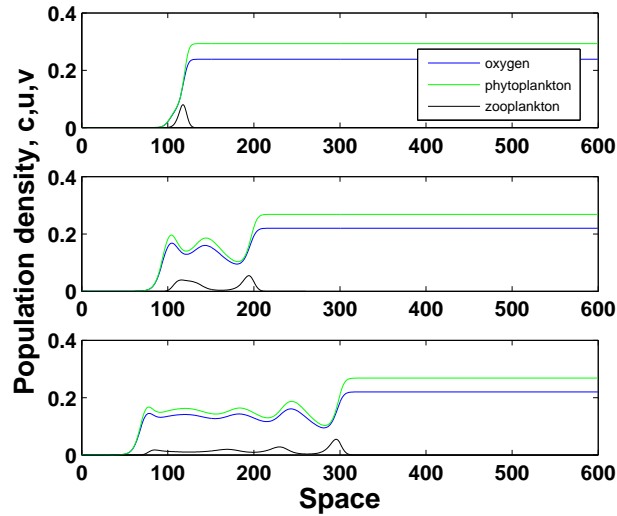


FIGURE 3.21: The spatial distribution of oxygen, phytoplankton and zooplankton for $t = 20$, $t = 100$ and $t = 200$ from top to bottom acquired at $A = 1$, $B = 1$, $c_1 = 0.6$, $\gamma = 1$, $\beta = 2$, $\mu = 0.6$, $h = 0.35$, for ($L = 600$) and the initial conditions are $c_0 = u_0 = 1, v_0 = 0.5$.

of oxygen and phytoplankton front is followed by a regular smooth distribution of oxygen and phytoplankton. Zooplankton density reaches its maximum position of the front. Note that the propagating waves are connecting $(\tilde{c}, \tilde{u}, 0)$. It is readily seen that the steady states of oxygen and phytoplankton converge to the zero zooplankton steady state with increasing time.

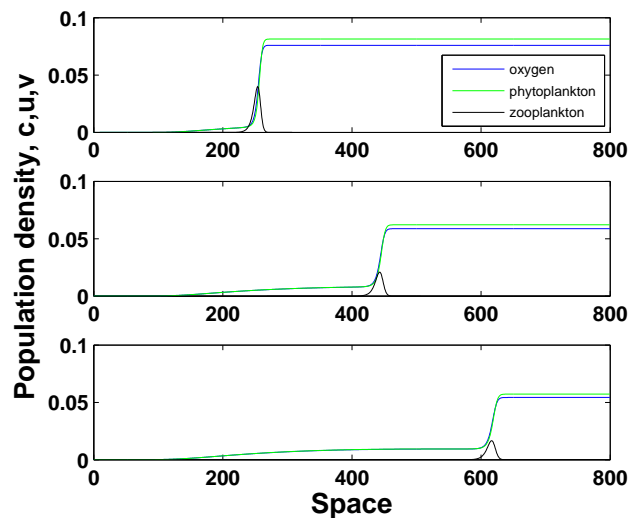


FIGURE 3.22: Oxygen, phytoplankton and zooplankton distribution over space obtained at different time values $t = 100$, $t = 250$ and $t = 400$ from top to bottom and $A = 1$, $B = 1$, $c_1 = 0.9$, $\gamma = 1$, $\beta = 2$, $\mu = 0.4$, $h = 0.1$, for ($L = 800$) and the initial conditions are $c_0 = u_0 = 1, v_0 = 0.5$.

For large time limit, the system's succession in Fig. 3.22 is seen as in Fig. 3.23. The steady state $(\tilde{c}, \tilde{u}, 0)$ is connected to the steady state $(\bar{c}, \bar{u}, \bar{v})$. It should be emphasized that as it is seen from Figs. 3.22–3.23, zooplankton density reaches its maximum and forms a peak when oxygen and phytoplankton densities stabilise. See the similar succession of the prey-predator system from [198] in Chapter 6. For all of the given cases Figs. 3.21–3.23, the directions of the propagation happens from left to right.

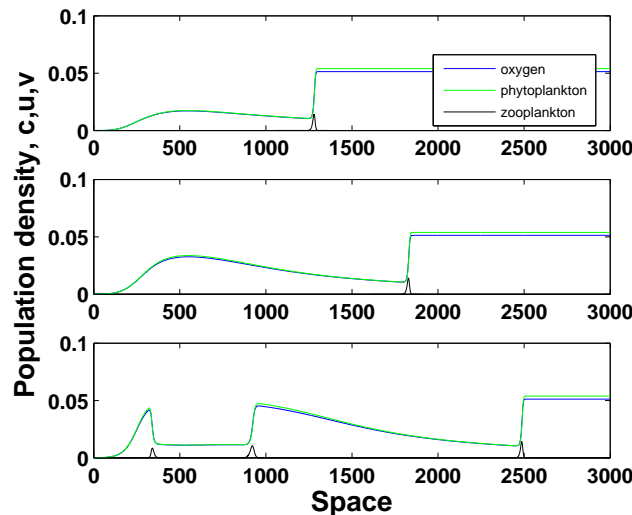


FIGURE 3.23: Oxygen, phytoplankton and zooplankton distribution over space for $t = 1000$, $t = 1500$, $t = 2100$ from top to bottom and the system parameters are same as previous figure, for $(L = 3000)$ and the initial conditions are $c_0 = u_0 = 1, v_0 = 0.5$.

We have extended our analytical results to include calculations of the asymptotic rate speed of travelling wave by taking system parameter values from Fig. 3.21 by linearising Eqs. (3.5–3.7) at the leading edge of travelling front [see Section 3.3 [135] and further references there in]. We consider the time values from $t = 100$ to $t = 200$. It is easy to see that $u \cong 0.27$ from Eq. (3.10) and from Fig. 3.21.

$$l(c, u, v) = \frac{\beta uv}{u + h} - \mu v \quad (3.23)$$

$$l_v(c, u, v) \cong \frac{0.27 * 2}{0.27 + 0.35} - 0.6 \cong 0.27 \quad (3.24)$$

$$c_{speed} = 2\sqrt{l_v(c, u, 0)D} \cong 1. \quad (3.25)$$

The front moves to the right with constant speed for different time moments. The travelling fronts propagate at the asymptotic rate of spread as obtained in Eq. (3.25).

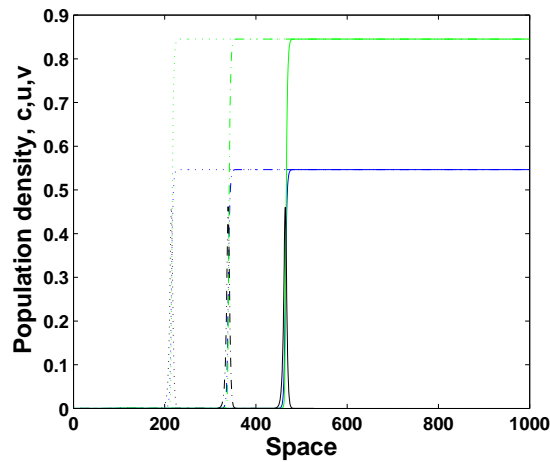


FIGURE 3.24: Distribution of oxygen (blue), phytoplankton (green) and zooplankton (black) over space at $t = 100$ (dotted line), $t = 200$ (dashed line) and $t = 300$ (solid line) obtained for parameters $A = 1$ and $c_1 = 0.1$ and the system parameters are same in Fig. 3.13 as in the text with chosen initials as $c_0 = u_0 = 1, v_0 = 0.5$.

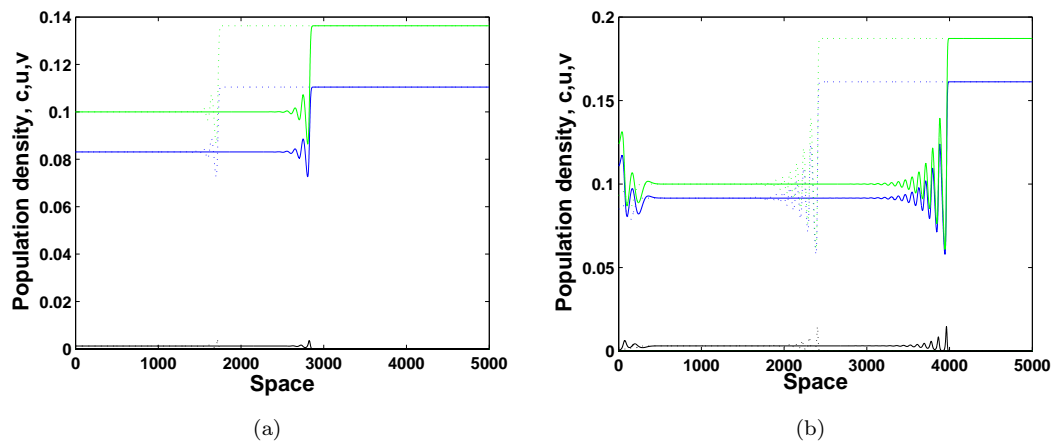


FIGURE 3.25: Snapshots of the density distribution over space for oxygen, phytoplankton and zooplankton at $t = 3000$ (dashed curves) and $t = 5000$ (solid curves) obtained for (a) $A = 0.9, c_1 = 0.7$, (b) $A = 1, c_1 = 0.7$. The corresponding nonspatial system is given by Fig. 3.14. The initial conditions are $c_0 = 0.0916$ and $u_0 = 0.1, v_0$ as in Eq. 3.22.

The effect of including a spatial component is often difficult to predict based on the dynamics of its nonspatial counterpart. In particular, Fig. 3.24 shows the evolution of the species spatial distribution over time obtained for the same parameter values as Fig. 3.13. As it should be expected, in the large-time limit the system goes extinct; however, at an intermediate time, the initial distribution evolves to a travelling wave. The distribution of oxygen and phytoplankton form travelling fronts separating the area where these quantities are approximately at their steady state values $c(x, t) = \tilde{c}$ and $u(x, t) = \tilde{u}$ (on the right of the front) from

the area where these quantities have gone extinct (on the left of the front). The zooplankton density forms a narrow peak at the position of the front. This solution of the model (3.17–3.19) apparently describes an interesting ecological situation. There is not enough oxygen everywhere in the system to support a stable existence of zooplankton; however, zooplankton can survive transiently (and over a relatively long time) at the interface between the area of partial depletion of oxygen and the area with no oxygen.

Figure 3.25 presents the simulation results in the spatial system (3.17–3.19) obtained for the parameters corresponding to Fig. 3.14. In particular, in Fig. 3.25a the coexistence state is a stable focus (the corresponding nonspatial dynamics is shown in Fig. 3.14a). It is readily seen that, in this case, the intermediate-time solution is given by an oscillating travelling front connecting the two steady states, i.e. the zooplankton-free state E_2 (on the right of the front) and the coexistence state E_3 (on the left of the front). The front propagates to the right so that, in the large-time limit, the species densities converge to the spatially uniform distribution $c(x, t) = \bar{c}$, $u(x, t) = \bar{u}$, $v(x, t) = \bar{v}$.

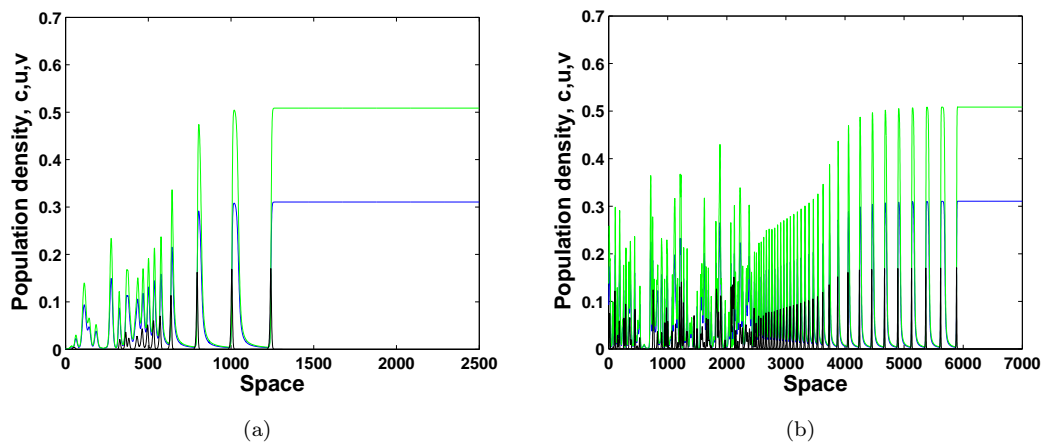


FIGURE 3.26: The effect of changes in parameter c_1 . The density of oxygen (blue), phytoplankton (green) and zooplankton (black) over space at (a) $t = 1000$, (b) $t = 5000$ obtained for other given parameter values and $A = 0.8$, $c_1 = 0.3$ and the initial conditions are as in Eq. 3.20 with $c_0 = 0.0385$, $u_0 = 0.1$.

In Fig. 3.26, the steady state is unstable; see real part of system steady states in Fig. 3.6. Remarkably, the travelling waves for oxygen and phytoplankton converge to the zooplankton-free state E_2 , which is the saddle for these parameter values. Irregular spatiotemporal oscillations grow with a large time limit. In both cases (Figs. 3.26a-b), periodic oscillations follow the onset of chaotic oscillations in the wake of travelling waves. But, this replacement is much more clear for a larger time limit (Fig. 3.26b). The irregular spatiotemporal dynamics are followed

by periodic oscillations increasing in amplitude which adjoin to population fronts converging to the zooplankton-free state. Biologically, it means that the absence of zooplankton results in the stability of the oxygen concentration and the phytoplankton population (see more simulations on prey-predator system in [147] and the references there in).

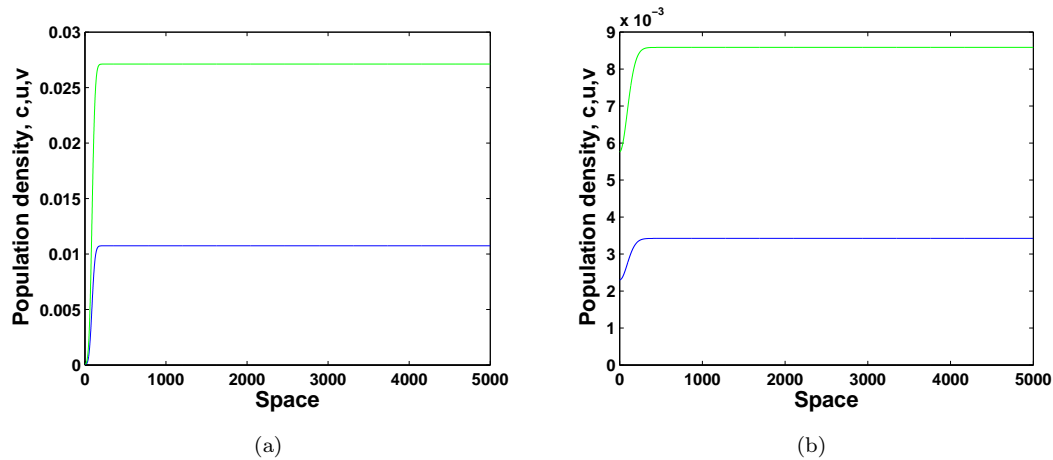


FIGURE 3.27: The density of oxygen (blue), phytoplankton (green) and zooplankton (black) over space at (a) $t = 500$, (b) $t = 5000$ obtained for other given parameter values $A = 0.4$, $c_1 = 0.4$ and initial conditions are as in (3.20–3.22) with $c_0 = 0.06$, $u_0 = 0.1$.

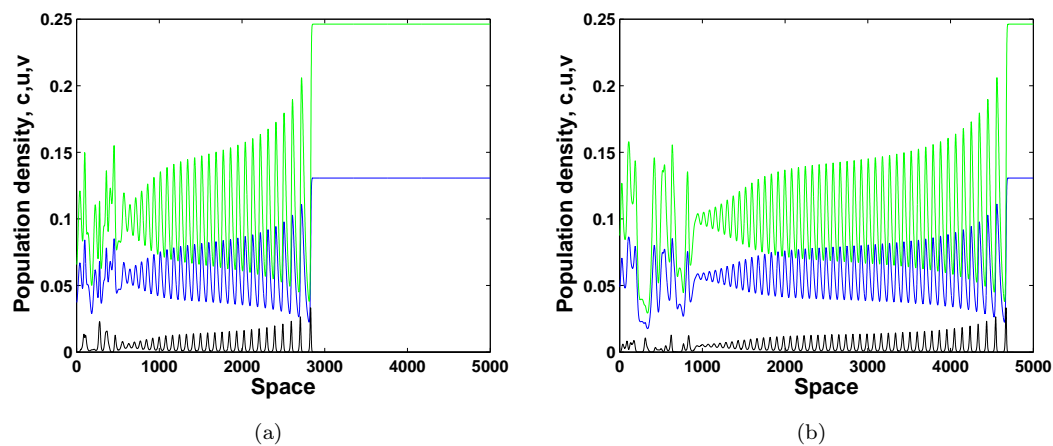


FIGURE 3.28: Distribution of oxygen (blue), phytoplankton (green) and zooplankton (black) over space at (a) $t = 3000$, (b) $t = 5000$ obtained for $A = 0.6$ and $c_1 = 0.4$ with the initial conditions $c_0 = 0.06$, $u_0 = 0.1$. Other parameters are given in the text, see the beginning of Section 3.3.2.

In Fig. 3.25b, the parameters are beyond the Hopf bifurcation so that the nonspatial system becomes oscillatory (see Fig. 3.14b). In this case, the spatial species distribution has somewhat counter-intuitive properties. A part of the spatial solution forms, similarly to the above, an oscillating travelling front connecting

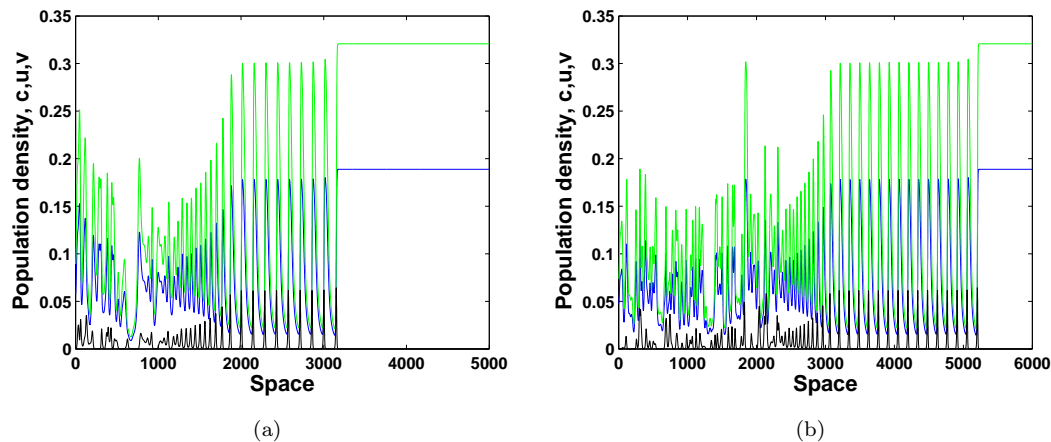


FIGURE 3.29: The density of oxygen (blue), phytoplankton (green) and zooplankton (black) over space at (a) $t = 3000$, (b) $t = 5000$ obtained for other given parameter values $A = 0.7$, $c_1 = 0.4$ and initial conditions are $c_0 = 0.06$, $u_0 = 0.1$ as in Eqs. (3.20–3.22).

E_2 on the right and E_3 on the left. However, the coexistence state E_3 is unstable and therefore cannot persist indefinitely. As the oscillating travelling front propagates to the right, far behind the front, i.e. behind the unstable plateau, irregular oscillations eventually develop; see the left-hand end of Fig. 3.14b. In the large-time limit, the irregular spatiotemporal oscillations eventually occupy the whole domain (not shown here). The system dynamics thus follow the generic scenario well-known for other reaction-diffusion systems, i.e. the onset of chaos in the wake of the front preceded by the so called dynamical stabilization of unstable equilibrium [145, 193, 196, 228].

The existence of the travelling front connecting E_2 to E_3 is not a general property of the system (3.17–3.19) though. The unstable plateau does not always exist and, alternatively, the spatially uniform distribution of oxygen and phytoplankton (corresponding to the zooplankton-free state E_2) may give way to a band of regular spatial oscillations of varying amplitude; see Fig. 3.28 obtained for parameters where the nonspatial system is oscillatory. The band of regular spatial oscillations is eventually displaced by the chaotic spatiotemporal oscillations which, in the course of time, occupy the whole domain.

We mention here that the onset of spatiotemporal chaos in the system (3.17–3.19) is, when the corresponding nonspatial system is oscillatory, a common property. A general tendency that we have observed in our simulations is that the spatial oscillations become more and more irregular with an increase in A (keeping other parameters fixed), i.e. when the point in the parameter plane moves further away from the Hopf bifurcation curve. An example of this situation is shown in

Fig. 3.29.

3.4 Discussion and Concluding remarks

Peculiarities of plankton dynamics in marine ecosystems have been a focus of significant interest and intense research for several decades. Considerable progress has been made in the understanding of factors and mechanisms underlying a variety of plankton phenomena, and there exists vast literature covering almost every aspect of plankton research. However, there is at least one aspect that has been rather poorly investigated on oxygen concentration of water body. Surprisingly, there are very few studies directly concerned with the dynamics of the oxygen-plankton coupling. In spite of its obvious importance, this issue remains clearly overlooked both in theoretical and field studies. Admittedly, plankton is not only the base of the ocean food chain (which is often mentioned as a practical reason justifying the effort behind scientific studies), it is also responsible for the production of about two thirds of the atmospheric oxygen.

In this chapter, we developed a conceptual three-component mathematical model of the oxygen-phyto-zooplankton system from the baseline model system given in Chapter 2. The model consists of three ordinary differential equations. We first consider the nonspatial version of the model which, in real-world terms, corresponds to a well-mixed system with spatially uniform distribution of species. The properties of the model have been studied both analytically and by simulations. In particular, we found analytical conditions for the existence of a (unique) positive equilibrium corresponding to the coexistence of all three components. In ecological terms, parameter values corresponding to the existence of the positive equilibrium may be regarded as safe (existence of system components), whilst the disappearance of this steady state should be regarded as an ecological disaster resulting in mass extinction of the plankton species.

As a next step, we consider the spatially explicit extension of our model which takes into account the transport of plankton and oxygen by the turbulent diffusion. The model is described by a system of three partial differential equations of reaction-diffusion type. Extensive numerical simulations were performed to show the properties of the system. We have shown that the model exhibits rich spatiotemporal dynamics, in particular, resulting in travelling fronts and spatiotemporal chaos. The observed properties of the system are therefore reminiscent of the dynamics of other ecologically relevant reaction-diffusion systems, e.g. see [147, 261], which helps to verify the model properties and to interpret the results.

With this chapter, we have focussed on the predation effect on water body oxygen concentration. On the other hand, the decrease of dissolved oxygen concentration in the water body affects the predation response of zooplankton community [21, 45, 175]. Therefore, the interaction between zooplankton predation and oxygen concentration can be extended in future studies.

The most interesting feature of this chapter is that zooplankton addition to the oxygen-phytoplankton model, results in our model system generating rich dynamics. In addition, as it is seen for particular parameter choices our oxygen-plankton model system illustrates similar dynamical successions to those observed in well known prey-predator system.

Chapter 4

Plankton Respiration Effect on Oxygen Dynamics

4.1 Introduction

Oxygen depletion in marine ecosystems is a severe ecological problem, often being responsible for the mass extinction of marine fauna. Therefore, oxygen production by marine phytoplankton due to its photosynthetic activity is thought to hold the key to a better understanding and forecasting of ecological disasters. Importantly, oxygen concentration is not only determined by primary production, but also depends on its consumption through plankton respiration [231]. In this chapter, we address this issue theoretically by considering an oxygen, phytoplankton and zooplankton model in order to make an insight into the effect of plankton respiration on oxygen dynamics¹.

Oxygen depletion has been a challenging ecological problem, thereby oxygen and plankton dynamics are explicitly included together in a model system to make an insight into this problem by several researchers [5, 57, 105, 106, 150, 160]. In particular, Marchettini et al. [150] studied a mathematical model of biochemical processes of a lagoon system. In an other study, Allegretto et al. [5] focused on the existence of periodic fluctuations, which is based on the Italian coastal lagoon. The dynamics of a plankton-nutrient system and its possible dynamical properties, excluding the dynamics of oxygen concentration was considered by Edwards and Brindley [57]. Moreover, an oxygen-algae model is introduced to detail oxygen depletion under some controlling external factors in [160]. Hull et al. [105] investigated dissolved oxygen concentration in a multi-component system, with the assistance of microbial and environmental forcing function (wind, solar

¹The majority of this chapter has been published in [226]

radiation and temperature) on lagoon dynamics. In another study, Hull et al. [106] investigated seasonal and daily dynamics of dissolved oxygen measurements in Mediterranean coastal lagoons, but in the modelling section dissolved oxygen is considered at sediment level together with CO_2 and organic matter, thereby the remaining water body oxygen concentration and its dependence on plankton respiration activity are overlooked. Therefore, we address the oxygen depletion problem by considering prey-predator interactions for plankton dynamics combined with water body dissolved oxygen dynamics, based on the model presented in [227] that describes the marine system oxygen dynamics without taking into account plankton respiration term.

In this chapter, we focus on the effects of plankton respiration on oxygen dynamics. We first extend the model presented in Chapter 3 describing predation effects, by addition of respiration terms accounting for both phytoplankton and zooplankton respiration. In what follows, oxygen, phytoplankton and zooplankton steady state stability are examined both analytically and numerically. Extensive numerical simulations are performed for both the nonspatial and corresponding spatial system in one-dimension and two-dimensions.

4.2 Model formulation

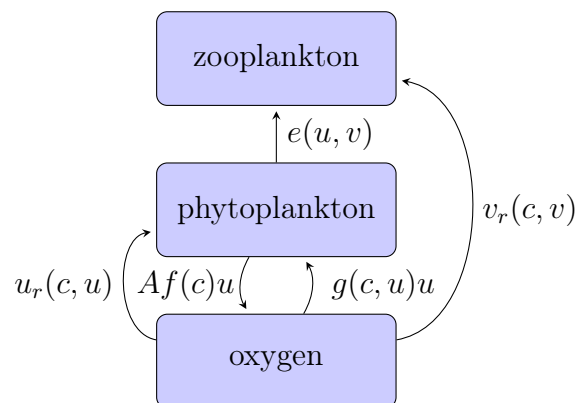


FIGURE 4.1: The structure of our conceptual model describing the interactions between oxygen, phytoplankton and zooplankton. Arrows show the flows of matter through the system, and the parametrizations of the rates are as labelled. Phytoplankton produces oxygen through photosynthesis during the day-time then consumes it during the night [36]. Zooplankton feeds on phytoplankton and consumes oxygen through breathing; for further details see in the text.

The model that we investigated is based on the oxygen-phytoplankton-zooplankton model of [227] which we extend by adding a plankton respiration

term and its expected consequences on the model structure to further develop the underlying properties of oxygen dynamics and to make our model system more ‘realistic’. The structure of the model is shown schematically in Fig. 4.1. Flows of matter through the system are indicated by arrows, and the model components of these flows are given on each arrow. The three equation coupled model system (4.1-4.3) illustrates the increase in oxygen concentration as a result of photosynthetic activity, governed mainly by phytoplankton; Then, the produced oxygen is consumed in metabolic activities involving respiration for both phytoplankton and zooplankton. Furthermore, phytoplankton are grazed upon by zooplankton. Therefore, in this model, the importance of zooplankton is twofold: controlling plankton density by predation and consuming oxygen.

We begin with the nonspatial system which applies to the case of a well-mixed ecosystem. The dynamics of oxygen, which in turn is being controlled by its main producer phytoplankton, which in turn is grazed by its predator zooplankton, is described by the following model:

$$\frac{dc}{dt} = Af(c)u - mc - u_r(c, u) - v_r(c, v), \quad (4.1)$$

$$\frac{du}{dt} = g(c, u)u - e(u, v) - \sigma u, \quad (4.2)$$

$$\frac{dv}{dt} = e(u, v) \varphi(c) - \mu v, \quad (4.3)$$

where c , u , and v are the concentration of dissolved oxygen, the density of phytoplankton and zooplankton respectively, at time t . The term $Af(c)$ describes the rate of oxygen production per unit phytoplankton mass, while $f(c)$ is the rate of increase in the concentration of the dissolved oxygen due to its transport from phytoplankton cells to the surrounding water, $g(c, u)$ is the per capita phytoplankton growth rate, $e(u, v)$ is the per capita zooplankton growth rate, A quantifies the rate of oxygen production affected by some external factors, and negative terms in Eq. (4.1) are the losses of oxygen with the coefficient of m due to natural depletion (e.g. due to biochemical reactions in the water), consumption terms by phytoplankton and zooplankton due to respiration, respectively. The first negative term of Eq. (4.2) corresponds to the grazing of zooplankton on phytoplankton, and thus the growth term of zooplankton consists of both predation and respiration. Therefore, function $e(u, v)$ describes predation, and σu describes the natural mortality of phytoplankton. The consumed phytoplankton biomass is transformed into the zooplankton biomass with efficiency φ , see the first term in the right-hand side of Eq. (4.3). Since the well-being of zooplankton obviously depends on the

oxygen concentration (so that, ultimately, it dies if there is not enough oxygen to breathe), we assume that $\varphi = \varphi(c)$. The term μv stands for the natural mortality of zooplankton, and stages of the model construction are detailed in [227] and in Chapters 2 and 3. For more detailed reasoning, (in order to understand the model formulation) based on prey-predator system, see [226].

An immediate question arising is what kind of interaction exists between respiration and phytoplankton growth. In view of the biological literature, there is a direct relation between oxygen concentration of water body and phytoplankton density [233]. On the other hand, phytoplankton need oxygen as other living organisms in aquatic environments to use in its metabolic processes, e.g. growth, respiration, etc. [105, 173, 191, 236]. We consider u_r (see the third term in the right-hand side of Eq. (4.1)) as a function of phytoplankton respiration and assume it has a functional response of Holling type II. Low oxygen concentration is unfavorable for phytoplankton and it is likely to depress its reproduction. In addition, a phytoplankton cell cannot take more oxygen than it needs. For this reason, u_r should be a monotonously increasing function of c tending to a constant value for $c \rightarrow \infty$; for further details see [226]. We neglected the consumption of oxygen by other living beings due to respiration, however this may be accounted for by natural depletion of oxygen as first term of Eq. (4.1). Under the above assumptions, the simplest parametrization for phytoplankton respiration function is as follows:

$$u_r = \frac{uc}{c + c_2}, \quad (4.4)$$

where c_2 is the half-saturation constant.

To construct a zooplankton respiration function, we have to understand the underlying mechanism of its biological standpoints. Here, the specific breathing rate (rate for per individual) of zooplankton is neglected. Detailed work on the relation between zooplankton body mass and respiration rate is found in [6, 35, 97]. Zooplankton respiration depends on oxygen concentration changes of surrounding water. The respiration rate of zooplankton varies with changing environmental conditions [31, 43, 76]. Therefore, the consumption rate usually shows a linear increase at small oxygen concentration but tends to a constant, saturating value at large oxygen concentration (cf. Fig.1 in [31]). Consider v_r as a function of zooplankton respiration. According to the above biological observations, this term has the following simplest parametrization:

$$v_r = \frac{\nu cv}{c + c_3}, \quad (4.5)$$

where ν is the maximum per capita zooplankton respiration rate and c_3 is the half-saturation constant.

Respiration rate of plankton is affected by some surrounding factors ,i.e., water temperature, light intensity, nutrient uptake etc. [8, 69, 252]. In addition, zooplankton metabolism is complex [69], and as a simplification of biological reality, we have chosen its coefficient ν as a constant to mathematically describe it.

The feeding efficiency of zooplankton as a function of the oxygen concentration, $\varphi(c)$, (i.e. zooplankton die if there is not enough oxygen to breathe). This function should be of a sigmoidal shape function under generic biological arguments, suggesting low efficiency at low oxygen concentration, i.e being approximately constant for the oxygen concentration above a certain threshold but promptly decays to zero for concentrations below the threshold [31]. Note that, proper understanding of respiration and its relation to zooplankton biomass and also its contribution to the other marine organisms' growth rate, is detailed in [7, 97]. The above explanations are quantitatively considered by the following parametrization:

$$\varphi(c) = \beta \frac{c^2}{c^2 + c_4^2}, \quad (4.6)$$

where β is the maximum feeding efficiency and c_4 is the half-saturation constant.

We introduce dimensionless variables, $t' = tm$, $c' = \frac{c}{c_0}$, $u' = \frac{u}{m}$, $v' = \frac{v}{m}$ and the new parameters $\hat{B} = \frac{B}{m}$, $\hat{A} = \frac{A}{c_0}$, $\hat{\nu} = \frac{\nu}{c_0}$, $\hat{\sigma} = \frac{\sigma}{m}$, $\hat{\mu} = \frac{\mu}{m}$, $\hat{\beta} = \frac{\beta}{m}$, $\hat{h} = \frac{h}{m}$, $\hat{c}_i = \frac{c_i}{c_0}$ where $i = 1, 2, 3, 4$. For notational convenience, primes and hats are omitted $t' \rightarrow t$, $c' \rightarrow c$, $u' \rightarrow u$, $v' \rightarrow v$, $\hat{A} \rightarrow A$, $\hat{B} \rightarrow B$, $\hat{\beta} \rightarrow \beta$, $\hat{\nu} \rightarrow \nu$, $\hat{\sigma} \rightarrow \sigma$, $\hat{\mu} \rightarrow \mu$, $\hat{h} \rightarrow h$ and $\hat{c}_i \rightarrow c_i$. In terms of the these new (dimensionless) variables, equations (4.1–4.3) then turn into the following form:

$$\frac{dc}{dt} = A \left(1 - \frac{c}{c+1} \right) u - c - \frac{uc}{c+c_2} - \frac{\nu cv}{c+c_3}, \quad (4.7)$$

$$\frac{du}{dt} = \left(\frac{Bc}{c+c_1} - u \right) \gamma u - \frac{uv}{u+h} - \sigma u, \quad (4.8)$$

$$\frac{dv}{dt} = \left(\frac{\beta uv}{u+h} \right) \frac{c^2}{c^2 + c_4^2} - \mu v. \quad (4.9)$$

In order to understand the ecological background of our model system, we have to look at oxygen production and consumption issues of marine ecosystems in detail. Dissolved oxygen level depends mainly on the relative amount of photosynthetic oxygen production and total plankton respiration [242]. Some amount of produced oxygen is consumed in the respiration process by phytoplankton and zooplankton

to use in their metabolic activities and zooplankton then feed on phytoplankton. So, our model system (4.7-4.9) keeps the idea to reveal the relation between the prey-predator system and water body oxygen concentration. Further discussion of possible parameter values in real ecosystems will be done in Section 5.3.

Note that, here, the difference between this model and the model presented in Chapter 3 is the recognition of the importance of plankton respiration on oxygen dynamics [23, 73, 105]. But here our main focus is plankton respiration as living organism contrary to the complex structure of marine system.

4.2.1 Equilibria analysis and steady states

Before proceeding to the spatial case of model system, understanding of nonspatial properties of the oxygen itself and the phytoplankton as its primary producer and zooplankton as phytoplanktons' main consumer becomes useful. System's stationary dynamics are solutions of $dc/dt = 0$, $du/dt = 0$, $dv/dt = 0$.

Note that the system (4.7–4.9) has four steady states, one is extinction state $(0, 0, 0)$ and the other two are zooplankton-free $(\dot{c}, \dot{u}, 0)$ $((\dot{c}_1, \dot{u}_1, 0), (\dot{c}_2, \dot{u}_2, 0))$ and the last one is the coexistence state $(\ddot{c}, \ddot{u}, \ddot{v})$, which lies in the domain $c > 0$, $u > 0$, $v > 0$.

1. The trivial equilibrium $E_1 = (0, 0, 0)$ corresponds to the extinction state. It is readily seen that this equilibrium always exists, without any dependence on the choice of parameter values.
2. The two semi-trivial equilibria $E_2^{(i)} = (\dot{c}_i, \dot{u}_i, 0)$ where $i = (1, 2)$. When $v = 0$, the system (4.7–4.9) returns into its oxygen and phytoplankton system given by Eqs. (4.10–4.11); therefore, there exist two positive steady states $(E_2^{(1)} = (\dot{c}_1, \dot{u}_1, 0), E_2^{(2)} = (\dot{c}_2, \dot{u}_2, 0))$. Note that the dot above a letter denotes the notation to prevent the confusion with the steady states used in previous chapters for zooplankton-free state while the double dot above a letter denotes the steady coexistence steady state.

The system's steady state values, \dot{c} and \dot{u} , are the solutions of the following system of equations:

$$A\left(1 - \frac{\dot{c}}{\dot{c} + 1}\right)\dot{u} - \dot{c} - \frac{\dot{u}\dot{c}}{\dot{c} + c_2} = 0, \quad (4.10)$$

$$\left(\frac{B\dot{c}}{\dot{c} + c_1} - \dot{u}\right)\gamma\dot{u} - \sigma\dot{u} = 0, \quad (4.11)$$

Equations (4.10–4.11) define two (null)isoclines of the system, which we call the oxygen isocline and the phytoplankton isocline, respectively. The oxygen and phytoplankton isoclines can be obtained as

$$u = \frac{c(c+1)(c+c_2)}{A(c+c_2) - c(c+1)}, \quad (4.12)$$

$$c = \frac{c_1(u\gamma + \sigma)}{B\gamma - u\gamma - \sigma}. \quad (4.13)$$

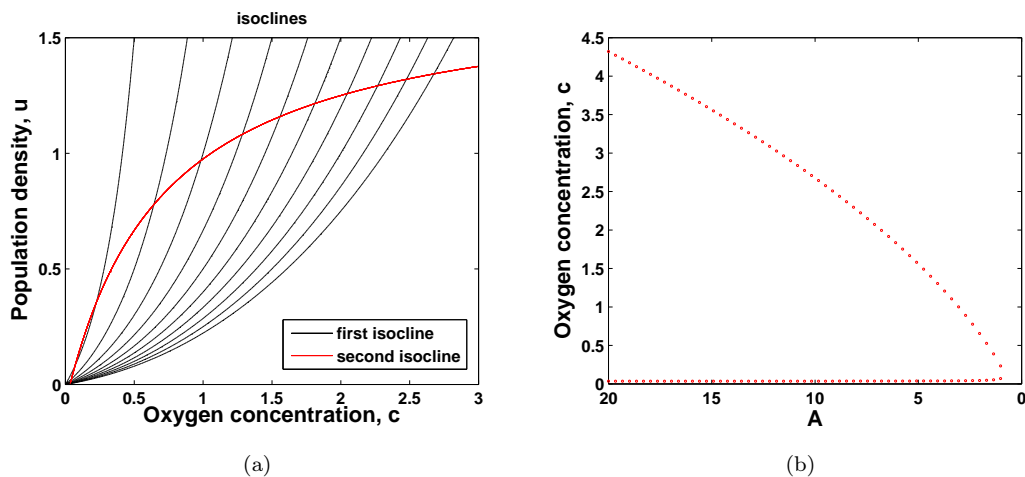


FIGURE 4.2: (a) The (null)-isoclines of the oxygen phytoplankton system (4.7–4.9) where $v = 0$. Black curves show the first (oxygen) isocline for $A = \{1, 2, \dots, 10\}$ from left to right; while red curve shows the second (phytoplankton) isocline. (b) Intersection points of two isoclines are shown in a (A, c) parameter map (the steady state values of c) and system other parameters are $B = 1.8$, $\gamma = 1.2$, $\sigma = 0.1$, $c_1 = 0.7$ and $c_2 = 1$.

System equilibria are non-negative intersection points of the oxygen zero growth isocline and phytoplankton zero growth isocline. The shape of zooplankton free steady states given by Eq. (4.12) and Eq. (4.13), null-cline figure is given in Fig. 4.2. Oxygen-phytoplankton steady states are obtained as the intersections points of the two isoclines. These two positive steady states value of the zooplankton-free state $(\dot{c}, \dot{u}, 0)$ are seen on Fig. 4.2b.

Parameter A determines the shape of the first isocline, as given by Eq. (4.12) in Fig. 4.2a. The succession of black curves Fig. 4.2a shows that taking sufficiently small A , the two positive steady states move towards each other, eventually they merge, and then disappear, thereby the only steady state remaining is the extinction state; see Fig. 4.2b. The intersection points of first (black) and second (red) isoclines are shown in Fig. 4.2b for varying values of A . A is considered as a controlling parameter (for reasons that

will be expanded upon in Chapter 5). It is readily seen that one of the positive steady states $E_2^{(1)}$ always stays close to the extinction state and the shape of the first isocline succession can be described as convergence of upper positive steady state ($E_2^{(2)}$) to the lower one ($E_2^{(1)}$). The convergence of systems' steady states to $E_2^{(1)}$ (the lower positive one) brings with it a most crucial ecological problem called depletion of oxygen concentration in water body.

We readily observe that $(0, 0, 0)$ is a steady state of the system. As for the positive equilibria (if any), it does not seem possible to solve Eqs. (4.12–4.13) explicitly. Instead, since system's equilibria are the intersection points of the two isoclines, important conclusions can be made by analyzing the mutual position of the corresponding curves. Figure 4.2a shows the isoclines given by Eq. (4.12) and Eq. (4.13) obtained for some hypothetical parameter values. Therefore, system (4.10-4.11) can have two positive equilibria $(\dot{c}_1, \dot{u}_1, 0)$ and $(\dot{c}_2, \dot{u}_2, 0)$. It is seen that the extinction state always exists, regardless of what the parameters are. However, the existence of the two positive steady states depends on the choice of controlling parameter A . These positive equilibria exist only if A is not too small, i.e. above certain critical value; see Fig. 4.2b. A similar tendency of the system properties is also observed as a result of an increase in c_1 or decrease in B (obtained results under the effect of different controlling parameters are not given here for the sake of brevity).

3. The positive (coexistence) equilibrium $E_3 = (\ddot{c}, \ddot{u}, \ddot{v})$.

The steady state values \ddot{c} , \ddot{u} and \ddot{v} are the solutions of the following system:

$$A\left(1 - \frac{\ddot{c}}{\ddot{c} + 1}\right) \ddot{u} - \ddot{c} - \frac{\ddot{u}\ddot{c}}{\ddot{c} + c_2} - \frac{\nu\ddot{c}\ddot{v}}{\ddot{c} + c_3} = 0, \quad (4.14)$$

$$\left(\frac{B\ddot{c}}{\ddot{c} + c_1} - \ddot{u}\right)\gamma \ddot{u} - \frac{\ddot{u}\ddot{v}}{\ddot{u} + h} - \sigma\ddot{u} = 0, \quad (4.15)$$

$$\left(\frac{\beta\ddot{u}\ddot{v}}{\ddot{u} + h}\right) \frac{\ddot{c}^2}{\ddot{c}^2 + c_4^2} - \mu\ddot{v} = 0. \quad (4.16)$$

In this case oxygen production is led by not only phytoplankton respiration, but also zooplankton respiration contrary to the semi-trivial equilibrium case. The system (4.14-4.16) can be solved as follows:

$$\ddot{c} = \frac{c_1(\ddot{u}\gamma + \frac{\ddot{v}}{\ddot{u}+h} + \sigma)}{B\gamma - \ddot{u}\gamma - \frac{\ddot{v}}{\ddot{u}+h} - \sigma}, \quad \ddot{u} = \frac{\mu h(\ddot{c}^2 + c_4^2)}{\beta\ddot{c}^2 - \mu(\ddot{c}^2 + c_4^2)}, \quad \ddot{v} = \frac{\ddot{c} + c_3}{\nu} \left(\frac{A\ddot{u}}{\ddot{c}(\ddot{c} + 1)} - 1 - \frac{\ddot{u}}{\ddot{c} + c_2} \right). \quad (4.17)$$

4.2.2 Stability analysis

In this section, a detailed discussion of steady states stability on E_1 , $E_2^{(1)}$, $E_2^{(2)}$ and E_3 is presented. (Steady states are the solutions to $dc/dt = du/dt = dv/dt = 0$). The stability of system steady states is obtained by the eigenvalues of the Jacobian matrix. The Jacobian matrix of system (4.14-4.16) is given by:

$$C = \begin{pmatrix} -\frac{Au}{(1+c)^2} - 1 - \frac{uc_2}{(c+c_2)^2} - \frac{\nu vc_3}{(c+c_3)^2} & \frac{A}{1+c} - \frac{c}{c+c_2} & -\frac{\nu c}{c+c_3} \\ \frac{Bc_1\gamma u}{(c+c_1)^2} & \frac{Bc\gamma}{c+c_1} - 2\gamma u - \frac{vh}{(u+h)^2} - \sigma & -\frac{u}{u+h} \\ \frac{\beta uv}{u+h} \frac{2cc_4^2}{(c^2+c_4^2)^2} & \frac{\beta vh}{(u+h)^2} \frac{c^2}{(c^2+c_4^2)} & \frac{\beta uc^2}{(u+h)(c^2+c_4^2)} - \mu \end{pmatrix}. \quad (4.18)$$

Let C_i be the corresponding matrix with the given steady states E_i where $i = 1, 2, 3$. Computation of the corresponding Jacobian matrices for given steady states are detailed in Appendix C.

- Extinction state E_1

For the stability of E_1 from matrix C , the eigenvalues of matrix C_1 given by matrix 4.18 are -1 , $-\sigma$, $-\mu$, thereby the extinction state is always stable.

- Oxygen-phytoplankton existence states $E_2^{(1)}$, $E_2^{(2)}$

For the oxygen-phytoplankton existence state stability from matrix C_2 , the eigenvalues are the solutions of the following characteristic equation:

$$\left[\left(-\frac{A\dot{u}}{(1+\dot{c})^2} - 1 - \frac{\dot{u}c_2}{(\dot{c}+c_2)^2} - \lambda \right) \left(\frac{B\dot{c}\gamma}{\dot{c}+c_1} - 2\dot{u}\gamma - \sigma - \lambda \right) - \left(\frac{A}{1+\dot{c}} - \frac{\dot{c}}{\dot{c}+c_2} \right) \left(\frac{Bc_1\gamma\dot{u}}{(\dot{c}+c_1)^2} \right) \right] \left(\frac{\beta\dot{u}}{\dot{u}+h} \left(\frac{\dot{c}^2}{\dot{c}^2+c_4^2} \right) - \mu - \lambda \right) = 0 \quad (4.19)$$

where \dot{c} and \dot{u} are given by Eqs. (4.12–4.13) and the solution of Eq. (4.19) is denoted by $E_2^{(1)}$ and $E_2^{(2)}$, which are shown in Fig. 4.2 as the first positive steady state (lower one), and the second positive steady state (upper one), respectively. Stability of this steady state E_2 is shown by extensive numerical simulations and by a corresponding bifurcation diagram presented in Fig. 4.13.

Steady state values of oxygen and phytoplankton for $E_2^{(1)}$ for the given range of parameter values A and c_1 are shown in Fig. 4.3. We fix other parameter values at some hypothetical values as $B = 1.8$, $\gamma = 1.2$, $\sigma = 0.1$, $c_2 = 1$ and vary A and c_1 . Note that for this steady state (zooplankton-free state) zooplankton steady state is denoted by zero surface and it is not shown here. Figure 4.4 shows

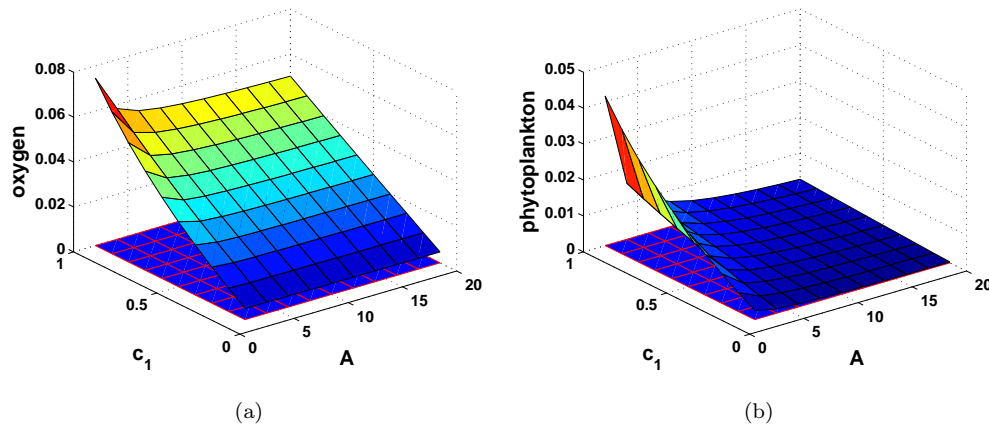


FIGURE 4.3: First positive steady state values ($E_2^{(1)}$) of oxygen and phytoplankton vs. A and c_1 (as given by the system (4.10-4.11)) with other given parameter values as in the text.

the eigenvalues of system (4.10-4.11) for $E_2^{(1)}$ vs. A and c_1 . As it is seen this steady state is always a saddle as a result of one eigenvalue always being positive for a given set of parameter values. Figure 4.5 shows the sketch of the eigenvalues vs. A for two hypothetical values of c_1 . In this case two of the eigenvalues are always negative, while the other one is positive. Therefore, for given parameter values $E_2^{(1)}$ is always a saddle.

The steady state value $E_2^{(2)}$ vs. A and c_1 is given in Fig. 4.6. It is obvious that for chosen parameter values oxygen and phytoplankton are always positive and reasonable from an ecological stand point. Figure 4.7 shows λ eigenvalues λ_1 , λ_2 and λ_3 as a function of the controlling parameters on the given range of A and c_1 . Figure 4.8 present the eigenvalues λ_1 , λ_2 and λ_3 as a controlling parameter A versus two different values of c_1 for $E_2^{(2)}$. This steady state for given parameter values can be stable or a saddle under the choice of system controlling parameters (see Fig. 4.7). For specific work on system eigenvalues in a large range of values of A see Table C.4 and for a small range of A see Table C.7 for $E_2^{(1)}$. For a similar tendency for $E_2^{(2)}$ see Table C.5 and Table C.8 in Appendix C, respectively.

- Oxygen-phytoplankton-zooplankton existence state E_3

For the oxygen-phytoplankton-zooplankton existence state stability from the corresponding matrix C_3 can be found in Appendix C. The characteristic equation of this steady state is rather bulky, thereby stability of this steady state is solved numerically.

The steady states of oxygen-phytoplankton-zooplankton vs. A and c_1 are given in Fig. 4.9. For this range of A and c_1 all system components are always

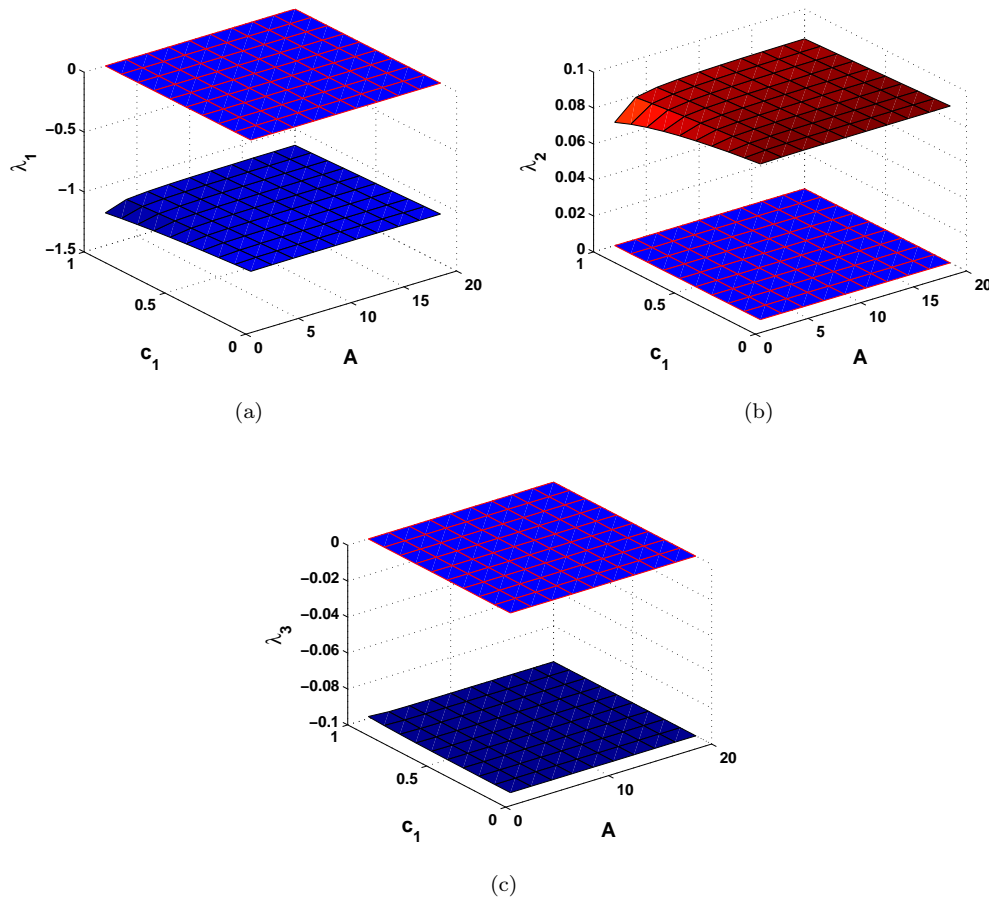


FIGURE 4.4: The eigenvalues of the system (4.10-4.11) linearised in the vicinity of the $(\bar{c}_1, \bar{u}_1, 0)$ vs. A and c_1 with other given parameter values as given in the text for given range of A and c_1 .

positive, thereby the ecological reality holds for the given set of system parameters. Figure 4.10 shows $Re\lambda$ (real part of eigenvalues) for each of the eigenvalues λ_1 , λ_2 and λ_3 as a function on the controlling parameter A and c_1 . As it is seen the real part of λ_1 is always negative. Hence, the stability of this steady state depends on the signs of λ_2 and λ_3 . They become negative, for a chosen range of controlling parameters: small A and large c_1 . For more details on the eigenvalues; see in Appendix C in Table C.9. Imaginary parts of the λ_1 , λ_2 and λ_3 are given in Fig. 4.11 to show that λ_2 and λ_3 are complex conjugates. Fig. 4.12 presents real parts of the eigenvalues λ_1 , λ_2 and λ_3 as functions of the controlling parameter A for two different values of c_1 for E_3 . An important step towards understanding the behavior of the systems' trajectories is identification of its eigenvalues. The oxygen-phytoplankton system eigenvalues, i.e. $E_2^{(1)}$ and $E_2^{(2)}$, are always real. However, the coexistence state, i.e. E_3 , is characterized by one negative real and by a pair of complex conjugate eigenvalues where their real part can be positive

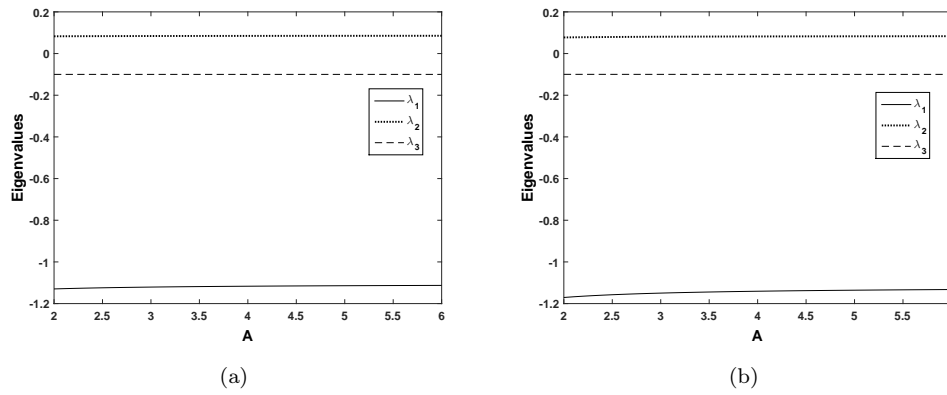


FIGURE 4.5: Eigenvalues vs. A for zooplankton-free, oxygen-phytoplankton state $E_2^{(1)}$ for (a) $c_1 = 0.4$, (b) $c_1 = 0.7$.

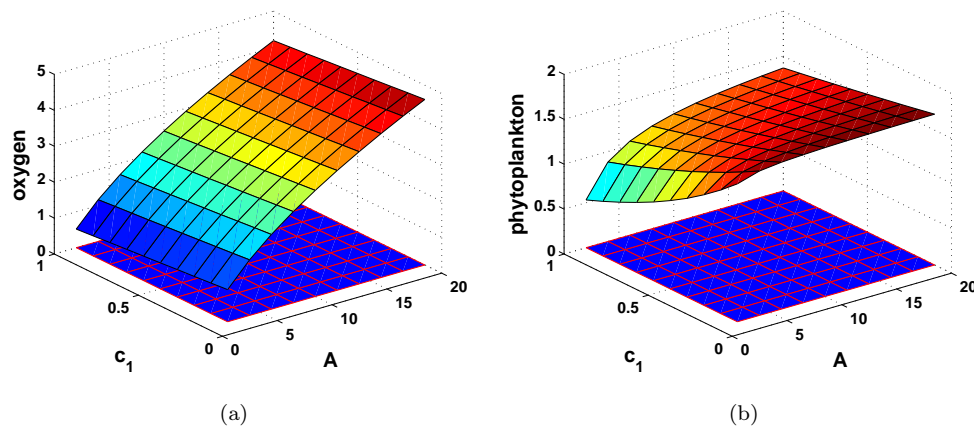


FIGURE 4.6: Second positive steady state $E_2^{(2)}$ values of oxygen and phytoplankton vs. A and c_1 (as given by the system (4.10-4.11)) for given range of A and c_1 and other system parameters are given in the text.

or negative depending on parameters.

Figure 4.13 summarizes the results of the steady state analysis as a map in parameter plane (A, c_1) for a small/large range of A . Here, again, c_1 is chosen as the controlling parameter because it describes the effect of oxygen on phytoplankton growth. In Fig. 4.13, blue stars show stable regions (negative eigenvalues), while black circles denote the saddle region (the pair of negative and positive eigenvalues). In Domain 2, for some intermediate values of A , E_3 is stable and $E_2^{(2)}$ is unstable. The system therefore exhibits bistability (recall that E_1 is always stable). With a decrease in A , $E_2^{(2)}$ becomes stable, so that for the parameters in Domain 1 the system exhibits tristability. With a further decrease in A , $E_2^{(2)}$ disappears (the further decrease in A , resulting in more domains beyond Domain 1, is not shown here for the convenience with the simulations). For approximately the

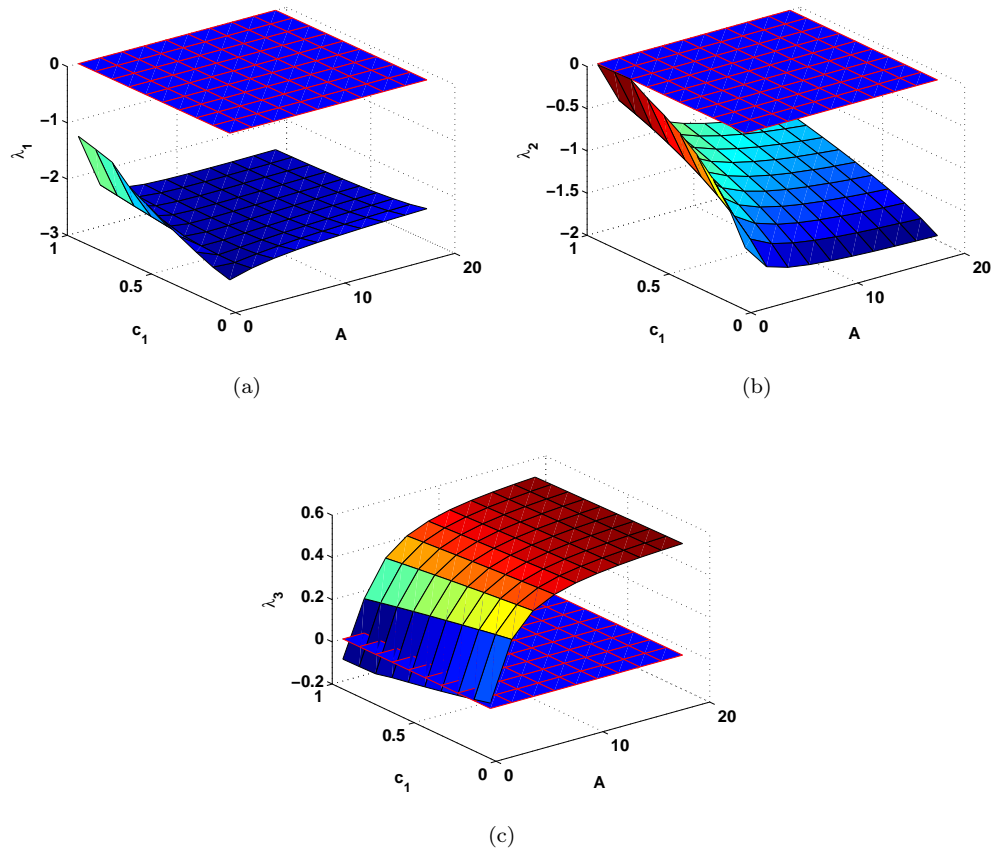


FIGURE 4.7: The eigenvalues of the system (4.10-4.11) linearised in the vicinity of the $(\hat{c}_2, \hat{u}_2, 0)$ vs. A and c_1 for their given range and other system parameters are given in the text.

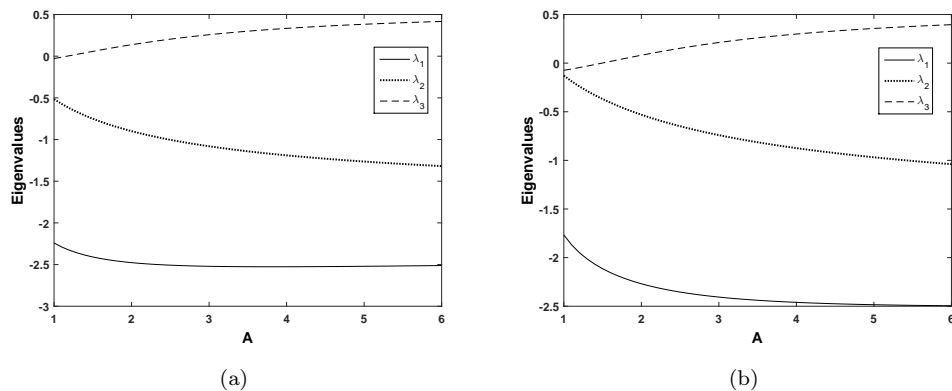


FIGURE 4.8: Eigenvalues vs. A for zooplankton-free, oxygen-phytoplankton state $E_2^{(2)}$ for (a) $c_1 = 0.4$, (b) $c_1 = 0.7$.

same value of A , the coexistence state disappears as well so that, for sufficiently small values of A , the only attractor of the system is the extinction state.

With an increase in A , in Domain 3, $E_2^{(2)}$ remains unstable (a saddle point) and E_3 loses its stability to become an unstable focus. For these parameters,

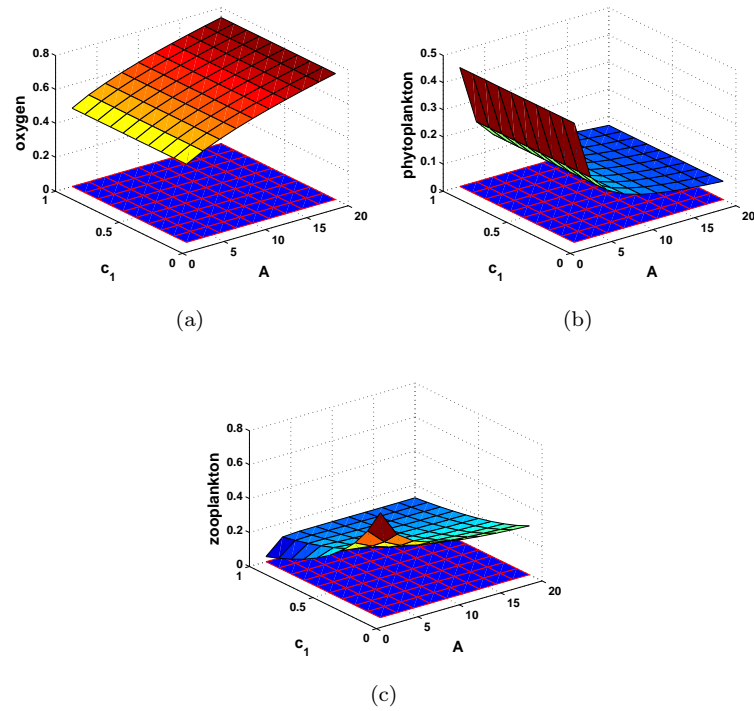


FIGURE 4.9: Steady state values of oxygen, phytoplankton and zooplankton vs. A and c_1 as given by the system (4.14–4.16) for given range of A and c_1 with other given parameter values as in the text.

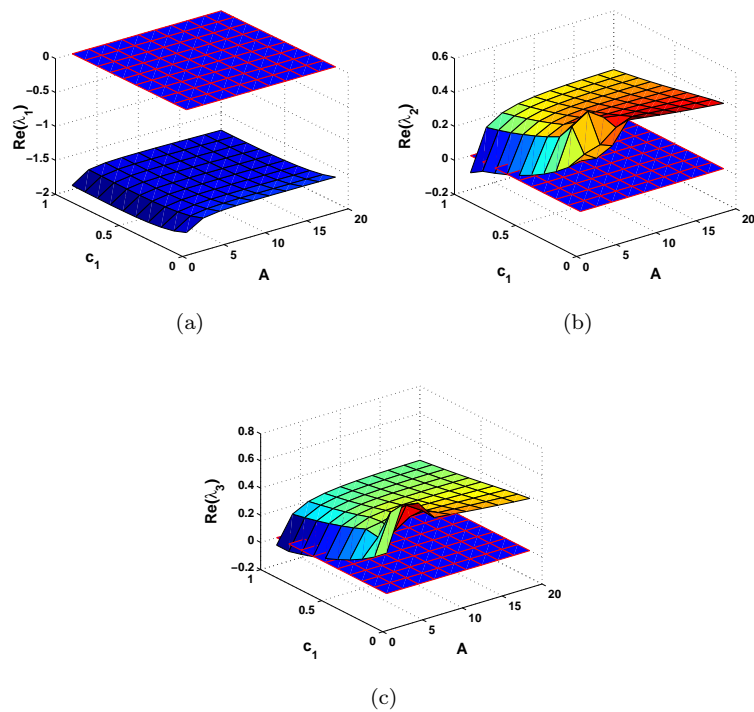


FIGURE 4.10: The eigenvalues real parts of the system (4.14–4.16) linearised in the vicinity of the $(\bar{c}, \bar{u}, \bar{v})$ steady state vs. A and c_1 for their given range with other given parameter values as in the text.

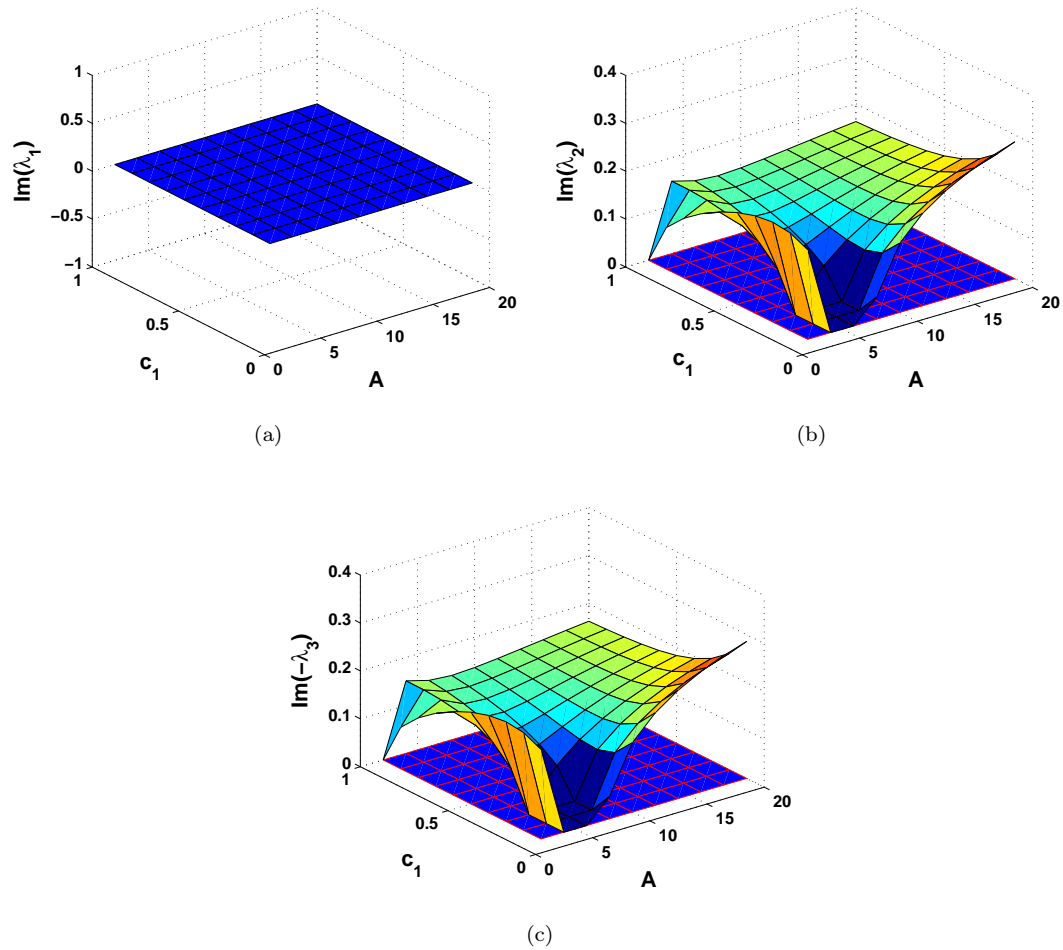


FIGURE 4.11: The eigenvalues imaginary parts of the system (4.14-4.16) linearised in the vicinity of the $(\check{c}, \check{u}, \check{v})$ steady state vs. A and c_1 for their given range with other given parameter values as in the text.

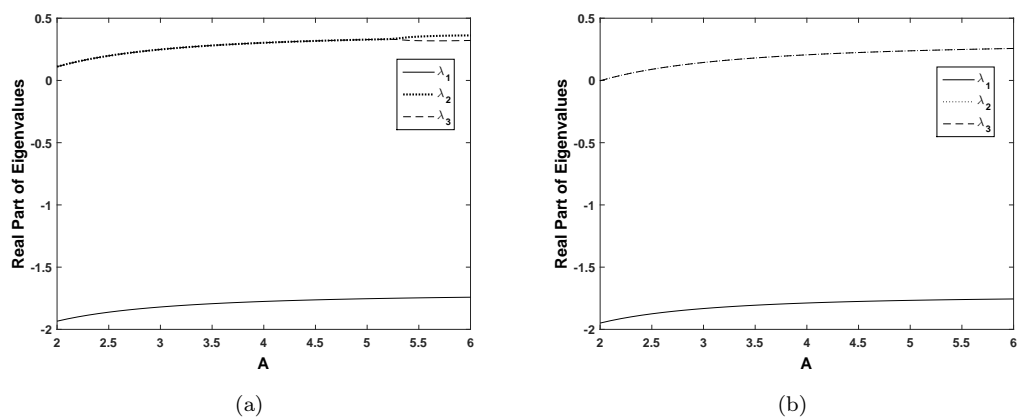


FIGURE 4.12: Eigenvalues vs. A for oxygen-phytoplankton-zooplankton state E_3 for (a) $c_1 = 0.4$, (b) $c_1 = 0.7$.

the unstable state E_3 is surrounded by a stable limit cycle that appears through the Hopf bifurcation when crossing from Domain 2 to Domain 3. With a further

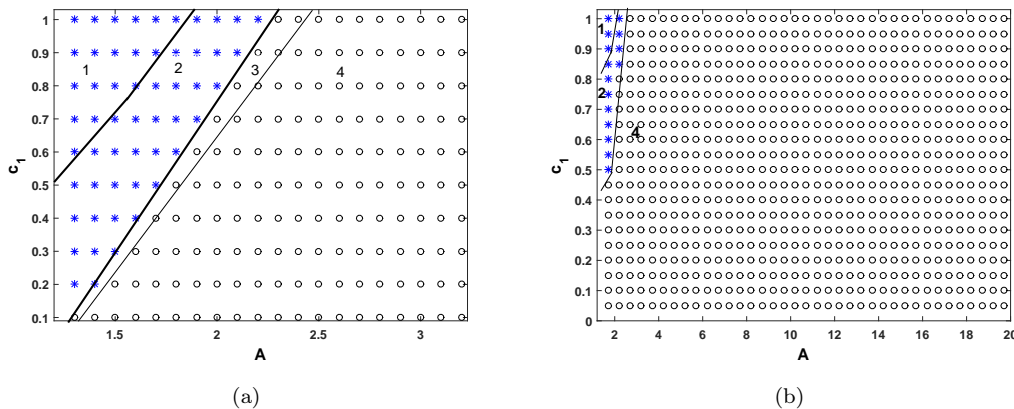


FIGURE 4.13: A map in the parameter plane (A, c_1) , for system (4.7-4.9), where different domains correspond to different stability of equilibria $E_2^{(2)}$ and E_3 ; see text for further details. Since the map is obtained in numerical simulations, the position of the domains boundaries is approximate. Other parameters are given in the text.

increase in A , the limit cycle disappears through a nonlocal bifurcation when crossing from Domain 3 to Domain 4. For parameter values from Domain 4, the only attractor of the system is the extinction state E_1 . Fig. 4.13b is given to show the system tendency in broadened range of A (see Tables C.4-C.9).

Note that for the eigenvalues versus A figures (Fig. 4.5, Fig. 4.8 and Fig. 4.12) are the specific form of the eigenvalues versus A - c_1 (Fig. 4.4, Fig. 4.7 and Fig. 4.10) for hypothetically chosen values of c_1 , respectively.

4.3 Numerical Simulations

4.3.1 Temporal dynamics

In light of steady states and their stability analysis given previously numerical simulations for the nonspatial system (4.7-4.9) are performed. In all following numerical simulations, we fix most of the parameters at some hypothetical value: $B = 1.8$, $\gamma = 1.2$, $\sigma = 0.1$, $c_2 = 1$, $c_3 = 1$, $c_4 = 1$, $\nu = 0.01$, $\beta = 0.7$, $\mu = 0.1$, $h = 0.1$ and vary A and c_1 in a broad range. Here, our interest lies in the temporal dynamics (4.7-4.9) under the effect of plankton respiration.

Figure 4.14 shows the oxygen concentration and phyto-zooplankton densities versus time obtained for the same value of $c_1 = 0.659$ and two different values of A chosen in Domain 3 (cf. Fig. 4.13a). For $A = 1.95$ (Fig. 4.14a), the damping oscillations were found to diminish in amplitude. However, for same c_1 , the situation is different for $A = 1.99$ (Fig. 4.14b) where the system develops periodic

oscillations and parameters are further away from the Hopf bifurcation (i.e. the boundary between Domains 2 and 3) so that the size of the limit cycle is increased.

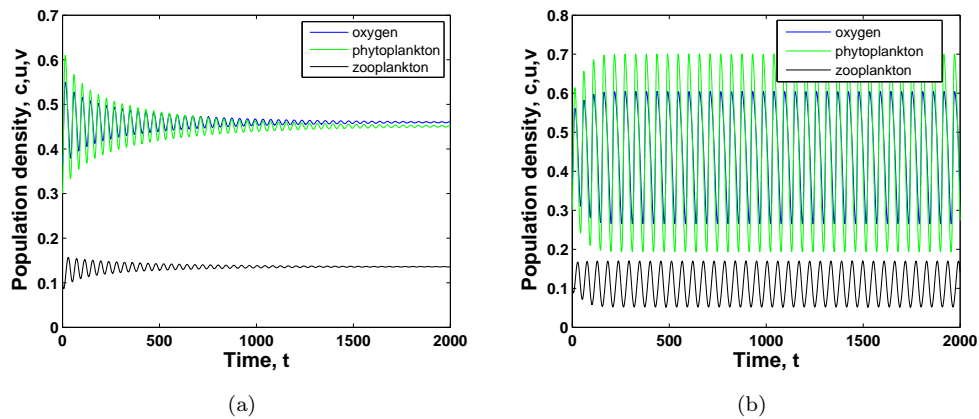


FIGURE 4.14: Effect of changes in parameter A . The density of oxygen, phytoplankton and zooplankton against time obtained for other given parameter values (a) $A = 1.95$, $c_1 = 0.659$, (b) $A = 1.99$, $c_1 = 0.659$. The initial conditions are $c_o = 0.385$, $u_o = 0.3$, $v_o = 0.1$. Other parameters are given in the text.

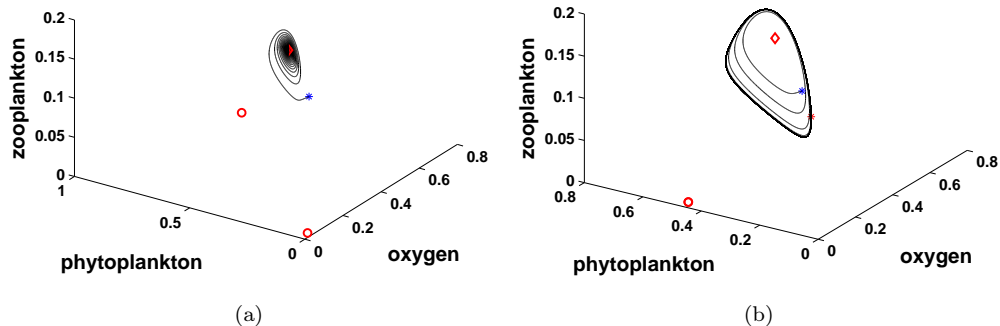


FIGURE 4.15: Trajectories of the oxygen-phyto-zooplankton dynamical system shown in the corresponding 3D phase space. Blue star shows initial values, red star for end point and red circle for steady state of the $(\dot{c}, \dot{u}, 0)$, while red diamond for $(\ddot{c}, \ddot{u}, \ddot{v})$ (a) $A = 1.95$, $c_1 = 0.659$, (b) $A = 1.99$, $c_1 = 0.659$. The initial conditions are $c_o = 0.385$, $u_o = 0.3$, $v_o = 0.1$; other parameters are the same as in Fig. 4.14.

The corresponding three dimensional phase space of Figure 4.14 is given by Figure 4.15 to trace the changes in system properties in another way. Here, in all phase spaces (Figs. 4.2a-b), red circles represent the positive steady states belonging to E_2 , while red diamond presents the coexistence steady state E_3 . The blue star shows the initial conditions, i.e. the starting point of the trajectory, while red star corresponds to end point of system trajectory reached over the given

simulation time. Special attention should be paid to Fig. 4.15b. There is only one red circle, meaning that for these specific values of A and c_1 , system isoclines do not intersect, they only touch each other at one point; see the illustration in Fig. 4.2a.

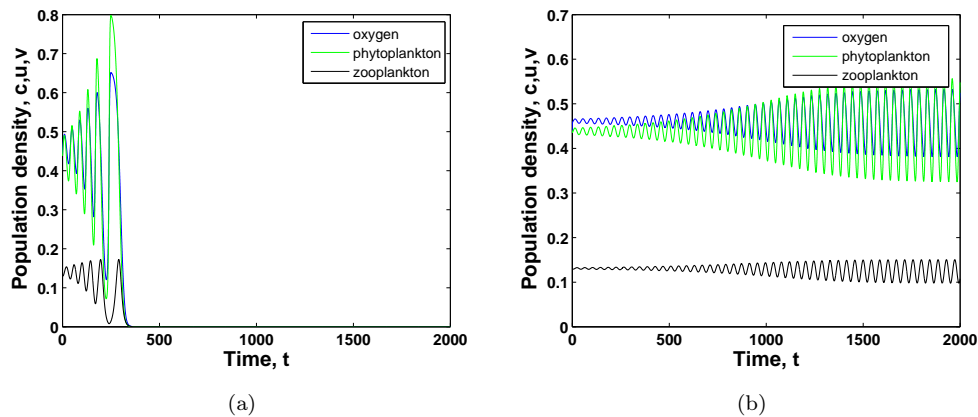


FIGURE 4.16: Effect of changes in parameter c_1 . The density of oxygen, phytoplankton and zooplankton against time obtained for other given parameter values (a) $A = 2$, $c_1 = 0.659$, (b) $A = 2$, $c_1 = 0.685$. The initial conditions are $c_o = 0.44$, $u_o = 0.44$, $v_o = 0.13$. Other parameters are given in the text.

Figure 4.16 shows the oxygen concentration and phyto-zooplankton densities versus time obtained for the same value of $A = 2$ and two different values of c_1 . The limit cycle disappears for parameters of Fig. 4.16a, so that the species densities go to extinction after just a few oscillations. For $c_1 = 0.685$ (Fig. 4.16b), parameters are further into Domain 3, and consequently the system eventually develops periodic oscillations. Figure 4.17 shows the corresponding three dimensional phase space for parameter values given in Fig. 4.16. It is seen that when initial conditions chosen around E_3 , the limit cycle grows in size and approaches the first saddle point, $E_2^{(1)}$, and then $E_2^{(2)}$ see Fig. 4.17a. Eventually, the trajectory goes to origin (extinction state) which is always stable. For an increase in c_1 (Fig. 4.17b), the trajectory grows in time then it retains its regular structure.

Figure 4.18 shows the oxygen concentration and plankton densities versus time for given parameter values. For $A = 4$ (Fig. 4.18a), system parameters are in Domain 4, so there is no limit cycle unsurprisingly the initial conditions promptly converge to zero. Note that extinction is preceded by an outbreak, so that the initial values first show a significant increase before all system components go extinct in the course of time and (Fig. 4.18b) the system possesses a stable limit

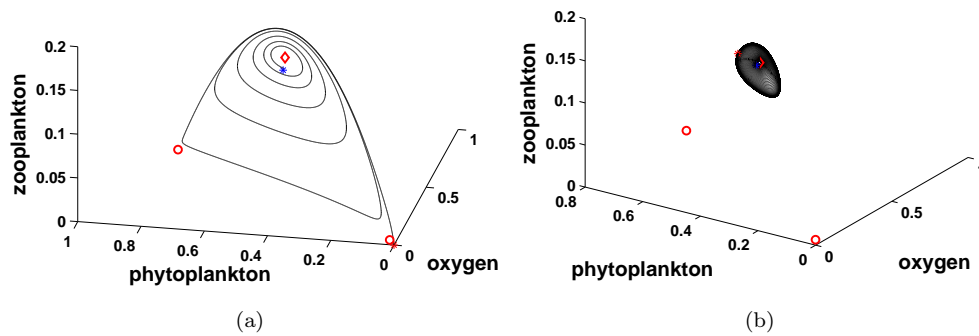


FIGURE 4.17: Trajectories of the oxygen-phyto-zooplankton dynamical system shown in the corresponding 3D phase space. Blue star show initial values, red star for end point and red circle for steady state of the $(\dot{c}, \dot{u}, 0)$, while red diamond for $(\ddot{c}, \ddot{u}, \ddot{v})$ (a) $A = 2$, $c_1 = 0.659$, (b) $A = 2$, $c_1 = 0.685$. The initial conditions are $c_o = 0.44$, $u_o = 0.44$, $v_o = 0.13$; other parameters are the same as in Fig. 4.16.

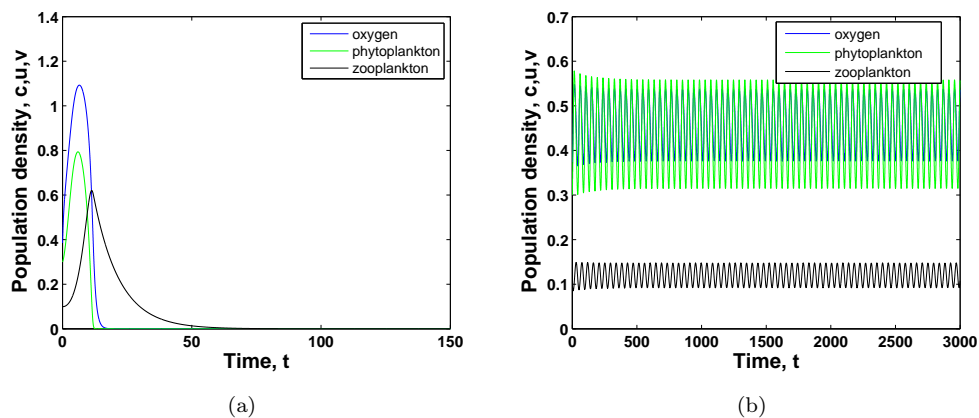


FIGURE 4.18: Effect of changes in parameter A . The density of oxygen, phytoplankton and zooplankton against time obtained for other given parameter values (a) $A = 4$, $c_1 = 0.7$, (b) $A = 2.02$, $c_1 = 0.7$. The initial conditions are $c_o = 0.385$, $u_o = 0.3$, $v_o = 0.1$. Other parameters are given in the text.

cycle (i.e. the parameters are in Domain 3), where the coexistence state E_3 is an unstable focus², system develops periodic oscillations.

Fig. 4.19 shows the corresponding three dimensional phase space of Fig. 4.18. Interestingly, in spite of the choice of the same initial value, the system dynamics move to different steady states. In the case of $A = 4$ (Fig. 4.18a and Fig. 4.19a), all system components go extinct. This is not a surprising ecological issue due to excessive increase on zooplankton density (see Eq. (4.17)), under the effect of increasing A) makes a decrease on phytoplankton density due to excessive predation

²This type of equilibrium exists when it has one real eigenvalue with the sign same to the sign of the real part of a pair of complex-conjugate eigenvalues.

effect and then oxygen concentration decreases below its critical level. However, for $A = 2.02$ (Fig. 4.18b), system components develop periodic oscillations with same amplitudes.

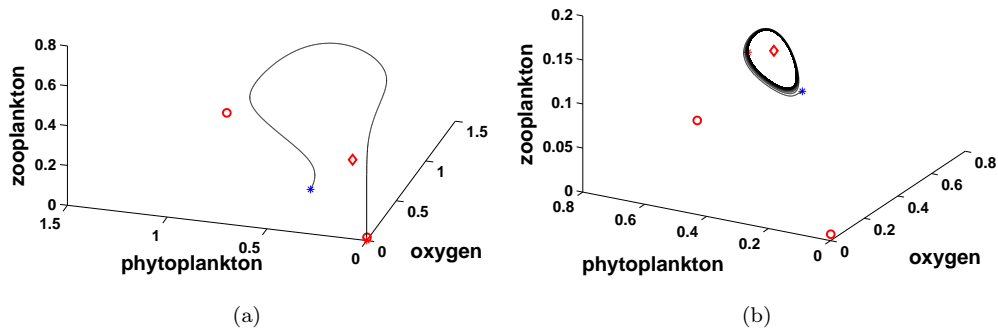


FIGURE 4.19: Trajectories of the oxygen-phyto-zooplankton dynamical system shown in the corresponding 3D phase space. Blue star shows initial values, red star for end points and red circle for steady state of the $(\dot{c}, \dot{u}, 0)$, while red diamond for $(\ddot{c}, \ddot{u}, \ddot{v})$ (a) $A = 4$, $c_1 = 0.7$, (b) $A = 2.02$, $c_1 = 0.7$. The initial conditions are $c_o = 0.385$, $u_o = 0.3$, $v_o = 0.1$; other parameters are the same as in Fig. 4.18.

The succession of dynamical regimes observed under the effect of an increase in parameter A is focused on in Figs. 4.20-4.21 (i.e. the parameters are chosen through Domain 3 to 4). Oxygen concentration and plankton densities are plotted against time for different values of A and a fixed value of c_1 . With increasing A , we observe an increase in amplitude of periodic oscillations for all components; see Figs. 4.20a-c. System's trajectories can be seen from corresponding phase spaces; see Figs. 4.21a-c and also Appendix C. However, a further increase in A leads to extinction, after just a few oscillations; see Figs. 4.20d and 4.21d. For initial values chosen around the coexistence steady state E_3 , the system remains in the vicinity of E_3 (see Figs. 4.20a-c) and limit cycle evolves around this steady state. The succession of Fig. 4.20d is an expected result of our dynamical system response to the further increase on A , as it is seen in Fig. 4.13a and Fig. 4.13b.

It should be emphasized that in the parameter range where the stable limit cycle exists, i.e. Domain 3, the system has two attractors: the limit cycle itself and the extinction state E_1 . Hence the dynamics depend on the initial conditions, i.e. which basin of attraction they belong to. For the results shown in Figs. 4.20a-c and 4.21a-c, the initial conditions were chosen from the attraction basin of the limit cycle. In case the initial conditions are chosen from the attraction basin

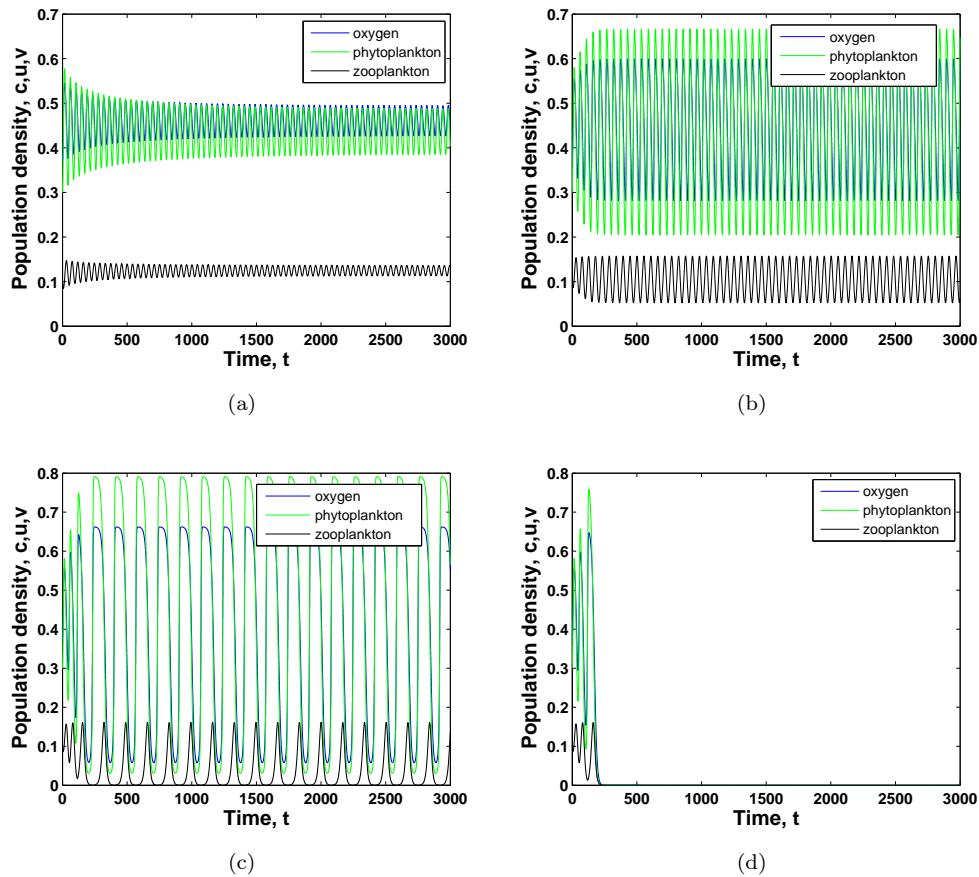


FIGURE 4.20: Effect of changes in parameter A . The density of oxygen, phytoplankton and zooplankton versus time obtained for (a) $A = 2.01$, $c_1 = 0.7$, (b) $A = 2.04$, $c_1 = 0.7$, (c) $A = 2.0534$, $c_1 = 0.7$, (d) $A = 2.054$, $c_1 = 0.7$. In all cases, the initial conditions are $c_o = 0.385$, $u_o = 0.3$, $v_o = 0.1$. Other parameters are the same as in previous ones.

of E_1 , the dynamics are less interesting as the trajectories approach the origin without any oscillations (not shown here).

Note that, the dynamical response of changing values of A is focused to understand the underlying properties of the dynamics around the system steady states. These results hold the key that oxygen production rate A is important to support the existence and stability of marine plankton systems. Therefore, in the following chapter (Chapter 5), we will focus on the issue of our systems' dynamical response to the changing environmental conditions, i.e. global climate change.

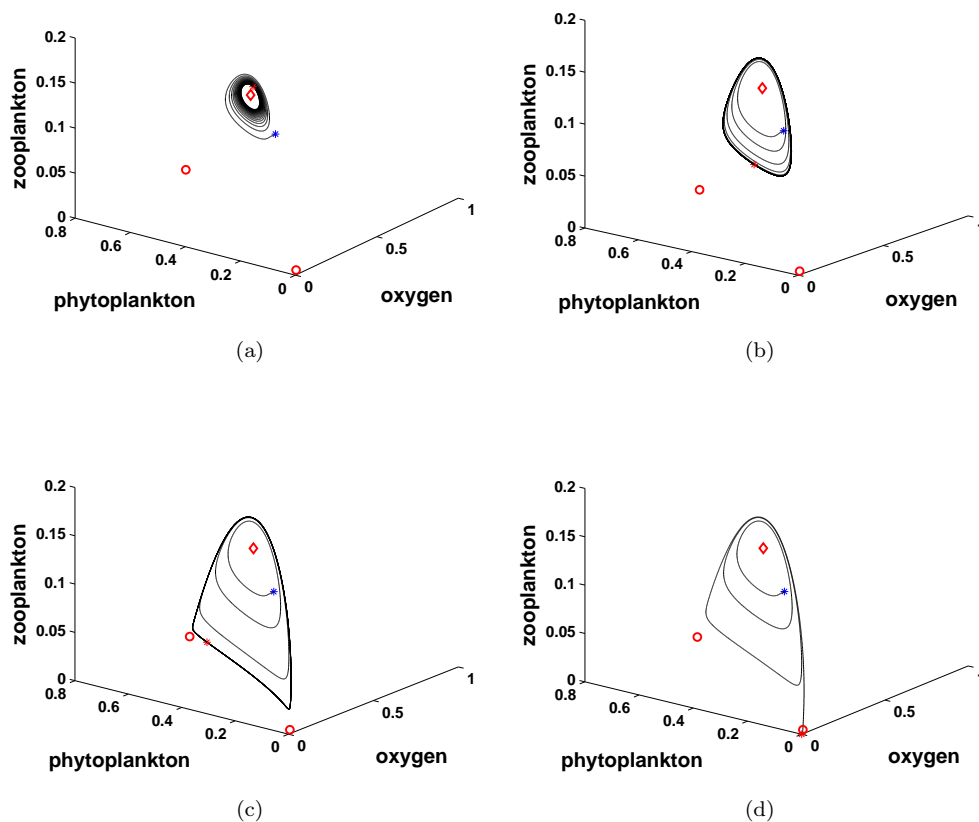


FIGURE 4.21: Phase space trajectory is given for oxygen-phytoplankton-zooplankton and blue star for initial values, red star for end points and red circle for steady state of the $(\dot{c}, \dot{u}, 0)$, while red diamond for $(\tilde{c}, \tilde{u}, \tilde{v})$ of the system components (a) $A = 2.01$, $c_1 = 0.7$, (b) $A = 2.04$, $c_1 = 0.7$, (c) $A = 2.0534$, $c_1 = 0.7$, (d) $A = 2.054$, $c_1 = 0.7$ and the initials are $c_o = 0.385$, $u_o = 0.3$, $v_o = 0.1$; other parameters are the same as in Fig. 4.20.

4.3.2 Spatial pattern in 1D

We now extend the model to include a spatial components which is described as follows:

$$\frac{\partial c}{\partial t} = D_T \frac{\partial^2 c}{\partial x^2} + A \left(1 - \frac{c}{c+1}\right) u - c - \frac{uc}{c+c_2} - \frac{\nu cv}{c+c_3}, \quad (4.20)$$

$$\frac{\partial u}{\partial t} = D_T \frac{\partial^2 u}{\partial x^2} + \left(\frac{Bc}{c+c_1} - u\right) \gamma u - \frac{uv}{u+h} - \sigma u, \quad (4.21)$$

$$\frac{\partial v}{\partial t} = D_T \frac{\partial^2 v}{\partial x^2} + \left(\frac{\beta uv}{u+h}\right) \frac{c^2}{c^2+c_4^2} - \mu v. \quad (4.22)$$

Here c , u and v have the previous meanings, i.e. $c = c(x, t)$ is the concentration of oxygen, $u = u(x, t)$ and $v = v(x, t)$ are the densities of phytoplankton

and zooplankton, respectively, at time t and position x with the coefficient of turbulent diffusion D_T [165, 183]. The specific form of the model Eqs. (4.20-4.22) and assumptions on the model construction can be easily found in [227].

The model system (4.20-4.22) is solved numerically in a finite domain $0 < x < L$ where L is the domain length, by the finite difference method with zero-flux boundary condition and mesh steps chosen to be $\Delta x = 0.5$ and $\Delta t = 0.01$. The magnitude of mesh steps has been checked to be sufficiently small in order to avoid numerical artefact. The spatial system (4.20-4.22) is in its dimensionless form where $A, B, \sigma, \gamma, \beta, \mu, c_1, c_2, c_3, c_4, \nu$ and h are defined through the original parameters as in Section 4.2.

4.3.3 System spatial dependence to the chosen initial conditions

The choice of the different initial conditions is a subtle issue and may result in very different spatiotemporal dynamics [147]. Therefore, in this section we focus on our dynamical system's (4.20-4.22) response to the different initial conditions. We assume the initial distributions as describing a zooplankton patch in space with uniformly distributed oxygen and phytoplankton at the level of their steady states:

$$c(x, 0) = c_0, \quad (4.23)$$

$$u(x, 0) = u_0, \quad (4.24)$$

$$v(x, 0) = v_0 \quad \text{for } |x_i| < \epsilon, \quad \text{otherwise } v(x, 0) = 0, \quad (4.25)$$

where c_0, u_0 and v_0 are the initial densities (as given by the positive equilibrium E_3 see Section 4.2.1) and ϵ is the patch diameter. The results shown below are obtained for $v_0 = 0.5$ and $\epsilon = 100$. We consider the dynamics of the system (4.20-4.22) for different values of A and time, while keeping other parameters fixed at some hypothetical values as $B = 1.8, \gamma = 1.2, \sigma = 0.1, c_2 = 1, c_3 = 1, c_4 = 1, \nu = 0.01, \beta = 0.7, \mu = 0.1, h = 0.1, L = 1000, c_1 = 0.7$ and vary A .

Figure 4.22 shows the spatial system's (4.20-4.22) response to the initial condition given by Eqs. (4.23–4.25) for two different time moments. In the wake of the population fronts chaotic oscillations emerge which are preceded by a plateau corresponding to system's steady states (see similar succession for prey-predator system in [147] in Chapter 10.)

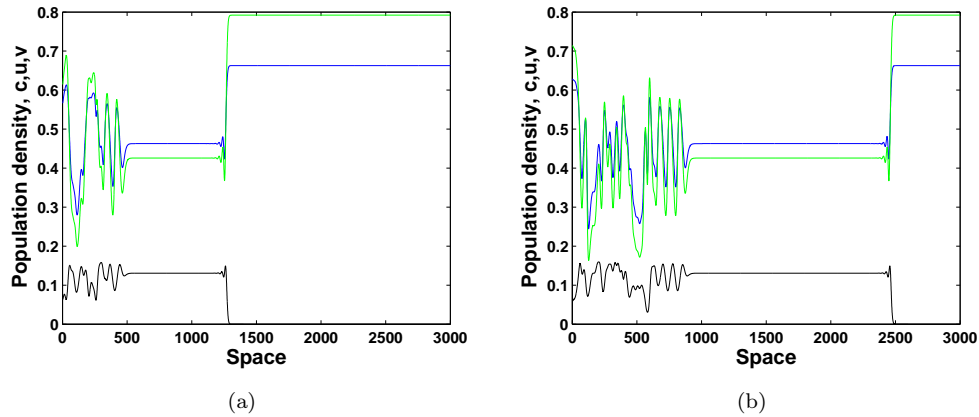


FIGURE 4.22: The density of oxygen-phytoplankton-zooplankton against space obtained for (a) $A = 2.054$, $t = 2000$, (b) $A = 2.054$, $t = 4000$ and system parameters are same as in nonspatial system with the initials $c_0 = 0.385$, $u_0 = 0.3$, $v_0 = v_0$. Other parameters are given in the text.

We now consider the choice of initial conditions as the perturbation of the homogeneous distribution in terms of zooplankton and the ‘constant-gradient’ distribution is as follows:

$$c(x, 0) = c_0, \quad (4.26)$$

$$u(x, 0) = u_0, \quad (4.27)$$

$$v(x, 0) = v_0 + \epsilon x + \delta \quad (4.28)$$

where c_0 , u_0 and v_0 are the steady states of the system components and ϵ , δ are parameters (see more details on the choice of initials (4.26–4.28) in [147] in Chapter 11). Figure 4.23 shows the system’s spatial response to the initial conditions (4.26–4.28) for $\epsilon = 10^{-5}$, $\delta = 0.01$. The system’s smooth spatial distribution is led by an irregular structure in space for both $t = 1000$ and $t = 3000$. For Fig. 4.23b, the irregular structure is followed by a plateau.

Figure 4.24 shows the spatial distribution of system (4.20–4.22) for initial conditions by given Eqs. (4.26–4.28) and for $\epsilon = 10^{-5}$, $\delta = -1.5 \cdot 10^{-2}$ for different time moments. In this case, the irregular dynamical pattern is restricted by a smooth spatial distribution from both the left and right-hand side. The size of the irregular structure grows with time. It seems that for the initial by Eqs. (4.26–4.28), the choice of δ affects the system’s spatial dynamics.

Figures 4.22–4.24 illustrate some technical work done on the choice of appropriate initial conditions. The obtained results from above simulations show that the spatial distribution of system components are sensitive to the chosen

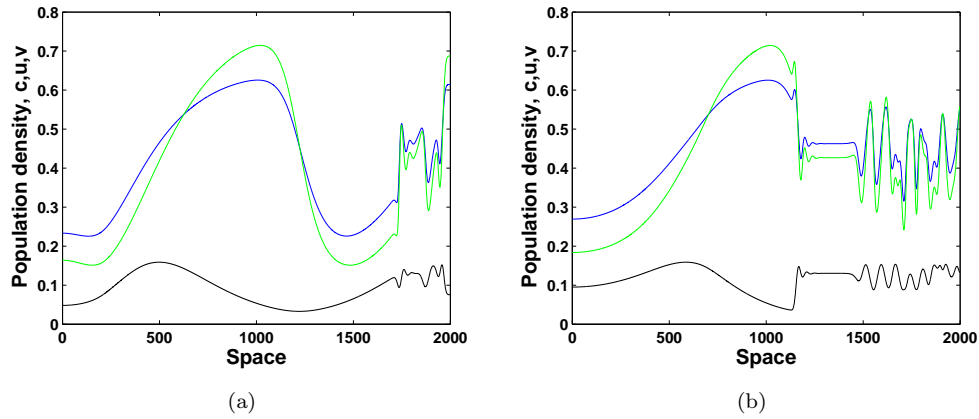


FIGURE 4.23: The density of oxygen-phytoplankton-zooplankton against space obtained for (a) $A = 2.05$, $t = 1000$, (b) $A = 2.05$, $t = 3000$. Other parameters are given in the text.

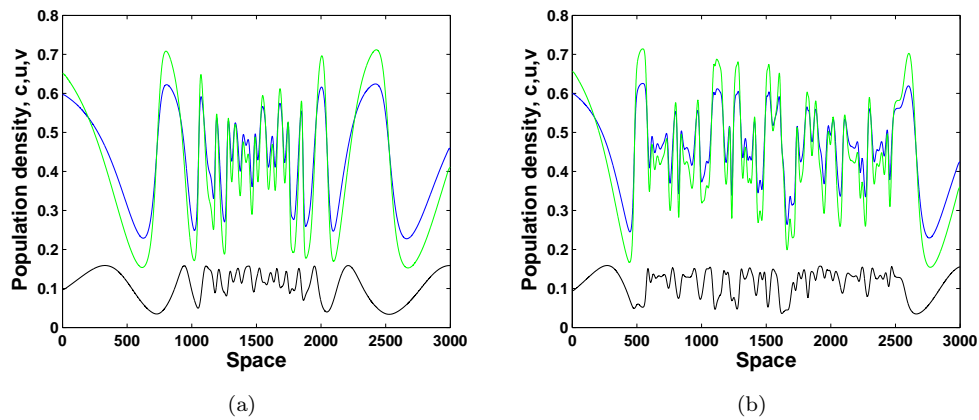


FIGURE 4.24: The density of oxygen-phytoplankton-zooplankton against space obtained for other given parameter values (a) $A = 2.05$, $t = 1000$, (b) $A = 2.05$, $t = 2000$. Other parameters are given in the text.

initial conditions.

Note that in real world systems, plankton's horizontal distribution in water body is not homogeneous but rather exhibits patchiness [256]. There are many papers on plankton patterns [48, 200, 210, 269]. Field research on plankton patchy structure shows that its spatial distribution is controlled by turbulence mixing and some biological process of the plankton community, such as growth, mortality, predation etc. [132, 190, 200, 246] (look further details on plankton patchiness in Chapter 1). In light of the literature on real plankton distribution, when we assume initial values as in Eqs.(4.29–4.31), numerical simulations generate appropriate patchiness corresponding to plankton distribution in nature. The initial species distribution is patchy for zooplankton with uniformly distributed oxygen

and phytoplankton in space:

$$c(x, 0) = c_0, \quad (4.29)$$

$$u(x, 0) = u_0, \quad (4.30)$$

$$v(x, 0) = \left(x - \frac{L}{2}\right) \frac{\epsilon}{L} + v_0, \quad (4.31)$$

where c_0 , u_0 and v_0 are the steady states of E_3 and ϵ is the patch diameter which is $\epsilon = 0.02$. In all our numerical simulations shown in this section, we fix parameters at some hypothetical values as $B = 1.8$, $\gamma = 1.2$, $\sigma = 0.1$, $c_2 = 1$, $c_3 = 1$, $c_4 = 1$, $\nu = 0.01$, $\beta = 0.7$, $\mu = 0.1$, $h = 0.1$, $\epsilon = 0.02$, $L = 1000$ and vary A and c_1 . Note that in all following spatial dynamics this initial distribution is used. The initial condition given by Eqs. (4.29–4.31) develops patchy structure and this patchiness is checked for different values of A , i.e. $A = 2.02$, $A = 2.05$, $A = 2.09$ and $A = 2.2$. The following series of Figs. 4.25–4.27 show the spatial structure of initial distribution of system components for different values of A . Here, the patchy structure obtained for $A = 2.09$ is not shown for the sake of brevity.

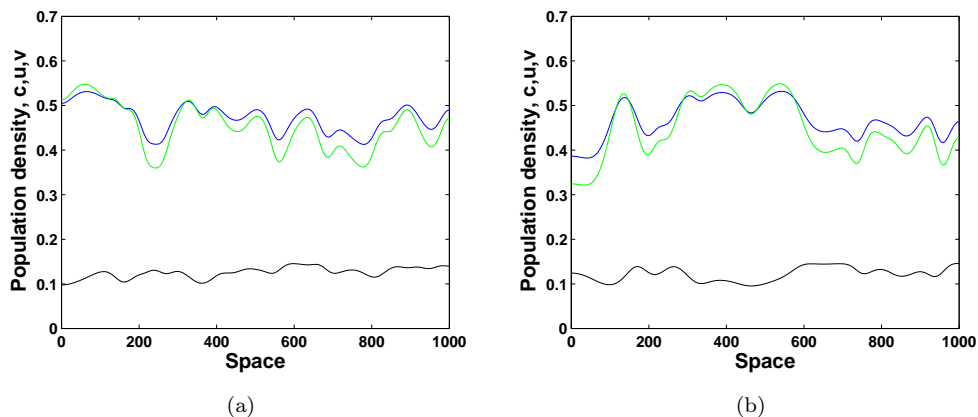


FIGURE 4.25: Initial distribution of oxygen-phytoplankton-zooplankton against space obtained for (a) $A = 2.02$, $t = 10000$, (b) $A = 2.02$, $t = 12000$ and other parameters are given in the text.

Spatial distributions of oxygen and plankton obtained from Eqs. (4.29–4.31) are given in Fig. 4.25a (obtained for $t = 10000$) and Fig. 4.25b (obtained for $t = 12000$) for $A = 2.02$. Spatial variations of the system components become remarkably irregular and qualitatively similar to what is observed in reality.

Figure 4.26 presents the initial distribution (4.29–4.31) for $A = 2.05$, for different time moments. Note that, the system develops more patchiness for Fig. 4.26

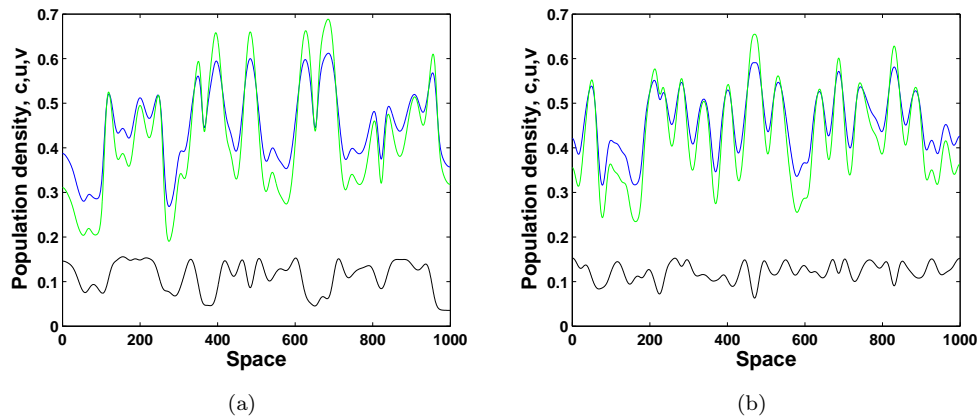


FIGURE 4.26: Initial distributions of oxygen-phytoplankton-zooplankton over space obtained for other given parameter values (a) $A = 2.05$, $t = 10000$, (b) $A = 2.05$, $t = 12000$ and system other parameters are given in the text.

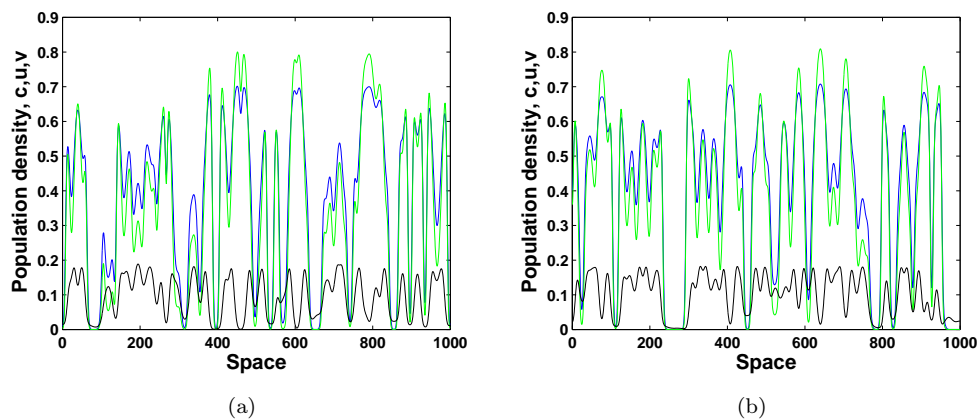


FIGURE 4.27: Initial distributions of oxygen-phytoplankton-zooplankton against space obtained for (a) $A = 2.2$, $t = 10000$, (b) $A = 2.2$, $t = 12000$ and other parameters are given in text.

than Fig. 4.25. Figure 4.27 shows the spatial distribution of model system (4.20–4.22) for $A = 2.2$ and for different time moments. In this case, the initial distributions (4.29–4.31) lead to the strongly irregular patch dynamics occupying the whole domain. Note that for different A parameters spatial distribution of oxygen and plankton obtained from Eqs. (4.20–4.22) is patchy and there is no notable qualitative difference between the distributions shown in Fig. 4.25a obtained for $t = 10000$ and Fig. 4.25b obtained for $t = 12000$, which indicates that the system has reached its dynamical equilibrium. Therefore, we consider distribution shown in Fig. 4.25a as ‘inherent’ and use it as the initial condition for the following simulations.

As a next step, having chosen appropriate initial condition we aim to investigate the effect of varying A and c_1 on plankton dynamics. Figure 4.28 shows the

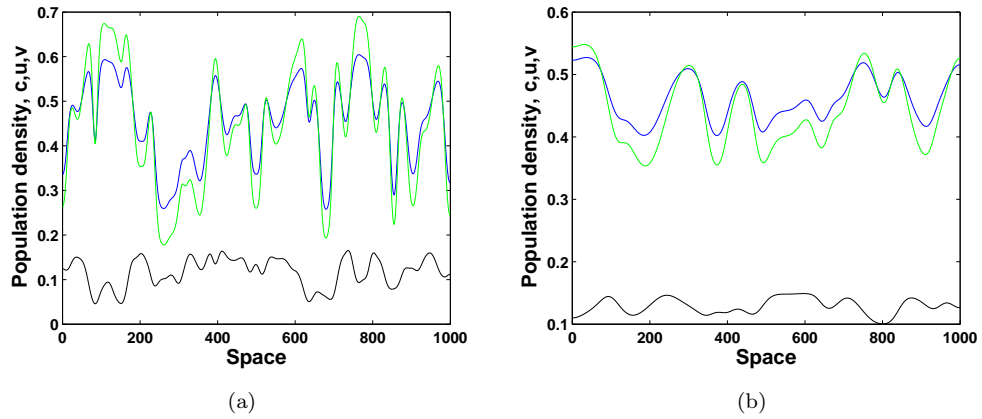


FIGURE 4.28: The effect of changes in parameter c_1 . The density of oxygen-phytoplankton-zooplankton over space obtained for (a) $A = 2$, $c_1 = 0.659$ and $t = 10000$, (b) $A = 2$, $c_1 = 0.685$ and $t = 10000$ and other parameters are as in Fig. 4.16. The initial conditions are shown as in Fig. 4.25a.

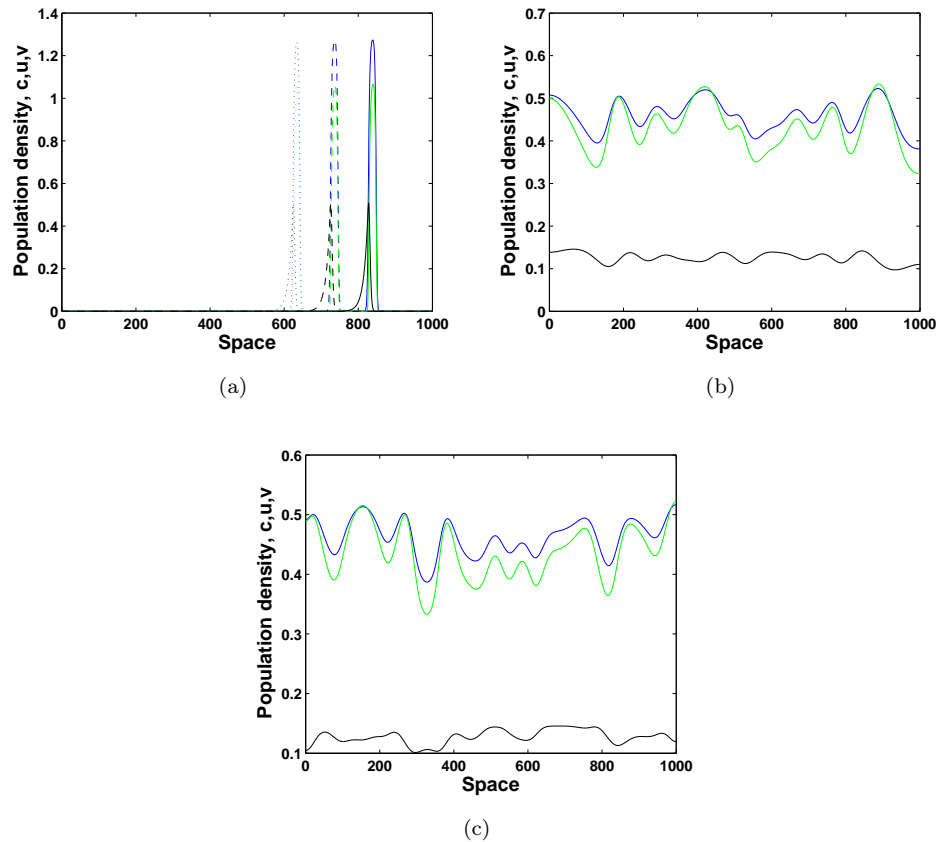


FIGURE 4.29: The effect of changes in parameter A to distributions of oxygen-phytoplankton-zooplankton over space obtained for other given parameter values (a) $A = 4$, $t = 150$ (dotted line), $t = 250$ (dashed line), $t = 350$ (solid line), (b) $A = 2.02$, $t = 3000$, (c) $A = 2.02$, $t = 10000$ for $c_1 = 0.7$ and other parameters are given in the text and same as in Fig. 4.18. The initial conditions are shown as in Fig. 4.25a.

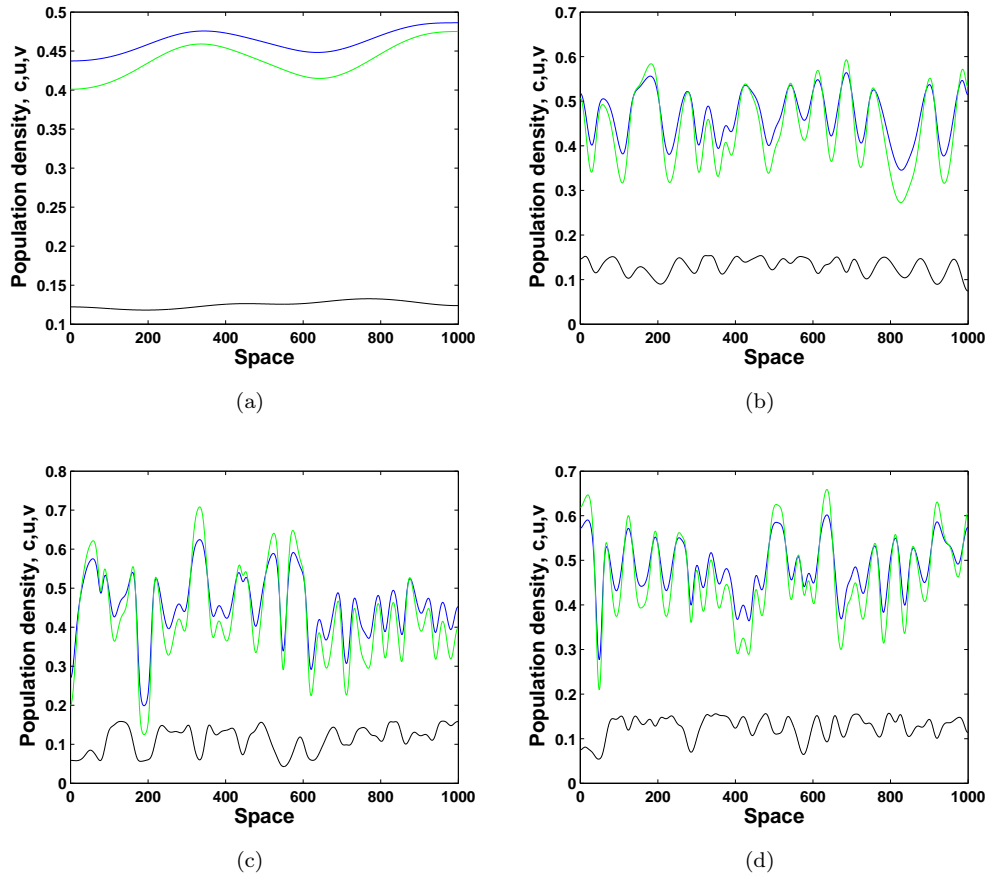


FIGURE 4.30: The effect of changes in parameter A distribution of oxygen, phytoplankton and zooplankton over space obtained for (a) $A = 2.01$, (b) $A = 2.04$, (c) $A = 2.0534$, (d) $A = 2.054$ for fixed $c_1 = 0.7$ at $t = 3000$ and the other parameters are as in Fig. 4.20. The initial conditions are shown as in Fig. 4.25a.

spatial distribution of corresponding nonspatial system given by Fig. 4.16. The initials (4.29–4.31) lead to a patchy distribution in the spatial case, while in the corresponding nonspatial case the local dynamics results in extinction and periodic oscillations; see Fig. 4.16a and Fig. 4.16b, respectively. In the spatially explicit case the system dynamics is proven to be sustainable and the irregular pattern persists.

Fig. 4.29a shows the spatial distribution of the corresponding nonspatial systems' oxygen, phytoplankton and zooplankton distribution in time given in Fig. 4.18. Corresponding to the species extinction in the nonspatial system, the spatial case results in travelling wave solutions for intermediate time, while the system components go extinct in the large time limit. In Fig. 4.29a, zooplankton density reaches its maximum before the moment that oxygen and phytoplankton reach their maxima. Fig. 4.29b and Fig. 4.29c show the system's formation of spatiotemporal patterns for different time moments $t = 3000$ and $t = 10000$. For

this values of A given in Fig. 4.18b, the local dynamics develop periodic oscillations.

Fig. 4.30 shows the evolution of the spatial distribution of system components for the same parameter values given in Fig. 4.20. Contrary to the nonspatial system, where species extinction was observed (Fig. 4.20d), the spatial system persists, and exhibits patchy distribution (Fig. 4.30d). For these value of A (Fig. 4.30), the nonspatial system develops periodic oscillations of different size depending the parameter values domain(see Fig.4.13). But in spatial case irregular spatiotemporal pattern persist and no extinction occurs.

So far, we have focused on one spatial dimension. We further this study to include two spatial dimensions.

4.3.4 Pattern formation in 2D

Throughout this section, we attempt to investigate spatiotemporal dynamics of the oxygen-plankton system (4.20-4.22) extended to two dimensions which is described as follows:

$$\frac{\partial c(x, y, t)}{\partial t} = D_T \left(\frac{\partial^2 c}{\partial x^2} + \frac{\partial^2 c}{\partial y^2} \right) + A \left(1 - \frac{c}{c+1} \right) u - c - \frac{uc}{c+c_2} - \frac{\nu cv}{c+c_3} \quad (4.32)$$

$$\frac{\partial u(x, y, t)}{\partial t} = D_T \left(\frac{\partial^2 u}{\partial x^2} + \frac{\partial^2 u}{\partial y^2} \right) + \left(\frac{Bc}{c+c_1} - u \right) \gamma u - \frac{uv}{u+h} - \sigma u, \quad (4.33)$$

$$\frac{\partial v(x, y, t)}{\partial t} = D_T \left(\frac{\partial^2 v}{\partial x^2} + \frac{\partial^2 v}{\partial y^2} \right) + \left(\frac{\beta uv}{u+h} \right) \frac{c^2}{c^2+c_4^2} - \mu v, \quad (4.34)$$

where all system notations have their usual previous meanings with $0 < x < L_x$ and $0 < y < L_y$. The length of the domain L_x and the width of the domain L_y are chosen equal and Neumann-boundary conditions are imposed at the domain boundaries. In order to examine the behavior of the system's dynamics, two different types of initial conditions are used. The first initial distribution case, describes spatially homogeneous distributions for both oxygen and phytoplankton at their steady states, while the second case describes spatially homogeneous distribution for only oxygen at its steady states with a constant-gradient plankton distribution. For the first case, the initial distribution of system components is as follows:

$$c(x, y, 0) = c_0, \quad (4.35)$$

$$u(x, y, 0) = u_0, \quad (4.36)$$

$$v(x, y, 0) = v_0 - \epsilon_2(x - 150) - \epsilon_3(y - 150), \quad (4.37)$$

where $\epsilon_2 = 3.10^{-5}$ and $\epsilon_3 = 6.10^{-5}$. For more details on initial conditions choice; see prey-predator system in [156]. Parameter values are chosen as in one-dimensional case Section 4.3.2 as $c_1 = 0.7$, $c_2 = 1$, $c_3 = 1$, $c_4 = 1$, $\nu = 0.01$, $B = 1.8$, $\gamma = 1.2$, $\beta = 0.7$, $\mu = 0.1$, $h = 0.1$, $\sigma = 0.1$ and for varying A values. The distribution of phytoplankton and oxygen exhibit qualitatively similar behavior, hence only the oxygen concentration is shown. Some snapshots of the system dynamics for initial conditions given by Eqs. (4.35-4.37) are shown for the following series of Figs. 4.31-4.37.

For the latter case, the initial distribution of system components is as follows:

$$c(x, y, 0) = c_0, \quad (4.38)$$

$$u(x, y, 0) = u_0 - \epsilon_1(x - 180)(x - 220) - \epsilon_2(y - 90)(y - 210), \quad (4.39)$$

$$v(x, y, 0) = v_0 - \epsilon_2(x - 150) - \epsilon_3(y - 150), \quad (4.40)$$

where $\epsilon_1 = 2.10^{-7}$, $\epsilon_2 = 6.10^{-7}$ and $\epsilon_3 = 3.10^{-5}$ (cf. [156] for the choice of the initial conditions). Some snapshots of the system dynamics for initial conditions given by Eqs. (4.38-4.40) are shown in the following series of Figs. 4.38-4.41.

Simulations were performed for a larger domain Fig. 4.42 for the following initials.

$$c(x, y, 0) = c_0, \quad (4.41)$$

$$u(x, y, 0) = u_0 - \epsilon_1(x - 180)(x - 420) - \epsilon_2(y - 90)(y - 210), \quad (4.42)$$

$$v(x, y, 0) = v_0 - \epsilon_2(x - 250) - \epsilon_3(y - 250), \quad (4.43)$$

where ϵ_1 , ϵ_2 and ϵ_3 have their previous values as in initial distributions (4.38-4.40).

This section begins with an insight into the pattern formation in two-dimensional case, with special attention paid to the system response to the changes in parameter A due to the reality on plankton patchiness have controlled by some environmental factors [47, 70, 192].

In Fig. 4.31, some snapshots of the oxygen concentration arising from the initial distributions given by Eqs. (4.35-4.37) for different t are shown for $A = 2.01$ with all other parameters kept as in one-dimension. It should be emphasized here that in two-dimensional case the scenario seems qualitatively similar to the one-dimensional case; see Fig. 4.30a. The distribution of oxygen concentration is rather smooth and persistent in time, except the size of stripes. Here the distribution of phytoplankton is quite similar with the concentration of oxygen. For this reason,

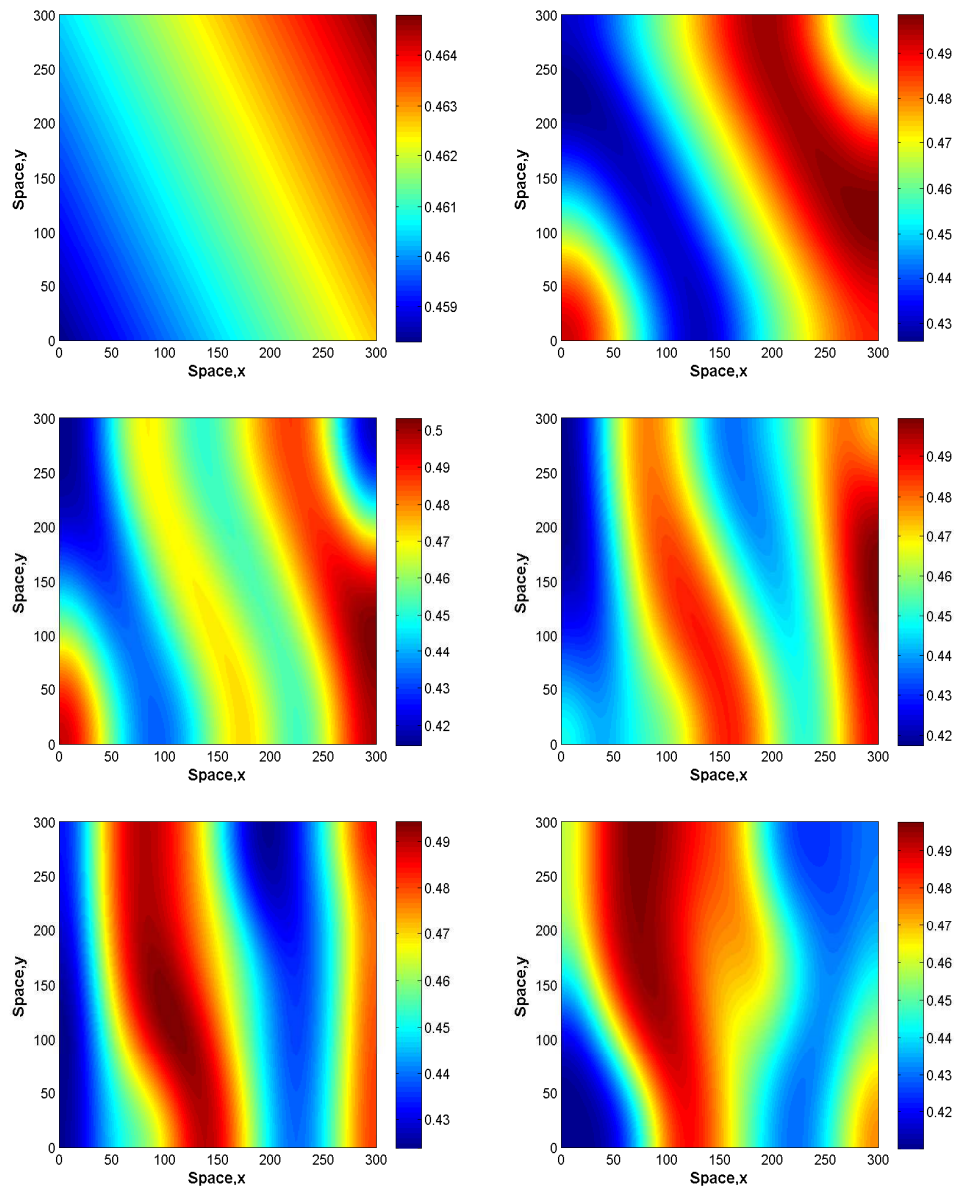


FIGURE 4.31: Spatial distribution of the oxygen concentration in the two-dimensional case for $t = 1$, $t = 1000$, $t = 3000$, $t = 4000$, $t = 5000$, and $t = 6000$ from left to right, top to bottom for $A = 2.01$ and the other parameters are as given in the text with given initials $c_0 = 0.4616$, $u_0 = 0.4360$, $v_0 = 0.1260$. The initial conditions are given by Eqs. (4.35-4.37). The distribution of phytoplankton exhibits qualitatively similar patterns. For large time limit the distribution of oxygen retains its shape with changing size of stripes.

we choose only the spatial distribution of oxygen in water body to show in the two-dimensional case.

Figure 4.32 shows snapshots of oxygen distribution at the same time moments as in Fig. 4.31. Although the initial distributions given by Eqs. (4.35-4.37) are same, here the smooth pattern at intermediate time is preceded by the patchy structure. Note that this patchy structure corresponds to the one dimensional case;

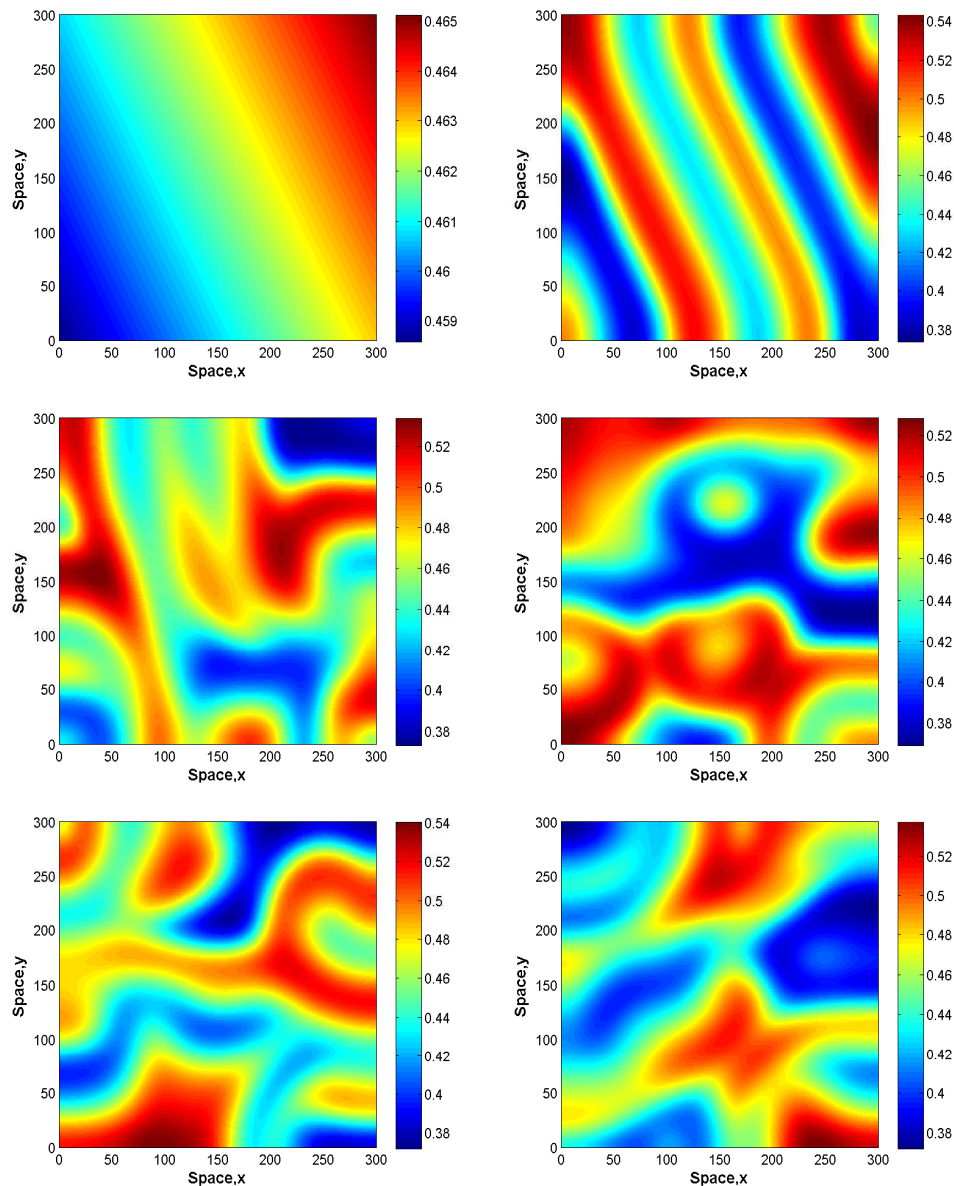


FIGURE 4.32: Spatial distribution of the oxygen concentration in the two-dimensional case for $t = 1$, $t = 1000$, $t = 3000$, $t = 4000$, $t = 5000$, and $t = 6000$ from left to right, top to bottom for $A = 2.02$ and the other parameters are as given in the text with given initials $c_0 = 0.4618$, $u_0 = 0.4337$, $v_0 = 0.1271$. The initial conditions are given by Eqs. (4.35-4.37). Oxygen concentration shows qualitatively similar behavior with phytoplankton spatial distribution. The patchy structure resulted from the destructions of stripy structures.

see Fig. 4.29b-c. For this value of A , both in one-dimension and in two-dimensions the system is sustainable and the irregular dynamics persist.

Figure 4.33 shows that the irregular patchy structure is preceded by the stripy structure; see Fig. 4.26 for the corresponding one dimensional case. It appears that a hypothesis can be made in relation to A and the evolution of the

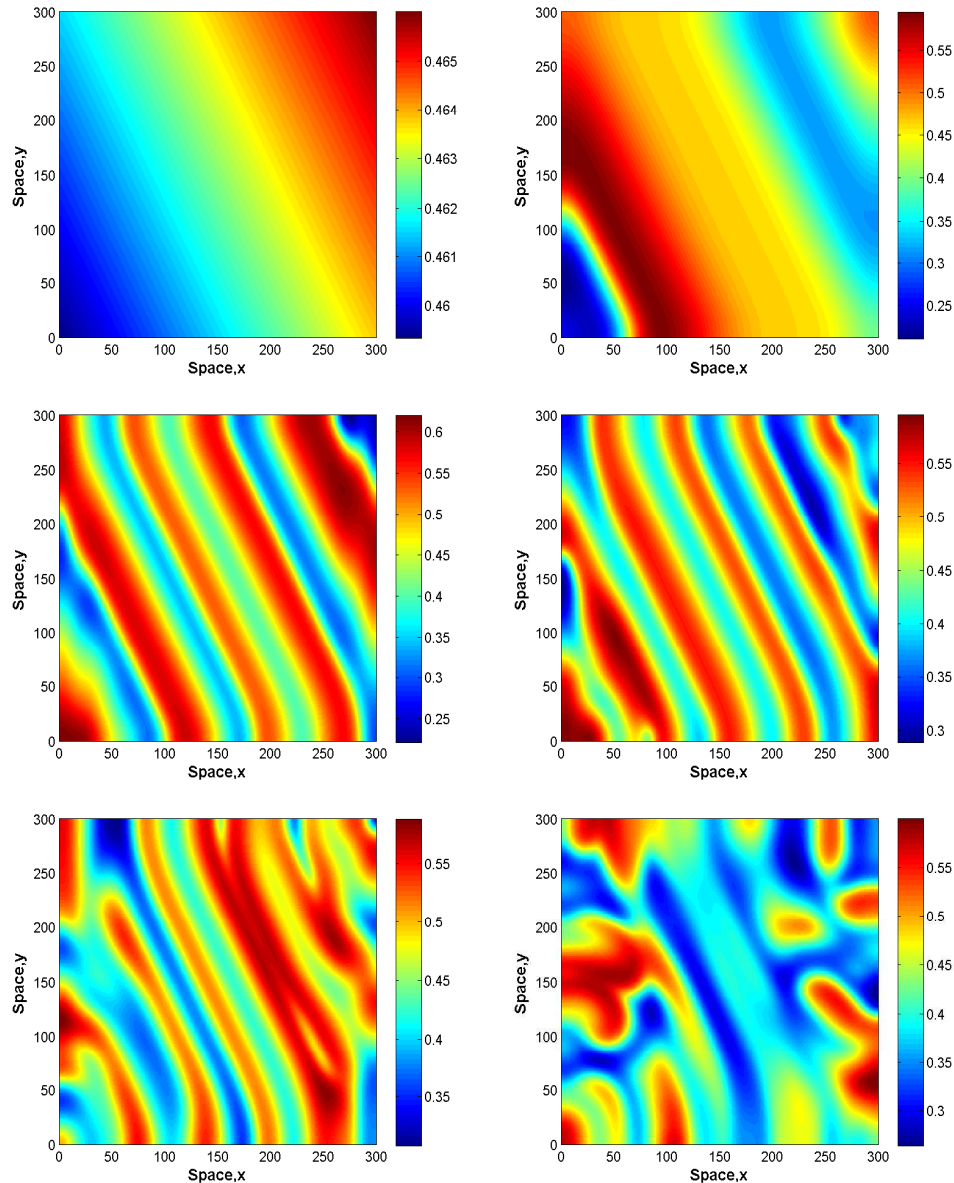


FIGURE 4.33: Spatial distribution of the oxygen concentration in the two-dimensional case for $t = 1$, $t = 200$, $t = 400$, $t = 600$, $t = 800$, and $t = 1100$ from left to right, top to bottom for $A = 2.05$ and the other parameters are as given in the text with given initials $c_0 = 0.4627$, $u_0 = 0.4267$, $v_0 = 0.1304$. The initial conditions are given by Eqs. (4.35-4.37). Oxygen concentration shows qualitatively similar behavior with phytoplankton spatial distribution. The patchy structure resulted in the destructions of stripy structures.

patchy structure: increasing A reduces the time of emergence of the irregular patchy structure. Again, the irregular patchy structure is preceded by a stripy structure for $A = 2.09$; see Fig. 4.34. Formation of the patchy structure starts around the domain with the destruction of the stripes, then it prevails over the whole domain by shrinking the stripy rolls in the center.

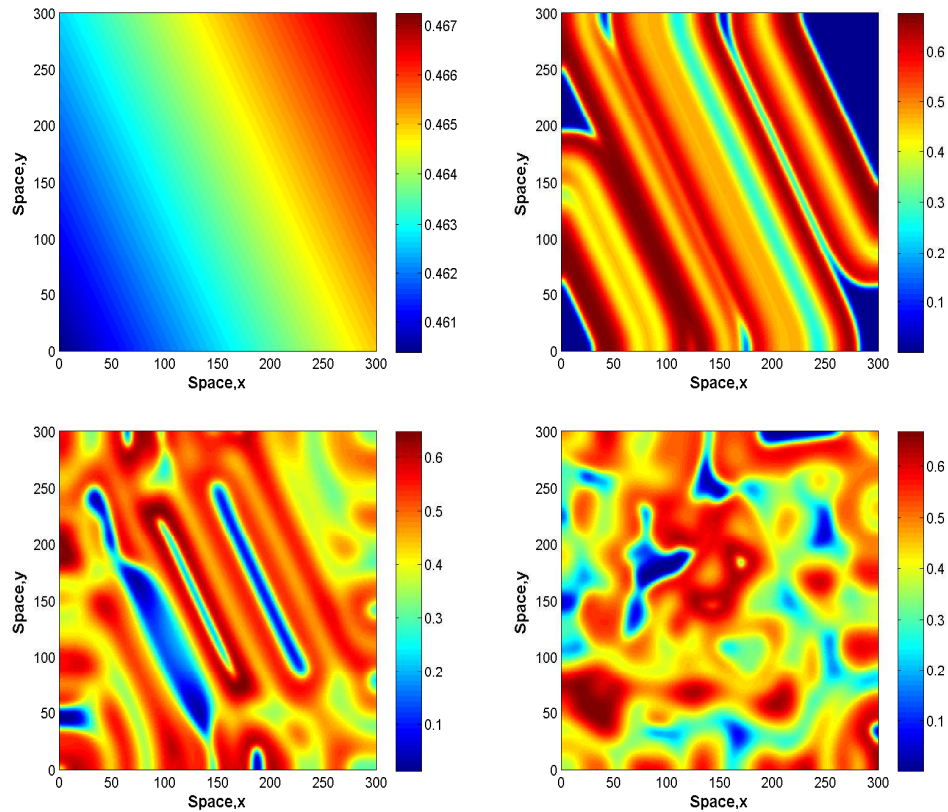


FIGURE 4.34: Spatial distribution of the oxygen concentration in the two-dimensional case for $t = 1$, $t = 200$, $t = 500$, and $t = 1100$ from left to right, top to bottom for $A = 2.09$ and the other parameters are as given in the text with the initials $c_0 = 0.4638$, $u_0 = 0.4179$, $v_0 = 0.1343$. The initial conditions are given by Eqs. (4.35-4.37). The distribution of phytoplankton exhibits qualitatively similar patterns. The patchy structure resulted in the destructions of stripy structures.

Figure 4.35 shows snapshots of the oxygen concentration for given time moments, arising from given initial distributions given by Eqs. (4.35-4.37). Although the destruction of the spiral is thought to be ended by the evolution of the patchy structure, the system does not evolve into the patchy structure as the spiral preserves its shape for larger time limit.

Figure 4.36 shows snapshots of the oxygen concentration at $t = 200$, $t = 2000$, $t = 2200$, $t = 2500$ from left to right, top to bottom for $A = 2.4$. The initial distribution of the oxygen is not given, but it is qualitatively the same with the previous ones. Again, the stripy structure is followed by spirals which are somewhat more regular than the previous one. Contrary to the previous cases, the spiral structure is not persistent in time and extinction happens for a further increase in time.

Figure 4.37 shows snapshots of the oxygen concentration for $A = 2.7$ and

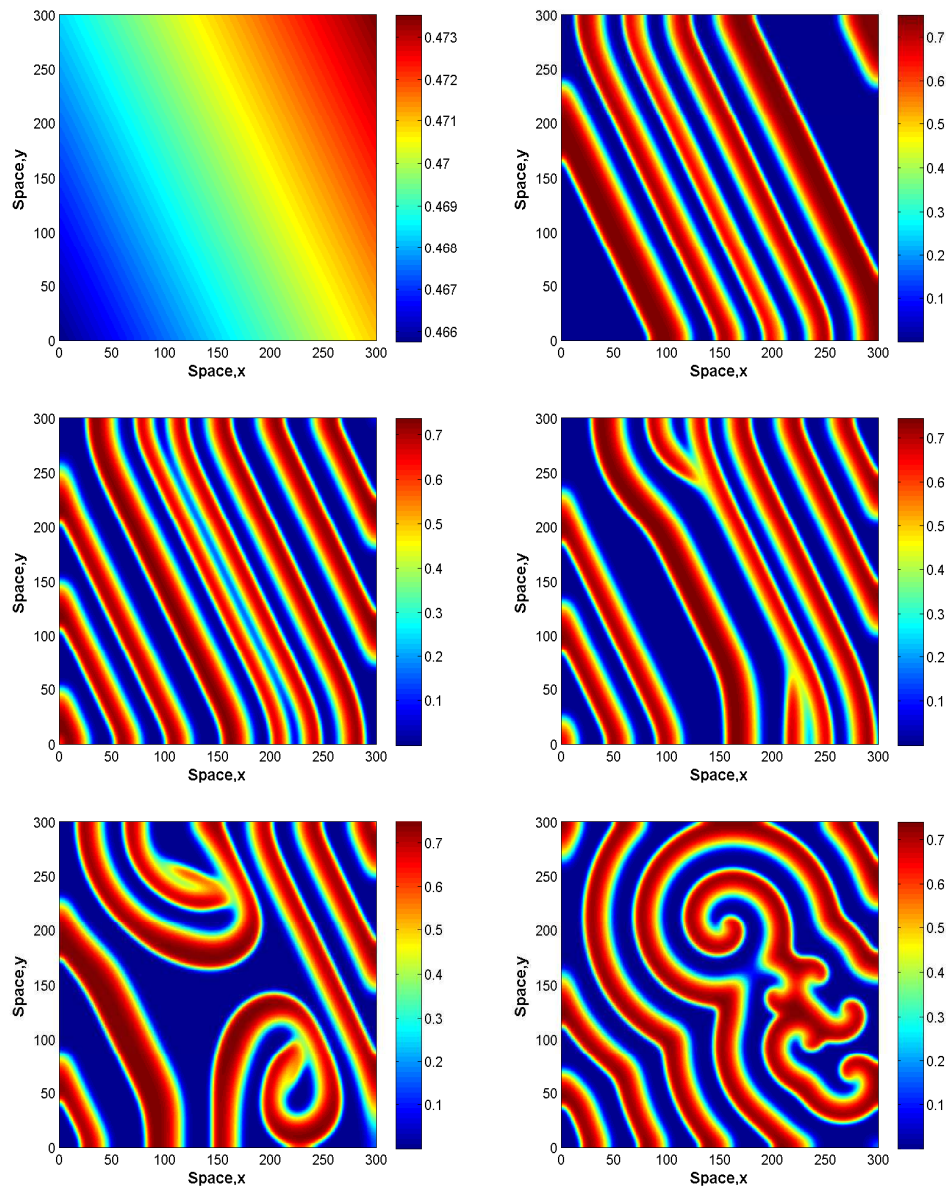


FIGURE 4.35: Spatial distribution of the oxygen concentration in the two-dimensional case for $t = 1$, $t = 200$, $t = 400$, $t = 700$, $t = 800$, $t = 2000$ from left to right, top to bottom for $A = 2.3$ and the other parameters are as given in the text with the initials $c_0 = 0.4696$, $u_0 = 0.3775$, $v_0 = 0.1501$. The initial conditions are given by Eqs. (4.35-4.37). The distribution of phytoplankton exhibits qualitatively similar patterns. The destruction of the spiral from its center is not resulted in patchy structure. The emerging pattern for $t = 2000$ retains its shape for even $t = 6000$.

for different time moments. In this case, the emerging stripy patterns leave the domain, without forming any spirals and then oxygen concentration becomes zero. We have seen that for the initial distribution given by Eqs. (4.35-4.37) and for small A values, the stripy structure gives way to a patchy structure, although for large A values the system ends up with a spiral structure or extinction.

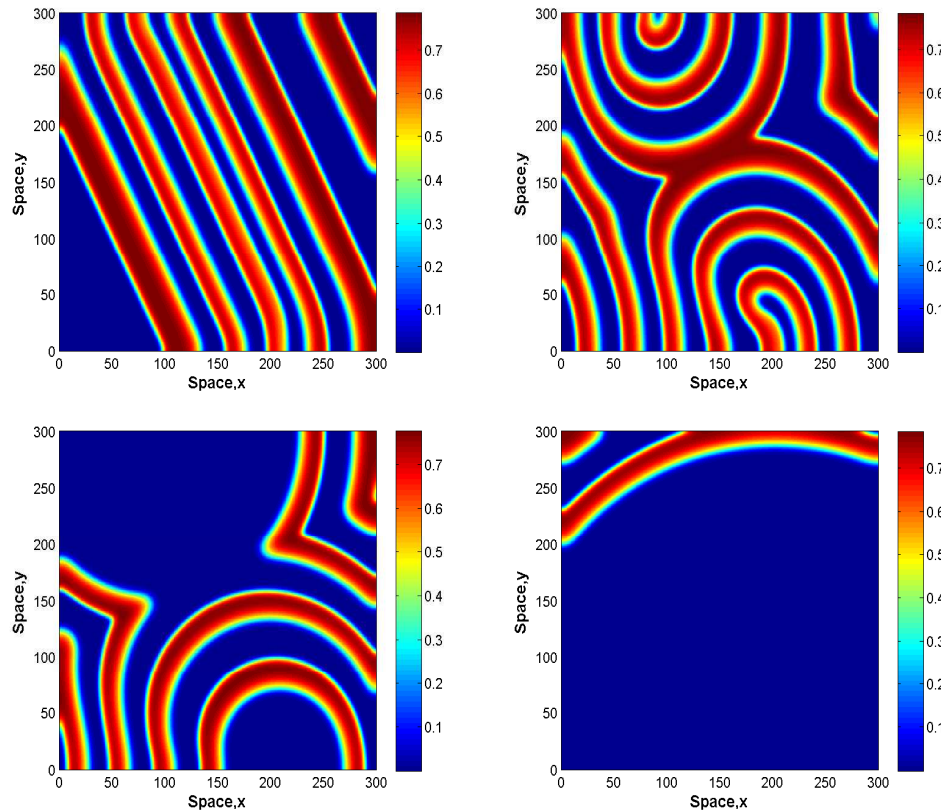


FIGURE 4.36: Spatial distribution of the oxygen concentration in the two-dimensional case for $t = 200$, $t = 2000$, $t = 2200$, $t = 2500$ from left to right, top to bottom for $A = 2.4$ and the other parameters are as given in the text with given initials as $c_0 = 0.4723$, $u_0 = 0.3612$, $v_0 = 0.1554$. The initial conditions are given by Eqs. (4.35-4.37). The distribution of phytoplankton exhibits qualitatively similar patterns. The emerging spirals leave the domain for larger time moments.

Figure 4.38 shows snapshots of the spatiotemporal dynamics of oxygen concentration for the initial distribution given by Eqs. (4.38-4.40). Contrary to the case in Fig. 4.32, for the same A value, the dynamics of the system is not succeeded by the formation of the irregular patchy structure. The formation of the patchy structure for $A = 2.06$ is shown in Fig. 4.39 for the initial conditions given by Eqs. (4.38-4.40).

Snapshots of oxygen concentration are given for $A = 2.4$ and for the initial conditions given by Eqs. (4.38-4.40) in Fig. 4.40. The spiral appears in the middle of the spatial domain in terms of space x and steadily increases in size and eventually occupies over the whole domain. Figure 4.41 shows snapshots for $A = 2.7$ arising from (4.38-4.40). The emerging regular patterns look similar with previous ones. It should be emphasized that when $A = 2.4$ and $A = 2.7$ the initial distributions given by Eqs. (4.35-4.37) evolve to the extinction state, while for the

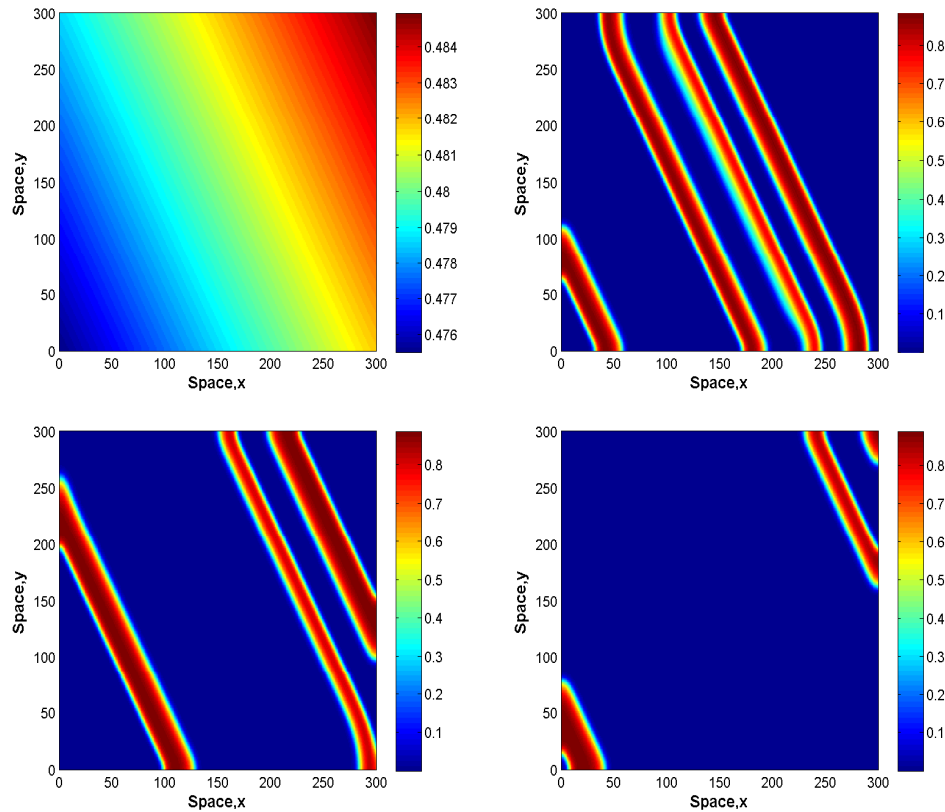


FIGURE 4.37: Spatial distribution of the oxygen concentration in the two-dimensional case for $t = 1$, $t = 120$, $t = 200$, $t = 300$ from left to right, top to bottom for $A = 2.7$ and the other parameters are given in the text with given initials as $c_0 = 0.4802$, $u_0 = 0.3206$, $v_0 = 0.1658$. The initial conditions are given by Eqs. (4.35-4.37). The distribution of phytoplankton exhibits qualitatively similar patterns. The emerging strips leave the domain when $t > 350$

initial distributions given by Eqs. (4.38-4.40) evolve to the regular structure.

Figure 4.42 shows snapshots of the oxygen concentration for a larger spatial domain and for initials given by Eqs. (4.41-4.43) when $A = 2.4$. The spatiotemporal dynamics are depicted by an elliptical distribution which increases in space with time. Eventually, the structure leaves the domain and extinction is inevitable. Regular pattern formation such as observed in our numerical simulations is readily observed in nature, in particular, by vegetations in arid and semiarid ecosystems [141, 142, 147].

It can be concluded that the type of system dynamics depends to a large extent on the choice of the initial distributions. Note that the appearance of the spirals are observed for larger A values. It may be assumed as an ecological warning signal for the upcoming extinction state in two-dimensional case; see Fig. 6.17 in Chapter 6. Interestingly, contrary to the one-dimensional case, for large value of A ($A > 2.28$ which is obtained as a critical threshold for extinction case; see

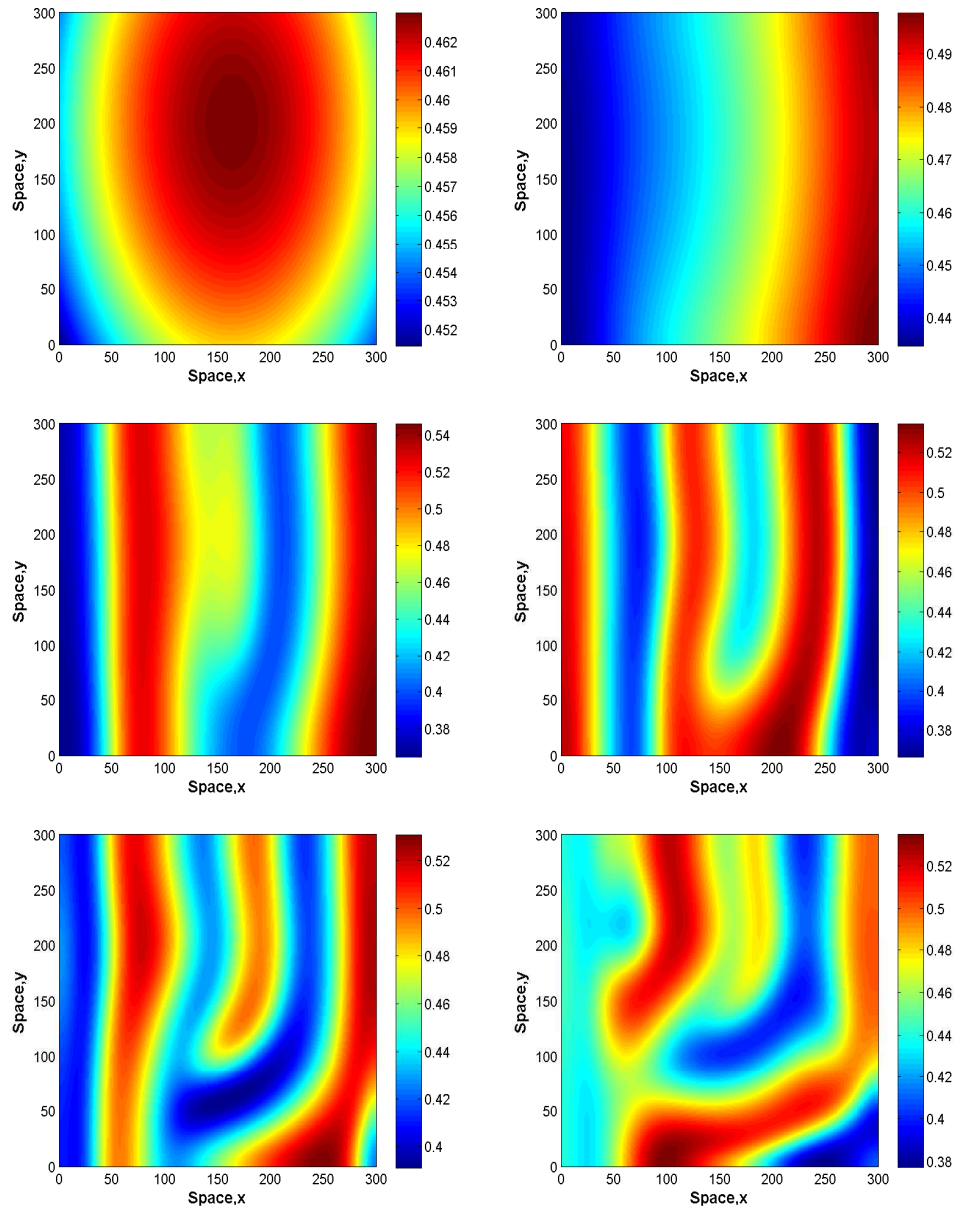


FIGURE 4.38: Spatial distribution of the oxygen concentration in the two-dimensional case for $t = 1$, $t = 300$, $t = 900$, $t = 1100$, $t = 1500$, and $t = 2000$ from left to right, top to bottom for $A = 2.02$ and the other parameters are as given in the text with the given initials $c_0 = 0.4618$, $u_0 = 0.4337$, $v_0 = 0.1271$. The initial conditions are given by Eqs. (4.38-4.40). The distribution of phytoplankton exhibits qualitatively similar patterns.

Chapter 6), the system dynamics are sustainable and somehow the regular spiral type pattern persists in two-dimensional case. Note that, transitions possible between these structures depending initial conditions and controlling parameter A . For small values of A , the system evolves stripy structure and for an increase in A the system results in distinct spirals. For a further increase in A stripes can leave the domain without evolving spirals.

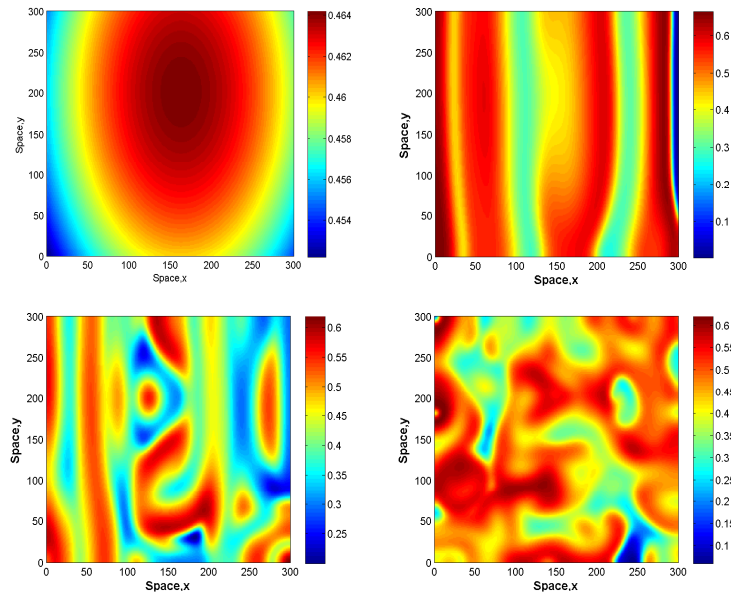


FIGURE 4.39: Spatial distribution of the oxygen concentration in the two-dimensional case for $t = 1$, $t = 300$, $t = 500$, $t = 900$ from left to right, top to bottom for $A = 2.06$ and the other parameters are as given in the text with the initials $c_0 = 0.4630$, $u_0 = 0.4245$, $v_0 = 0.1314$. The initial conditions are given by Eqs. (4.38-4.40). The distribution of phytoplankton exhibits qualitatively similar patterns.

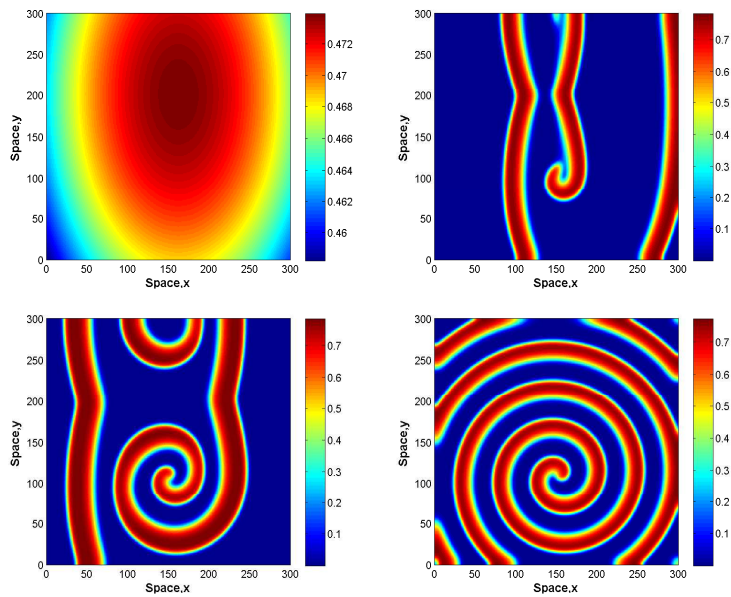


FIGURE 4.40: Spatial distribution of the oxygen concentration in the two-dimensional case for $t = 1$, $t = 120$, $t = 200$, $t = 1200$ from left to right, top to bottom for $A = 2.4$ and the other parameters are as given in the text and the initials are $c_0 = 0.4723$, $u_0 = 0.3612$, $v_0 = 0.1554$. The initial conditions are given by Eqs. (4.38-4.40).

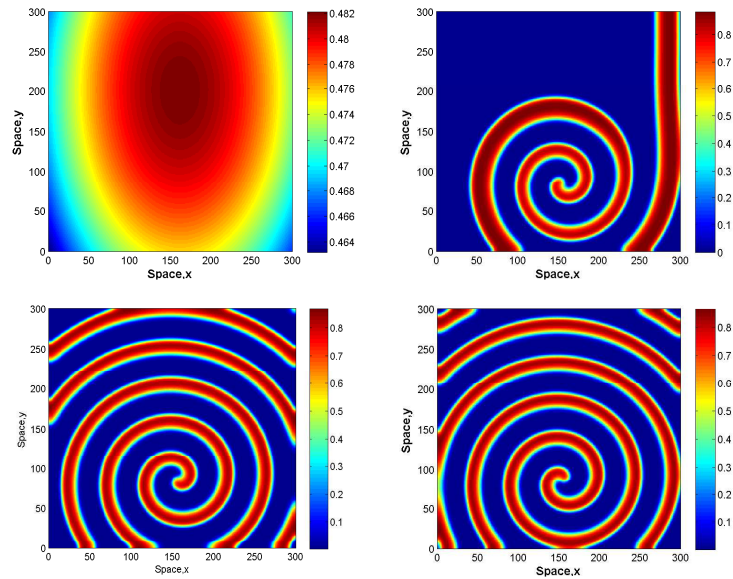


FIGURE 4.41: Spatial distribution of the oxygen concentration in the two-dimensional case for $t = 1$, $t = 200$, $t = 500$, and $t = 2000$ from left to right, top to bottom for $A = 2.7$ and the other parameters are as given in the text with given initials $c_0 = 0.4802$, $u_0 = 0.3206$, $v_0 = 0.1658$. The initial conditions are given by Eqs. (4.38-4.40). The distribution of phytoplankton exhibits qualitatively similar patterns. The irregular patchy structure is not arise for a large time limit, i.e $t = 6000$ and still retains its shape.

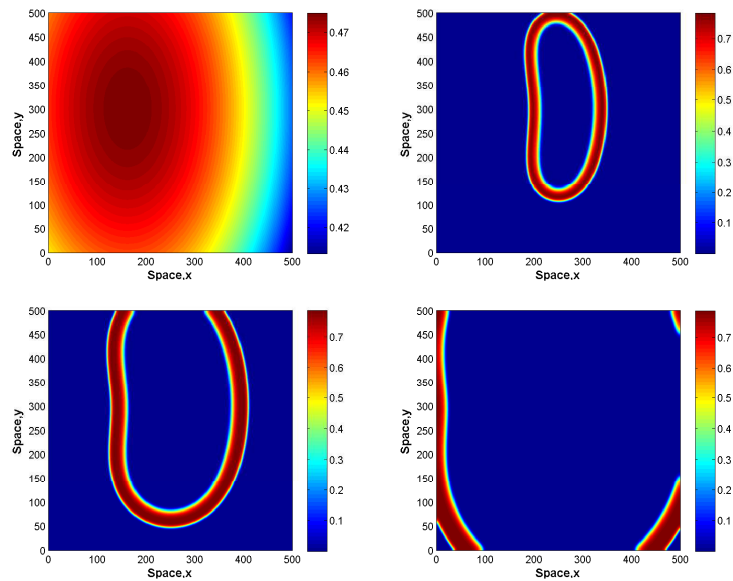


FIGURE 4.42: Spatial distribution of the oxygen concentration in the two-dimensional case and spread of oxygen concentration through expanding ellipse for $t = 1$, $t = 120$, $t = 200$, and $t = 400$ from left to right, top to bottom for $A = 2.4$ and the other parameters are as given in the text and with given initials $c_0 = 0.4723$, $u_0 = 0.3612$, $v_0 = 0.1554$. The initial conditions are given by Eqs. (4.41 -4.43). The species absent both outside and inside the shape. The distribution of phytoplankton exhibits qualitatively similar patterns.

4.4 Discussion and Concluding remarks

We have studied the oxygen, phytoplankton and zooplankton dynamics by using a mathematical model which takes into account both the effect of zooplankton predation on phytoplankton and plankton respiration. On the other hand, ocean planktonic respiration allows us to gain a better awareness of the major air-sea CO_2 flux [46].

The model is described by a system of three coupled ordinary differential equations in the nonspatial case and by three corresponding diffusion-reaction PDEs in the spatially explicit case. The system dynamics have been revealed by some analytical approaches and by extensive numerical simulations. We first consider a nonspatial system to reveal the structure of the parameter range, namely, we show that the system is sustainable only for an intermediate value of the oxygen production rate. We also show that for a sufficiently low oxygen production rate, outside that range, the dynamics are not sustainable resulting in phytoplankton extinction which in turn results in oxygen depletion. Therefore, for the oxygen-phytoplankton system, the system is sustainable unless the production rate becomes too low (see Fig. 4.13).

We then consider a spatially explicit extension of our model where plankton and oxygen are carried around by turbulent water flows and the diffusion-reaction models of phyto-zooplankton dynamics have previously been used to describe this phenomenon, e.g. see [183], also [146, 147, 156] and references therein. It is shown that spatiotemporal dynamics result in the formation of patchy patterns. In the parameter range for which the nonspatial system possesses a stable limit cycle, the spatial system exhibits the formation of irregular spatiotemporal patterns. Note that the patterns are self organised, namely, they are not caused by any predefined spatial structure. Here we recall that plankton patchiness is a very common property of marine ecosystems [2, 64, 81, 143, 245] and our results support this ecological reality.

We then considered a spatially explicit extension of the one-dimensional case to two-dimensions and have shown that the model exhibits rich spatiotemporal dynamics. In particular one-dimensional case, resulting in strongly irregular patchy distribution for large A . However, for small A , the system components distributions are rather smooth spatially. However, in the two-dimensional case, for small A values the distribution of oxygen is patchy. For a further increase in value of this controlling parameter would lead to a regular structure, which was shown in Section 4.3.4. Moreover, a further increase in A would lead to extinction

regardless of what the initial conditions are. We also want to point out that for different initial values the patterns in two-dimensions are very different; such as “mushroom-like” structure, “snaky” structure or different sort of spirally structure are not shown here for the sake of brevity.

Chapter 5

The Effect of Temperature

5.1 Introduction

As it is mentioned in the previous chapters, marine system dynamics are controlled by external factors, such as wind intensity, light, salinity, eutrophication, temperature, etc. In particular, temperature is regarded as one of the basic controlling factors of oxygen concentration in water body, hence it holds the responsibility for the changes affecting primary production in marine systems [101]. Any changes in surrounding water temperature prominently affect phytoplankton photosynthetic mechanisms as this changes limit phytoplankton growth and limit their photosynthetic rates [7, 60, 101, 136, 243]. However, zooplankton predation is decreased at low temperatures due to a decrease on fish feeding rates [270]. Furthermore, temperature plays a role on aquatic organisms' metabolism. Warmer water leads to faster metabolism and respiration due to an increase of cell division under the influence of increasing temperature [4, 59, 117]. Due to the relation between metabolism and respiration, respiration rate of ecosystem increases with increasing temperature [22, 59, 92, 170]. If we want to support this idea with real field data, it can be said that the respiration rate of phytoplankton increases slightly when temperatures are between $5^{\circ}C$ and $13^{\circ}C$, and increases steeply when temperatures are between $17^{\circ}C$ and $21^{\circ}C$ [117]¹.

The effect of water warming on phytoplankton dynamics has not been considered until now. Therefore, we address this issue theoretically by considering our oxygen-phytoplankton-zooplankton model in order to make an insight into the effect of changing environmental conditions. Specifically, we consider how the system dynamics can be affected by continuously increasing water temperature.

¹The majority of this chapter has been published in [226]

Combining analytical investigation of the system's properties with extensive numerical simulations, we show that oxygen depletion can occur if the temperature exceeds a certain critical level, where the latter can be a result of the global climate change.

Interestingly, in spite of recognition of the marine system importance on global climate change, there is no directly relevant mathematical research on oxygen-plankton dynamics under the control of increasing/decreasing temperature in marine systems up until now. Correspondingly, we attempt to model the effect of global climate change on the oxygen production in marine ecosystems. This approach is the main factor that distinguishes our work from the models usually mentioned in the literature. Therefore, we address the oxygen depletion problem considering prey-predator interactions for plankton dynamics combined with water body dissolved oxygen dynamics, based on the model presented in [227] and in Chapter 4 that describes the marine system oxygen dynamics without taking into account the warming of surrounding water effect.

In this Chapter, we review recent biological advances on the oxygen depletion problem due to global climate change in marine ecosystems and focus on this issue by means of mathematical modelling and numerical simulations. We first extend the model in Chapter 4 by taking into account a sufficiently large increase or decrease in the controlling parameters (in particular, in the rate of oxygen production and in the phytoplankton growth term) in the manner of addition of temperature changes in time to the model system to understand the underlying possible reasons of the oxygen depletion problem under the climate change effect. We then consider the responses of our mathematical model by extensive numerical simulations corresponding to both the nonspatial and spatial system. We observe that a sufficiently large increase in water temperature (presumably as a result of global warming) leads to an ecological disaster when the oxygen production suddenly drops to zero.

5.2 Numerical Simulations

Temporal Dynamics

The model that we considered is the same as model in Chapter 4. We show the model here for the convenience of reading. For the formulation of the model system and its steady state analysis see Chapter 4 (Sections 4.2–4.2.1).

The considered model consists of oxygen itself, phytoplankton as oxygen's main producer and zooplankton as phytoplankton's predator and oxygen's consumer due to respiration:

$$\frac{dc}{dt} = A\left(1 - \frac{c}{c+1}\right)u - c - \frac{uc}{c+c_2} - \frac{\nu cv}{c+c_3}, \quad (5.1)$$

$$\frac{du}{dt} = \left(\frac{Bc}{c+c_1} - u\right)\gamma u - \frac{uv}{u+h} - \sigma u, \quad (5.2)$$

$$\frac{dv}{dt} = \left(\frac{\beta uv}{u+h}\right)\frac{c^2}{c^2+c_4^2} - \mu v, \quad (5.3)$$

where $c(x, 0) > 0$, $u(x, 0) > 0$ and $v(x, 0) > 0$. In the system (5.1-5.3) all notations keep their usual previous meanings. Some of the system parameters are fixed at their hypothetical values as in previous chapters (see for details Section 4.3.1): $B = 1.8$, $\gamma = 1.2$, $\sigma = 0.1$, $c_2 = 1$, $c_3 = 1$, $c_4 = 1$, $\nu = 0.01$, $\beta = 0.7$, $\mu = 0.1$, $h = 0.1$ and we vary A and c_1 in a certain range.

Surrounding water temperature can have an effect on the photosynthesis rate and hence on the net amount of oxygen produced over the daily cycle [85, 217]. In our model (5.1–5.3), the rate of oxygen production is quantified by parameter A . In order to reflect the effect of temperature T on photosynthesis, A becomes a function of T . In its turn, the temperature is a function of time, hence A becomes a function of time too. Therefore, we consider $A = A(t)$ but keep other parameters fixed for the sake of simplicity.

Water temperature is known to fluctuate significantly on all temporal scales, e.g. hourly, daily, monthly and annually [105]. A “realistic” function $A(t)$ taking into account those fluctuations is likely to be very complicated. However, since the purpose of this study is to consider the effect of global warming conceptually rather than predictively, this level of details seems to be excessive. Instead, in order to account for the general trend (and not for details), we consider the simplest possible choice of $A(t)$, i.e. the linear function (Thus assuming for simplicity that A depend on T linearly.):

$$A = A_0 \quad \text{for } t < t_1, \quad A = A_0 + \omega (t - t_1) \quad \text{for } t \geq t_1. \quad (5.4)$$

Here t_1 is the moment when the global warming started, A_0 is the rate of net oxygen production ‘before changes’, and parameter ω quantifies the rate of global warming.

Available data remains unclear on what the typical phytoplankton response

to an increase in the water temperature is, i.e. whether the rate of oxygen production by phytoplankton actually decreases or increases. Therefore, we consider two possible scenarios: The first one where a higher water temperature facilitates oxygen production (when $\omega > 0$) and the second one where a higher temperature hampers oxygen production (when $\omega < 0$). Since global warming is a slow process, we consider ω to be very small, i.e. $|\omega| \ll \min\{A, B, \delta, \sigma, \mu, \nu\beta\}$. For the initial value of A , we assume that prior to the climate change the ecosystem was in a ‘safe state’, i.e. with the coexistence steady state E_3 either being stable (Domain 2 in Fig. 4.13) or unstable, but surrounded by a stable limit cycle (Domain 3), so that A_0 is chosen accordingly.

Note that, with A now being a function of t , the system (4.7–4.9) becomes non-autonomous and strictly speaking, the results of the previous section do not immediately apply. However, having assumed that $A(t)$ is a slow changing function, we expect that the properties of the corresponding autonomous system (i.e. with $A = \text{const}$) in different parameter ranges (see Fig. 4.13) can provide a convenient backbone for understanding the effect of changes.

5.2.1 Effect of decreasing A

Simulations on different values of oxygen production rate show the importance of A values for our dynamical system. In the previous chapters, A is assumed as a constant, but here, contrary to the previous one, A will be considered as a function in time. It is observed in previous chapters (see Fig. 4.13a-b), that positive equilibria exist only if A is not too small, i.e. above a certain critical value. Decreasing A results in the merging of the two positive steady states, $E_2^{(1)}$ and $E_2^{(2)}$, which eventually disappear; see the succession of the system in Figs. 4.2a-b. For this reason, we will take into account the effect of decreasing A on system dynamics. It is assumed that the decrease of A can be taken as an evidence of a catastrophe. Hence we will focus on the systems’ temporal response to decreasing A to its critical value, in time and by considering $\omega < 0$:

$$A = A_0 \quad \text{for} \quad t < t_1, \quad A = A_0 + \omega (t - t_1) \quad \text{for} \quad t \geq t_1. \quad (5.5)$$

Here, A is assumed to be a continuously decreasing function in time with upper initial point A_0 and t_1 corresponds to the starting moment of global warming; see Fig. 5.1. A is shown by the thick black line in following simulations.

This appears to be in full agreement with our simulation results. The system is expected to develop, in the course of time, oscillations of decreasing

amplitude as A decreases, whereby the system moves into Domain 1, further away from Domain 2; see bifurcation analysis in Chapter 4 (Section 4.2.2). If the decrease continues for a sufficiently long time, resulting in A becoming sufficiently small, all species go extinct and the only steady state is the extinction one.

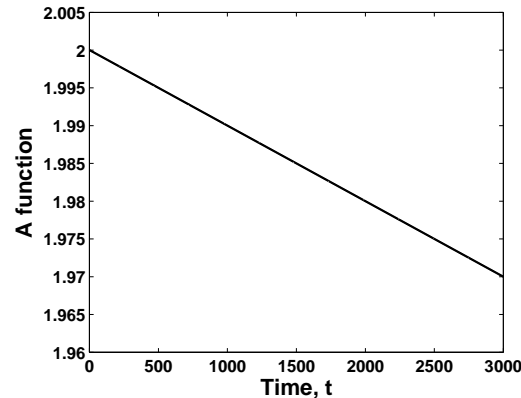


FIGURE 5.1: Sketch of the continuously decreasing A function as in Eq. (5.5) for given parameter values, $A_0 = 2$ and $\omega = -10^{-5}$.

An interesting succession of dynamical regimes is observed for a sequence of decreasing A_0 in Fig. 5.2. In the case for $A_0 = 1.97$ (Fig. 5.2a), the system components eventually converge to the steady state values after a sequence of damping oscillations for the rate of decreasing $\omega = -10^{-5}$. However, the convergence of the steady states happens without any oscillations for smaller A_0 ; (see Figs. 5.2b–d). The system converges to the zooplankton free state between $A_0 = 1.54$ and $A_0 = 1.4$, so that the system dynamics jump from the oxygen-phytoplankton-zooplankton system to the oxygen-phytoplankton system. A further decrease in A_0 , i.e. $A_0 \leq 1.33$ leads the system dynamics to the extinction state E_1 . Correspondingly, for Fig. 5.2a, for $A = 1.97$ the final value of the oxygen production rate is $A = 1.96$ which is still in Domain 2 so that the oscillations eventually die out. However, in case of Fig. 5.2d, the final value of the oxygen production rate is $A_0 > 1.33$, corresponding to parameters in Domain 1, results in the zooplankton free state in the course of time. Hence, the corresponding phase space structure of Fig. 5.2 is given in Fig. 5.3. In case $A_0 \leq 1.4$, (Figs. 5.2c-d), oxygen and phytoplankton lie on zooplankton-free plane in course of time. The system succession for the catastrophic case when the system jumps from the oxygen-phytoplankton state to the extinction state can be seen in Figs. 5.4–5.5. In this case system trajectories directly go to the extinction state regardless of what the initial conditions are. Here, in phase structure, the blue and red star keep the previous meanings.

Since it is difficult to distinguish the ω is small or not too small we performed numerical simulations choosing the ω by different magnitude. It is observed that

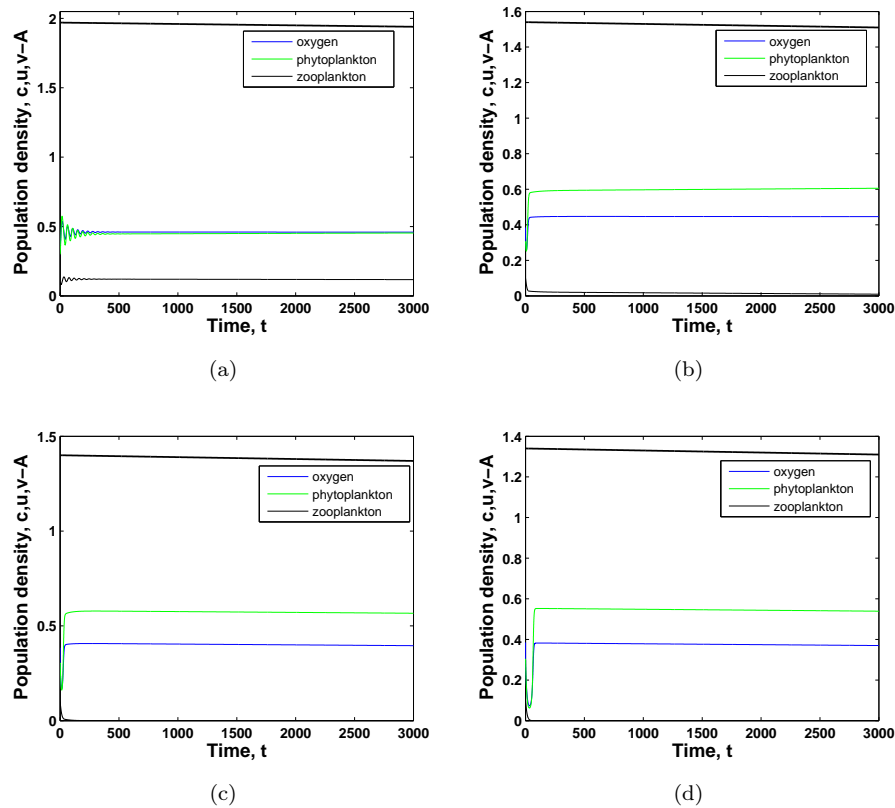


FIGURE 5.2: Effect of decrease in parameter A . The density of oxygen-phytoplankton-zooplankton against time obtained for other given parameter values (a) $A_0 = 1.97$, (b) $A_0 = 1.54$, (c) $A_0 = 1.4$, (d) $A_0 = 1.34$; $\omega = -10^{-5}$ for fixed $c_1 = 0.7$ and the initial values $c_0 = 0.385$, $u_0 = 0.3$, $v_0 = 0.1$ and systems' other parameters are given in the text (see Section 4.3.1).

at least for values of $\omega = -10^{-3}$, the properties of the system are reduced to the properties of the corresponding system with constant A for relevant values of A [14, 127]. We mention here that it was necessary to check the validity of the adiabatic approximation because there are examples when the properties of similar systems depend on the transition rate [194]. We have also performed these simulations for the corresponding spatial model, whereby the results are the same in these sense that the distribution of species converges to a uniform one. Indeed, it is intuitively expected because as we showed in Fig. 5.2 the system steady states are always stable and there is no pattern formation. Importantly for small values of A , ($A_0 \leq 1.33$), the spatial distribution of system components corresponds to the temporal dynamics and all species go extinct.

Now, we consider the case when the coefficient of oxygen concentration is gradually increasing with time; for marine systems it can be consequence of increasing water temperature.

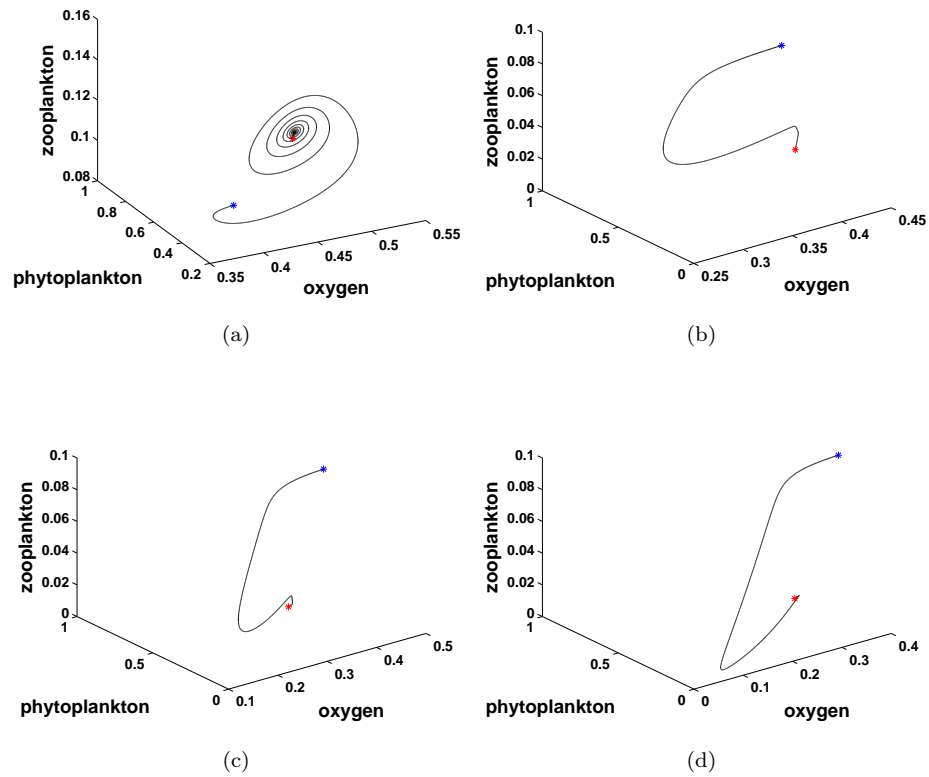


FIGURE 5.3: Phase space structure for corresponding temporal dynamics Fig. 5.2. (a) $A_0 = 1.97$, (b) $A_0 = 1.54$, (c) $A_0 = 1.4$, (d) $A_0 = 1.34$, $\omega = -10^{-5}$ and fixed $c_1 = 0.7$ and the initial values $c_0 = 0.385$, $u_0 = 0.3$, $v_0 = 0.1$; other parameters are the same as in previous figure.

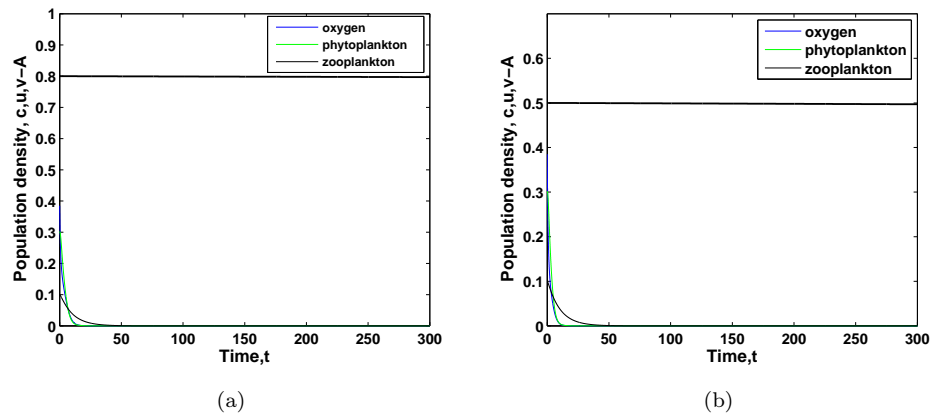


FIGURE 5.4: Effect of decrease in parameter A . The density of oxygen-phytoplankton-zooplankton against time obtained for other given parameter values (a) $A_0 = 0.8$, (b) $A_0 = 0.5$; $\omega = -10^{-5}$ for fixed $c_1 = 0.7$ and the initial values $c_0 = 0.385$, $u_0 = 0.3$, $v_0 = 0.1$ and systems' other parameters are given in the text (see Section 4.3.1).

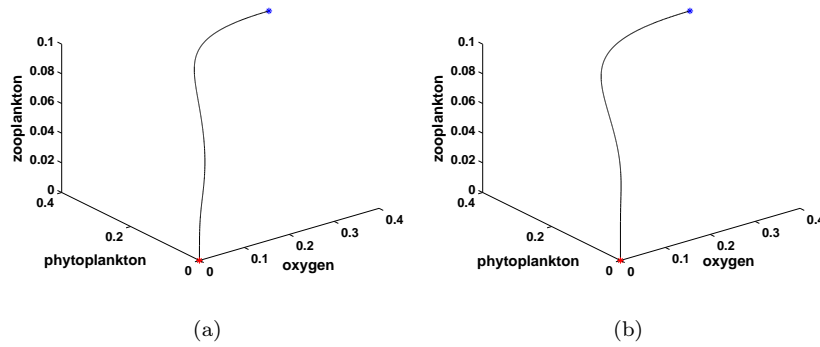


FIGURE 5.5: Phase space structure for corresponding temporal dynamics Fig. 5.4. (a) $A_0 = 0.8$, (b) $A_0 = 0.5$; $\omega = -10^{-5}$ and fixed $c_1 = 0.7$ and the initial values $c_0 = 0.385$, $u_0 = 0.3$, $v_0 = 0.1$; other parameters are the same as in previous figure.

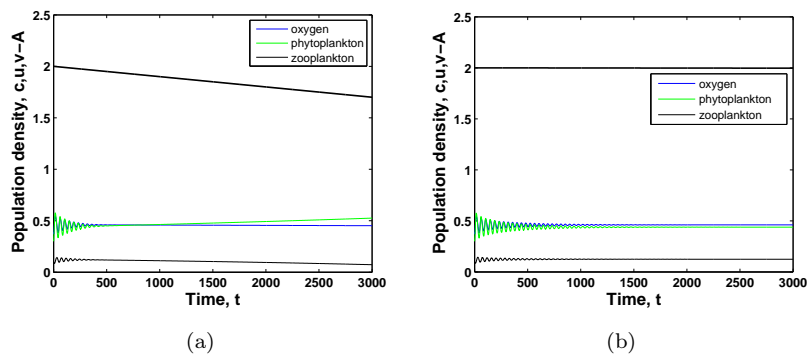


FIGURE 5.6: Effect of changes in parameter ω . The density of oxygen-phytoplankton-zooplankton against time obtained for other given parameter values (a) $\omega = -10^{-4}$, (b) $\omega = -10^{-6}$ for fixed $A_0 = 2$ and system other parameters are as given in the text. In all cases, the initial conditions are $c_0 = 0.385$, $u_0 = 0.3$, $v_0 = 0.1$.

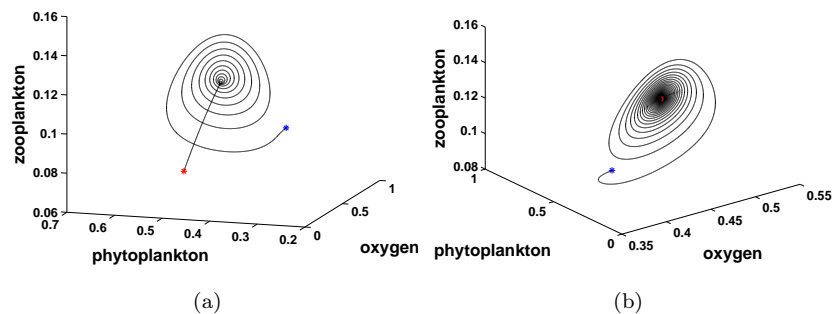


FIGURE 5.7: Phase space structure for corresponding temporal dynamics Fig. 5.6. (a) $\omega = -10^{-4}$, (b) $\omega = -10^{-6}$ for fixed $A_0 = 2$ and other parameters are the same as in previous figure. In all cases, the initial conditions are $c_0 = 0.385$, $u_0 = 0.3$, $v_0 = 0.1$.

5.2.2 Effect of increasing A

Here we consider the case $\omega > 0$ where an increase in water temperature facilitates oxygen production. Then A function is as follows:

$$A = A_0 \quad \text{for } t < t_1, \quad A = A_0 + \omega (t - t_1) \quad \text{for } t \geq t_1. \quad (5.6)$$

A function, with lower limit A_0 , corresponds to the continuously increasing function (see Fig. 5.8) where t_1 is the moment when the global warming started. We assume the oxygen concentration is below the solubility limit, which decreases with increasing temperature [20, 25, 84, 121, 174, 230]. Fig. 5.8 shows the rate of oxygen production change versus time obtained for $c_1 = 0.7$ with the slope of ω and the initial time moment $t_1 = 0$. The thick straight black line shows the function of A in time.

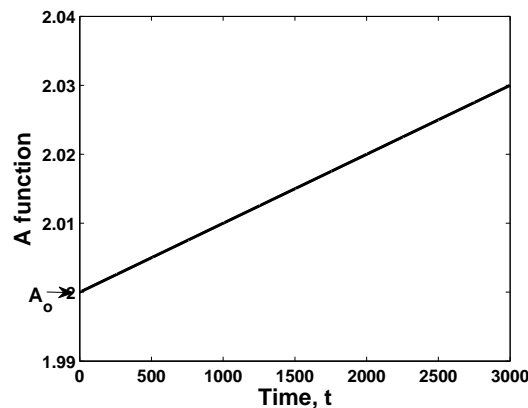


FIGURE 5.8: Sketch of the continuously increasing A function in time from Eq. (5.6) for given parameter values, $A_0 = 2$ and $\omega = 10^{-5}$.

This intuition seems to be in full agreement with the following simulations. In this case, the system is expected to develop, in the course of time, oscillations of increasing amplitude with increasing A , i.e. the system moves further into Domain 3. If the temperature keeps increasing for a sufficiently long time, which results in A becoming sufficiently large, one can expect that all species go extinct once the system moves to Domain 4, where the only steady state is the extinction.

Fig. 5.9 shows the oxygen concentration and plankton density versus time obtained for different lower bounds of the temperature function, A_0 , and for a fixed value of $c_1 = 0.7$. For $A_0 = 1.97$ (Fig. 5.9a), the system components eventually converge to its steady state after a sequence of damping oscillations. However, the system develops periodic oscillations of different amplitude for $A_0 = 2$ (Fig. 5.9b). In both cases, A_0 is in the parameter range where E_3 is a stable focus, i.e. Domain

2. Correspondingly, in both cases, at early times the system dynamics result in

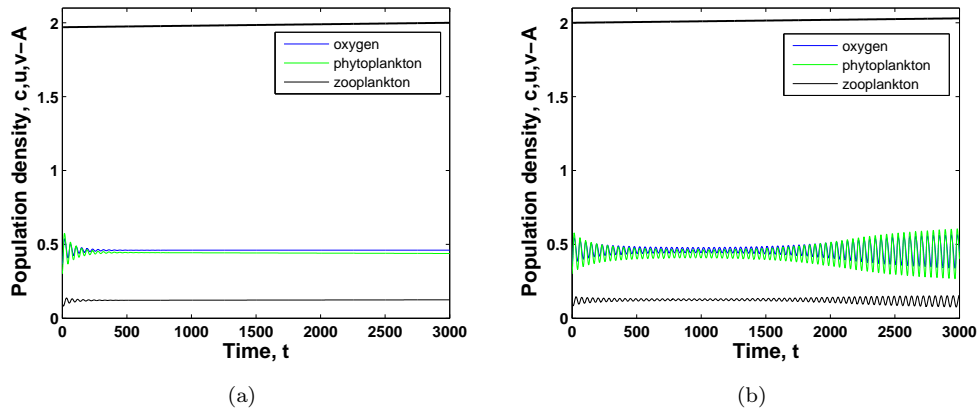


FIGURE 5.9: Effect of changes in parameter A . The density of oxygen-phytoplankton-zooplankton against time obtained for other given parameter values (a) $A_0 = 1.97$, (b) $A_0 = 2$, $\omega = 10^{-5}$ for fixed $c_1 = 0.7$ and the initial values $c_0 = 0.385$, $u_0 = 0.3$, $v_0 = 0.1$ and other system parameters are given in the text.

oscillations of decreasing amplitude as the system converges to the stable steady state. In the case of Fig. 5.9a, the final value of the oxygen production rate is $A = 2$ which is below the Hopf bifurcation value ($A_{Hop} \approx 2.01$) so the oscillations decrease. However, for Fig. 5.9b, the final value of the oxygen production rate is $A = 2.03$ ($A > A_{Hop}$). As a result, oscillations start increasing when the system passes the Hopf bifurcation point. The phase space structure of Fig. 5.9 is given in Fig. 5.10, respectively.

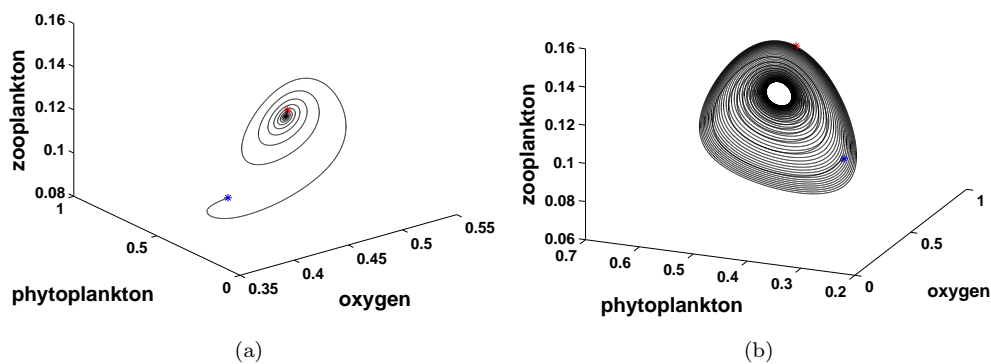


FIGURE 5.10: Phase space structure for corresponding temporal dynamics Fig.5.9 for (a) $A_0 = 1.97$, (b) $A_0 = 2$, $\omega = 10^{-5}$; other parameters are the same as in Fig. 5.9.

Fig. 5.11 shows the oxygen concentration and plankton densities over time obtained for two different values of A_0 for the rate of warming $\omega = 10^{-5}$ and

for the same value of $c_1 = 0.7$. In both cases, A_0 lies in the parameter range where E_3 is an unstable focus surrounded by a stable limit cycle (Domain 3). For $A_0 = 2.024$ in Fig. 5.11a, the system develops periodic oscillations with an increase in period. However, a further increase on A_0 results in extinction following a sequence of oscillations increasing in period, phytoplankton suddenly goes extinct and the oxygen concentration falls to zero. This dramatic change of the system occurs when A moves, in the course of time, to the parameter range where there is no limit cycle and the only attractor of the corresponding autonomous system is extinction (Domain 4). Figure 5.12 shows the corresponding phase structure of Fig. 5.11.

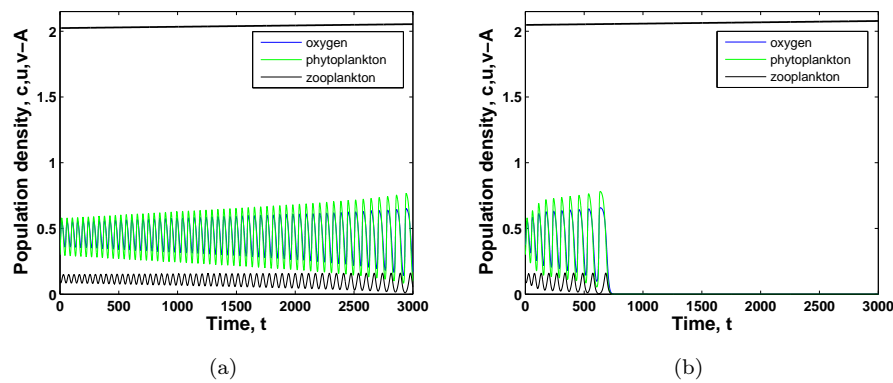


FIGURE 5.11: Effect of changes in parameter A . The density of oxygen-phytoplankton-zooplankton against time obtained for other given parameter values (a) $A_0 = 2.024$, (b) $A_0 = 2.048$, $\omega = 10^{-5}$ and for $c_1 = 0.7$ and the initial values are $c_0 = 0.385$, $u_0 = 0.3$, $v_0 = 0.1$ and system parameters are given in the text.

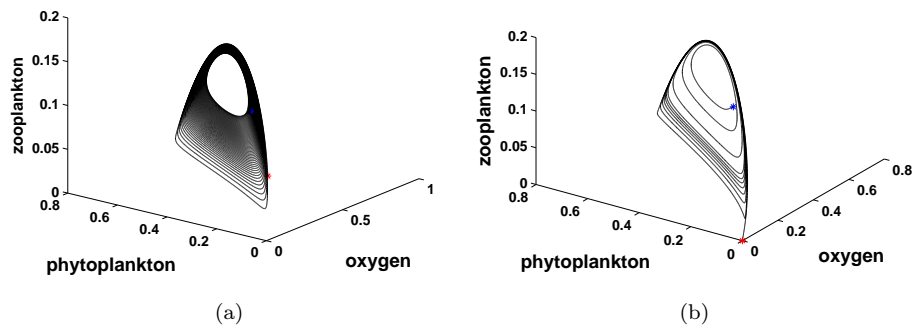


FIGURE 5.12: Phase space structure for corresponding temporal dynamics for (a) $A_0 = 2.024$, (b) $A_0 = 2.048$, $\omega = 10^{-5}$, $c_1 = 0.7$ and the initial values $c_0 = 0.385$, $u_0 = 0.3$, $v_0 = 0.1$ other parameters are the same as in Fig. 5.11.

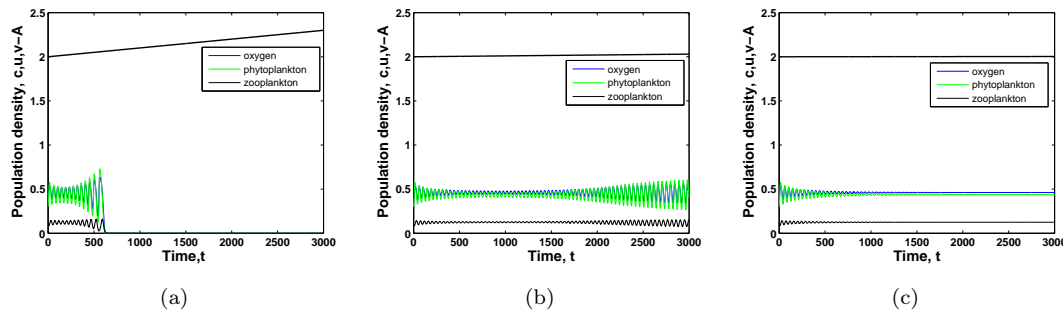


FIGURE 5.13: Effect of changes in parameter ω . The density of oxygen-phytoplankton-zooplankton against time obtained for other given parameter values (a) $\omega = 10^{-4}$ (b) $\omega = 10^{-5}$ (c) $\omega = 10^{-6}$ for fixed $A_0 = 2$ and system other parameters are as given in the text for the initial conditions are $c_0 = 0.385$, $u_0 = 0.3$, $v_0 = 0.1$.

The effect of a decrease in parameter ω may have a more subtle effect on the system's dynamical response; see Figs. 5.13a-c. Therefore, we observe an interesting succession of dynamical regimes obtained for three different values of ω (slope of A function). Figure 5.13a obtained for $\omega = 10^{-4}$ shows that all system components go extinct in the course of time. It shows that the dramatic change can occur for smaller values of A (safe) with higher global warming rate. A close look at $A(t)$ (black line) shows that the disaster occurs for almost the same value of A as in Fig. 5.11b, i.e. for $A \approx 2.055$. However, the decrease on the slope of temperature function results in a limit cycle with varying period in size and damping oscillation, Fig. 5.13b-c, respectively. This dynamical response to the different values of ω corresponds to its ecological meaning. Once the oxygen production coefficient A is not large enough, plankton extinction is not observed and oxygen concentration becomes sufficient to support the life of marine ecosystems.

5.2.3 Effect of decreasing c_1

In this section we focus on the issue of what would the response of phytoplankton growth be to the changing environmental conditions. In particular, here we attempt to observe the system's response to the change in environmental conditions induced by reducing c_1 . It is assumed that this parameter quantifies the growth rate of phytoplankton under the situation that oxygen concentration in water body is at the edge of depletion.

In our model system (5.1-5.3), c_1 is the half saturation constant for phytoplankton density. The varying c_1 describes the effect of oxygen on phytoplankton

growth. The effect of temperature on the release of oxygen molecules to the surrounding water will be considered through varying c_1 , and we will keep A constant. Here, we assume c_1 is a continuously decreasing function as follows:

$$c_1 = c_0 \quad \text{for } t < t_1, \quad c_1(t) = c_0 - \omega (t - t_1) \quad \text{for } t \geq t_1. \quad (5.7)$$

with upper limit c_0 , (see Fig. 5.14). The thick straight black line shows the function of c_1 in time. Figure 5.14 shows the changes in c_1 in time for $c_0 = 0.7$ with the given slope of ω and for $t = 3000$. In this case, the bifurcation diagram should be evaluated in terms of decreasing tendency of c_1 (see Fig. 4.13).

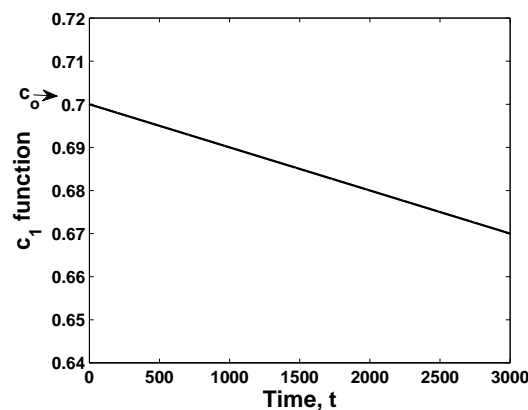


FIGURE 5.14: Sketch of the continuously decreasing c_1 function as in Eq. (5.7) for given parameter values, $c_0 = 0.7$ and $\omega = 10^{-5}$.

Figure 5.15 shows the oxygen concentration and plankton density versus time obtained for different upper bound c_0 for fixed $A = 2.01$. For $c_0 = 0.721$ (Fig. 5.15a), the system components eventually converge to its steady state after a sequence of damping oscillations. However, the system develops different sort of periodic oscillations for $c_0 = 0.71$ (Fig. 5.15b). In both cases, at early times the system exhibits oscillations decreasing in size. In Fig. 5.15a, the final value of c_1 is $c_1 = 0.691$ which is above the Hopf bifurcation. In Fig. 5.15b the final value of c_1 is $c_1 = 0.68$ which is a sufficiently large value leading the system to pass the Hopf bifurcation point, thereby resulting in the oscillations increasing in amplitude. The system's dynamic with given parameter values are qualitatively similar with Fig. 5.9. The Hopf bifurcation occur when c_0 value changes from $c_0 = 0.721$ to $c_0 = 0.71$. The phase space structure for the corresponding temporal dynamics of Fig. 5.15 is given in Fig. 5.16.

Figure 5.17 shows the oxygen concentration and plankton densities versus time for a fixed upper bound c_0 and two different values of A . For $A = 2.01$ (Fig. 5.17a), the system develops periodic oscillations decreasing in amplitude

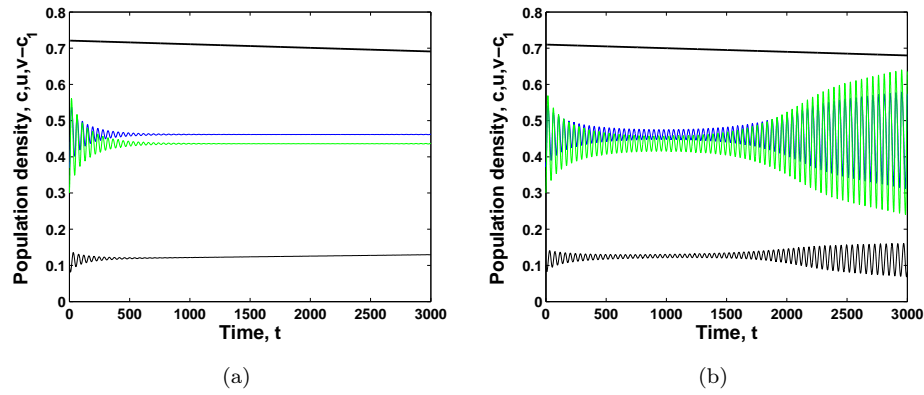


FIGURE 5.15: Effect of changes in parameter c_0 and for fixed $A = 2.01$. The density of oxygen-phytoplankton-zooplankton against time obtained for other given parameter values (a) $c_0 = 0.721$, (b) $c_0 = 0.71$, $\omega = 10^{-5}$ and the initial values $c_o = 0.385$, $u_o = 0.3$, $v_o = 0.1$ and system parameters are given in the text.

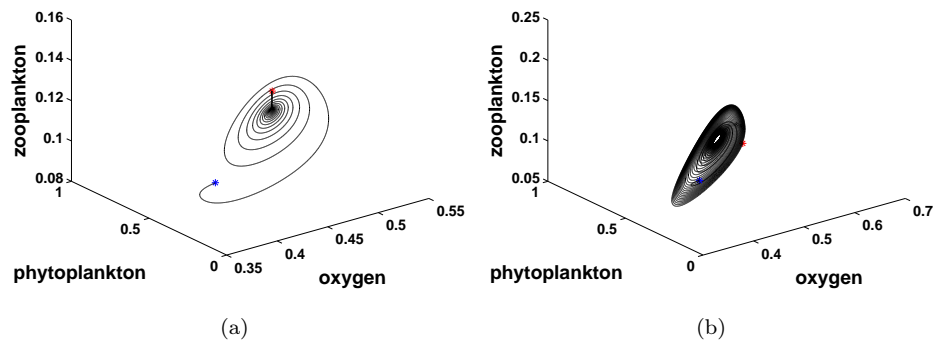


FIGURE 5.16: Phase space structure for corresponding temporal dynamics Fig. 5.15 (a) $c_0 = 0.721$, (b) $c_0 = 0.71$, $\omega = 10^{-5}$ and the initial values $c_o = 0.385$, $u_o = 0.3$, $v_o = 0.1$ and other parameters are the same as in Fig. 5.15.

at the beginning followed by oscillations increasing in amplitude. However, the situation is different for an increase in A : when $A = 2.05$ (Fig. 5.17b), the densities of plankton goes extinct and the oxygen concentration falls to zero after just a few sequence of oscillations. This sudden and dramatic change in the dynamics happens when A increases and moves, in the course of time, from Domain 3 to Domain 4 (see Fig. 4.13). Corresponding phase space structure of Fig. 5.17 is given in Fig. 5.18.

The effect of a decrease in parameter ω on the system's dynamical response is given in Figs. 5.19a–c. An interesting succession of dynamical regimes is obtained for three different values of ω that is the slope of the decreasing c_1 function.

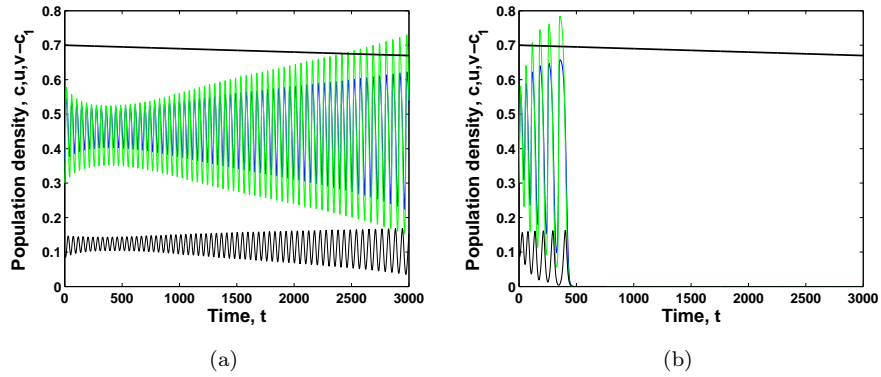


FIGURE 5.17: Effect of changes in parameter A . The density of oxygen-phytoplankton-zooplankton against time obtained for other given parameter values (a) $A = 2.01$, (b) $A = 2.05$, $\omega = 10^{-5}$ and the initial values $c_o = 0.385$, $u_o = 0.3$, $v_o = 0.1$ and system parameters are same with previous figure for fixed $c_0 = 0.7$.

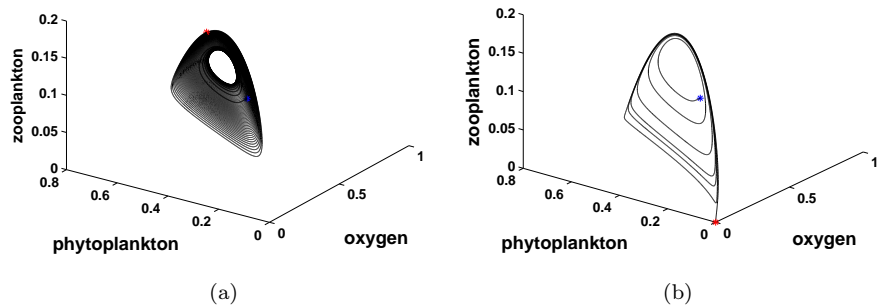


FIGURE 5.18: Phase space structure for corresponding temporal dynamics 5.17 (a) $A = 2.01$, (b) $A = 2.05$, $\omega = 10^{-5}$ and the initial values $c_o = 0.385$, $u_o = 0.3$, $v_o = 0.1$ and for fix $c_0 = 0.7$; other parameters are the same as in Fig. 5.17.

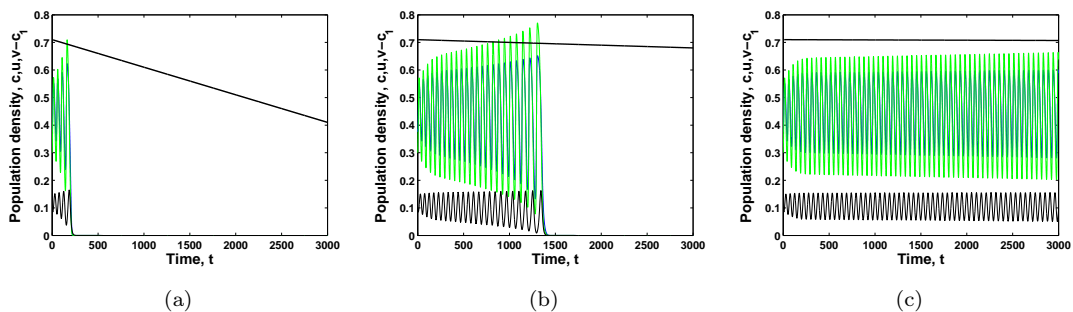


FIGURE 5.19: Effect of changes in parameter ω . The density of oxygen-phytoplankton-zooplankton against time obtained for other given parameter values (a) $\omega = 10^{-4}$, (b) $\omega = 10^{-5}$, (c) $\omega = 10^{-6}$ for fixed $A = 2.05$, $c_0 = 0.71$ with given parameter values as in text for given initials $c_o = 0.385$, $u_o = 0.3$, $v_o = 0.1$.

Fig. 5.19a obtained for $\omega = 10^{-4}$ shows that the trajectory shoots away to the extinction state, which is always stable, and then all system components go extinct after staying in the vicinity of oxygen-phytoplankton-zooplankton steady state (E_3). Moreover, the decrease in the slope of c_1 results in limit cycle behaviour with increased in a sequence in size; see Fig. 5.19b. In case $\omega = 10^{-6}$ (Fig. 5.19c), the system dynamics become periodical with the densities obviously following the stable limit cycle after a some sequence of oscillations. In the case shown in Fig. 5.19a the final value of c_1 is $c_1 = 0.41$ which is below the line crossing from Domain 3 to Domain 4. For Fig. 5.19b, the final value of c_1 is $c_1 = 0.68$ and for Fig. 5.19c the final value of c_1 is $c_1 = 0.697$, which explains the system succession (see Fig. 4.13).

5.2.4 Spatial dynamics

Throughout this section, we are going to focus on the spatial oxygen-plankton system under the effect of changing environmental conditions.

$$\frac{\partial c}{\partial t} = D_T \frac{\partial^2 c}{\partial x^2} + A \left(1 - \frac{c}{c+1}\right) u - c - \frac{uc}{c+c_2} - \frac{\nu cv}{c+c_3}, \quad (5.8)$$

$$\frac{\partial u}{\partial t} = D_T \frac{\partial^2 u}{\partial x^2} + \left(\frac{Bc}{c+c_1} - u\right) \gamma u - \frac{uv}{u+h} - \sigma u, \quad (5.9)$$

$$\frac{\partial v}{\partial t} = D_T \frac{\partial^2 v}{\partial x^2} + \left(\frac{\beta uv}{u+h}\right) \frac{c^2}{c^2+c_4^2} - \mu v. \quad (5.10)$$

Here c , u and v have the previous usual meanings at time t and position x . In numerical simulations we used the initial conditions given by Eqs. (4.29–4.31) for given parameter values. As it is mentioned in previous chapter, there is no qualitative difference between the distributions shown in Fig. 4.25a (obtained for $t = 10000$) and Fig. 4.25b (obtained for $t = 12000$). Correspondingly, we choose Fig. 4.25a as initials for the following simulations to provide a convenient comparison with Chapter 4.

In Fig. 5.20, the response of system's spatial dynamics to the increasing temperature is obtained for the parameters corresponding to the nonspatial system in Fig. 5.9. In this case, patchy distribution in spatial dynamics corresponds with nonspatial systems' limit cycle. It is clear that for different initial values, A_0 , spatial variations of the system components become remarkably irregular and fit well with the biological reality of plankton patchiness [47, 49, 70, 81, 147].

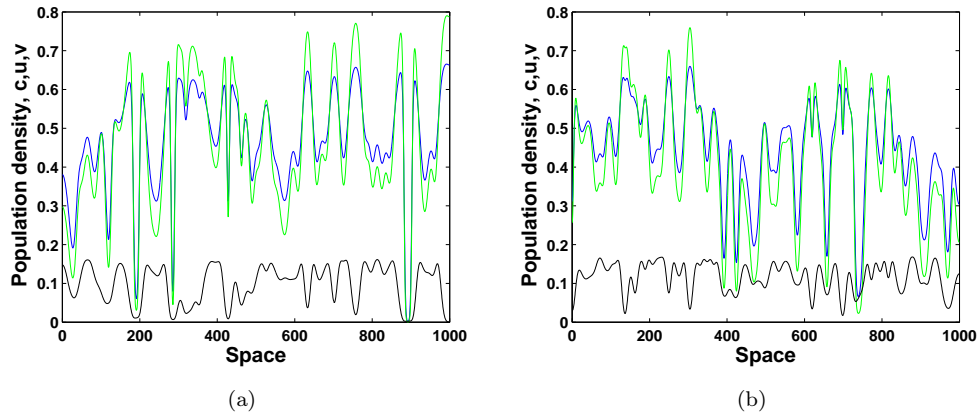


FIGURE 5.20: The effect of changing parameter A_0 and fix $c_1 = 0.7$ distribution of oxygen, phytoplankton and zooplankton over space obtained for other given parameter values (a) $A_0 = 1.97$, (b) $A_0 = 2$, $\omega = 10^{-5}$ for $t = 10000$ other parameters are same in Fig. 5.9. The initial conditions are shown as in Fig. 4.25a.

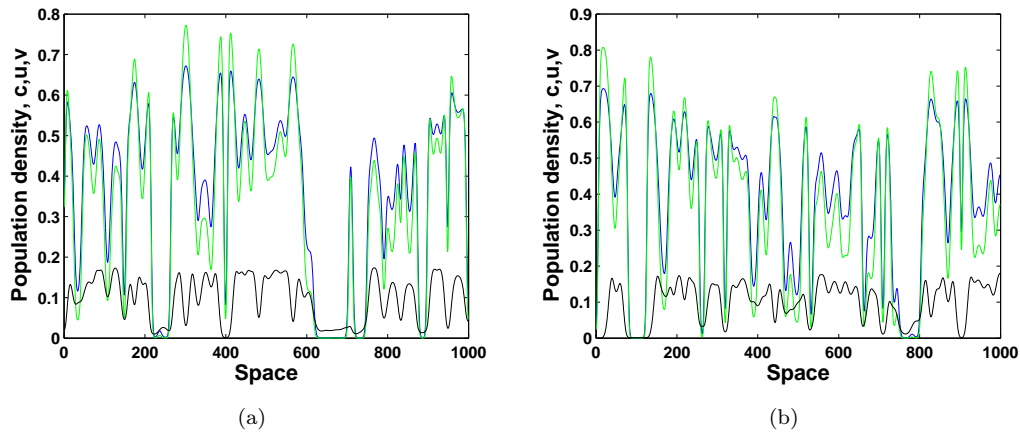


FIGURE 5.21: The effect of changing parameter A_0 and fix $c_1 = 0.7$ distribution of oxygen, phytoplankton and zooplankton over space obtained for given parameter values (a) $A_0 = 2.024$, (b) $A_0 = 2.048$, $\omega = 10^{-5}$ for $t = 10000$. Other parameters are same in Fig. 5.11. The initial conditions are shown as in Fig. 4.25a.

Figure 5.21 shows the effect of increasing temperature on the system's spatial dynamics obtained for the same parameters as in the nonspatial system given by Fig. 5.11. The patches invade the whole domain, with the system dynamics being sustainable and irregular, in Fig. 5.21a–b, although the species distributions go extinct in the nonspatial system in Fig. 5.11b.

Figure 5.22 shows the oxygen and plankton distributions obtained at $t = 10000$ for $A_0 = 2$ for the corresponding nonspatial system in Fig. 5.13. Systems' species spatial distributions are quite interesting under the influence of decreasing ω . When ω becomes presumably high enough ($\omega = 10^{-4}$), species go extinct in

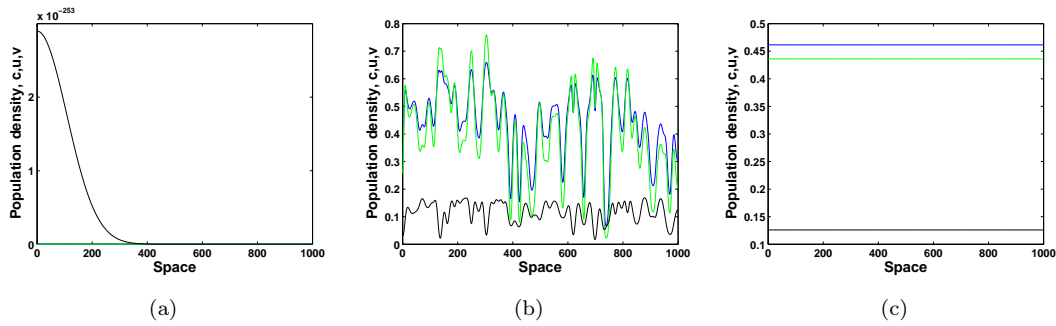


FIGURE 5.22: The effect of changing parameter ω and fix $A_0 = 2$ distribution of oxygen, phytoplankton and zooplankton over space obtained for same parameter values as in Fig. 5.13 for (a) $\omega = 10^{-4}$, (b) $\omega = 10^{-5}$, (c) $\omega = 10^{-6}$ and $t = 10000$. The initial conditions are shown as in Fig. 4.25a.

space. However, the whole numerical domain is invaded by species patchy distribution at $\omega = 10^{-5}$. In Fig. 5.13c, in spite of the corresponding nonspatial case, the spatial structure of the system's components evolve to a uniform distributions, i.e. the species densities are constant at their steady state values. Therefore, a decrease in ω turns the extinction to the one-dimensional patchy structure and a further decrease in ω leads the patchy structure to the spatially simple uniform structure.

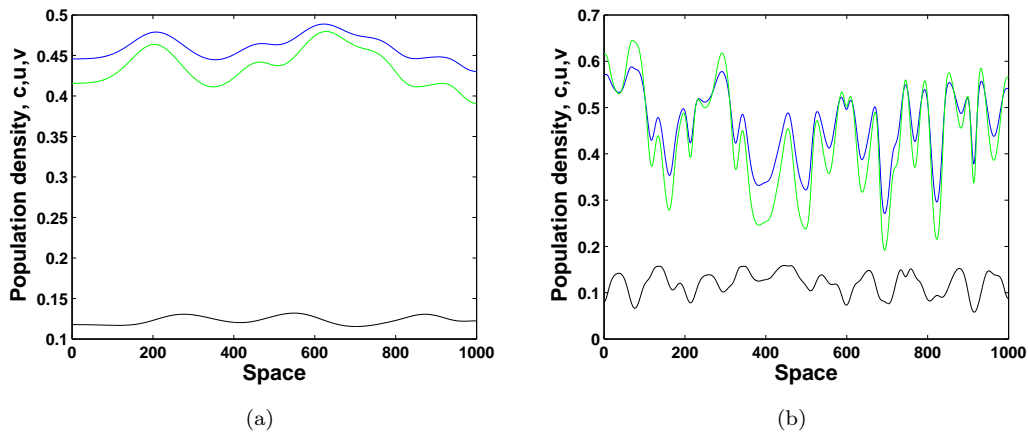


FIGURE 5.23: The effect of changing parameter c_1 and fix $c_0 = 0.7$ for different A values for distribution of oxygen, phytoplankton and zooplankton over space obtained for given parameter values (a) $A = 2.01$, (b) $A = 2.05$ and $t = 10000$ and the system other parameters are as in Fig. 5.17. The initial conditions are shown as in Fig. 4.25a.

Figure 5.23 shows the dynamical response of the system (5.8–5.10) to the changes in c_1 as in Eq. 5.7 for corresponding Fig. 5.17 for two different values of A . For $A = 2.01$ (Fig. 5.23a), the distribution of system components are rather smooth. But, for a slight difference in A , for $A = 2.05$ (Fig. 5.23b), the domain

is occupied by irregular distributions. Although, the temporal behavior of the system components consist of periodic and extinction (see Fig. 5.17), the spatial distributions of the system are dominated by the irregular structure (see Fig. 5.23).

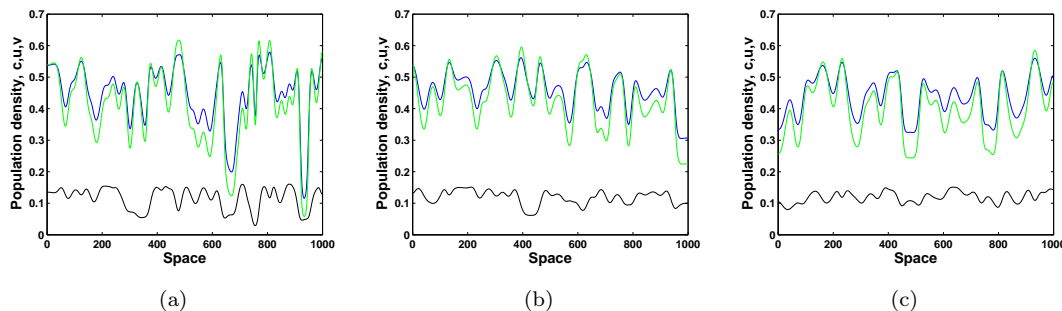


FIGURE 5.24: The effect of changes in parameter ω and fix $A = 2.05$, $c_0 = 0.71$. Distribution of oxygen, phytoplankton and zooplankton over space obtained for given parameter values (a) $\omega = 10^{-4}$, (b) $\omega = 10^{-5}$, (c) $\omega = 10^{-6}$ and $t = 10000$ and other system parameters are same as in Fig. 5.19. The initial conditions are shown as in Fig. 4.25a.

Figure 5.24 shows the simulation results in spatial system (5.8–5.10) for the corresponding nonspatial system (5.1–5.3) in Fig. 5.19. For a different set of ω , the dynamics of the system show the irregular patchy distribution, in spite of the corresponding nonspatial system demonstrating a different structure for different ω ; see Fig. 5.19. Recall that, for the parameter values of Figs. 5.24a–b, the nonspatial system goes extinct already at $t \approx 250$ and at $t \approx 1480$, cf. Figs. 5.19a–b, respectively. However, in the spatial case irregular spatiotemporal patterns persist and no extinction is observed. As a summary of the obtained results, in this chapter the spatial dynamics can be classified as patchy, regular or extinction; see Figs. 5.9–5.28.

5.3 Ecology catastrophe and paths to extinction

Throughout this section we will focus on pattern formation resulting in regular, patchy structure and extinction. To do that, our model's dynamical response to the different boundary conditions is detailed. Based on previous numerical simulations with Neumann boundary conditions we have observed some spatial dynamics resulting in extinction. Correspondingly, in this section we detail the system's dynamics as a response to the different boundary conditions, i.e. Neumann boundary conditions, (which is used in all previous simulations to describe an environment surrounded by dispersal barriers), and periodic boundary conditions (in order to avoid boundary effects on system dynamics).

Here, we define the spatially averaged densities $\langle c \rangle (t)$, $\langle u \rangle (t)$ and $\langle v \rangle (t)$ as

$$\langle k \rangle = \frac{1}{L} \int_0^L k(x, t) dx, \quad (5.11)$$

where $k = c, u, v$. Figure 5.25 shows our system's (5.8–5.10) response to two different boundary conditions. The left-top corner figure shows the maximum (solid line) and minimum (dotted line) values of oxygen concentration and plankton densities in the spatial system for large time limit. The left-bottom corner shows the corresponding average concentration of oxygen (to understand the underlying reason of extinction scenario to do that the rate of increase/decrease in size of oxygen concentration per unit time is given by the integration of its spatial distribution; see Eq. (5.11)). It is obvious that a gradual decrease of the average densities is followed by a sudden catastrophe after a range of regular distribution. For $t = 60000$ the left-top corner of Fig. 5.25, species densities suddenly drop to zero, after which the system dynamics follow a long-living transient. Extinction of system components is seen from corresponding average oxygen concentration versus time figure (see left-bottom corner of Fig. 5.25). Here, we do not give the temporal extinction scenario of plankton community for the sake of brevity, but they exhibit qualitatively similar behavior. On the other hand, this extinction scenario is not present by using different type of boundary conditions. As it is seen from the right hand side top figure maximum values of system components follow a line after a sequence of oscillations. The corresponding average oxygen concentration versus time figure (bottom, right) shows the persistency of system components for a long time limit. The time is intentionally chosen large to prove the persistence of system components.

It should be emphasized that for both of the chosen boundary conditions for the average density of oxygen in Fig. 5.25, there is a narrow regular structure between the patchy distribution and sudden drop resulting in extinction/persistence. Prompted by these two types of dynamical responses, i.e. extinction or persistence, a relevant question regarding species spatiotemporal dynamics arises. In this context, Fig. 5.26 and Fig. 5.27 give snapshots of oxygen concentration and plankton community densities for periodic boundary conditions for $A_0 = 2.02$ and $A_0 = 2.05$ for $\omega = 10^{-3}$ to illustrate the persistence and extinction scenario in space. Note that the spatial distribution to illustrate the dynamics persistence and extinction are qualitatively similar to periodic boundary conditions (see Figs. 5.26–5.27). Even if the system parameters are different in Fig. 5.26 and in

Fig. 5.27, the extinction and persistence scenario look pretty similar to the case of Fig. 5.25.

An important question is what is the rate of predicted oxygen depletion in real time units. It does not seem possible at the moment to give a reliable estimate all parameter values as the accuracy of such estimate is usually very low and can differ as much as a few orders of magnitude [113]. However, we can indeed provide an estimate for parameter m as this parameter that determines the rate of changes in the system dynamics. In particular, there is some references on real data for oxygen depletion problem [42, 99, 140].

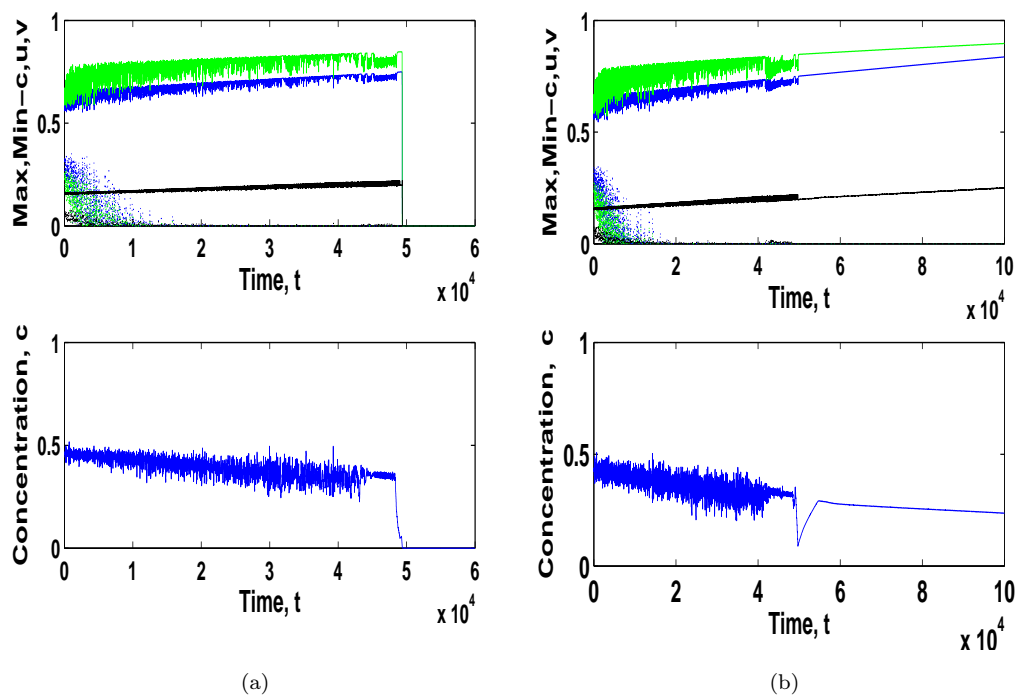


FIGURE 5.25: Maximum (solid line) - minimum (dotted line) values the density in spatial system of oxygen-phytoplankton-zooplankton and the integration of oxygen (average) concentration (a) $t = 60000$ with Neumann boundary condition, (b) $t = 100000$ with periodic boundary condition. Initials are chosen for $A = 2.05$, $t = 12000$, (see Fig. 4.26b) for $\omega = 10^{-6}$.

The snapshots of oxygen concentration and phyto-zooplankton density are shown for different time moments from top to bottom in Fig. 5.26 as an example of persistence behavior (see the similar succession in Fig. 5.25b bottom). The pattern is patchy for smaller time moments, but it is not given here for the sake of brevity. The region seems invaded by groups of patches. The groups of patches interact with each other and then some of them become extinct. The interaction between the group of patches becomes on two pulses merge each other and then extinct. Note that the merging patches phytoplankton community is grazed upon from

zooplankton community coming from a different direction. Finally the domain is invaded by only two pulses and remains the same for larger time moments. See similar succession of the dynamical system on biological invasion and biological control model in [198].

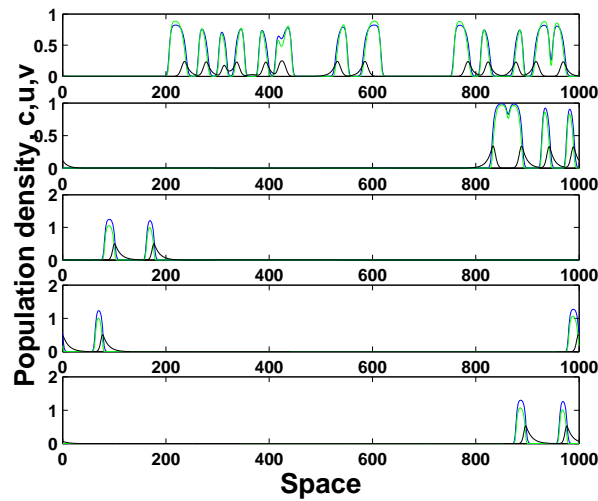


FIGURE 5.26: Snapshots of the spatial distributions of oxygen, phytoplankton and zooplankton with periodic boundary condition and with given time moments are given as $t = 500$, $t = 1000$, $t = 1900$, $t = 2000$, $t = 2100$ from top to bottom. $A_0 = 2.02$, $\omega = 10^{-3}$.

Figure 5.27 is shown as an example to illustrate the spatial distribution of oxygen concentration and plankton densities for different time moments in the case of extinction (see the similar succession in Fig. 5.26a bottom). In this case, patches move towards each other and then merge in the middle of the domain. The merging patches disappear and the new patches are not generated. This scenario happens until all of the system components go extinct. From an ecological standpoint, this situation can be interpreted by excessive predation or some kind of environmental external factors. In terms of predation, we can say that phytoplankton community in the interacting patches are attacked by zooplankton from the left and right hand side, thereby there is no way around to escape and to survive. Remarkably, the attack is continued until there is no survival. Hence, the extinction of primary producer brings the primary productivity to the edge of extinction.

This observed regularity in species distribution invokes a question about whether dynamics are actually periodic. To clarify this issue, power spectrum analysis should be made as a proof of periodicity. In order to address regular and patchy structure issues, we have to look closer into the corresponding spatial dynamics. For that purpose, we give spatial distribution of oxygen concentration and plankton densities versus space as initials conditions $A = 2.05$ obtained for

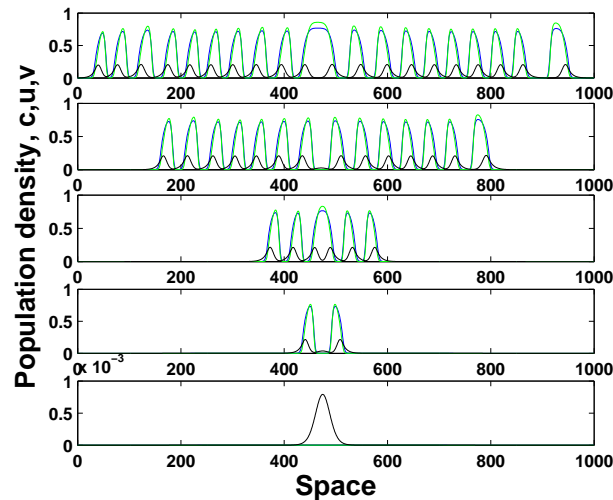


FIGURE 5.27: Snapshots of the spatial distributions of oxygen, phytoplankton and zooplankton with periodic boundary condition and with given time moments are given as $t = 3000$, $t = 3200$, $t = 3500$, $t = 3600$, $t = 3700$ from top to bottom.

$$A_0 = 2.05, \omega = 10^{-4}.$$

$t = 12000$; see the initial distributions for this parameter in Fig. 4.26b. Since the spatial distribution of system components show a qualitatively similar structure, we show only the results obtained for oxygen. Hence, we construct two different columns in Fig. 5.28. Fig. 5.28a shows the system components spatial distributions for $t = 42000$ and the Fig. 5.28c shows the corresponding power spectrum analysis and distribution function of oxygen concentration for given spatial dynamics. Similarly, Fig. 5.28b illustrates the oxygen concentration and plankton densities distributions for $t = 47000$ and the Fig. 5.28d shows the power spectrum analysis and distribution function of oxygen for given spatial distribution.

Power spectrum or spectral density is used to show the distribution of ‘signal’ of a time series over different frequencies to check the periodicity of the given system [17]. Therefore, power spectrum analysis can be used as evidence that the model system given by Eqs. (5.8–5.10) is capable of developing periodic spatial patterns. The spatial distribution remains patchy for $t = 42000$ (top-left of Fig. 5.28), in particular being prominently irregular, however at a later time $t = 47000$ (top-right of Fig. 5.28) the distribution becomes almost spatially periodic. For regular structure, Fig. 5.28b, some leading frequencies are obviously distinguished for its corresponding power spectrum figure. But for the patchy structure top-left in Fig. 5.28, periodicity is not observed and it can be said that the system is clearly non-periodic.

Figures 5.28e–f show the distribution function of oxygen concentration obtained for exactly the same parameters as in their spatial distribution and power

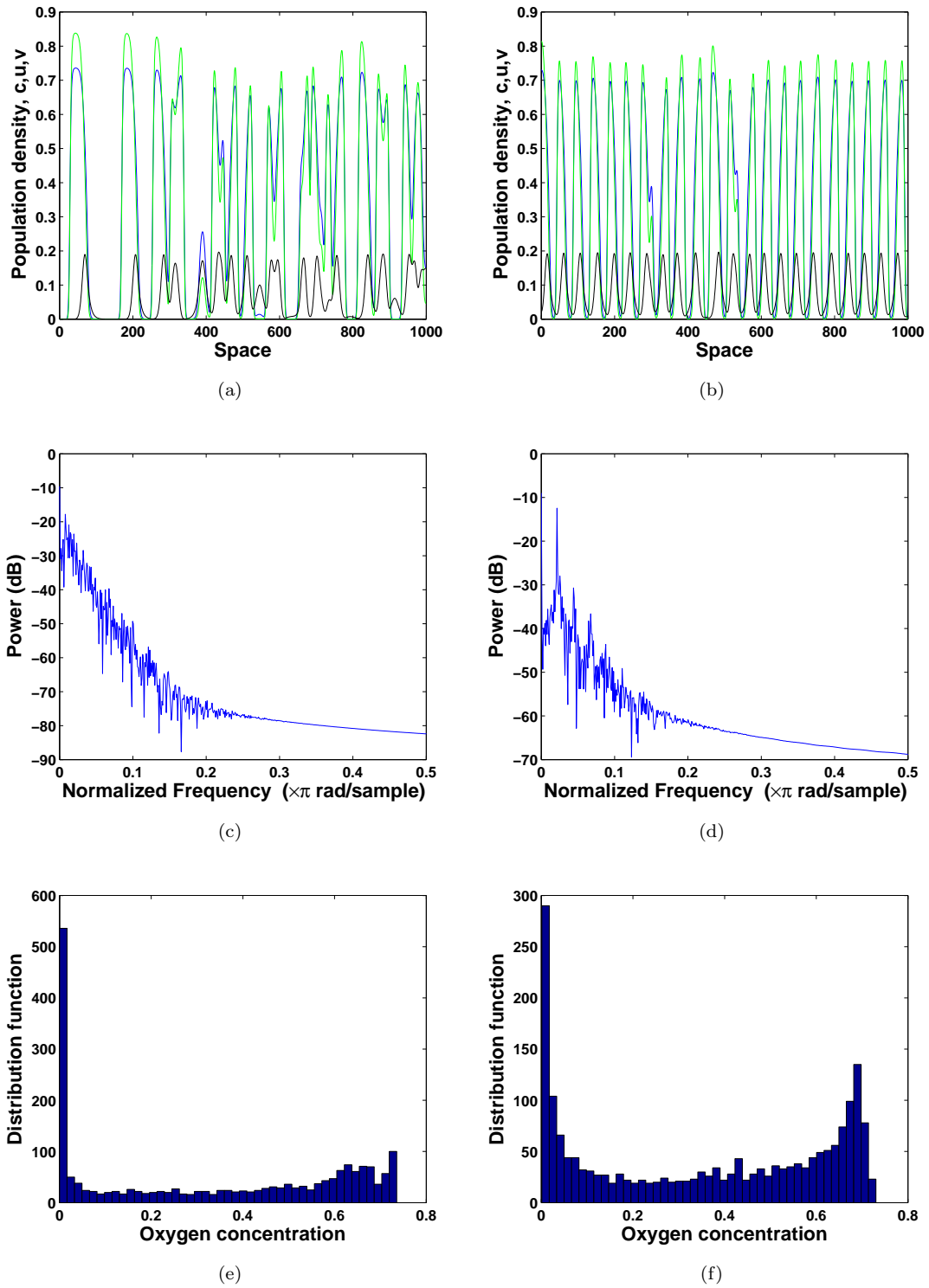


FIGURE 5.28: Spatial distribution of oxygen, phytoplankton and zooplankton for same initials as $A = 2.05$ obtained for $t = 12000$ (see in Fig. 4.26b) (a) $t = 42000$, (b) $t = 47000$, Periodogram power spectrum estimate for oxygen concentration for (c) $t = 42000$, (d) $t = 47000$, and Distribution function with Histogram (e) $t = 42000$, (f) $t = 47000$.

spectrum analysis. The obtained histogram for patchy distribution and regular distribution look somewhat similar except for the distinct maximum level where oxygen concentration equals to zero.

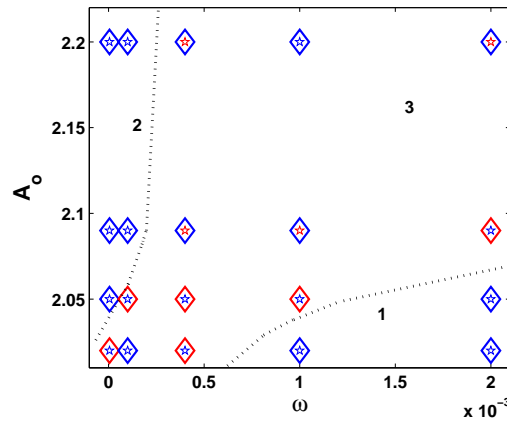


FIGURE 5.29: Sketch for paths to extinction for different initials. Blue color is used for alive and red for extinction, stars for initial conditions obtained at $t = 10000$ and diamonds for $t = 12000$, e.g. the stars lie on the line $A_0 = 2.05$ is obtained for chosen initial as in Fig. 4.26a and diamonds in the same line for the initial for Fig. 4.26b.

Based on the numerous simulations performed, we observe extinction or persistence of system components for some lower limit A_0 and for some values of ω . Figure. 5.29 is given to understand whether there is any relation between the slope of the increasing temperature and the initial limit point of the A function between the system components at extinction or persistence. Moreover, two different initial conditions are used to show that there is any dependence on existence/persistence for chosen initial conditions and with periodic boundary conditions. The x-axis shows the slope of increase (ω) in temperature, while the y-axis shows A_0 , the lower limit of temperature function. Stars show the initial conditions obtained for $t = 10000$, while the diamonds present the initials for $t = 12000$ and the blue color is used for existence and red color is for extinction. The dotted curves between Domain 1-3 and between Domain 2-3 determine the region for the system components persistence for both initial conditions. Namely, the right top corner shape with blue diamond and red star explain that the system components go extinct for chosen initial conditions $A_0 = 2.2$ and $\omega = 0.002$ when $t = 10000$. However, the blue diamond around the red star means that the species persist for chosen initial conditions when $t = 12000$. Therefore, in view of the obtained results we can say that the extinction or persistence of system components do not pursue any path and in terms of increasing/decreasing slope of temperature,

and chosen lower limit of A_0 , i.e. there is no association with the chosen initial conditions.

5.4 Discussion and Concluding remarks

In this Chapter, we have studied the oxygen-plankton dynamics by using a mathematical model taking into account the effect of zooplankton predation on phytoplankton and the plankton respiration under the effect of global climate change. The model is described by a system of three coupled ordinary differential equations in the nonspatial (well-mixed) case and by three corresponding diffusion-reaction PDEs in the spatially explicit case. The system's dynamics have been revealed by some analytical approaches and through extensive numerical simulations. We first consider a nonspatial system to reveal the structure of the parameter space. We then consider the dynamics of the spatially explicit system to show that it exhibits complicated spatiotemporal dynamics typically resulting in the formation of transient patchy patterns. Here we recall that plankton patchiness is a very common property of marine ecosystems [2, 64, 81, 143, 245] and the diffusion-reaction models of phyto-zooplankton dynamics have previously been used to describe this phenomenon, e.g. see [183], also [146, 147, 156] and references therein.

We then consider the dynamics of the corresponding non-autonomous system where some of the parameters slowly change with time to take into account the increase in the water temperature due to climate change. We show that a sufficiently large increase or decrease in the controlling parameters (in particular, in the rate of oxygen production and phytoplankton growth) can result in a sequence of bifurcations leading to a sudden decline in oxygen production and plankton extinction.

We have focused on the extinction/persistence issue to understand the underlying dynamical properties of our system; see Figure. 6.18. However, we could not find any tendency to clarify the exact reason of extinction due to the dependence on chosen initials, or slope of increasing temperature, or chosen lower limit of temperature function or on different type of the chosen boundary conditions. Importantly, we have observed that the system develops a periodic structure in time for different initial conditions and for different boundary conditions. Then follows the question whether this regularity may be used as an early warning signal as an ecological response to changing environmental conditions. This issue is going to be the focus of the following chapter.

On the other hand, our results have important implications. A lot has been said about detrimental consequences of the global warming such as, for instance, possible extinction of some species (and the corresponding biodiversity loss) and the large-scale flooding resulting from melting Antarctic ice. In this work, however, we have shown that the danger to be stifled is probably more real than to be drowned. Using a model of coupled oxygen-plankton dynamics, we have identified another possible consequence of the global warming that can potentially be more dangerous than all others. We have shown that the oxygen production by marine phytoplankton can stop suddenly if the water temperature exceeds a certain critical value. Since the ocean plankton produces altogether more than one half of the total atmospheric oxygen, it would mean oxygen depletion not only in the water but also in the air. Should it happen, it would obviously damage the marine life and ocean health.

Chapter 6

Temperature Effect, Long-living Transient

6.1 Introduction

Dissolved oxygen concentration (amount of oxygen in solution) changes during day time due to photosynthesis (existence of sunlight) and respiration (all the time) in water body [233]. This concentration becomes lowest before the sunrise and highest in the late afternoon in water body [23]. Oxygen dynamical behavior is handled in Chapter 5 in terms of increasing surrounding water temperature. Its importance is concluded and supported by results obtained in the previous chapter. It determines water body oxygen concentration by affecting primary production [101]. Therefore, the main reason is that it acts as a controlling factor on phytoplankton by changing photosynthetic mechanisms [136, 243], thereby limiting phytoplankton growth rate and photosynthetic rate by temperature [7, 60, 101]¹.

On the other hand, temperature effects on aquatic ecosystem cannot be restricted only to photosynthetic activity. It also affects the solubility rate of oxygen. Because, solubility of oxygen concentration in water body decreases under the effect of increasing temperature [20, 25, 74, 84, 95, 121, 153, 174, 230, 220], in turn dissolved oxygen concentration decreases in deep water. This process also has an impact on the rate of salinity and ventilation [153], but these factors are disregarded in this dissertation.

Temperature also has an effect on the metabolism of aquatic organisms and so on their growth. The warmer water temperature causes higher metabolism and respiration rates, within the organisms optimal temperature range [4, 59, 117]. Phytoplankton reproduction rates and upper limit of the growth are related with

¹The majority of this chapter has been prepared [225]

temperature due to the maximum rate of cell division increasing with increasing temperature [4].

In Chapter 5 we have realized the importance of increasing temperature on our dynamical system, but we did not observe any distinct result with regards to what the dynamical response of our system can be, e.g. the relation between extinction and the rate of global warming, ω , under the influence of a linearly increasing/decreasing function. To make an insight into the system's dynamical response in time, we choose the temperature function as a piecewise linear instead of linear function, contrary to Chapter 5. For that purpose, we examine the mathematical model of oxygen-plankton dynamics under the influence of changing environmental conditions by taking into account the assumption that if somehow we manage to stop the global climate change, what would the dynamical response of our model system be. Moreover, can we prevent the extinction of species and water body oxygen depletion to save aquatic life.

We used the same model system given in Chapter 4 (same model covered by Chapter 5). We then consider global warming effects on oxygen concentration and plankton densities where the rate of oxygen production changes by a "hypothetical" piecewise linear function in time to account for changing global climate. Then we consider the properties of the model by extensive numerical simulations both in the spatial and nonspatial case. Finally, we highlight the ecological and mathematical importance of our results.

6.2 Parametrization of "A" and " c_1 " functions

The model that we considered is the same model in Chapters 4 and 5. We show the model here again for the convenience of reading. For more details on the formulation of the model system and the analysis of the steady states; see Chapter 4 (Section 4.2).

$$\frac{dc}{dt} = A\left(1 - \frac{c}{c+1}\right)u - c - \frac{uc}{c+c_2} - \frac{\nu cv}{c+c_3}, \quad (6.1)$$

$$\frac{du}{dt} = \left(\frac{Bc}{c+c_1} - u\right)\gamma u - \frac{uv}{u+h} - \sigma u, \quad (6.2)$$

$$\frac{dv}{dt} = \left(\frac{\beta uv}{u+h}\right)\frac{c^2}{c^2+c_4^2} - \mu v, \quad (6.3)$$

where $c(x,0) > 0$, $u(x,0) > 0$ and $v(x,0) > 0$ and all system components and parameters have the previous, usual, meanings.

In this section, we will focus on again the external factor, i.e. temperature. Contrary to Chapter 5, the temperature function is chosen as a piecewise linear instead of a linear function to understand the population dynamics under the control of the constant and varying environmental cases.

In Chapter 5, the richness of our dynamical system is shown by choosing A and c_1 as a linearly decreasing/increasing and decreasing function, respectively. We assume that at the beginning the external factor is constant in time, then it linearly decreases or increases until a certain time, and eventually the decrease/increase stops and stabilises at a constant value. It should be emphasized that in our model system (6.1–6.3), A quantifies the rate of oxygen production, hence here we are interested in the case when changing environmental condition affects the release of oxygen molecule to the surrounding environment. To reflect the effect of temperature on photosynthesis, A again becomes a function of temperature. Then, temperature becomes a function of time resulting in A becoming a function of time with the same approach of the previous chapter. Therefore, A is taken as $A = A(t)$.

We intentionally choose the continuously changing part of c_1 as a decreasing function where higher temperature hampers phytoplankton growth ($\frac{c_1^{(2)} - c_1^{(1)}}{t_2 - t_1} < 0$). Since global warming is a slow process, we consider the rate of change in both A and c_1 to be very small (see the similar assumption in Section 5.2). Because, the increase of temperature is not favour of phytoplankton growth continuously. There is a certain temperature range for optimum phytoplankton growth. It means that if temperature exceeds this range, it results in phytoplankton death [16, 34, 208, 211, 238]. Hence, changing temperature response to phytoplankton growth is taken into account by assuming c_1 as a piecewise function decreasing in a range of time.

Specifically, we use A and c_1 functions as follows:

$$A(t) = \begin{cases} A_0, & 0 \leq t \leq t_1 \\ A_0 + \frac{A_1 - A_0}{t_2 - t_1}(t - t_1), & t_1 \leq t \leq t_2 \\ A_1, & t_2 \leq t, \end{cases} \quad (6.4)$$

$$c_1(t) = \begin{cases} c_1^{(1)}, & 0 \leq t \leq t_1 \\ c_1^{(1)} + \frac{c_1^{(2)} - c_1^{(1)}}{t_2 - t_1}(t - t_1), & t_1 \leq t \leq t_2 \\ c_1^{(2)}, & t_2 \leq t. \end{cases} \quad (6.5)$$

Here t_1 is the moment when the global warming starts, A_0 is the rate of oxygen

production ‘before change’, A_1 is the rate of oxygen production ‘after change’ and the parameter $(\frac{A_1 - A_0}{t_2 - t_1})$ quantifies the rate of global warming. In the same manner, $c_1^{(1)}$ is the change on growth of phytoplankton ‘before change’ and the parameter $(\frac{c_1^{(2)} - c_1^{(1)}}{t_2 - t_1})$ quantifies the rate of global warming; see Figs. 6.1a-b for the sketch of A and c_1 functions versus time. The thick straight black line shows the function of A and c_1 for all other parameters are constant in the course of time.

Note that the system succession for increasing A and decreasing c_1 take our attention. For the initial values of A and $c_1^{(1)}$, we assume that the ecosystem was in a ‘safe state’, namely, E_3 either being stable (Domain 2) in Fig. 4.13 or unstable and surrounded by a limit cycle (Domain 3), so that A_0 and $c_1^{(1)}$ are chosen accordingly.

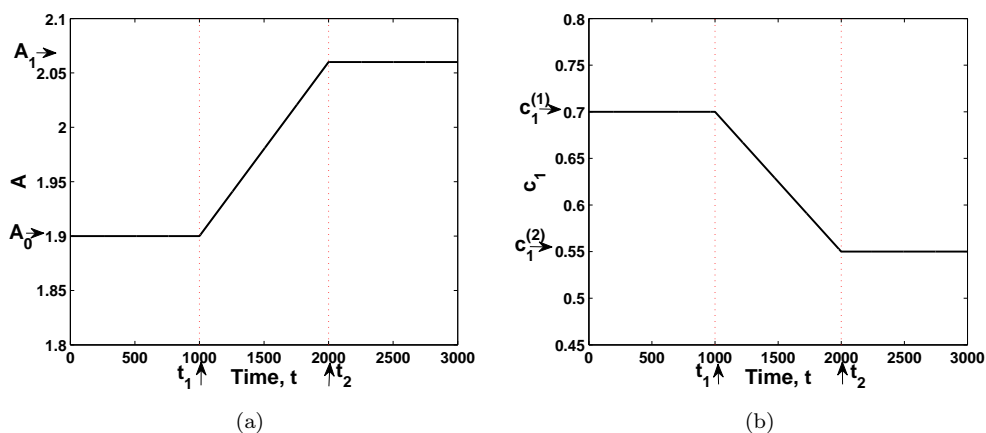


FIGURE 6.1: Sketch of A and c_1 functions vs. time for (a) $A_0 = 1.9$, $A_1 = 2.06$ and fixed $c_1 = 0.7$ for $t_2 = 2000$, $t_1 = 1000$, (b) $c_1^{(1)} = 0.7$, $c_1^{(2)} = 0.55$ and fixed $A = 1.9$ for $t_2 = 2000$, $t_1 = 1000$ and .

6.3 Numerical Simulations

6.3.1 Temporal dynamics

In this section, we perform numerical simulations on the oxygen and plankton non-spatial system (6.1-6.3). In all following numerical simulations, we fix parameters at some hypothetical values as in previous chapters: $B = 1.8$, $\gamma = 1.2$, $\sigma = 0.1$, $c_2 = 1$, $c_3 = 1$, $c_4 = 1$, $\nu = 0.01$, $\beta = 0.7$, $\mu = 0.1$, $h = 0.1$ and vary A and c_1 in a certain range. Here we focus on the temporal dynamics response of changes in A as a piecewise linear function.

The system is expected to develop, in the course of time, oscillations with an increase in A and eventually the system moves into Domain 3, hence further

away from the Hopf bifurcation curve. If the warming continues this, results in A becoming sufficiently large and reaching a critical value whereby the plankton density should go extinct; therefore the system moves to Domain 4 where the only steady state of the autonomous system is extinction.

Figure 6.2 shows the oxygen concentration and plankton densities versus time obtained for two different values of A_0 and for fixed $c_1 = 0.7$. For $A_0 = 2$ (Fig. 6.2a), population fronts propagate through decaying oscillations. The amplitude of the oscillations decreases at the beginning, it starts increasing when the system passes the Hopf bifurcation point. The increasing amplitude of oscillations up to a certain time is followed by species extinction when $A \approx 2.1$ depicting an ecological disaster (cf. Domain 4 in Fig. 4.13). For $A_0 = 2.048$ (Fig. 6.2b), the system develops periodic oscillations after which all of the species go extinct after temperature starts to increase. The increase in A ($A_0 = 2$) results in an ecological

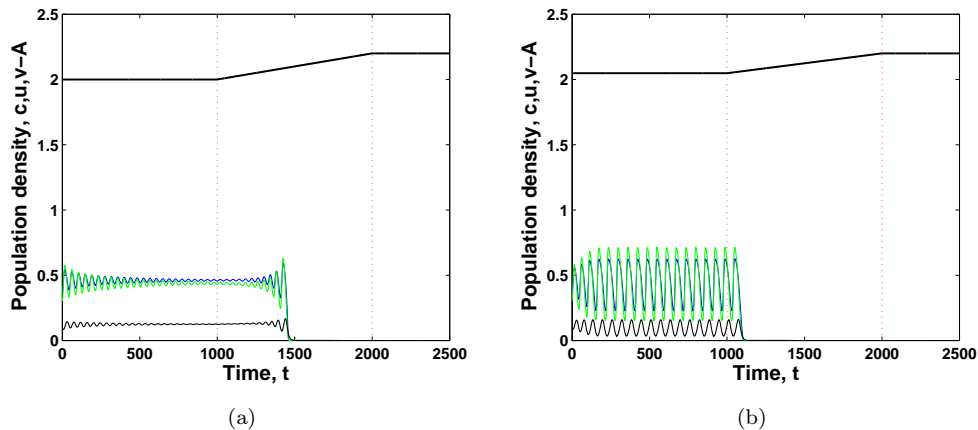


FIGURE 6.2: Effect of changes in parameter A_0 . Oxygen concentration (blue) and phytoplankton and zooplankton densities (green and black, respectively) against time obtained for other given parameter values (a) $A_0 = 2$, $A_1 = 2.2$, (b) $A_0 = 2.048$, $A_1 = 2.2$ for the chosen initial values as $c_0 = 0.385$, $u_0 = 0.3$, $v_0 = 0.1$ for fix $c_1 = 0.7$ and system parameters are given in the text. The thick black line at the top shows $A(t)$.

disaster where after a number of oscillations of increasing amplitude, plankton extinction propagates oxygen depletion in time. This dramatic and sudden change happens when A moves, in the course of time, to the parameter range where there is no limit cycle and the only existing attractor is extinction. The corresponding phase space structure for Fig. 6.2 is given by Fig. 6.3. For both of the initial values of A (A_0), the system's trajectory goes to the extinction steady state (E_1) which is always stable.

Oxygen concentration and plankton density versus time obtained for different final values of (A_1) and for fixed $c_1 = 0.7$ are shown in Figs. 6.4a-b. Fig. 6.4a,

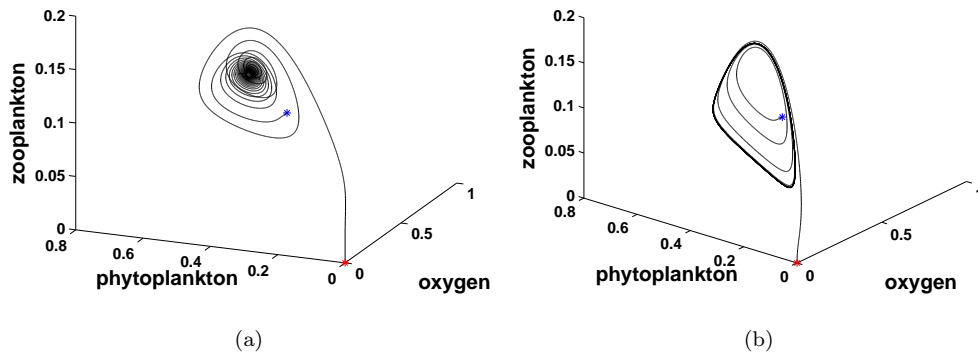


FIGURE 6.3: 3D Phase space structure for corresponding system trajectories shown in Figs. 6.2a-b. (a) $A_0 = 2$, $A_1 = 2.2$, (b) $A_0 = 2.048$, $A_1 = 2.2$ with the chosen initial values as $c_0 = 0.385$, $u_0 = 0.3$, $v_0 = 0.1$ for fix $c_1 = 0.7$; other parameters are the same as in Fig. 6.2.

the dynamics of the system develops periodic oscillations and retains its regular structure. For a slightly larger value of A_1 , Fig. 6.4b, system species go to extinction at the moment when $t_2 = 2000$. The final value of oxygen production rate determines the system succession being in the Domain 3 and in Domain 4 for Fig. 6.4a ($A_1 = 2.05$) and for Fig. 6.4b ($A_1 = 2.06$), respectively. Therefore, it can be said that the dramatic change which results in extinction or persistency happens when A moves to the parameter range in Domain 4 and in Domain 3, respectively. Figure 6.5 shows the corresponding phase space structure for Fig. 6.4.

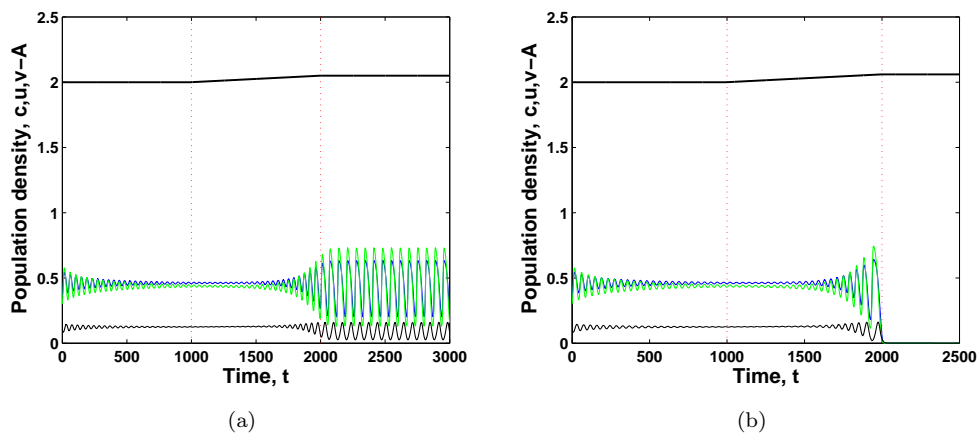


FIGURE 6.4: Effect of changes in parameter A_1 . Oxygen concentration (blue) and phytoplankton and zooplankton densities (green and black, respectively) against time obtained for other given parameter values (a) $A_0 = 2$, $A_1 = 2.05$, (b) $A_0 = 2$, $A_1 = 2.06$ for the chosen initial values $c_0 = 0.385$, $u_0 = 0.3$, $v_0 = 0.1$ for fix $c_1 = 0.7$ and system parameters are as given in the text. The thick black line at the top shows $A(t)$.

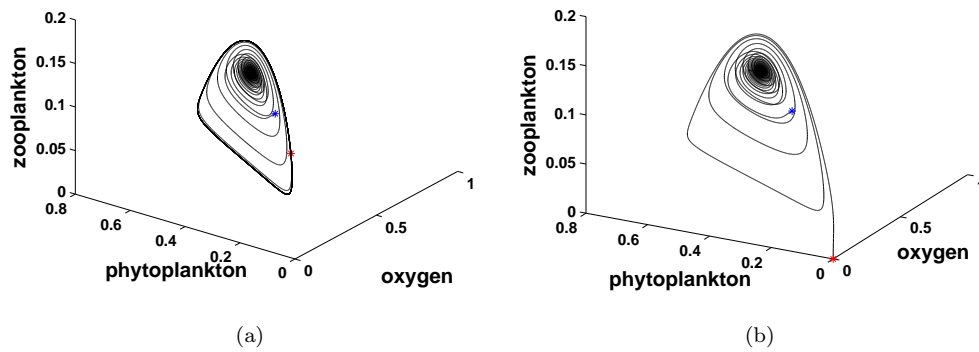


FIGURE 6.5: 3D Phase space structure of corresponding system trajectories shown in Figs. 6.4a–b. (a) $A_0 = 2$, $A_1 = 2.05$, (b) $A_0 = 2$, $A_1 = 2.06$ and the initial values $c_0 = 0.385$, $u_0 = 0.3$, $v_0 = 0.1$ for fix $c_1 = 0.7$; other parameters are the same as in Fig. 6.4.

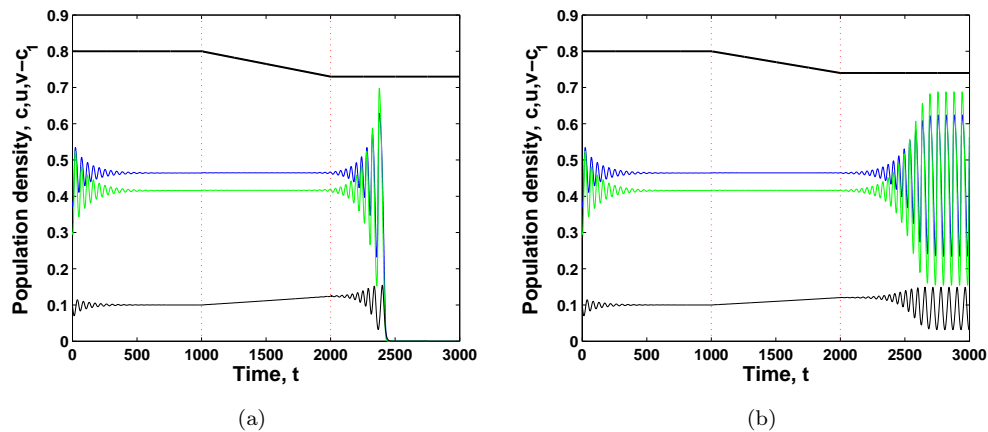


FIGURE 6.6: Effect of changes in parameter c_1 . Oxygen concentration (blue) and phytoplankton and zooplankton densities (green and black, respectively) against time obtained for other given parameter values (a) $c_1^{(1)} = 0.8$, $c_1^{(2)} = 0.73$, (b) $c_1^{(1)} = 0.8$, $c_1^{(2)} = 0.74$ and the initial values $c_0 = 0.385$, $u_0 = 0.3$, $v_0 = 0.1$ and system parameters are given in the text and for fix $A = 2.1$. The thick black line at the top shows $c_1(t)$.

The changes in the final value of parameter c_1 , $c_1^{(2)}$, for fixed $A = 2.1$ has a more subtle effect on system dynamical response; see Figs. 6.6a–b. For Fig. 6.6, oxygen concentration and plankton densities converge to their steady state value before c_1 start to decrease. In both cases, $c_1^{(1)}$ is in the parameter range where E_3 is a stable focus (Domain 3). Correspondingly, in both cases, at early times the system develops oscillations with a decreasing amplitude as the system converging to the stable steady state. For Fig. 6.6a, the final value of c_1 is $c_1 = 0.73$ which is below the Hopf bifurcation value so the oscillations decay in the course of time. It

is seen that, for Fig. 6.6a, the system exhibits oscillations of increasing amplitude up to a certain time but then suddenly go to extinction. However, for Fig. 6.6b, the final value of c_1 is $c_1 = 0.74$ above the Hopf bifurcation curve, hence oscillations keep its size in time (in this case bifurcation diagram Fig. 4.13 should be evaluated in the direction of increasing/decreasing c_1 value for fixed A). As it is readily seen from Figs. 6.6a-b, oxygen and phytoplankton densities stay stable for the region of emerging plateau, while the density of zooplankton grows steadily in time in the whole range $[t_2, t_1]$. Figure 6.7 shows the corresponding phase space structure

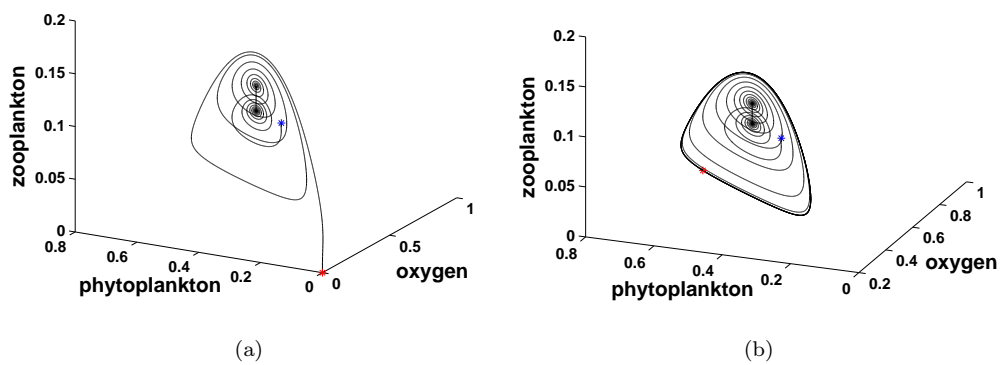


FIGURE 6.7: Phase space structure of corresponding Figs. 6.6a–b. (a) $c_1^{(1)} = 0.8$, $c_1^{(2)} = 0.73$, (b) $c_1^{(1)} = 0.8$, $c_1^{(2)} = 0.74$ for the chosen initial values as $c_0 = 0.385$, $u_0 = 0.3$, $v_0 = 0.1$ and for fix $A = 2.1$; other parameters are the same as in Fig. 6.6.

for Fig. 6.6. Then limit cycle further increases in size and approaches the steady state of E_3 , a stable focus, and then eventually goes to extinction; see Fig. 6.7a. Obviously, the separated limit cycle emerges due to the increase in zooplankton density in the range of t_2-t_1 for both cases Figs. 6.7a-b.

The effect of changes in parameter $c_1^{(1)}$ is given for fixed $c_1^{(2)} = 0.55$ in Fig. 6.8. For $c_1^{(1)} = 0.735$ (Fig. 6.8a), the system components develop periodic oscillations with constant amplitude t_1 and then after a number oscillations of increasing in amplitude the system eventually goes to extinction. For $c_1^{(1)} = 0.8$ (Fig. 6.8b), the properties of the system dynamics are qualitatively similar with Fig. 6.6a. However, here the system goes extinct when c_1 continues to decrease. For Fig. 6.8a, $c_1 \approx 0.698$ and for Fig. 6.8b, $c_1 \approx 0.675$, hence in both cases c_1 value drops below the Hopf bifurcation value. The corresponding phase plane is presented by Fig. 6.9.

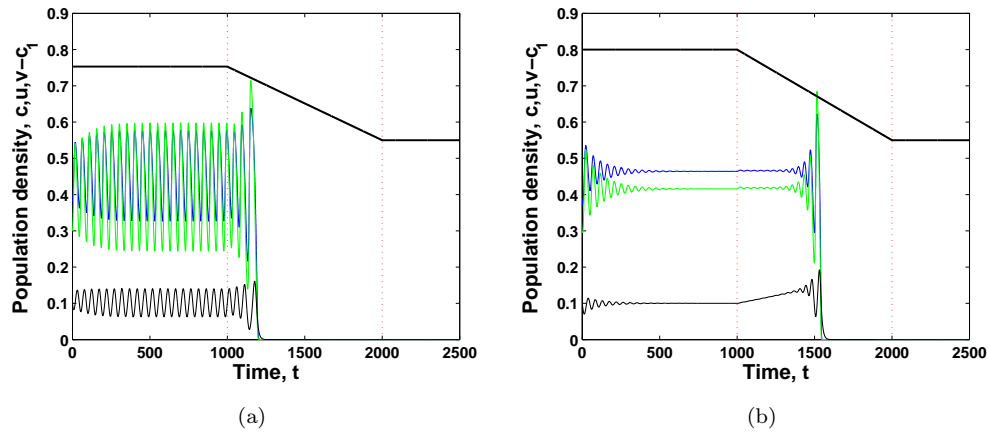


FIGURE 6.8: Effect of changes in parameter c_1 . Oxygen concentration (blue) and phytoplankton and zooplankton densities (green and black, respectively) against time obtained for other given parameter values (a) $c_1^{(1)} = 0.735$, $c_1^{(2)} = 0.55$, (b) $c_1^{(1)} = 0.8$, $c_1^{(2)} = 0.55$ for fix $A = 2.1$ and for the chosen initial values $c_0 = 0.385$, $u_0 = 0.3$, $v_0 = 0.1$ and system parameters are given in the text. The thick black line at the top shows $c_1(t)$.

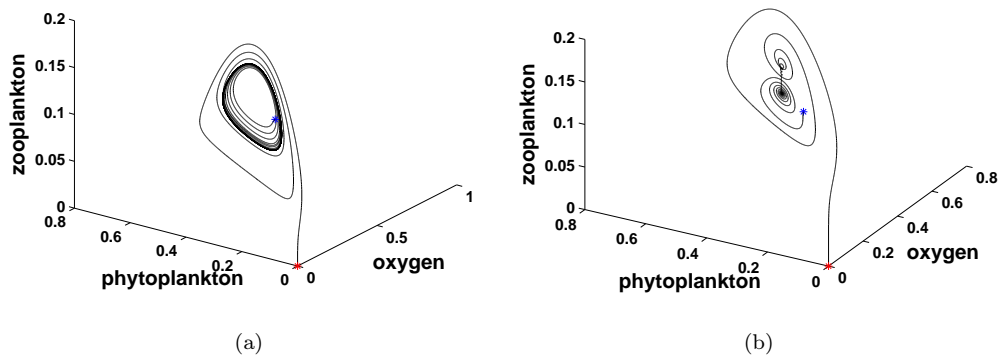


FIGURE 6.9: 3D Phase space structure of corresponding system trajectories shown in Figs. 6.8a-b, (a) $c_1^{(1)} = 0.735$, $c_1^{(2)} = 0.55$, (b) $c_1^{(1)} = 0.8$, $c_1^{(2)} = 0.55$ and the initial values $c_0 = 0.385$, $u_0 = 0.3$, $v_0 = 0.1$ for fix $A = 2.1$; other parameters are the same as in Fig. 6.8.

6.3.2 Spatial dynamics

In this section, we will focus on the spatiotemporal dynamics of the oxygen-plankton system described by the following equations as in previous chapters

(Chapters 4 and 5):

$$\frac{\partial c}{\partial t} = D_T \frac{\partial^2 c}{\partial x^2} + A \left(1 - \frac{c}{c+1}\right) u - c - \frac{uc}{c+c_2} - \frac{\nu cv}{c+c_3}, \quad (6.6)$$

$$\frac{\partial u}{\partial t} = D_T \frac{\partial^2 u}{\partial x^2} + \left(\frac{Bc}{c+c_1} - u\right) \gamma u - \frac{uv}{u+h} - \sigma u, \quad (6.7)$$

$$\frac{\partial v}{\partial t} = D_T \frac{\partial^2 v}{\partial x^2} + \left(\frac{\beta uv}{u+h}\right) \frac{c^2}{c^2+c_4^2} - \mu v. \quad (6.8)$$

Here c , u and v keeps the usual previous meanings as concentration of oxygen, densities of phytoplankton and zooplankton, respectively at time t and position x . The specific form of the model Eqs. (6.6–6.8) and assumptions on the model structure can be easily found in Chapters 2–4. Eqs. (6.6–6.8) are solved numerically, in a finite domain $0 < x < L$ where L is the domain length, by the finite difference method with zero-flux boundary conditions. The mesh steps are chosen as $\Delta x = 0.5$ and $\Delta t = 0.01$ and a further decrease in mesh step size is checked to prevent numerical artifacts.

In this chapter, the initial species distribution is patchy for zooplankton with uniformly distributed oxygen and phytoplankton at their steady states which is described in Chapter 4 and Chapter 5 (Eqs. (4.29–4.31)).

Similarly, the results from the previous chapters (Chapter 4–Chapter 5) show that spatial distributions are classified as patchy, regular (distribution) and extinction and are valid for this chapter too. For this purpose, the aim of this chapter is to closer look into the path of extinction and understand the behavior of our system (6.6–6.8) under the effect of chosen controlling parameters A and c_1 as in Eqs. (6.4–6.5).

Figure 6.10 shows simulation results of the spatial system (6.6–6.8). Fig. 6.10, for $A_0 = 2$, it seems that the domain is invaded separated patches. However, for $A_0 = 2.048$ (Fig. 6.10), this separation is not obvious. For some parameter values we have observed more clear separation of patches more than in Fig. 6.10a; see Fig. 6.11b. Some of the patches disappear as a result of patch interaction and the remaining patches seem as a separated as in Fig. 6.11b (see the similar succession in Chapter 5 from Figs. 5.26–5.27).

Figure 6.12 shows the snapshots of oxygen and plankton distribution for the parameters corresponding to the nonspatial system given in Fig. 6.4. The local system (see Fig. 6.4) exhibits extinction, however the spatial system's dynamics are sustainable with irregular spatiotemporal pattern persisting and no extinction.

Figure 6.13 shows snapshots of oxygen and plankton distribution for the corresponding nonspatial system given in Fig. 6.6. For a slight change in $c_1^{(2)}$ the

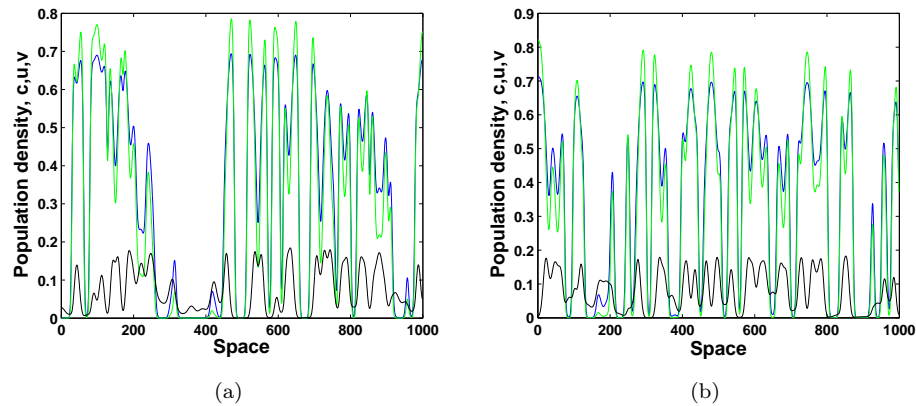


FIGURE 6.10: The effect of changes in parameter A_0 and fix $c_1 = 0.7$ on distribution of oxygen, phytoplankton and zooplankton over space obtained for other given parameter values (a) $A_0 = 2$, $A_1 = 2.2$, (b) $A_0 = 2.048$, $A_1 = 2.2$, $t = 10000$ and time difference ($\tau = (t_2 - t_1) = 1000$) for $t_2 = 2000$, $t_1 = 1000$; other parameters are same in Fig. 6.2. The initial conditions are shown as in Fig. 4.25a.

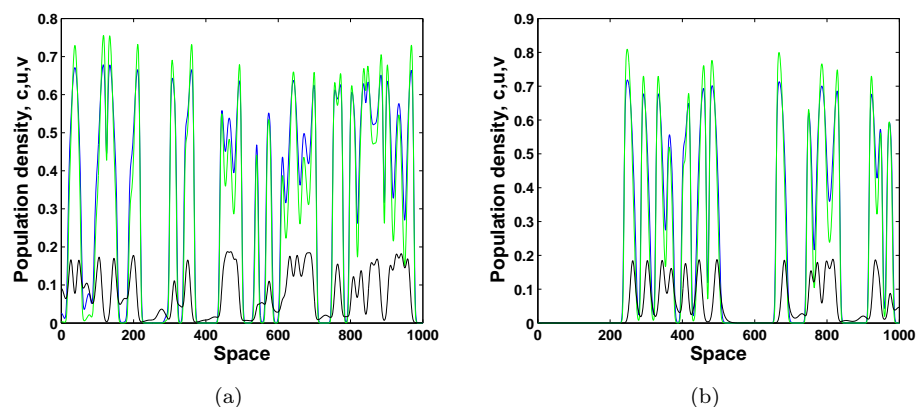


FIGURE 6.11: The density of oxygen-phytoplankton-zooplankton against space obtained for other given parameter values (a) $A_0 = 2.05$, $A_1 = 2.2$, (b) $A_0 = 2.05$, $A_1 = 2.25$ $t = 10000$, other system parameters are given in the text. The initial conditions are shown as in Fig. 4.25a.

system persists through formation of spatiotemporal patterns. However, we recall that, for this value of $c_1^{(2)}$, Fig. 6.6a, the corresponding nonspatial system goes to extinction.

Figure 6.14 shows simulation results for the spatial system corresponding to parameter values of the nonspatial system in Fig. 6.8. The corresponding nonspatial system exhibits extinction for both cases of $c_1^{(1)}$ Figs. 6.8a–b. But in the spatial system, extinction is observed for only the second case $c_1^{(1)} = 0.8$ Fig. 6.14b. For a lower value of $c_1^{(1)} = 0.735$ the system's spatial dynamics form a regular structure and the distribution becomes almost spatially periodical.

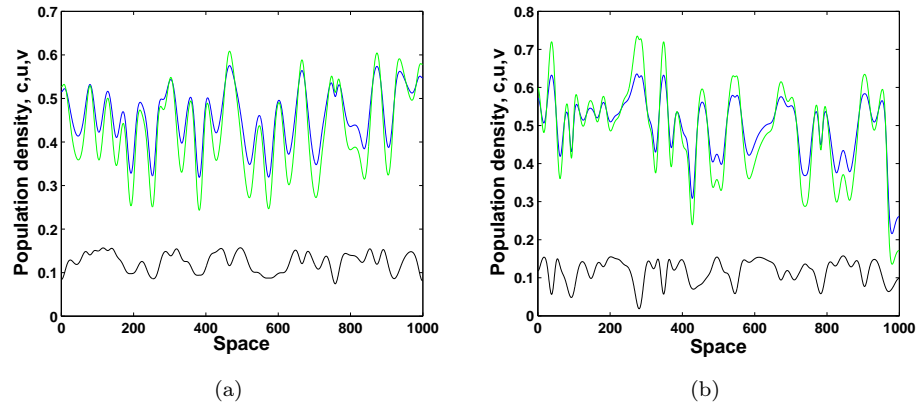


FIGURE 6.12: The effect of changes in parameter A_1 and fix $c_1 = 0.7$ distribution of oxygen, phytoplankton and zooplankton over space obtained for other given parameter values (a) $A_0 = 2$, $A_1 = 2.05$, (b) $A_0 = 2$, $A_1 = 2.06$, $t = 10000$ for $t_2 = 2000$, $t_1 = 1000$ and other system parameters are same as in Fig. 6.4. The initial conditions are shown as in Fig. 4.25a.

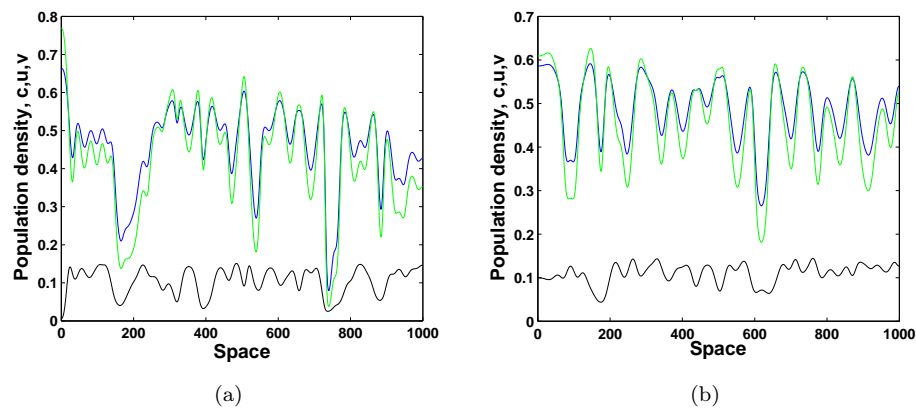


FIGURE 6.13: The effect of changes in parameter $c_1^{(2)}$ and fix $A = 2.1$ distribution of oxygen, phytoplankton and zooplankton over space obtained for other given parameter values (a) $c_1^{(1)} = 0.8$, $c_1^{(2)} = 0.73$, (b) $c_1^{(1)} = 0.8$, $c_1^{(2)} = 0.74$, $t = 10000$ for time difference ($\tau = 1000$) for $t_2 = 2000$, $t_1 = 1000$, other system parameters are same in Fig. 6.6 The initial conditions are shown as in Fig. 4.25a.

6.4 Extinction, early warning signals and intermittency

As it is shown in the previous chapters (Chapter 4 and Chapter 5), the model system (6.1-6.3) spatial distribution is lead by patchy, regular or extinction structure. Different types of system spatial distribution invokes a question that the existence of the early warning signal of the approaching ecological disaster.

For a different values of A_1 and for fixed A_0 , the system's spatial distribution is given by Fig. 6.15. As it is seen that for $A_1 = 2.1$ (Fig. 6.15a), the domain is

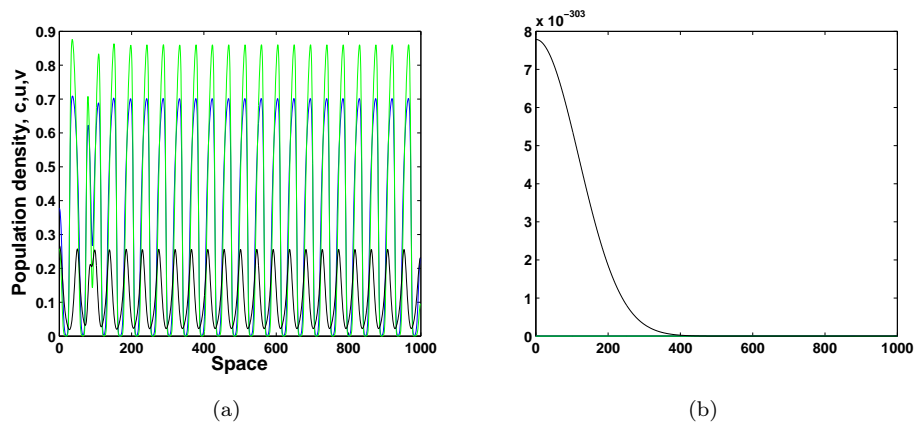


FIGURE 6.14: The effect of changes parameter $c_1^{(1)}$ and fix $A = 2.1$ distribution of oxygen, phytoplankton and zooplankton over space obtained for other given parameter values (a) $c_1^{(1)} = 0.735$, $c_1^{(2)} = 0.55$, (b) $c_1^{(1)} = 0.8$, $c_1^{(2)} = 0.55$, $t = 10000$ and time difference ($\tau = 1000$) for $t_2 = 2000$, $t_1 = 1000$ other system parameters are same as in Fig. 6.8. The initial conditions are shown as in Fig. 4.25a.

invaded by a strongly irregular patchy structure. Although, for a larger value of A_1 , $A_1 = 2.27789$, (Fig. 6.15b), the region is occupied by an almost regular structure. This regularity is happen for different value of A_1 ; see Fig. 6.15d. A further increase in A_1 , $A_1 = 2.277967$, shown in Fig. 6.15c, leads to the formation of separate patches. Note that, the systems' A_1 values depicted in Fig. 6.17, which shows the corresponding spatial distribution on line chart.

As before Chapter 5, we need to prove the periodicity of the system. For this reason, we choose two different values of A_1 from Fig. 6.15. The first column corresponds to $A_1 = 2.1$, (Fig. 6.15a). Left-top corner of Fig. 6.16 shows the maximum (solid line) and minimum (dotted line) values of oxygen concentration for corresponding figure (Fig. 6.15a). The below figure, left column second row shows the average concentration of oxygen (see Eq. (5.11)). For $t = 12000$ the left-top corner of Fig. 6.16, oxygen concentration and plankton densities follow a long-living transient. The corresponding oxygen concentration versus time figure (second row, left) shows the persistence of oxygen concentration for a long time limit. The left bottom panel of Fig. 6.16 shows the periodicity of the system dynamics. Distinct peaks are not observed for the given set of parameters, hence the system is not periodic (see more details on periodicity in Section 5.3).

The second column of Fig. 6.16 is for $A_1 = 2.27789$, as in Fig. 6.15b. The system components maximum and minimum values follow a different path from Fig. 6.16 top-left corner. The system has some irregularity in terms of maximum-minimum vs. time and average density of oxygen vs. time, it is clear from its

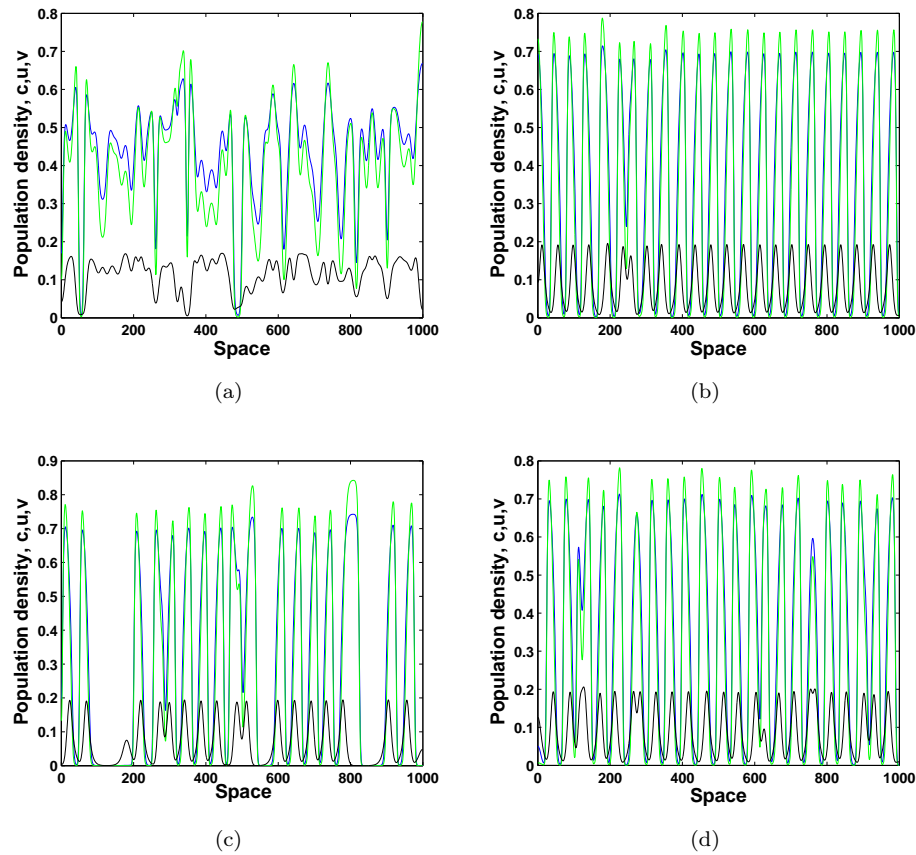


FIGURE 6.15: The effect of changes in parameter A_1 , taking values from Fig.6.17, on distribution of oxygen, phytoplankton and zooplankton over space obtained for other given parameter values (a) $A_0 = 2.05, A_1 = 2.1$, (b) $A_0 = 2.05, A_1 = 2.27789$, (c) $A_0 = 2.05, A_1 = 2.277967$, (d) $A_0 = 2.05, A_1 = 2.283$, initial conditions and time difference ($\tau = 170$) for $t_2 = 270, t_1 = 100$ and $t = 12000$; other parameters are same as in the text. The initial conditions are shown as in Fig. 4.25a.

power spectrum analysis that some leading frequencies are observed for Fig. 6.16 (bottom-right). In this case, it can be said that the decrease on A_1 lets the periodicity disappear .

Figure 6.17 shows spatial succession of the pattern formation for fixed A_0 and τ ($\tau = t_2 - t_1$). The x-axis formed by varying A_1 values with given order. Systems' patchy distribution, periodic structure and extinction are illustrated by green, yellow and red bars, respectively. For small A_1 values, the system results in the formation of irregular patchy distributions. The patchy distribution is preceded by a regular structure as it is given in Fig. 6.15b. Interestingly, this regular spatial distribution is preceded by the extinction of oxygen concentration and plankton densities. But an increase in A_1 , plankton densities and oxygen concentration become patchy and the scenario is followed by this kind of path (first patchy, second regular and then extinction) as it is defined in Fig. 6.17 from

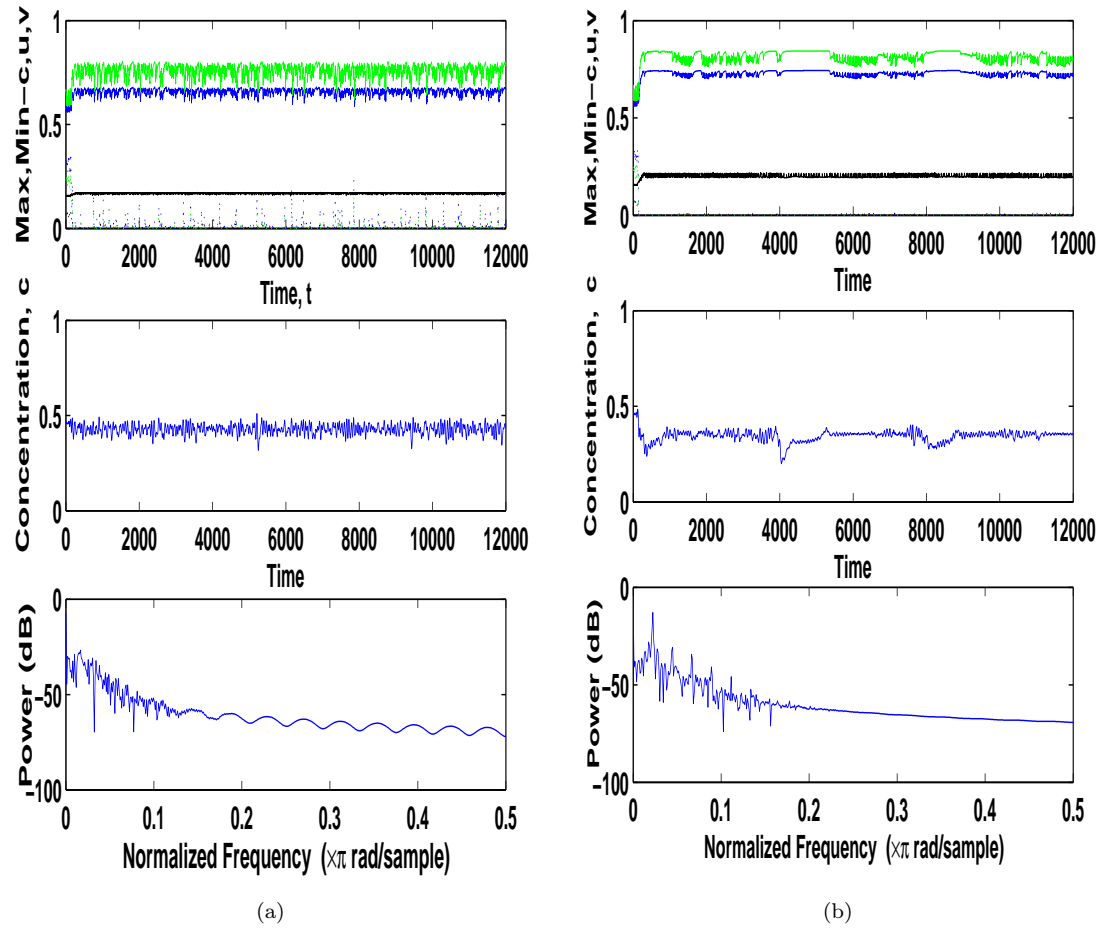


FIGURE 6.16: Maximum-minimum values of oxygen, plankton densities in spatial system, average concentration of oxygen concentration and the power spectrum analyse. (a) $A_0 = 2.05$, $A_1 = 2.1$ $t = 12000$, (b) $A_0 = 2.05$, $A_1 = 2.27789$, $t = 12000$ Initial conditions are same $A_0 = 2.05$ and $t = 12000$. The initial conditions are shown as in Fig. 4.25a.

left to right in the direction of given arrow. It should be emphasized here that after the last red column, we did not observe any evidence of the existence of system components. Therefore, the last red column on the right hand side shows the final stage of the given system and it is followed by red columns.

To observe this kind of pattern, system spatial dynamics has been checked by over 4000 numerical simulations to understand underlying structure for different initial values, where $A_0 = 2.02$, $A_0 = 2.05$, $A_0 = 2.09$ and $A_0 = 2.09$ and for different $\tau = 10$, $\tau = 20$, $\tau = 50$, $\tau = 100$, $\tau = 170$, $\tau = 300$ and $\tau = 500$. It is shown that extinction state is preceded by regular structure and the regular structure is preceded by patchy structure, in turn. The corresponding sketch of the system structure for given time difference $\tau = 170$ and for $A_0 = 2.05$ is given by Fig. 6.17. Here $A_1^{(i)}$ where $i = 1, 2, \dots, 7$ show the first observation points

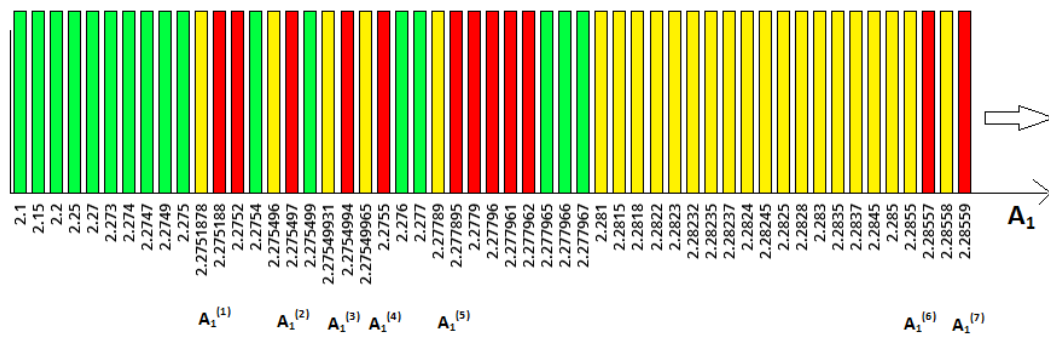


FIGURE 6.17: The oxygen-plankton system pattern formation for time difference $\tau = 170$ for $t_2 = 270$, $t_1 = 100$ for $A_0 = 2.05$ and $t = 12000$, yellow bar (regular), red bar (extinction), green bar (existence).

of extinction. These values are given to show the general structure of system dynamics, but they can be enhanced by choosing their closest values.

The biological standpoint, in reality, increasing temperature is highly connected with changes in plankton dynamics and subsequently affecting species life cycle and food web dynamics [222]. It is observed that, there is a recovery on plankton community to support life being in oxygen production is not too small or high. For this reason dynamical scheme of model system is formed as cascade pattern as it is seen in Fig. 6.17.

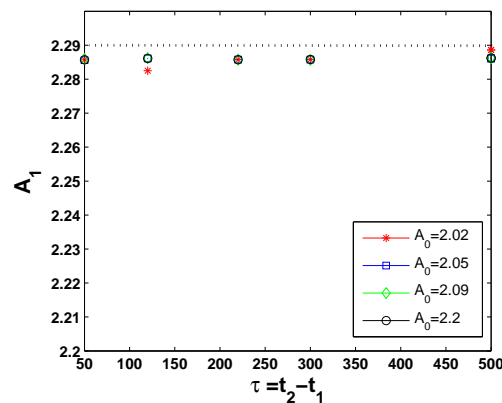


FIGURE 6.18: The oxygen-plankton system extinction diagram for different initial values of A_0 . The extinction tendency of these initial values are roughly shown by dashed line with given colors.

Critical thresholds are observed in many complex dynamical systems. In this case, early warning signal may be an important indicator of future catastrophic ecological events [221]. Fig. 6.18 shows the collection of data points for detection of extinction for different initial values $A_0 = 2.02$, $A_0 = 2.05$, $A_0 = 2.09$, $A_0 = 2.2$,

which are shown for different signs shown as in figure label and for different time difference, i.e. τ . The line chart in Fig. 6.17 is a specific illustration for $\tau = 170$ for Fig. 6.18. The most interesting part of this result is that for different time differences, i.e. τ , we can draw a threshold line for the extinction. It can be seen in Fig. 6.18 that the difference in lower limits of the net oxygen production rate before changes, A_0 , does not effect the threshold level. If we call the threshold level as θ , we can say that the level of the threshold $\theta \approx 2.29$. Remarkably, the interesting point here is that when the system parameters are close to the threshold value, the spatial distributions of system dynamics show a regular structure for a large range of A_1 ; see the yellows charts for the given range, i.e. (2.281, 2.2855), which can be regarded as an early warning signal of the approaching catastrophe.

6.5 Discussion and Concluding remarks

In aquatic system, plankton spatial distribution is highly inhomogeneous and many external factors play a role in the formation of the plankton patches such as nutrients availability, temperature, predation etc. [2, 64, 81, 143, 245]. But here, we only concentrate on the temperature factor by taking into account the effect of temperature on oxygen production rate and oxygen production effect on phytoplankton growth.

This issue is addressed theoretically by considering a model of a coupled plankton-oxygen dynamics where the rate of oxygen production and its effect on phytoplankton growth change as a piecewise function with time to account for the global climate change.

The model is described by a system of three coupled ODEs in the non-spatial case and by three corresponding diffusion-reaction PDEs in the spatially explicit case. The system dynamics have been revealed by some extensive numerical simulation under the effect of changing temperature response to oxygen production rate and phytoplankton growth with time, respectively. We showed that a sufficiently large increase in the oxygen production rate results in a sudden plankton extinction and oxygen depletion. Similarly, we showed that a sufficiently large increase in the oxygen production effect on phytoplankton growth is resulted in the same ecological disaster.

The results (extinction case) shown in Figs. 6.2, 6.4b, 6.8, 6.14b are supported by the oxygen minimum zone biological study. According to this biological observation, plankton density is undetectable when oxygen concentration is minimum, whilst it is detectable when oxygen exceeds its certain critical level (0.2 ml

l^{-1}) [50, 151]. Moreover, respiration and photosynthesis increase with increasing temperature up to a certain level, but the increase in respiration is more rapid than photosynthetic rate [138].

Our study leaves a number of open questions on changing temperatures. At high temperatures, oxygen concentration becomes low which explains some ecological events such as decline on oxygen solubility, the increase on the decomposition of sediment and the increase on respiration [28]. Generally, higher oxygen consumption rates occur at higher temperatures due to the temperature effect on metabolic activities [32]. However, our results show that the further increase of the final value of A (A_1) of the temperature function resulted in extinction. Also, if water temperature exceeds the optimum temperature level for algal growth, produced algal biomass and amount of algae that enter the water body from outside is decreased. Thereby, increasing temperature causes decrease of oxygen level due to decrease of existing plankton population [95].

Chapter 7

Conclusions

Plankton dynamics in marine ecosystem have been a focus of significant interest for several decades. There is a plenitude of literature addressing various aspects of plankton functioning by using mathematical modelling and numerical simulations, usually regarding the phytoplankton and zooplankton coupling as a prey-predator system. However, neither oxygen production by phytoplankton nor the effect of oxygen on the plankton dynamics have been considered systematically. Moreover, to the best of our knowledge, the plankton-oxygen dynamics subject to the climate change has never been considered at all, in spite of its obvious ecological importance.

Understanding of the temporal dynamics creates a convenient framework for the understanding of the complex dynamics skeleton of the spatiotemporal system, thus in this dissertation our main goal was to examine oxygen-plankton system in the sense of both temporal and spatial pattern formation. The underlying structure of this work can be summarized as follows: the basic oxygen-phytoplankton model is improved by taking into account the effect of predation together with plankton respiration. The model also considered how the system dynamics can be affected by changing water temperature. We observe that the impact of increasing water temperature induces oxygen depletion in aquatic systems. This result has been supported through numerous simulations which give rise to interesting nonspatial and spatial plankton dynamics. A consequence of changing global temperatures includes the sudden stop of photosynthetic activity of phytoplankton which results in oxygen depletion.

In all of the performed numerical simulations one controlling parameter (oxygen production rate A) is chosen and the changes in temporal and spatial structure is considered subject to its variation, while all other system parameters are fixed at their hypothetical values to provide relevant comparisons between the

different models.

Chapter 1 provides a biological literature review of oxygen and plankton dynamics thereby enhancing the understanding of underlying ecological mechanisms of our subsequent models. In Chapter 2 we present the two-component (oxygen-phytoplankton) mathematical model which we refer to as the “baseline model”. The nonspatial case is described by a system of two coupled ordinary differential equations and its spatially explicit counterpart takes into account the transport of phytoplankton and oxygen through turbulent diffusion which results in a system of two coupled reaction diffusion equations. It should be emphasized here that in this thesis we are interested in the possibility of non-Turing patterns, hence the diffusivity is chosen same for all of the system components and it is assumed that this situation stems from the same turbulent mixing. Results presented include a combination of analytical and numerical simulations for the temporal case, whilst the results for the considerably more complex spatial case were solved numerically. Since our model takes into account only very general, generic interactions in the oxygen-plankton system, we believe that the model predictions possess a considerable degree of generality.

Our first observation here is that for our oxygen-phytoplankton system, the concentration of oxygen and density of phytoplankton remain close to their steady state or go to extinction where the baseline model has two steady states (see Chapter 2 for further details). The observed properties of the system are therefore reminiscent of the dynamics of other ecologically relevant reaction-diffusion systems, e.g. see [147, 261], which helps to verify the model properties and to interpret the results. Perhaps the most interesting property of our ‘baseline’ oxygen-phytoplankton model is that phytoplankton is predicted to survive only if the rate of oxygen production is above a certain critical value; see condition given by Eq. (2.22). Since the rate of oxygen production may be expected to depend on the properties of the environment, it makes our model a convenient and relevant theoretical tool that can be used for the purposes of nature conservation and marine ecosystem management.

To make our model more realistic we incorporate the effects of predation keeping in mind the properties of the well known prey-predator model [147]. Therefore, in Chapter 3, we consider oxygen-phytoplankton-zooplankton model dynamics to make an insight into the basic properties of the plankton-oxygen interactions and in particular the effect of predation on oxygen dynamics. The system dynamics have been revealed by some analytical approaches and by extensive numerical

simulations. We first consider the nonspatial model and show that it predicts possible oxygen depletion under certain environmental conditions. We then consider the spatially explicit model and show that it exhibits a rich variety of spatiotemporal patterns including travelling fronts of oxygen depletion, dynamical stabilization of unstable equilibrium and spatiotemporal chaos.

Understanding the predation effect on our oxygen-plankton model system led us to develop more comprehensive model. Therefore, the model presented in Chapter 4 extends the existing model through the addition of plankton respiration. We focus on the stability analysis of the system's steady states through bifurcation diagrams. As a next step we investigate the system's spatial distribution dependence on the chosen initial conditions to ensure phytoplankton patchiness, as observed in nature. In particular, the one dimensional case resulted in a strongly irregular patchy distribution for large values of A . However, for small values of A , the system's spatial distribution becomes smooth. Finally, we present how these results can be extended to the two-dimensional case. In the two-dimensional case, small values of A lead to the patchy distribution of oxygen and an increase in A results in a more regular structure. Perhaps the most interesting result of this chapter is that a further increase in A would lead to extinction regardless of the initial conditions. For larger values of A in the two-dimensional case, a pattern of stripes is observed rather than patches. In some cases, the stripes keep their position for the course of time or leave the domain by moving to the boundary.

In Chapter 5 we revisit the model presented in Chapter 4 and extend our interest to the effects of global climate change. Namely, we consider the dynamics of the corresponding nonspatial system with parameters as linear functions of time. The increase/decrease in controlling parameters (in particular, oxygen production rate and phytoplankton growth) results in a sequence of bifurcations leading to a sudden plankton extinction and oxygen depletion. The decreasing values of A effect in Section 5.2.1 and the increasing values of A effect in Section 5.2.2, it can probably be said that the system dynamics always leads to system components extinction for sufficiently large decrease in A (low oxygen production rate) and for sufficiently large increase in A (high oxygen production rate). Recall that in corresponding model the global warming is assumed to continue indefinitely. Therefore, there is a safe parameter range of A for the persistence of all system components. Another focus of interest was to investigate how the chosen boundary conditions affect the emergence of extinction. Is there any difference on system's species sustainability in the one dimensional system's (4.7-4.9) dynamics with zero-flux Neumann boundary conditions compared to periodic boundary conditions? In

both cases, it is observed that the system evolves into a periodical spatiotemporal structure. However, as it is seen in Fig. 6.18, there is no dependence for the emergence of the periodical structure to the chosen boundary conditions.

Prompted by the existing results we were interested in investigating whether extinction can be stopped by stabilising the increase/decrease in A as a piecewise function. For this reason, in Chapter 6 we revisit the model presented in Chapter 4. We investigate the power spectra of plankton time series to prove the system's species regular distribution. We have found the pattern of extinction emergence. For increasing A , the patchy distribution is displaced by regular pattern formation and this structure persists until the species eventually goes extinct. Extinction occurs when the surrounding water temperature reaches a certain (intermediate) critical threshold value. This sequence of regular-patchy-extinction repeats itself several times for increasing A . However, when A reaches its final critical value, species go extinct and oxygen is depleted.

Note that it was not our aim here to calculate precise critical values of the oxygen production rate. Instead, our aim is to identify the new threat in principle rather than to link our analysis to specific plankton species or specific marine ecosystems. Similarly, we do not attempt to estimate the value of the model parameters. In contrast to other simulation studies where complicated 'realistic' marine ecosystem models were used (e.g. [28, 65, 106]), our model is relatively simple. One benefit of this approach is that the model becomes tractable semi-analytically (see Sections 2.2.1, 3.2.1, 4.2.1) and the change in model's properties in response to relevant factors can be revealed and understood relatively easy, cf. Sections 2.2.1, 4.2.1.

The downside of the model's simplicity is that many processes are left out of the scope. Thus, our study leaves a number of open questions. Firstly, in our model, the ocean hydrodynamics is taken into account very schematically (i.e. as the turbulent diffusion). However, the amount of oxygen entering the atmosphere through the ocean surface is known to depend on details of the ocean circulation [84, 95, 121, 153, 220]. Although it does not seem likely that ocean hydrodynamics can alter the dependence of oxygen production on temperature, it seems probable that it can delay the oxygen transport through the sea-air interface. How this delay may affect the atmospheric oxygen budget remains to be investigated. Secondly, our model does not take into account the effect of oxygen saturation and its dependence on temperature. Meanwhile, the solubility of oxygen in water is known to decline with water temperature, which can be another factor reducing the oxygen concentration [4, 95]. Thirdly, phytoplankton community consists of

hundreds of different species. To the best of our knowledge, data on the temperature dependence of the oxygen production rate are currently available only for a handful of species [85, 217]. How general is the observed response to an increase in water temperature remains to be seen.

Further recognition on sedimentation importance on water body oxygen concentration issue can be extended with a proper mathematical model as a future work. Phytoplankton is a major oxygen producer, both phytoplankton and zooplankton as well as macrophytes are also oxygen consumers [160], in particular through the decomposition process of marine sediment in bottom of the ocean. The importance of plankton decomposition process in relation to oxygen balance in aquatic ecosystems is discussed in [265]. In addition to what is happening in the pelagic zone, marine sediments are formed by dead algae and macrophytes. These particles sink to the bottom of the ocean and are exposed to a biochemical process. Large amounts of dissolved oxygen are utilized by these biochemical processes [18, 41, 57, 93, 106, 179, 215, 231, 237, 260]. Sediment decomposition process needs oxygen and dissolved oxygen is utilized for this process. This, in turn, can cause the ocean's dissolved oxygen concentration to become low. Addressing these questions should become a subject of future research.

So far as from the obtained results, it can be said that they have important implications. A lot has been said about detrimental consequences of global climate change, such as possible extinction of some species resulting in corresponding biodiversity loss and the large scale of flooding as a result of melting glaciers. In this dissertation, we have identified another possible consequence of the global climate change that can be more dangerous than all others by using coupled oxygen-plankton model. It is shown that the oxygen production by marine phytoplankton can stop suddenly if the water temperature exceeds a certain critical value ($\theta \approx 2.29$). As a result, since the ocean plankton produce more than one half of the total atmospheric oxygen, it would mean oxygen depletion is not restricted only to water but also to the Earth's surface. If these results can be linked and supported by ecological field data, it would be encouraging as this approach can predict and potentially prevent future ecological disasters.

Appendix A

Simplifying a Model System

A complex mathematical model can be reduced to our model system by ignoring some external factors. For this reason, Mocenni's model Eqs. (A.1–A.5) is transformed to our 'baseline' model system to understand the fundamental properties of the dissolved oxygen produced by phytoplankton.

Eqs. (A.1–A.5) consist of four coupled differential equations where x_1 is phytoplankton density, x_2 is herbivore consumers biomass (zooplankton), x_3 is the concentration of dissolved oxygen, while x_4 is the nutrient variable, consisting of nitrogen and phosphorus compounds in water and sediments [163]. In this model system, it is assumed that $u_1(t)$ is photo-period annual variation, $u_2(t)$ is temperature and $u_3(t)$ is average wind intensity. Growth of phytoplankton is affected by some restricting external factors shown as $u_4(t)$ and k_i describe model coefficients for $i=0,1,\dots,12$. System coefficients (k_{AN} , k_{AE} , k_P , k_T and k_X) are all nonnegative due to their ecological meanings and k_P shows the half saturation value. The model system A.1–A.5 takes into account phytoplankton, zooplankton, dissolved oxygen and nutrients, respectively [163].

Phytoplankton density x_1 is given by

$$\frac{dx_1}{dt} = k_1 u_1 u_4 x_1 \left(\frac{x_4}{k_0 + x_4} \right) - k_2 x_1^2 - k_3 x_2 \left(\frac{x_1}{k_p + x_1} \right). \quad (\text{A.1})$$

The first term of Eq. (A.1) corresponds to photosynthetic activity leading to the increase of phytoplankton biomass. This term is mainly controlled by light intensity and restricted by temperature and nutrient availability. The second term of Eq. (A.1) accounts for natural mortality. Therefore, the combination of growth and mortality term can be described by logistic type dynamics [172]. The last term of Eq. (A.1) represents grazing of zooplankton.

Zooplankton growth x_2 is described by

$$\frac{dx_2}{dt} = k_4 x_2 \left(\frac{x_1}{k_p + x_1} \right) - k_5 x_2. \quad (\text{A.2})$$

The first term of Eq. (A.2) represents the growth rate of zooplankton due to predation. The second term of Eq. (A.2) is natural mortality and intraspecific competition.

Dissolved oxygen concentration x_3 is given by

$$\frac{dx_3}{dt} = k_6 u_3 + k_7 u_1 u_4 x_1 \left(\frac{x_4}{k_0 + x_4} \right) - k_8 f_\alpha(x_3) - \quad (\text{A.3})$$

$$k_9 f_\beta(x_3) + k_{10} \left(\frac{C_s(u_2) - x_3}{k_T + x_2} \right) - k_{11} x_1 x_3 - k_{12} x_2 x_3, \quad (\text{A.4})$$

where $f_\alpha(x_3) = \left(\frac{x_3^2}{k_{AE} + x_3^2} \right)$ and $f_\beta(x_3) = \left(\frac{x_3}{k_{AN} + x_3^2} \right)$.

The first two positive terms of Eq. (A.3) represent wind re-aeration and oxygen production due to photosynthesis. The third and fourth terms of Eq. (A.3) account for the decreases due to bacterial activity and the last two terms account for decrease on oxygen concentration due to phytoplankton and zooplankton respiration, respectively. The fifth term of Eq. (A.3) represents the equilibrium of the physical-chemical reaction between gaseous oxygen and dissolved oxygen due to the effect of changing temperature in water body; for more details see [163] and the references therein. Temperature is one of the limiting factor represented by k_T . The biochemical process $[C_s(u_2) - x_3]$ is associated with the over/under saturated level of water body oxygen concentration x_3 . Functions f_α and f_β account for aerobic and anaerobic activities dependence accounted for dissolved oxygen concentration in Eq. (A.3), respectively, and f_α and f_β are determined by k_{AE} and k_{AN} .

The nutrient variable growth can be modelled by

$$\frac{dx_4}{dt} = k_{13} f_\alpha(x_3) + k_{14} f_\beta(x_3) - k_{15} u_1 u_4 x_1 \left(\frac{x_4}{k_0 + x_4} \right) - k_{16} \left(\frac{x_4}{k_X + x_4} \right), \quad (\text{A.5})$$

where x_4 indicates nitrogen and phosphorus compounds in water and sediments. The nutrient fixation half saturation constant is represented by k_X . The first two terms of Eq. (A.5) refer to aerobic and anaerobic production of nitrogen and phosphorus due to the mineralization of organic matter, respectively. The loss terms of Eq. (A.5) stem from photosynthetic activity and fixation in the sediment. The system formulation has been studied in much detail by [163].

As it is seen, the model system (A.1–A.5) contains many external factors. Instead of using all of these factors, here we simplify the model to better understanding the relation between oxygen and phytoplankton. For this reason, some components from model system (A.1–A.5) are ignored by assuming them as constants. Hence, herbivore consumers' biomass is not of interest for our baseline model system in Chapter 2. Therefore, we disregard Eq. (A.2) and the consumption term due to zooplankton respiration of Eq. (A.1). This means that the herbivore density x_2 kept constant, so differentiation of x_2 equals to zero, i.e. $\dot{x}_2 = 0$. This assumption is not at all ecologically unrealistic and may be supported by the fact that zooplanktons' dynamics change more slower than phytoplanktons'. A similar assumption can be made for x_4 and hence phosphor and nitrogen compounds are also not of interest for this work. It means that x_4 is assumed as a constant and $\dot{x}_4 = 0$. In addition, wind-reaeration, bacterial activity, and zooplankton respiration terms are neglected. Following these simplifications, we form our basic model, and rename components: c is oxygen concentration (instead of x_3) and u is phytoplankton density (instead of x_1).

In view of above the discussions, we construct a mathematical model which concentrates on phytoplankton and oxygen components to understand the underlying dynamics.

The dynamical equation of phytoplankton is

$$\dot{x}_1 = k_1 u_1 u_4 \left(\frac{x_4}{k_0 + x_4} \right) x_1 - k_2 x_1^2 - k_3 x_2 \left(\frac{x_1}{k_P + x_1} \right). \quad (\text{A.6})$$

with the assumption of

$$\dot{x}_2 = 0 \quad \text{and} \quad \dot{x}_4 = 0, \quad (\text{A.7})$$

and the first term is constant in Eq. (A.3). The steps to deriving our model are as follows:

1. It is assumed $x_1 \ll k_P$ for Eq. (A.6), therefore the last consumption term of Eq. (A.6) converges to zero.

$$\dot{x}_1 = \tilde{B}x_1 - \gamma_1 x_1^2, \quad (\text{A.8})$$

where $k_2 = \gamma_1$, then

$$\dot{x}_1 = (\tilde{B} - \gamma_1 x_1)x_1, \quad (\text{A.9})$$

2. Assume $\tilde{B} = \tilde{B}(c)$ is an increasing function.

Choose $\tilde{B} = \frac{Bc}{c+c_1}$ where x_1 is replaced with u in our model system. Therefore,

$$\frac{du}{dt} = \left(\frac{Bc}{c+c_1} - \gamma_1 u \right) u, \quad (\text{A.10})$$

using the previous expressions for u , we have derived the equation for phytoplankton as Eq. (A.10).

The dynamical system of oxygen is

$$\dot{x}_3 = Z + Ax_1 - k_8 f_\alpha(x_3) - k_9 f_\beta(x_3) + k_{10} \left(\frac{C_s(u_2) - x_3}{k_T + x_2} \right) - mx_3 - k_{12} x_2 x_3$$

here Z corresponds with $k_6 u_3$ and assumed as constant, A is replaced with the term $(k_7 u_1 u_4 x_1 (\frac{x_4}{k_0 + x_4}))$, while m is replaced with $k_{11} x_2$ and the zooplankton respiration term $(k_{12} x_2 x_3)$ is neglected.

In Mocenni's model equation $\beta = 2$, but in our model system it is assumed that $\beta = 1$, where $f_\alpha(x_3) = \frac{x_3^\beta}{c_0 + x_3^\beta}$ in [163].

3. Assume that anaerobic activity is not make any change on oxygen dynamics. Therefore, we neglect the term by taking it as $f_\beta \equiv 0$ and where x_3 is named as c in our model system.

Then, the oxygen concentration dynamical equation becomes as follows:

$$\frac{dc}{dt} = Z + Au - mc - \frac{\tilde{A}c}{c + c_0}. \quad (\text{A.11})$$

We assume $Z = 0$ by ignoring the wind effect on our model system.

4. Assume that rate of decomposition of death phytoplankton should depend on phytoplankton concentration in per unit. This means that $\tilde{A} \sim u$.

Assume $\tilde{A}(u) = Au$. Then we obtain:

$$\frac{dc}{dt} = A \left(1 - \frac{c}{c+1} \right) u - c, \quad (\text{A.12})$$

Following these assumptions we get our baseline model system (2.5–2.6).

Appendix B

Dimensionless Form

In order to simplify analytical and numerical calculations we rescale our model, thereby decreasing the number of parameters. Referring back to the system (2.5–2.6), it is easily seen that the system contains six free parameters which are A , c_0 , m , B , c_1 and γ . However, their number can be reduced by choosing dimensionless variables. The scaled mathematical model has only three free parameters.

We scale the model to dimensionless variables as follows:

$$\begin{cases} \frac{dc}{dt} = A \left(1 - \frac{c}{c+c_0}\right) u - mc, \\ \frac{du}{dt} = \left(\frac{Bc}{c+c_1} - \gamma u\right) u, \end{cases} \quad (\text{B.1})$$

this transformation is performed by $\hat{t} = tm$ and acquire

$$\begin{cases} \frac{dc}{d\hat{t}} = \frac{A}{m} \left(1 - \frac{c}{c+c_0}\right) u - c, \\ \frac{du}{d\hat{t}} = \frac{1}{m} \left(\frac{Bc}{c+c_1} - \gamma u\right) u, \end{cases} \quad (\text{B.2})$$

We then choose $\hat{A} = \frac{A}{m}$, $\hat{B} = \frac{B}{m}$, $\hat{\gamma} = \frac{\gamma}{m}$,

$$\begin{cases} \frac{dc}{d\hat{t}} = \hat{A} \left(1 - \frac{c}{c+c_0}\right) u - c, \\ \frac{du}{d\hat{t}} = \left(\hat{B} \frac{c}{c+c_1} - \hat{\gamma} u\right) u, \end{cases} \quad (\text{B.3})$$

and $\hat{c} = \frac{c}{c_0}$

$$\begin{cases} \frac{d\hat{c}}{d\hat{t}} = \frac{\hat{A}}{c_0} \left(1 - \frac{\hat{c}}{\hat{c}+1}\right) u - \hat{c}, \\ \frac{du}{d\hat{t}} = \left(\frac{\hat{B}\hat{c}}{\hat{c}+\frac{c_1}{c_0}} - \hat{\gamma} u\right) u, \end{cases} \quad (\text{B.4})$$

and $\hat{u} = \hat{\gamma}_1 u$

$$\begin{cases} \frac{d\hat{c}}{d\hat{t}} = \frac{\hat{A}}{c_0} \left(1 - \frac{\hat{c}}{\hat{c}+1}\right) \frac{\hat{u}}{\hat{\gamma}} - \hat{c}, \\ \frac{d\hat{u}}{d\hat{t}} = \left(\hat{B} \frac{\hat{c}}{\hat{c}+\frac{c_1}{c_0}} - \hat{u}\right) \hat{u}, \end{cases} \quad (\text{B.5})$$

so that

$$\begin{cases} \frac{d\hat{c}}{d\hat{t}} = \frac{\hat{A}}{c_0\hat{\gamma}_1} \left(1 - \frac{\hat{c}}{\hat{c}+1}\right) \hat{u} - \hat{c}, \\ \frac{d\hat{u}}{d\hat{t}} = \left(\hat{B} \frac{\hat{c}}{\hat{c}+\frac{c_1}{c_0}} - \hat{u}\right) \hat{u}. \end{cases} \quad (\text{B.6})$$

Therefore, the last step to obtain the dimensionless equation is to choose $\hat{A} = \frac{\hat{A}}{c_0\hat{\gamma}_1}$ and $\hat{c} = \frac{c_1}{c_0}$

$$\begin{cases} \frac{dc}{dt} = \hat{A} \left(1 - \frac{c}{c+1}\right) u - c, \\ \frac{du}{dt} = \left(\hat{B} \frac{c}{c+\hat{c}} - u\right) u, \end{cases} \quad (\text{B.7})$$

For convenience, we now simplify the notations by omitting the hats and double hats, i.e. by changing $\hat{A} \rightarrow A$, $\hat{c} \rightarrow c$ and $\hat{u} \rightarrow u$. To reiterate, Eqs. (B.7) then take the following form:

$$\frac{dc}{dt} = A \left(1 - \frac{c}{c+1}\right) u - c \equiv f(c, u), \quad (\text{B.8})$$

$$\frac{du}{dt} = \left(\frac{Bc}{c+c_1} - u\right) u \equiv g(c, u). \quad (\text{B.9})$$

where all variables and parameters are now dimensionless.

Appendix C

Linearized System Matrix

C.0.1 Baseline model linearized system

The linearized system's matrix is as follows:

$$A = \begin{pmatrix} -\frac{Au}{(1+c)^2} - 1 & A\left(1 - \frac{c}{1+c}\right) \\ \frac{Bc_1u}{(c+c_1)^2} & \frac{Bc}{c+c_1} - 2u \end{pmatrix}. \quad (\text{C.1})$$

- Extinction steady state: $(0, 0)$.

Matrix C.1 takes the following form:

$$\det(A_{(0,0)} - \lambda I) = \begin{vmatrix} -1 - \lambda & A \\ 0 & -\lambda \end{vmatrix} = 0,$$

so that the characteristic equation is defined by

$$\Rightarrow (0 - \lambda)(-1 - \lambda) = 0. \quad (\text{C.2})$$

From Eq. (C.2), $\lambda_1 = -1$ and $\lambda_2 = 0$. Therefore, the origin has one negative real eigenvalue and one zero eigenvalue.

- Oxygen-phytoplankton steady state: (\tilde{c}, \tilde{u}) .

The corresponding form is:

$$\det(A_{(\tilde{c}, \tilde{u})} - \lambda I) = \begin{vmatrix} -\frac{A\tilde{u}}{(1+\tilde{c})^2} - 1 - \lambda & A\left(1 - \frac{\tilde{c}}{1+\tilde{c}}\right) \\ \frac{Bc_1\tilde{u}}{(\tilde{c}+c_1)^2} & \frac{B\tilde{c}}{\tilde{c}+c_1} - 2\tilde{u} - \lambda \end{vmatrix} = 0,$$

so that

$$\det(A_{(\tilde{c}, \tilde{u})} - \lambda I) = \left(-\frac{A\tilde{u}}{(1+\tilde{c})^2} - 1 - \lambda \right) \left(\frac{B\tilde{c}}{\tilde{c}+c_1} - 2\tilde{u} - \lambda \right) - \frac{A}{1+\tilde{c}} \frac{Bc_1\tilde{u}}{(\tilde{c}+c_1)^2} = 0, \quad (\text{C.3})$$

where \tilde{u} and \tilde{c} defined as in Eq. (2.11) and Eq.(2.13).

$$\lambda_{1,2} = \frac{-\rho \pm \sqrt{\rho^2 - 4\Delta}}{2} \quad (\text{C.4})$$

where

$$\rho = \frac{A\tilde{u}}{(1+\tilde{c})^2} - \frac{B\tilde{c}}{\tilde{c}+c_1} + 2\tilde{u} + 1 \quad (\text{C.5})$$

$$\Delta = \frac{2A\tilde{u}^2}{(1+\tilde{c})^2} - \frac{AB\tilde{u}\tilde{c}}{(1+\tilde{c})^2(\tilde{c}+c_1)} - \frac{B\tilde{c}}{\tilde{c}+c_1} - \frac{ABc_1\tilde{u}}{(1+\tilde{c})(\tilde{c}+c_1)^2} + 2\tilde{u} \quad (\text{C.6})$$

C.0.2 Linearized system for predation effect model

The linearized system's matrix is as follows:

$$B = \begin{pmatrix} -\frac{Au}{(1+c)^2} - 1 & A(1 - \frac{c}{1+c}) & 0 \\ \frac{Bc_1u}{(c+c_1)^2} & \frac{Bc}{c+c_1} - 2u - \frac{vh}{(u+h)^2} & -\frac{u}{u+h} \\ 0 & \frac{\beta vh}{(u+h)^2} & \frac{\beta u}{u+h} - \mu \end{pmatrix}. \quad (\text{C.7})$$

- Extinction steady state: $(0, 0, 0)$.

Matrix C.7 takes the following form:

$$\det(B_{(0,0,0)} - \lambda I) = \begin{vmatrix} -1 - \lambda & A & 0 \\ 0 & -\lambda & 0 \\ 0 & 0 & -\mu - \lambda \end{vmatrix} = 0,$$

so that the characteristic equation is defined by

$$\Rightarrow (-\mu - \lambda)(0 - \lambda)(-1 - \lambda) = 0. \quad (\text{C.8})$$

From Eq. (C.8), $\lambda_1 = -\mu$, $\lambda_2 = 0$ and $\lambda_3 = -1$. Therefore, the origin has two negative real eigenvalues and one zero eigenvalue.

- Zooplankton-free steady state: $(\tilde{c}, \tilde{u}, 0)$.

TABLE C.1: Eigenvalues for (\tilde{c}, \tilde{u})

		<i>A</i>									
		0.1	0.2	0.3	0.4	0.5	0.6	0.7	0.8	0.9	1
c_1	1	-1 0	-1 0	-1 0	-1 0	-1 0	-1 0	-1 0	-1 0	-1 0	-1 0
	0.9	-1 0	-1 0	-1 0	-1 0	-1 0	-1 0	-1 0	-1 0	-1 0	-1.0976 -0.1499
	0.8	-1 0	-1 0	-1 0	-1 0	-1 0	-1 0	-1 0	-1 0	-1.1078 -0.0065	-1.1905 -0.0206
	0.7	-1 0	-1 0	-1 0	-1 0	-1 0	-1 0	-1 0	-1.1204 -0.0087	-1.2092 -0.0266	-1.2782 -0.0477
	0.6	-1 0	-1 0	-1 0	-1 0	-1 0	-1 0	-1.1362 -0.0119	-1.2317 -0.0352	-1.3035 -0.0617	-1.3599 -0.0884
	0.5	-1 0	-1 0	-1 0	-1 0	-1 0	-1.1565 -0.0170	-1.2591 -0.0483	-1.3330 -0.0820	-1.3891 -0.1146	-1.4336 -0.1452
	0.4	-1 0	-1 0	-1 0	-1 0	-1.1835 -0.0257	-1.2929 -0.0689	-1.13670 -0.1125	-1.4213 -0.1528	-1.4630 -0.1892	-1.4964 -0.2220
	0.3	-1 0	-1 0	-1 0	-1.2211 -0.0421	-1.3346 -0.1041	-1.4054 -0.1613	-1.4546 -0.2111	-1.4912 -0.2542	-1.5199 -0.2917	-1.5432 -0.3245
	0.2	-1 0	-1 0	-1.2758 -0.0780	-1.3843 -0.1707	-1.4441 -0.2462	-1.4830 -0.3068	-1.5111 -0.3563	-1.5327 -0.3976	-1.5502 -0.4326	-1.5649 -0.4627
	0.1	-1 0	-1.3546 -0.1810	-1.4282 -0.3226	-1.4613 -0.4166	-1.4822 -0.4839	-1.4979 -0.5348	-1.5108 -0.5749	-1.5220 -0.6075	-1.5321 -0.6346	-1.5413 -0.6575

Eigenvalues are produced by given parameter values $B = 1$, A and c_1 changes with given ranges as it seen on table.

The corresponding form is:

$$\det(B_{(\tilde{c}, \tilde{u}, 0)} - \lambda I) = \begin{vmatrix} -\frac{A\tilde{u}}{(1+\tilde{c})^2} - 1 - \lambda & A(1 - \frac{\tilde{c}}{1+\tilde{c}}) & 0 \\ \frac{Bc_1\tilde{u}}{(\tilde{c}+c_1)^2} & \frac{B\tilde{c}}{\tilde{c}+c_1} - 2\tilde{u} - \lambda & -\frac{\tilde{u}}{\tilde{u}+h} \\ 0 & 0 & \frac{\beta\tilde{u}}{\tilde{u}+h} - \mu - \lambda \end{vmatrix} = 0,$$

so that

$$\det(B_{(\tilde{c}, \tilde{u}, 0)} - \lambda I) = \left[\left(-\frac{A\tilde{u}}{(1+\tilde{c})^2} - 1 - \lambda \right) \left(\frac{B\tilde{c}}{\tilde{c}+c_1} - 2\tilde{u} - \lambda \right) - \frac{A}{1+\tilde{c}} \frac{Bc_1\tilde{u}}{(\tilde{c}+c_1)^2} \right] \left(\frac{\beta\tilde{u}}{\tilde{u}+h} - \mu - \lambda \right) = 0, \quad (\text{C.9})$$

where \tilde{u} and \tilde{c} defined as in Eqs. (2.11) and (2.13).

$$\lambda_1 = \frac{\beta\tilde{u}}{\tilde{u}+h} - \mu \quad \text{and} \quad \lambda_{2,3} = \frac{-\rho \pm \sqrt{\rho^2 - 4\Delta}}{2}, \quad (\text{C.10})$$

where

$$\rho = \frac{A\tilde{u}}{(1+\tilde{c})^2} - \frac{B\tilde{c}}{\tilde{c}+c_1} + 2\tilde{u} + 1, \quad (\text{C.11})$$

$$\Delta = \frac{2A\tilde{u}^2}{(1+\tilde{c})^2} - \frac{AB\tilde{u}\tilde{c}}{(1+\tilde{c})^2(\tilde{c}+c_1)} - \frac{B\tilde{c}}{\tilde{c}+c_1} - \frac{ABc_1\tilde{u}}{(1+\tilde{c})(\tilde{c}+c_1)^2} + 2\tilde{u}. \quad (\text{C.12})$$

- Coexistence steady state: $(\bar{c}, \bar{u}, \bar{v})$.

$$\det(B_{(\bar{c}, \bar{u}, \bar{v})} - \lambda I) = \begin{vmatrix} -\frac{A\bar{u}}{(1+\bar{c})^2} - 1 - \lambda & A(1 - \frac{\bar{c}}{1+\bar{c}}) & 0 \\ \frac{Bc_1\bar{u}}{(\bar{c}+c_1)^2} & \frac{B\bar{c}}{\bar{c}+c_1} - 2\bar{u} - \frac{\bar{v}h}{(\bar{u}+h)^2} - \lambda & -\frac{\bar{u}}{\bar{u}+h} \\ 0 & \frac{\beta\bar{v}h}{(\bar{u}+h)^2} & \frac{\beta\bar{u}}{\bar{u}+h} - \mu - \lambda \end{vmatrix} = 0,$$

so that

$$\det(B_{(\bar{c}, \bar{u}, \bar{v})} - \lambda I) = \frac{\beta\bar{u}\bar{v}h}{(\bar{u}+h)^3} \left(-\frac{A\bar{u}}{(1+\bar{c})^2} - 1 - \lambda \right) + \left(\frac{\beta\bar{u}}{\bar{u}+h} - \mu - \lambda \right) \left[\left(-\frac{A\bar{u}}{(1+\bar{c})^2} - 1 - \lambda \right) \left(\frac{B\bar{c}}{\bar{c}+c_1} - 2\bar{u} - \frac{\bar{v}h}{(\bar{u}+h)^2} - \lambda \right) - \frac{A}{1+\bar{c}} \cdot \frac{Bc_1\bar{u}}{(\bar{c}+c_1)^2} \right] = 0, \quad (\text{C.13})$$

where \bar{c} , \bar{u} and \bar{v} defined by Eq. (3.11).

Let

$$\phi = \frac{\beta\bar{u}}{\bar{u}+h} - \mu - \frac{A\bar{u}}{(1+\bar{c})^2} - 1 + \frac{B\bar{c}}{\bar{c}+c_1} - 2\bar{u} - \frac{\bar{v}h}{(\bar{u}+h)^2},$$

$$\begin{aligned} \varepsilon = & \frac{A\beta\bar{u}^2}{(1+\bar{c})^2(\bar{u}+h)} + \frac{\beta\bar{u}}{\bar{u}+h} - \frac{\beta B\bar{u}\bar{c}}{(\bar{c}+c_1)(\bar{u}+h)} + \frac{2\bar{u}^2\beta}{\bar{u}+h} - \frac{A\bar{u}\mu}{(1+\bar{c})^2} - \mu \\ & + \frac{B\bar{c}\mu}{\bar{c}+c_1} - 2\bar{u}\mu - \frac{\bar{v}h\mu}{(\bar{u}+h)^2} + \frac{AB\bar{u}\bar{c}}{(1+\bar{c})^2(\bar{c}+c_1)} - \frac{2A\bar{u}^2}{(1+\bar{c})^2} - \frac{A\bar{u}\bar{v}h}{(1+\bar{c})^2(\bar{u}+h)^2} \\ & + \frac{B\bar{c}}{\bar{c}+c_1} - 2\bar{u} - \frac{\bar{v}h}{(\bar{u}+h)^2} + \frac{AB\bar{u}c_1}{(1+\bar{c})(\bar{c}+c_1)^2}, \end{aligned}$$

and

$$\begin{aligned} \rho = & -\frac{A\beta\bar{u}^2\bar{v}h}{(\bar{u}+h)^3(1+\bar{c})^2} - \frac{\beta\bar{u}\bar{v}h}{(\bar{u}+h)^3} - \frac{AB\beta\bar{u}^2\bar{c}}{(1+\bar{c})^2(\bar{c}+c_1)(\bar{u}+h)} + \frac{2A\bar{u}^3\beta}{(1+\bar{c})^2(\bar{u}+h)} \\ & + \frac{A\beta\bar{u}^2\bar{v}h}{(1+\bar{c})^2(\bar{u}+h)^3} - \frac{B\beta\bar{u}\bar{c}}{(\bar{c}+c_1)(\bar{u}+h)} + \frac{2\beta\bar{u}^2}{\bar{u}+h} + \frac{\beta\bar{u}\bar{v}h}{(\bar{u}+h)^3} \\ & - \frac{AB\beta\bar{u}^2c_1}{(1+\bar{c})(\bar{c}+c_1)^2(\bar{u}+h)} + \frac{AB\bar{u}\bar{c}\mu}{(1+\bar{c})^2(\bar{c}+c_1)} - \frac{2A\bar{u}^2\mu}{(1+\bar{c})^2} - \frac{A\bar{u}\bar{v}h\mu}{(1+\bar{c})^2(\bar{u}+h)^2} \\ & + \frac{B\bar{c}\mu}{\bar{c}+c_1} - 2\bar{u}\mu - \frac{\bar{v}h\mu}{(\bar{u}+h)^2} + \frac{ABc_1\bar{u}\mu}{(1+\bar{c})(\bar{c}+c_1)^2}. \end{aligned}$$

Then the eigenvalues of system (C.13) are the solutions of the following cubic equation:

$$\lambda^3 - \phi\lambda^2 - \varepsilon\lambda - \rho = 0, \quad (\text{C.14})$$

The roots of Eq. (C.14) are:

$$\begin{aligned} \lambda_1 = & \frac{\phi}{3} + \frac{2^{\frac{1}{3}}(-\phi^2 - 3\varepsilon)}{3(-27\rho - 2\phi^3 - 9\phi\varepsilon + 3\sqrt{3}\sqrt{27\rho^2 + 4\rho\phi^3 + 18\rho\phi\varepsilon - \phi^2\varepsilon^2 - 4\varepsilon^3})^{\frac{1}{3}}} \\ & - \frac{(-27\rho - 2\phi^3 - 9\phi\varepsilon + 3\sqrt{3}\sqrt{27\rho^2 + 4\rho\phi^3 + 18\rho\phi\varepsilon - \phi^2\varepsilon^2 - 4\varepsilon^3})^{\frac{1}{3}}}{3 \cdot 2^{\frac{1}{3}}}, \\ \lambda_2 = & \frac{\phi}{3} - \frac{(1+i\sqrt{3})(-\phi^2 - 3\varepsilon)}{3 \cdot 2^{\frac{2}{3}}(-27\rho - 2\phi^3 - 9\phi\varepsilon + 3\sqrt{3}\sqrt{27\rho^2 + 4\rho\phi^3 + 18\rho\phi\varepsilon - \phi^2\varepsilon^2 - 4\varepsilon^3})^{\frac{1}{3}}} \\ & + \frac{(1-i\sqrt{3})(-27\rho - 2\phi^3 - 9\phi\varepsilon + 3\sqrt{3}\sqrt{27\rho^2 + 4\rho\phi^3 + 18\rho\phi\varepsilon - \phi^2\varepsilon^2 - 4\varepsilon^3})^{\frac{1}{3}}}{6 \cdot 2^{\frac{1}{3}}}, \\ \lambda_3 = & \frac{\phi}{3} - \frac{(1-i\sqrt{3})(-\phi^2 - 3\varepsilon)}{3 \cdot 2^{\frac{2}{3}}(-27\rho - 2\phi^3 - 9\phi\varepsilon + 3\sqrt{3}\sqrt{27\rho^2 + 4\rho\phi^3 + 18\rho\phi\varepsilon - \phi^2\varepsilon^2 - 4\varepsilon^3})^{\frac{1}{3}}} \\ & + \frac{(1+i\sqrt{3})(-27\rho - 2\phi^3 - 9\phi\varepsilon + 3\sqrt{3}\sqrt{27\rho^2 + 4\rho\phi^3 + 18\rho\phi\varepsilon - \phi^2\varepsilon^2 - 4\varepsilon^3})^{\frac{1}{3}}}{6 \cdot 2^{\frac{1}{3}}}. \end{aligned}$$

Therefore, the equilibrium $(\bar{c}, \bar{u}, \bar{v})$ has one real and two complex conjugate eigenvalues; hence, it is a mixed focus-type equilibrium.

Eigenvalue Tables C.2 and C.3 are presented to show the scheme of eigenvalues magnitude and sign. These two tables represent the eigenvalues for parameters A and c_1 changing from 0.1 to 1, while other parameters are fixed at some hypothetical values as $B = 1$, $\gamma = 1$, $\beta = 1$, $\mu = 0.5$, $h = 0.1$, $\epsilon = 0.001$. The only difference between Table C.2 and Table C.3 are the steady state values.

Table C.2 shows the $(\tilde{c}, \tilde{u}, 0)$ steady state associated with real eigenvalues. It is seen that for the negative steady state area (see Fig. 3.2 and Fig. 3.5) one of the eigenvalues is always equal to zero. In this case, we use numerical simulations to determine the stability of the given steady state instead of using some theoretical and analytical calculations. Note that, the zooplankton-free state $(\tilde{c}, \tilde{u}, 0)$ corresponds to the basic model oxygen-phytoplankton steady state (\tilde{c}, \tilde{u}) ; cf. Table C.1 and Table C.2.

Table C.3 demonstrates the eigenvalues for $(\bar{c}, \bar{u}, \bar{v})$ given by Eq.(3.11). Table C.2's zero eigenvalues area corresponds with the Table C.3's real eigenvalues area. Table C.3 is used to understand the steady state behaviour of the coexistence state while Table C.2 is for the zooplankton-free state. However, demonstration of both tables is a powerful tool to investigate and predict the system's behavior in two dimensions without zooplankton and in three dimension with zooplankton in terms of phase plane/space structure ¹.

Both of the tables are given to distinguish between the different behavior of system dynamic in two and in three dimensions. The steady state's $(\tilde{c}, \tilde{u}, 0)$ dynamics shows the dynamical system in two dimensions with respect to the absence of zooplankton. The steady state's $(\bar{c}, \bar{u}, \bar{v})$ dynamics represent the dynamical system in three dimensions. Having these two different steady state dynamical system's provide information regarding the effect of zooplankton concentration on our baseline model.

The behavior of the system's dynamical response can be identified by the points chosen in Table C.2 and in Fig. 3.3. For example, the point defined by $A = 1$ and $c_1 = 0.1$ with other given parameters as in Fig.3.3 behaves as a saddle point. However, when $A = 0.9$ and $c_1 = 0.8$ are as defined, the system's steady state is stable. The corresponding oxygen-phytoplankton steady state can be seen from Fig. 3.2 and Fig. 3.5.

¹Here the word dimension is used to define the phase plane or phase space, i.e. oxygen-phytoplankton system trajectories lie on the phase plane (two-dimensions), while oxygen-phyto-zooplankton system trajectories lie on the phase space structure (three-dimensions)

TABLE C.2: Eigenvalues for $(\tilde{c}, \tilde{u}, 0)$

		<i>A</i>										
		0.1	0.2	0.3	0.4	0.5	0.6	0.7	0.8	0.9	1	
c_1	1	-1 -0.5 0	-1 -0.5 0	-1 -0.5 0	-1 -0.5 0	-1 -0.5 0	-1 -0.5 0	-1 -0.5 0	-1 -0.5 0	-1 -0.5 0	-1 -0.5 0	
	0.9	-1 -0.5 0	-1 -0.5 0	-1 -0.5 0	-1 -0.5 0	-1 -0.5 0	-1 -0.5 0	-1 -0.5 0	-1 -0.5 0	-1 -0.5 0	-1.0976 -0.0050 -0.1499	
	0.8	-1 -0.5 0	-1 -0.5 0	-1 -0.5 0	-1 -0.5 0	-1 -0.5 0	-1 -0.5 0	-1 -0.5 0	-1 -0.5 0	-1.1078 -0.0065 -0.1129	-1.1905 -0.0206 -0.0371	
	0.7	-1 -0.5 0	-1 -0.5 0	-1 -0.5 0	-1 -0.5 0	-1 -0.5 0	-1 -0.5 0	-1 -0.5 0	-1.1204 -0.0087 -0.0708	-1.2092 -0.0266 0.0768	-1.2782 -0.0477 0.1518	
	0.6	-1 -0.5 0	-1 -0.5 0	-1 -0.5 0	-1 -0.5 0	-1 -0.5 0	-1 -0.5 0	-1 -0.5 0	-1.1362 -0.0119 -0.0229	-1.2317 -0.0352 0.1192	-1.3035 -0.0617 0.1878	
	0.5	-1 -0.5 0	-1 -0.5 0	-1 -0.5 0	-1 -0.5 0	-1 -0.5 0	-1 -0.5 0	-1.1565 -0.0170 0.0314	-1.2591 -0.0483 -0.1641	-1.3330 -0.0820 0.2248	-1.3891 -0.1146 0.2597	
	0.4	-1 -0.5 0	-1 -0.5 0	-1 -0.5 0	-1 -0.5 0	-1.1835 -0.0257 0.0927	-1.2929 -0.0689 0.2112	-1.4054 -0.1613 0.3000	-1.4546 -0.2111 0.3218	-1.4213 -0.1528 0.2909	-1.4630 -0.1892 0.3093	-1.4964 -0.2220 0.0322
	0.3	-1 -0.5 0	-1 -0.5 0	-1 -0.5 0	-1.2211 -0.0421 0.1614	-1.3346 -0.1041 0.2600	-1.4441 -0.2462 0.3374	-1.4830 -0.3068 0.3521	-1.5111 -0.3563 0.3613	-1.4912 -0.2542 0.3357	-1.5199 -0.2917 0.3453	-1.5432 -0.3245 0.3523
	0.2	-1 -0.5 0	-1 -0.5 0	-1.2758 -0.0780 0.2377	-1.3843 -0.1707 0.3098	-1.4441 -0.2462 0.3374	-1.4830 -0.3068 0.3521	-1.5111 -0.3563 0.3613	-1.5327 -0.3976 0.3676	-1.5327 -0.3976 0.3676	-1.5502 -0.4326 0.3722	-1.5649 -0.4627 0.3757
	0.1	-1 -0.5 0	-1.3546 -0.1810 0.3207	-1.4282 -0.3226 0.3599	-1.4613 -0.4166 0.3740	-1.4822 -0.4839 0.3813	-1.4979 -0.5348 0.3858	-1.5108 -0.5749 0.3889	-1.5220 -0.6075 0.3911	-1.5220 -0.6075 0.3911	-1.5321 -0.6346 0.3929	-1.5413 -0.6575 0.3942

Eigenvalues are produced by given parameter values $B = 1, \gamma = 1, \beta = 1, \mu = 0.5, h = 0.1$. A and c_1 changes from 0.1 to 1 as seen on table.

TABLE C.3: Eigenvalues for $(\bar{c}, \bar{u}, \bar{v})$

A										
	0.1	0.2	0.3	0.4	0.5	0.6	0.7	0.8	0.9	1
1	-1.0215 -0.1785 0	-1.0412 -0.1588 0	-1.0593 -0.1407 0	-1.0762 -0.1238 0	-1.0919 -0.1081 0	-1.1067 -0.0933 0	-1.1205 -0.0795 0	-1.1336 -0.0664 0	-1.1460 -0.0540 0	-1.1577 -0.0423 0
0.9	-1.0227 -0.1762 0	-1.0434 -0.1545 0	-1.0623 -0.1346 0	-1.0798 -0.1162 0	-1.0961 -0.0991 0	-1.1112 -0.0831 0	-1.1254 -0.0682 0	-1.1388 -0.0541 0	-1.1514 -0.0408 0	-1.1633 -0.0282 0
0.8	-1.0242 -0.1733 0	-1.0461 -0.1492 0	-1.0660 -0.1272 0	-1.0842 -0.1070 0	-1.1010 -0.0882 0	-1.1167 -0.0708 0	-1.1313 -0.0545 0	-1.1449 -0.0392 0	-1.1578 -0.0249 0	-1.1699 -0.0063+i0.0244 -0.0063-i0.0244
0.7	-1.0262 -0.1697 0	-1.0495 -0.1425 0	-1.0705 -0.1179 0	-1.0896 -0.0954 0	-1.1071 -0.0746 0	-1.1232 -0.0555 0	-1.1382 -0.0376 0	-1.1522 -0.0210 0	-1.1654 -0.0041+i0.0373 -0.0041-i0.0373	-1.1779 0.0009+i0.0601 0.0009-i0.0601
0.6	-1.0287 -0.1649 0	-1.0539 -0.1337 0	-1.0762 -0.1058 0	-1.0963 -0.0804 0	-1.1146 -0.0573 0	-1.1313 -0.0360 0	-1.1467 -0.0163 0	-1.1612 -0.0015+i0.0489 -0.0015-i0.0489	-1.1747 0.0044+i0.0703 0.0044-i0.0703	-1.1874 0.0099+i0.0855 0.0099-i0.0855
0.5	-1.0322 -0.1582 0	-1.0597 -0.1218 0	-1.0838 -0.0895 0	-1.1051 -0.0605 0	-1.1242 -0.0342 0	-1.1415 -0.005+i0.0206 -0.005-i0.0206	-1.1576 0.002+i0.0608 0.002-i0.0608	-1.1725 0.009+i0.0817 0.009-i0.0817	-1.1862 0.0154+i0.097 0.0154-i0.097	-1.1989 0.0212+i0.1093 0.0212-i0.1093
0.4	-1.0372 -0.1485 0	-1.0680 -0.1045 0	-1.0941 -0.0663 0	-1.1168 -0.0324 0	-1.1370 -0.002+i0.038 -0.002-i0.038	-1.1552 0.0068+i0.0741 0.0068-i0.0741	-1.1717 0.0153+i0.0952 0.0153-i0.0952	-1.1867 0.0229+i0.1109 0.0229-i0.1109	-1.2004 0.0298+i0.1235 0.0298-i0.1235	-1.2131 0.0362+i0.1341 0.0362-i0.1341
0.3	-1.0451 -0.1328 0	-1.0804 -0.0775 0	-1.1092 -0.0305 0	-1.1337 0.0018+i0.0561 0.0018-i0.0561	-1.1550 0.0140+i0.090 0.0140-i0.090	-1.1736 0.0247+i0.1125 0.0247-i0.1125	-1.1901 0.0342+i0.1288 0.0342-i0.1288	-1.2049 0.0425+i0.1419 0.0425-i0.1419	-1.2182 0.0500+i0.1528 0.0500-i0.1528	-1.2303 0.0567+i0.1621 0.0567-i0.1621
0.2	-1.0594 -0.1032 0	-1.1013 -0.0286 0	-1.1337 0.0095+i0.0780 0.0095-i0.0780	-1.1598 0.0267+i0.1142 0.0267-i0.1142	-1.1811 0.041+i0.1372 0.041-i0.1372	-1.1991 0.0530+i0.1543 0.0530-i0.1543	-1.2144 0.0632+i0.1679 0.0632-i0.1679	-1.2277 0.0720+i0.1792 0.0720-i0.1792	-1.2393 0.0797+i0.1889 0.0797-i0.1889	-1.2497 0.0864+i0.1974 0.0864-i0.1974
0.1	-1.0932 -0.0265 0	-1.1449 0.0288+i0.1558 0.0288-i0.1558	-1.1780 0.0563+i0.1558 0.0563-i0.1558	-1.2007 0.0763+i0.1806 0.0763-i0.1806	-1.21717 0.091+i0.1988 0.091-i0.1988	-1.2295 0.1034+i0.2132 0.1034-i0.2132	-1.2392 0.1129+i0.2253 0.1129-i0.2253	-1.2471 0.1206+i0.2356 0.1206-i0.2356	-1.2536 0.1269+i0.2447 0.1269-i0.2447	-1.2592 0.1322+i0.2528 0.1322-i0.2528

Eigenvalues are produced by given parameter values $B = 1, \gamma = 1, \beta = 1, \mu = 0.5, h = 0.1$. A and c_1 changes from 0.1 to 1 as seen on table.

C.0.3 Linearized system for respiration effect model

The linearised system matrix is as follows:

$$C = \begin{pmatrix} -\frac{Au}{(1+c)^2} - 1 - \frac{uc_2}{(c+c_2)^2} - \frac{\nu vc_3}{(c+c_3)^2} & \frac{A}{1+c} - \frac{c}{c+c_2} & -\frac{\nu c}{c+c_3} \\ \frac{Bc_1\gamma u}{(c+c_1)^2} & \frac{Bc\gamma}{c+c_1} - 2\gamma u - \frac{vh}{(u+h)^2} - \sigma & -\frac{u}{u+h} \\ \frac{\beta uv}{u+h} \frac{2cc_4^2}{(c^2+c_4^2)^2} & \frac{\beta vh}{(u+h)^2} \frac{c^2}{(c^2+c_4^2)} & \frac{\beta uc^2}{(u+h)(c^2+c_4^2)} - \mu \end{pmatrix}. \quad (C.15)$$

- Extinction state stability: E_1 .

Matrix C.15 takes the following form:

$$\det(C_{(0,0,0)} - \lambda I) = \begin{vmatrix} -1 - \lambda & A & 0 \\ 0 & -\sigma - \lambda & 0 \\ 0 & 0 & -\mu - \lambda \end{vmatrix} = 0$$

so the characteristic equation is defined by

$$\Rightarrow (-1 - \lambda)(-\sigma - \lambda)(-\mu - \lambda) = 0 \quad (C.16)$$

from Eq. (C.16) $\lambda_1 = -1$, $\lambda_2 = -\sigma$ and $\lambda_3 = -\mu$. Therefore, the origin is always stable.

- Oxygen-phytoplankton existence state: $E_2 = (\dot{c}, \dot{u}, 0)$

For oxygen-phytoplankton existence state (E_2)

$$\det(C_{(\dot{c}, \dot{u}, 0)} - \lambda I) = \begin{vmatrix} -\frac{A\dot{u}}{(1+\dot{c})^2} - 1 - \frac{\dot{u}c_2}{(\dot{c}+c_2)^2} - \lambda & \frac{A}{\dot{c}+1} - \frac{\dot{c}}{\dot{c}+c_2} & -\frac{\nu\dot{c}}{\dot{c}+c_3} \\ \frac{Bc_1\gamma\dot{u}}{(\dot{c}+c_1)^2} & \frac{B\dot{c}\gamma}{\dot{c}+c_1} - 2\gamma\dot{u} - \sigma - \lambda & -\frac{\dot{u}}{\dot{u}+h} \\ 0 & 0 & \frac{\beta\dot{u}}{\dot{u}+h} \frac{\dot{c}^2}{\dot{c}^2+c_4^2} - \mu - \lambda \end{vmatrix} = 0$$

$$\det(C_{(\dot{c}, \dot{u}, 0)} - \lambda I) = \left(\left(-\frac{A\dot{u}}{(1+\dot{c})^2} - 1 - \frac{\dot{u}c_2}{(\dot{c}+c_2)^2} - \lambda \right) \left(\frac{B\dot{c}\gamma}{\dot{c}+c_1} - 2\gamma\dot{u} - \sigma - \lambda \right) - \left(\frac{Bc_1\gamma\dot{u}}{(\dot{c}+c_1)^2} \right) \left(\frac{A}{\dot{c}+1} - \frac{\dot{c}}{\dot{c}+c_2} \right) \right) \left(\frac{\beta\dot{u}}{\dot{u}+h} \frac{\dot{c}^2}{\dot{c}^2+c_4^2} - \mu - \lambda \right) = 0 \quad (C.17)$$

where \dot{u} and \dot{c} defined in Eqs. (4.12-4.13).

- Oxygen-phytoplankton-zooplankton coexistence steady state: $E_3 = (\ddot{c}, \ddot{u}, \ddot{v})$

$$\det(C_{(\check{c}, \check{u}, \check{v})} - \lambda I) =$$

$$\begin{vmatrix} -\frac{A\check{u}}{(1+\check{c})^2} - 1 - \frac{\check{u}c_2}{(\check{c}+c_2)^2} - \frac{\nu\check{v}c_3}{(\check{c}+c_3)^2} - \lambda & \frac{A}{1+\check{c}} - \frac{\check{c}}{\check{c}+c_2} & -\frac{\nu\check{c}}{\check{c}+c_3} \\ \frac{Bc_1\gamma\check{u}}{(\check{c}+c_1)^2} & \frac{B\check{c}\gamma}{\check{c}+c_1} - 2\gamma\check{u} - \frac{\check{v}h}{(\check{u}+h)^2} - \sigma - \lambda & -\frac{\check{u}}{\check{u}+h} \\ \frac{\beta\check{u}\check{v}}{\check{u}+h} \frac{2\check{c}c_4^2}{(\check{c}^2+c_4^2)^2} & \frac{\beta\check{v}h}{(\check{u}+h)^2} \frac{c^2}{(\check{c}^2+c_4^2)} & \frac{\beta\check{u}c^2}{(\check{u}+h)(\check{c}^2+c_4^2)} - \mu - \lambda \end{vmatrix} = 0 \quad (\text{C.18})$$

where \check{c} , \check{u} and \check{v} defined in Eq. (3.11). The stability of the coexistence state $(\check{c}, \check{u}, \check{v})$ is detailed with extensive numerical simulations in Chapter 4.

TABLE C.4: Eigenvalues for $(\dot{c}, \dot{u}, 0)^{(1)}$

		A									
		2	4	6	8	10	12	14	16	18	20
0.1		-1.0972	-1.0946	-1.0938	-1.0934	-1.0931	-1.0930	-1.0929	-1.0928	-1.0927	-1.0926
	c_1	0.0866	0.0870	0.0871	0.0872	0.0872	0.0872	0.0872	0.0872	0.0872	0.0873
0.2		-0.1	-0.1	-0.1	-0.1	-0.1	-0.1	-0.1	-0.1	-0.1	-0.1
	c_1	-1.1073	-1.1017	-1.1000	-1.0991	-1.0986	-1.0983	-1.0980	-1.0978	-1.0977	-1.0976
0.3		0.0855	0.0863	0.0865	0.0866	0.0867	0.0867	0.0868	0.0868	0.0868	0.0868
	c_1	-0.1	-0.1	-0.1	-0.1	-0.1	-0.1	-0.1	-0.1	-0.1	-0.1
0.4		-1.1180	-1.1091	-1.1063	-1.1049	-1.1041	-1.1036	-1.1032	-1.1029	-1.1027	-1.1025
	c_1	0.0842	0.0855	0.0859	0.0861	0.0862	0.0863	0.0863	0.0864	0.0864	0.0864
0.5		-0.1	-0.1	-0.1	-0.1	-0.1	-0.1	-0.1	-0.1	-0.1	-0.1
	c_1	-1.1296	-1.1166	-1.1127	-1.1108	-1.1097	-1.1089	-1.1084	-1.1080	-1.1077	-1.1075
0.6		0.0828	0.0847	0.0853	0.0855	0.0857	0.0858	0.0859	0.0859	0.0860	0.0860
	c_1	-0.1	-0.1	-0.1	-0.1	-0.1	-0.1	-0.1	-0.1	-0.1	-0.1
0.7		-1.1421	-1.1244	-1.1192	-1.1167	-1.1152	-1.1143	-1.1136	-1.1131	-1.1127	-1.1124
	c_1	0.0812	0.0839	0.0846	0.0850	0.0852	0.0853	0.0854	0.0855	0.0855	0.0856
0.8		-0.0999	-0.1	-0.1	-0.1	-0.1	-0.1	-0.1	-0.1	-0.1	-0.1
	c_1	-1.1557	-1.1324	-1.1258	-1.1227	-1.1208	-1.1196	-1.1188	-1.1182	-1.1177	-1.1173
0.9		0.0794	0.0830	0.0840	0.0844	0.0847	0.0848	0.0849	0.0850	0.0851	0.0852
	c_1	-0.0999	-0.0999	-0.1	-0.1	-0.1	-0.1	-0.1	-0.1	-0.1	-0.1
1		-1.1706	-1.1407	-1.1325	-1.1287	-1.1265	-1.1250	-1.1240	-1.1233	-1.1227	-1.1222
	c_1	0.0773	0.0821	0.0833	0.0838	0.0841	0.0843	0.0845	0.0846	0.0847	0.0847
0.1		-0.0997	-0.0999	-0.0999	-0.1	-0.1	-0.1	-0.1	-0.1	-0.1	-0.1
	c_1	-1.1871	-1.1493	-1.1394	-1.1348	-1.1322	-1.1305	-1.1293	-1.1284	-1.1277	-1.1271
0.2		0.0749	0.0811	0.0826	0.0832	0.0836	0.0839	0.0840	0.0841	0.0842	0.0843
	c_1	-0.0996	-0.0999	-0.0999	-0.0999	-0.1	-0.1	-0.1	-0.1	-0.1	-0.1
0.3		-1.2056	-1.1582	-1.1464	-1.1410	-1.1379	-1.1359	-1.1345	-1.1335	-1.1327	-1.1320
	c_1	0.0721	0.0801	0.0818	0.0826	0.0831	0.0834	0.0836	0.0837	0.0838	0.0839
0.4		-0.0993	-0.0998	-0.0999	-0.0999	-0.0999	-0.0999	-0.1	-0.1	-0.1	-0.1
	c_1	-1.2268	-1.1674	-1.1535	-1.1472	-1.1437	-1.1414	-1.1398	-1.1386	-1.1377	-1.1369
0.5		0.0686	0.0789	0.0811	0.0820	0.0825	0.0829	0.0831	0.0833	0.0834	0.0835
	c_1	-0.0989	-0.0997	-0.0998	-0.0999	-0.0999	-0.0999	-0.0999	-0.0999	-0.0999	-0.0999

Eigenvalues are produced by given parameter values $c_2 = 1, c_3 = 1, c_4 = 1, B = 1.8, \gamma = 1.2, \beta = 0.7, \mu = 0.1, h = 0.1, \sigma = 0.1, A$ changes from 2 to 20 and c_1 changes from 0.1 to 1 as seen on table.

TABLE C.5: Eigenvalues for $(\dot{c}, \dot{u}, 0)^{(2)}$

		A									
		2	4	6	8	10	12	14	16	18	20
c_1	0.1	-2.5564	-2.4672	-2.4144	-2.3793	-2.3539	-2.3345	-2.3189	-2.3061	-2.2954	-2.2861
		-1.5693	-1.7001	-1.7524	-1.7820	-1.8017	-1.8159	-1.8269	-1.8356	-1.8429	-1.8490
		0.1924	0.3649	0.4358	0.4715	0.4923	0.5057	0.5150	0.5218	0.5269	0.5309
	0.2	-2.5653	-2.5170	-2.4733	-2.4410	-2.4164	-2.3968	-2.3809	-2.3675	-2.3560	-2.3461
		-1.2863	-1.4911	-1.5764	-1.6255	-1.6583	-1.6823	-1.7008	-1.7157	-1.7280	-1.7385
		0.1744	0.3549	0.4297	0.4672	0.4891	0.5032	0.5129	0.5200	0.5253	0.5295
	0.3	-2.5310	-2.5308	-2.5008	-2.4741	-2.4522	-2.4341	-2.4188	-2.4058	-2.3946	-2.3847
		-1.0720	-1.3272	-1.4369	-1.5010	-1.5441	-1.5758	-1.6003	-1.6201	-1.6365	-1.6503
		0.1562	0.3445	0.4233	0.4629	0.4858	0.5006	0.5107	0.5181	0.5237	0.5281
	0.4	-2.4769	-2.5263	-2.5118	-2.4921	-2.4739	-2.4581	-2.4442	-2.4321	-2.4215	-2.4120
	-0.8993	-1.1898	-1.3185	-1.3947	-1.4463	-1.4844	-1.5140	-1.5378	-1.5576	-1.5744	
	0.1377	0.3337	0.4167	0.4583	0.4824	0.4979	0.5085	0.5162	0.5220	0.5266	
0.5	-2.4126	-2.5108	-2.5126	-2.5006	-2.4868	-2.4736	-2.4616	-2.4507	-2.4409	-2.4321	
	-0.7559	-1.0712	-1.2149	-1.3009	-1.3598	-1.4033	-1.4371	-1.4646	-1.4873	-1.5067	
	0.1191	0.3226	0.4099	0.4537	0.4790	0.4951	0.5062	0.5143	0.5203	0.5251	
0.6	-2.3424	-2.4880	-2.5064	-2.5025	-2.4934	-2.4832	-2.4732	-2.4638	-2.4551	-2.4471	
	-0.6345	-0.9669	-1.1225	-1.2168	-1.2816	-1.3298	-1.3675	-1.3980	-1.4234	-1.4450	
	0.1003	0.3111	0.4029	0.4489	0.4754	0.4923	0.5039	0.5123	0.5186	0.5235	
0.7	-2.2690	-2.4603	-2.4951	-2.4996	-2.4954	-2.4883	-2.4806	-2.4728	-2.4653	-2.4582	
	-0.5303	-0.8740	-1.0391	-1.1402	-1.2102	-1.2625	-1.3035	-1.3368	-1.3645	-1.3882	
	0.0814	0.2992	0.3956	0.4439	0.4717	0.4894	0.5015	0.5103	0.5168	0.5220	
0.8	-2.1935	-2.4290	-2.4801	-2.4930	-2.4938	-2.4901	-2.4846	-2.4785	-2.4723	-2.4662	
	-0.4399	-0.7909	-0.9932	-1.0700	-1.1445	-1.2003	-1.2442	-1.2799	-1.3098	-1.3352	
	0.0625	0.2868	0.3881	0.4388	0.4679	0.4864	0.4991	0.5082	0.5150	0.5204	
0.9	-2.1165	-2.3952	-2.4623	-2.4835	-2.4894	-2.4891	-2.4860	-2.4817	-2.4769	-2.4719	
	-0.3607	-0.7155	-0.8936	-1.0052	-1.0835	-1.1424	-1.1888	-1.2268	-1.2585	-1.2856	
	0.0436	0.2741	0.3802	0.4335	0.4640	0.4833	0.4965	0.5060	0.5132	0.5187	
1	-2.0380	-2.3596	-2.4423	-2.4718	-2.4827	-2.4858	-2.4852	-2.4828	-2.4794	-2.4755	
	-0.2906	-0.6471	-0.8296	-0.9450	-1.0266	-1.0882	-1.1370	-1.1768	-1.2103	-1.2389	
	0.0248	0.2610	0.3722	0.4280	0.4600	0.4802	0.4940	0.5039	0.5113	0.5171	

Eigenvalues are produced by given parameter values $c_2 = 1, c_3 = 1, c_4 = 1, B = 1.8, \gamma = 1.2, \beta = 0.1, h = 0.1, \mu = 0.1, \sigma = 0.1$. A changes from 2 to 20 and c_1 changes from 0.1 to 1 as seen on table.

TABLE C.6: Eigenvalues for $(\ddot{c}, \dot{u}, \dot{v})$

	A									
	2	4	6	8	10	12	14	16	18	20
0.1	-1.8100 0.2982+0.1870i 0.2982-0.1870i	-1.6673 0.6196 -0.1	-1.6352 0.5965 -0.1	-1.6241 0.4551+0.0463i 0.4551-0.0463i	-1.6201 0.4421+0.1447i 0.4421-0.1447i	-1.6191 0.4289+0.1930i 0.4289-0.1930i	-1.6195 0.4164+0.2262i 0.4164-0.2262i	-1.6207 0.4050+0.2509i 0.4050-0.2509i	-1.6224 0.3945+0.2702i 0.3945-0.2702i	-1.6242 0.3850+0.2858i 0.3850-0.2858i
0.2	-1.8770 0.2233+0.2042i 0.2233-0.2042i	-1.7255 0.2730 0.5161	-1.6915 0.3009 0.5353	-1.6796 0.3746 0.4608	-1.6751 0.4111+0.1057i 0.4111-0.1057i	-1.6737 0.4028+0.1524i 0.4028-0.1524i	-1.6738 0.3943+0.1842i 0.3943-0.1842i	-1.6747 0.3861+0.2081i 0.3861-0.2081i	-1.6760 0.3784+0.2270i 0.3784-0.2270i	-1.6776 0.3712+0.2423i 0.3712-0.2423i
0.3	-1.9139 0.1619+0.2083i 0.1619-0.2083i	-1.7579 0.4004 0.2897	-1.7236 0.4612 0.2935	-1.7118 0.3973 0.3693	-1.7076 0.3815+0.0937i 0.3815-0.0937i	-1.7065 0.3771+0.1329i 0.3771-0.1329i	-1.7068 0.3717+0.1608i 0.3717-0.1608i	-1.7080 0.3661+1823i 0.3661-1823i	-1.7095 0.3606+0.1996i 0.3606-0.1996i	-1.7113 0.3553+0.2139i 0.3553-0.2139i
0.4	-1.9342 0.1107+0.2032i 0.1107-0.2032i	-1.7756 0.3027+0.0775i 0.3027-0.0775i	-1.7415 0.3617 0.3214	-1.7303 0.3523+0.0565i 0.352-0.0565i	-1.7267 0.3543+0.0967i 0.3543-0.0967i	-1.7261 0.3528+0.1261i 0.3528-0.1261i	-1.7269 0.3499+0.1490i 0.3499-0.1490i	-1.7285 0.3464+0.1673i 0.3464-0.1673i	-1.7305 0.3427+0.1825i 0.3427-0.1825i	-1.7326 0.3389+0.1953i 0.3389-0.1953i
0.5	-1.9446 0.0674+0.1915i 0.0674-0.1915i	-1.7845 0.2660+0.1123i 0.2660-0.1123i	-1.7510 0.3100+0.0725i 0.3100-0.0725i	-1.7404 0.3245+0.0824i 0.3245-0.0824i	-1.7374 0.3294+0.1048i 0.3294-0.1048i	-1.7374 0.3303+0.1260i 0.3303-0.1260i	-1.7388 0.3294+0.1440i 0.3294-0.1440i	-1.7409 0.3276+0.1592i 0.3276-0.1592i	-1.7433 0.3253+0.1721i 0.3253-0.1721i	-1.7458 0.3228+0.1832i 0.3228-0.1832i
0.6	-1.9489 0.0301+0.1744i 0.0301-0.1744i	-1.7880 0.2340+0.1310i 0.2340-0.1310i	-1.7550 0.2820+0.0990i 0.2820-0.0990i	-1.7451 0.2995+0.1003i 0.2995-0.1003i	-1.7427 0.3068+0.1136i 0.3068-0.1136i	-1.7433 0.3097+0.1287i 0.3097-0.1287i	-1.7452 0.3104+0.1427i 0.3104-0.1427i	-1.7478 0.3099+0.1550i 0.3099-0.1550i	-1.7506 0.3089+0.1659i 0.3089-0.1659i	-1.7535 0.3074+0.1754i 0.3074-0.1754i
0.7	-1.9493 -0.0023+0.1524i -0.0023-0.1524i	-1.7881 0.2059+0.1419i 0.2059-0.1419i	-1.7556 0.2571+0.1153i 0.2571-0.1153i	-1.7463 0.2771+0.1132i 0.2771-0.1132i	-1.7444 0.2863+0.1214i 0.2863-0.1214i	-1.7455 0.2907+0.1323i 0.2907-0.1323i	-1.7480 0.2928+0.1431i 0.2928-0.1431i	-1.7510 0.2935+0.1532i 0.2935-0.1532i	-1.7543 0.2934+0.1623i 0.2934-0.1623i	-1.7576 0.2928+0.1704i 0.2928-0.1704i
0.8	-1.9473 -0.0307+0.1245i -0.0307-0.1245i	-1.7859 0.1809+0.1480i 0.1809-0.1480i	-1.7539 0.2348+0.1261i 0.2348-0.1261i	-1.7552 0.2568+0.1227i 0.2568-0.1227i	-1.7438 0.2676+0.1278i 0.2676-0.1278i	-1.7454 0.2733+0.1358i 0.2733-0.1358i	-1.7483 0.2765+0.1443i 0.2765-0.1443i	-1.7517 0.2781+0.1526i 0.2781-0.1526i	-1.7553 0.2789+0.1601i 0.2789-0.1601i	-1.7590 0.2791+0.1671i 0.2791-0.1671i
0.9	-1.9436 -0.0560+0.0867i -0.0560-0.0867i	-1.7822 0.1586+0.1507i 0.1586-0.1507i	-1.7508 0.2147+0.1333i 0.2147-0.1333i	-1.7425 0.2384+0.1295i 0.2384-0.1295i	-1.7416 0.2505+0.1328i 0.2505-0.1328i	-1.7436 0.2574+0.1389i 0.2574-0.1389i	-1.7468 0.2614+0.1457i 0.2614-0.1457i	-1.7506 0.2639+0.1525i 0.2639-0.1525i	-1.7546 0.2654+0.1589i 0.2654-0.1589i	-1.7586 0.2662+0.1648i 0.2662-0.1648i
1	-1.9388 -0.1015 -0.0556	-1.7777 0.1386+0.1511i 0.1386-0.1511i	-1.7466 0.1965+0.1380i 0.1965-0.1380i	-1.7388 0.2216+0.1344i 0.2216-0.1344i	-1.7382 0.2348+0.1367i 0.2348-0.1367i	-1.7406 0.2426+0.1414i 0.2426-0.1414i	-1.7442 0.2475+0.1470i 0.2475-0.1470i	-1.7484 0.2507+0.1526i 0.2507-0.1526i	-1.7527 0.2528+0.1581i 0.2528-0.1581i	-1.7570 0.2541+0.1632i 0.2541-0.1632i

Eigenvalues are produced by given parameter values $c_2 = 1, c_3 = 1, c_4 = 1, B = 1.8, \gamma = 1.2, \beta = 0.7, \mu = 0.1, h = 0.1, \sigma = 0.1$. A changes from 2 to 20 and c_1 changes from 0.1 to 1 as seen on table.

TABLE C.7: Eigenvalues for $(\dot{c}, \dot{u}, 0)^{(1)}$

		A										
		1.9	2	2.01	2.02	2.03	2.04	2.05	2.06	2.07	2.08	2.09
0.1		-1.0974	-1.0972	-1.0971	-1.0971	-1.0971	-1.0971	-1.0970	-1.0970	-1.0970	-1.0970	-1.0969
		0.0866	0.0866	0.0866	0.0867	0.0867	0.0867	0.0867	0.0867	0.0867	0.0867	0.0867
		-0.1000	-0.1000	-0.1000	-0.1000	-0.1000	-0.1000	-0.1000	-0.1000	-0.1000	-0.1000	-0.1000
0.2		-1.1079	-1.1073	-1.1072	-1.1071	-1.1071	-1.1070	-1.1070	-1.1069	-1.1069	-1.1068	-1.1068
		0.0854	0.0855	0.0855	0.0855	0.0855	0.0855	0.0855	0.0855	0.0856	0.0856	0.0856
		-0.1000	-0.1000	-0.1000	-0.1000	-0.1000	-0.1000	-0.1000	-0.1000	-0.1000	-0.1000	-0.1000
0.3		-1.1190	-1.1180	-1.1179	-1.1179	-1.1178	-1.1177	-1.1176	-1.1175	-1.1174	-1.1173	-1.1172
		0.0841	0.0842	0.0842	0.0843	0.0843	0.0843	0.0843	0.0843	0.0843	0.0843	0.0843
		-0.1000	-0.1000	-0.1000	-0.1000	-0.1000	-0.1000	-0.1000	-0.1000	-0.1000	-0.1000	-0.1000
0.4		-1.1311	-1.1296	-1.1295	-1.1293	-1.1292	-1.1291	-1.1289	-1.1288	-1.1287	-1.1285	-1.1284
		0.0826	0.0828	0.0828	0.0829	0.0829	0.0829	0.0829	0.0829	0.0830	0.0830	0.0830
		-0.1000	-0.1000	-0.1000	-0.1000	-0.1000	-0.1000	-0.1000	-0.1000	-0.1000	-0.1000	-0.1000
0.5		-1.1442	-1.1421	-1.1419	-1.1417	-1.1415	-1.1414	-1.1412	-1.1410	-1.1408	-1.1406	-1.1404
		0.0809	0.0812	0.0813	0.0813	0.0813	0.0813	0.0814	0.0814	0.0814	0.0815	0.0815
		-0.0999	-0.0999	-0.0999	-0.0999	-0.0999	-0.0999	-0.0999	-0.0999	-0.0999	-0.0999	-0.0999
0.6		-1.1586	-1.1557	-1.1555	-1.1552	-1.1549	-1.1547	-1.1544	-1.1542	-1.1539	-1.1537	-1.1535
		0.0790	0.0794	0.0795	0.0795	0.0795	0.0796	0.0796	0.0797	0.0797	0.0797	0.0798
		-0.0998	-0.0999	-0.0999	-0.0999	-0.0999	-0.0999	-0.0999	-0.0999	-0.0999	-0.0999	-0.0999
0.7		-1.1744	-1.1706	-1.1703	-1.1699	-1.1696	-1.1692	-1.1689	-1.1686	-1.1683	-1.1679	-1.1676
		0.0767	0.0773	0.0774	0.0775	0.0775	0.0776	0.0776	0.0777	0.0777	0.0778	0.0778
		-0.0997	-0.0997	-0.0997	-0.0997	-0.0997	-0.0997	-0.0998	-0.0998	-0.0998	-0.0998	-0.0998
0.8		-1.1921	-1.1871	-1.1867	-1.1862	-1.1858	-1.1853	-1.1849	-1.1845	-1.1840	-1.1836	-1.1832
		0.0741	0.0749	0.0750	0.0751	0.0752	0.0752	0.0753	0.0754	0.0755	0.0755	0.0756
		-0.0995	-0.0996	-0.0996	-0.0996	-0.0996	-0.0996	-0.0996	-0.0996	-0.0996	-0.0996	-0.0996
0.9		-1.2122	-1.2056	-1.2050	-1.2044	-1.2039	-1.2033	-1.2027	-1.2022	-1.2016	-1.2011	-1.2005
		0.0709	0.0721	0.0722	0.0723	0.0724	0.0725	0.0726	0.0727	0.0728	0.0729	0.0730
		-0.0992	-0.0993	-0.0993	-0.0993	-0.0993	-0.0993	-0.0993	-0.0993	-0.0993	-0.0993	-0.0993
1		-1.2356	-1.2268	-1.2260	-1.2252	-1.2244	-1.2237	-1.2229	-1.2222	-1.2215	-1.2208	-1.2201
		0.0669	0.0686	0.0688	0.0689	0.0691	0.0692	0.0693	0.0695	0.0696	0.0698	0.0699
		-0.0987	-0.0989	-0.0989	-0.0989	-0.0989	-0.0989	-0.0989	-0.0989	-0.0990	-0.0990	-0.0990

Eigenvalues are produced by given parameter values $c_2 = 1, c_3 = 1, c_4 = 1, B = 1.8, \gamma = 1.2, \beta = 0.7, \mu = 0.1, h = 0.1, \sigma = 0.1$. A changes from 1.9 to 2.09 and c_1 changes from 0.1 to 1 as seen on table.

TABLE C.8: Eigenvalues for $(\dot{c}, \dot{u}, 0)^{(2)}$

		A									
	1.9	2	2.01	2.02	2.03	2.04	2.05	2.06	2.07	2.08	2.09
0.1	-2.5622	-2.5564	-2.5558	-2.5552	-2.5546	-2.5541	-2.5535	-2.5529	-2.5524	-2.5518	-2.5512
	-1.5569	-1.5693	-1.5705	-1.5717	-1.5728	-1.5740	-1.5751	-1.5763	-1.5774	-1.5785	-1.5796
0.2	0.1785	0.1924	0.1937	0.1951	0.1964	0.1978	0.1991	0.2004	0.2017	0.2030	0.2043
	-2.5662	-2.5653	-2.5652	-2.5651	-2.5649	-2.5648	-2.5647	-2.5645	-2.5644	-2.5643	-2.5641
0.3	-1.2674	-1.2863	-1.2881	-1.2898	-1.2916	-1.2934	-1.2951	-1.2969	-1.2986	-1.3003	-1.3020
	0.1601	0.1744	0.1758	0.1772	0.1786	0.1800	0.1814	0.1827	0.1841	0.1855	0.1868
0.4	-2.5266	-2.5310	-2.5313	-2.5317	-2.5321	-2.5324	-2.5328	-2.5331	-2.5335	-2.5338	-2.5341
	-1.0491	-1.0720	-1.0742	-1.0763	-1.0785	-1.0806	-1.0827	-1.0849	-1.0869	-1.0890	-1.0911
0.5	0.1415	0.1562	0.1577	0.1591	0.1605	0.1619	0.1633	0.1647	0.661	0.1675	0.1689
	-2.4674	-2.4769	-2.4778	-2.4787	-2.4795	-2.4804	-2.4812	-2.4820	-2.4828	-2.4836	-2.4843
0.6	-0.8740	-0.8993	-0.9017	-0.9042	-0.9066	-0.9089	-0.9113	-0.9137	-0.9160	-0.9183	-0.9206
	0.1227	0.1377	0.1392	0.1407	0.1421	0.1436	0.1450	0.1465	0.1479	0.1494	0.1508
0.7	-2.3981	-2.4126	-2.4139	-2.4152	-2.4165	-2.4178	-2.4191	-2.4204	-2.4216	-2.4228	-2.4240
	-0.7290	-0.7559	-0.7585	-0.7611	-0.7636	-0.7661	-0.7687	-0.7712	-0.7737	-0.7761	-0.7786
0.8	0.1038	0.1191	0.1206	0.1221	0.1236	0.1251	0.1265	0.1280	0.1295	0.1309	0.1324
	-2.3233	-2.3424	-2.3442	-2.3460	-2.3477	-2.3494	-2.3511	-2.3528	-2.3545	-2.3561	-2.3577
0.9	-0.6068	-0.6345	-0.6372	-0.6398	-0.6425	-0.6451	-0.6477	-0.6503	-0.6529	-0.6554	-0.6580
	0.0849	0.1003	0.1018	0.1033	0.1049	0.1064	0.1079	0.1094	0.1109	0.1123	0.1138
1	-2.2454	-2.2690	-2.2712	-2.2734	-2.2755	-2.2777	-2.2798	-2.2819	-2.2839	-2.2860	-2.2880
	-0.5022	-0.5303	-0.5330	-0.5357	-0.5384	-0.5411	-0.5437	-0.5464	-0.5490	-0.5516	-0.5542
0.1	0.0659	0.0814	0.0830	0.0845	0.0860	0.0876	0.0891	0.0906	0.0921	0.0936	0.0951
	-2.1655	-2.1935	-2.1961	-2.1987	-2.2013	-2.2038	-2.2063	-2.2088	-2.2112	-2.2137	-2.2161
0.2	-0.4117	-0.4399	-0.4427	-0.4454	-0.4481	-0.4508	-0.4534	-0.4561	-0.4587	-0.4613	-0.4639
	0.0470	0.0625	0.0641	0.0656	0.0671	0.0687	0.0702	0.0717	0.0733	0.0748	0.0763
0.3	-2.0840	-2.1165	-2.1195	-2.1225	-2.1255	-2.1284	-2.1314	-2.1342	-2.1371	-2.1399	-2.1427
	-0.3326	-0.3607	-0.3634	-0.3662	-0.3689	-0.3715	-0.3742	-0.3768	-0.3795	-0.3821	-0.3847
0.4	0.0281	0.0436	0.0452	0.0467	0.0483	0.0498	0.0513	0.0529	0.0544	0.0559	0.0574
	-2.0007	-2.0380	-2.0414	-2.0449	-2.0483	-2.0517	-2.0550	-2.0583	-2.0616	-2.0648	-2.0680
0.5	-0.2626	-0.2906	-0.2933	-0.2960	-0.2987	-0.3014	-0.3041	-0.3067	-0.3093	-0.3119	-0.3145
	0.0093	0.0248	0.0263	0.0278	0.0294	0.0309	0.0324	0.0340	0.0355	0.0370	0.0385

Eigenvalues are produced by given parameter values $c_2 = 1, c_3 = 1, c_4 = 1, B = 1.8, \gamma = 1.2, \beta = 0.7, \mu = 0.1, h = 0.1, \sigma = 0.1$. A changes from 1.9 to 2.09 and c_1 changes from 0.1 to 1 as seen on table.

TABLE C.9: Eigenvalues for $(\ddot{c}, \dot{u}, \dot{v})$

A													
	1.9	2	2.01	2.02	2.03	2.04	2.05	2.06	2.07	2.08	2.09		
0.1	-1.8285 0.2748+0.2078i 0.2748-0.2078i	-1.8100 0.2982+0.1870i 0.2982-0.1870i	-1.8083 0.3004+0.1848i 0.3004-0.1848i	-1.8066 0.3025+0.1827i 0.3025-0.1827i	-1.8049 0.3046+0.1805i 0.3046-0.1805i	-1.8033 0.3067+0.1783i 0.3067-0.1783i	-1.8016 0.3087+0.1761i 0.3087-0.1761i	-1.8000 0.3107+0.1740i 0.3107-0.1740i	-1.7985 0.3127+0.1717i 0.3127-0.1717i	-1.7969 0.3146+0.1695i 0.3146-0.1695i	-1.7953 0.3165+0.1673i 0.3165-0.1673i		
0.2	-1.9345 0.1991+0.2172i 0.1991-0.2172i	-1.9139 0.2233+0.2042i 0.2233-0.2042i	-1.8751 0.2256+0.2028i 0.2256-0.2028i	-1.8733 0.2278+0.2014i 0.2278-0.2014i	-1.8715 0.2299+0.2001i 0.2299-0.2001i	-1.8698 0.2321+0.1987i 0.2321-0.1987i	-1.8680 0.2342+0.1973i 0.2342-0.1973i	-1.8663 0.2363+0.1959i 0.2363-0.1959i	-1.8646 0.2383+0.1945i 0.2383-0.1945i	-1.8630 0.2403+0.1931i 0.2403-0.1931i	-1.8613 0.2423+0.1917i 0.2423-0.1917i		
0.3	-1.9342 0.1372+0.2154i 0.1372-0.2154i	-1.9139 0.1619+0.2083i 0.1619-0.2083i	-1.9120 0.2256+0.2028i 0.2256-0.2028i	-1.9101 0.2278+0.2014i 0.2278-0.2014i	-1.9083 0.2299+0.2001i 0.2299-0.2001i	-1.9065 0.2321+0.1987i 0.2321-0.1987i	-1.9047 0.2342+0.1973i 0.2342-0.1973i	-1.9029 0.2363+0.1959i 0.2363-0.1959i	-1.9011 0.2383+0.1945i 0.2383-0.1945i	-1.8994 0.2403+0.1931i 0.2403-0.1931i	-1.9553 0.1815+0.2008i 0.1815-0.2008i		
0.4	-1.9342 0.0856+0.2051i 0.0856-0.2051i	-1.9322 0.1107+0.2032i 0.1107-0.2032i	-1.9303 0.1642+0.2075i 0.1642-0.2075i	-1.9284 0.1154+0.2026i 0.1154-0.2026i	-1.9265 0.1176+0.2022i 0.1176-0.2022i	-1.9247 0.1199+0.2019i 0.1199-0.2019i	-1.9229 0.1221+0.2015i 0.1221-0.2015i	-1.9211 0.1243+0.2011i 0.1243-0.2011i	-1.9193 0.1264+0.2007i 0.1264-0.2007i	-1.9176 0.1285+0.2003i 0.1285-0.2003i	-1.9660 0.1306+0.1998i 0.1306-0.1998i		
0.5	-1.9660 0.0419+0.1883i 0.0419-0.1883i	-1.9446 0.0674+0.1915i 0.0674-0.1915i	-1.9426 0.0697+0.1916i 0.0697-0.1916i	-1.9406 0.0721+0.1917i 0.0721-0.1917i	-1.9387 0.0744+0.1918i 0.0744-0.1918i	-1.9368 0.0766+0.1919i 0.0766-0.1919i	-1.9349 0.0789+0.1919i 0.0789-0.1919i	-1.9331 0.0811+0.1919i 0.0811-0.1919i	-1.9313 0.0833+0.1919i 0.0833-0.1919i	-1.9295 0.0854+0.1919i 0.0854-0.1919i	-1.9277 0.0876+0.1919i 0.0876-0.1919i		
0.6	-1.9705 0.0044+0.1658i 0.0044-0.1658i	-1.9489 0.0301+0.1744i 0.0301-0.1744i	-1.9469 0.0325+0.1750i 0.0325-0.1750i	-1.9449 0.0349+0.1760i 0.0349-0.1760i	-1.9429 0.0372+0.1761i 0.0372-0.1761i	-1.9410 0.0395+0.1767i 0.0395-0.1767i	-1.9391 0.0418+0.1771i 0.0418-0.1771i	-1.9373 0.0440+0.1776i 0.0440-0.1776i	-1.9354 0.0462+0.1780i 0.0462-0.1780i	-1.9336 0.0484+0.1784i 0.0484-0.1784i	-1.9318 0.0506+0.1787i 0.0506-0.1787i		
0.7	-1.9712 -0.0281+0.1369i -0.0281-0.1369i	-1.9493 -0.0023+0.1524i -0.0023-0.1524i	-1.9473 0.0001+0.1536i 0.0001-0.1536i	-1.9453 0.0025+0.1547i 0.0025-0.1547i	-1.9433 0.0049+0.1557i 0.0049-0.1557i	-1.9414 0.0072+0.1568i 0.0072-0.1568i	-1.9395 0.0095+0.1577i 0.0095-0.1577i	-1.9376 0.0117+0.1586i 0.0117-0.1586i	-1.9358 0.0140+0.1595i 0.0140-0.1595i	-1.9340 0.0162+0.1603i 0.0162-0.1603i	-1.9322 0.0183+0.1611i 0.0183-0.1611i		
0.8	-1.9692 -0.0568+0.0981i -0.0568-0.0981i	-1.9473 -0.0307+0.1245i -0.0307-0.1245i	-1.9452 -0.0283+0.1264i -0.0283-0.1264i	-1.9432 -0.0259+0.1283i -0.0259-0.1283i	-1.9413 -0.0236+0.1300i -0.0236-0.1300i	-1.9393 -0.0212+0.1317i -0.0212-0.1317i	-1.9374 -0.0189+0.1333i -0.0189-0.1333i	-1.9355 -0.0166+0.1348i -0.0166-0.1348i	-1.9337 -0.0144+0.1363i -0.0144-0.1363i	-1.9318 -0.0122+0.1377i -0.0122-0.1377i	-1.9300 -0.0100+0.1390i -0.0100-0.1390i		
0.9	-1.9656 -0.0821+0.0201i -0.0821-0.0201i	-1.9436 -0.0560+0.0867i -0.0560-0.0867i	-1.9415 -0.0535+0.0901i -0.0535-0.0901i	-1.9395 -0.0511+0.0933i -0.0511-0.0933i	-1.9376 -0.0488+0.0963i -0.0488-0.0963i	-1.9356 -0.0464+0.0991i -0.0464-0.0991i	-1.9337 -0.0441+0.1017i -0.0441-0.1017i	-1.9318 -0.0418+0.1043i -0.0418-0.1043i	-1.9299 -0.0395+0.1066i -0.0395-0.1066i	-1.9281 -0.0373+0.1089i -0.0373-0.1089i	-1.9263 -0.0351+0.1110i -0.0351-0.1110i		
1	-1.9609 -0.1985 -0.0112	-1.9388 -0.1015 -0.0556	-1.9368 -0.0761+0.0134i -0.0761-0.0134i	-1.9348 -0.0737+0.0294i -0.0737-0.0294i	-1.9328 -0.0713+0.0392i -0.0713-0.0392i	-1.9309 -0.0689+0.0467i -0.0689-0.0467i	-1.9289 -0.0666+0.0531i -0.0666-0.0531i	-1.9270 -0.0643+0.0586i -0.0643-0.0586i	-1.9252 -0.0620+0.0635i -0.0620-0.0635i	-1.9233 -0.0597+0.0679i -0.0597-0.0679i	-1.9215 -0.0575+0.0719i -0.0575-0.0719i		

Eigenvalues are produced by given parameter values $c_2 = 1, c_3 = 1, c_4 = 1, B = 1.8, \gamma = 1.2, \beta = 0.7, \mu = 0.1, h = 0.1, \sigma = 0.1$. A changes from 1.9 to 2.09 and c_1 changes from 0.1 to 1 as seen on table.

Appendix D

Numerical Method: Finite Differences

In this section, we will concentrate on computational methods for partial differential equations, in particular the finite difference method for diffusion-reaction equations with matching initial and boundary conditions.

Diffusion-reaction systems are frequently used to model ecological pattern formation. Firstly, diffusion-reaction systems were utilized to describe ecological pattern formation processes by [254] and after by [224]. A similar approach was used in modelling plankton pattern formation [124, 132].

We assume that the space-domain and time-domain are $[a, b] \subset R$ and $[0, T_f]$ for final time T_f , respectively. We build equally distributed grid points for both space and time as follows:

$a = x_1, x_2 = x_1 + h_x, x_3 = x_2 + h_x, \dots, x_{N_x} = b,$ and $0 = t_1, t_2 = t_1 + \tau, t_3 = t_2 + \tau, \dots, t_{N_t} = T_f.$ where $i = 1, 2, \dots, N_x$ and $n = 1, 2, \dots, N_t.$

Therefore, we have $h_x = (b - a)/(N_x - 1)$ and $\tau = h_x^2/4D$ where $L = b - a.$ τ is rather small in the interest of accuracy of our numerical simulations. We want to find an approximate solution of diffusion-reaction equation, such that

$$c_t(x, t) = Dc_{xx}(x, t) + f(c, u) \quad (D.1)$$

$$u_t(x, t) = Du_{xx}(x, t) + g(c, u) \quad (D.2)$$

for all $x \in [a, b]$ and $t \in [0, T_f],$

with the initial conditions

$$c(x, 0) = c_0(x_i) = p \quad (D.3)$$

$$u(x, 0) = u_0(x_i) = 0.5 \quad \text{if } |x| < \varepsilon; \quad \text{otherwise } u(x, 0) = 0 \quad (D.4)$$

where p and ε are dimensionless variables; in our baseline model $p = 0.2$, $\varepsilon = 100$ and $x_i = (i - 1)h_x$ for $i = 1, 2, \dots, N_x$.

We will show numerical simulations only for u as the only dissimilarity between c and u is the functional response.

Neumann-boundary conditions can be given, such as

$$u_0 = 0 \quad \text{and} \quad u_i = 0. \quad (\text{D.5})$$

$$u_i = E_i u_{i+1} + F_i \quad (\text{D.6})$$

Indeed, we look for E_i and F_i . The left-side Neumann-boundary condition from Eq. (D.5):

$$\frac{\partial u(0, t)}{\partial x} = 0 \quad (\text{D.7})$$

$$\frac{u_1 - u_0}{\Delta_x} = 0 \quad (\text{D.8})$$

$$\Rightarrow u_1 = u_0 \quad (\text{D.9})$$

From (D.6)

$$u_0 = E_0 u_1 + F_0 \quad (\text{D.10})$$

$$\Rightarrow E_0 = 1 \quad \text{and} \quad F_0 = 0. \quad (\text{D.11})$$

The right-side Neumann- boundary condition:

$$\frac{\partial u(L, t)}{\partial x} = 0 \quad (\text{D.12})$$

$$\frac{u_{N_x} - u_{N_x-1}}{\Delta_x} = 0 \quad (\text{D.13})$$

$$\Rightarrow u_{N_x} = u_{N_x-1} \quad (\text{D.14})$$

From Eq. (D.6)

$$u_{N_x-1} = E_{N_x-1} u_{N_x} + F_{N_x-1} \quad (\text{D.15})$$

$$u_{N_x} = E_{N_x-1} u_{N_x} + F_{N_x-1} \quad (\text{D.16})$$

$$\Rightarrow u_{N_x} = \frac{F_{N_x-1}}{1 - E_{N_x-1}}. \quad (\text{D.17})$$

Dirichlet boundary condition can be given by

$$u_0^n = 0 = u_{N_x}^n \quad n = 0, 1, \dots, N_t \quad (\text{D.18})$$

Our aim is to find approximations u_i^n for function values $u(x_i, t_n)$ and c_i^n for function values $c(x_i, t_n)$ for $i = 1, 2, \dots, N_x$ and $n = 1, 2, \dots, N_t$. We construct the following approximations, using the backward difference and central second difference method for

time and space derivatives, respectively. The approximation is as follows:

$$\frac{u(x_i, t_{n+1}) - u(x_i, t_n)}{\tau} = D \frac{u(x_{i+1}, t_{n+1}) - 2u(x_i, t_{n+1}) + u(x_{i-1}, t_{n+1})}{h_x^2} + \quad (\text{D.19})$$

$$g(c(x_i, t_n), u(x_i, t_n)), \quad (\text{D.20})$$

The key is to find approximations u_i^n for function values $u(x_i, t_n)$ from Eq. (D.2). Then we obtain the following system of equations:

$$\frac{u_i^{n+1} - u_i^n}{\tau} = D \frac{u_{i+1}^{n+1} - 2u_i^{n+1} + u_{i-1}^{n+1}}{h_x^2} + g(c_i^n, u_i^n), \quad (\text{D.21})$$

when multiplying by τ and rearranged becomes,

$$u_i^{n+1} - u_i^n = \frac{D\tau}{h_x^2} (u_{i+1}^{n+1} - 2u_i^{n+1} + u_{i-1}^{n+1}) + g(c_i^n, u_i^n)\tau, \quad (\text{D.22})$$

$$-\mu u_{i+1}^{n+1} + (1 + 2\mu)u_i^{n+1} - \mu u_{i-1}^{n+1} = u_i^n + g(c_i^n, u_i^n)\tau, \quad (\text{D.23})$$

where $\mu := \frac{\tau D}{h_x^2}$ is called the *Courant number*.

$$A_i = \mu, \quad B_i = 1 + 2\mu, \quad C_i = \mu \quad \text{and} \quad D_i = u_i^n \quad (\text{D.24})$$

$$\Rightarrow -A_i u_{i+1}^{n+1} + B_i u_i^{n+1} - C_i u_{i-1}^{n+1} = D_i + g(c_i^n, u_i^n)\tau. \quad (\text{D.25})$$

Our aim is to determine E_i and F_i in Eq. (D.6) from Eq. (D.25). The result can be written by u_i^n and u_{i+1}^{n+1} as

$$u_i^n = \frac{A_i}{B_i - C_i E_{i-1}} u_{i+1}^{n+1} + \frac{D_i + C_i F_{i-1}}{B_i - C_i E_{i-1}} + \frac{g(c_i^n, u_i^n)\tau}{B_i - C_i E_{i-1}} \quad (\text{D.26})$$

where

$$E_i = \frac{A_i}{B_i - C_i E_{i-1}} \quad \text{and} \quad F_i = \frac{D_i + C_i F_{i-1}}{B_i - C_i E_{i-1}}. \quad (\text{D.27})$$

Taking larger time-steps (τ) resulted in a decrease in convergence. For this reason to reduce computation time we have used $\tau = 0.1$. All numerical simulations were tested with smaller time steps to ensure the accuracy of results.

Appendix E

Different Parametrizations of Oxygen-Phytoplankton Model

Model 1

In this section we show that the system's steady states behaviour remains qualitatively similar under the choice of different coupled oxygen-phytoplankton system; see the following series of different model system isocline figures. Some of the system parameters are fixed at their hypothetical values as $c_1 = 1$, $B = 5$, $\gamma = 2.5$, $h = 0.5$, $m = 1$ and $\sigma = 0.1$.

The first model system is:

$$\frac{dc}{dt} = A\left(1 - \frac{c}{c+1}\right)u - mc - uc, \quad (\text{E.1})$$

$$\frac{du}{dt} = \left(\frac{Bc}{c+c_1} - \gamma u\right)u - \sigma u, \quad (\text{E.2})$$

where all system notations keep their usual meaning as in Chapter 2. The difference of system (E.1–E.2) comes from the sedimentation term. Plankton die out and sink to the bottom of the lake forming detritus (sediment). This component is converted into nutrients through biochemical processes. In this process huge amounts of dissolved oxygen are utilized [44, 106, 122, 123, 164, 260]. Therefore, the oxygen consumption term comes from the decomposition process too. Current climate change promotes the eutrophication (excessive sedimentation) [206, 231] and this model may be enhanced by this point of view as a future work.

The system (E.1–E.2) isoclines are as follows:

$$u = \frac{mc(c+1)}{A - c(c+1)} \quad (I), \quad u = \frac{Bc - \sigma(c+c_1)}{(c+c_1)\gamma_1} \quad (II). \quad (\text{E.3})$$

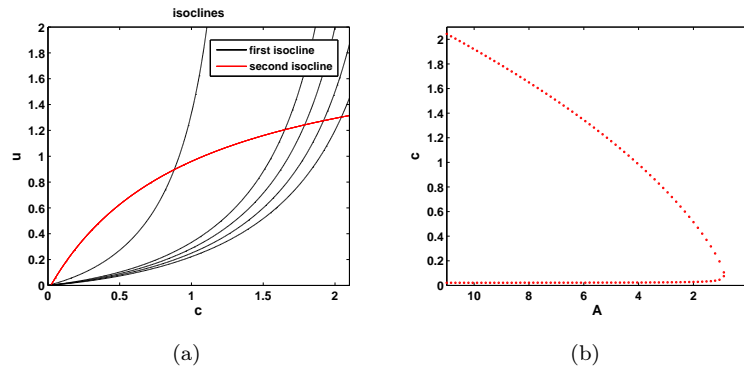


FIGURE E.1: (a) The (null)-isoclines of the oxygen-phytoplankton system for Model 1. Black curves show the oxygen isocline for $A = 3.5, 8, 9, 10, 11$ from left to right; while red curve shows the phytoplankton isocline. (b) Intersection points of two (red-black curves) isoclines are shown by A vs. phytoplankton steady states for various A values and the other parameters are given in the text.

Model 2

A Holling type II predator response is used for the consumption term of phytoplankton, while one of the consumption term of oxygen comes from sedimentation. But here we focus on the relation between oxygen and phytoplankton, so the term of zooplankton is chosen as a constant ($v = 0.3$). For more details see Chapter 4 for consumption term of phytoplankton.

$$\frac{dc}{dt} = A\left(1 - \frac{c}{c+1}\right)u - mc - uc, \quad (\text{E.4})$$

$$\frac{du}{dt} = \left(\frac{Bc}{c+c_1} - u\right)\gamma u - \frac{uv}{u+h}. \quad (\text{E.5})$$

The system E.4–E.5 isoclines are as follows:

$$u = \frac{c(c+1)}{A - c(c+1)} \quad (I), \quad c = \frac{c_1\left(\frac{v}{(u+h)\gamma} + u\right)}{B - \left(\frac{v}{(u+h)\gamma} + u\right)} \quad (II). \quad (\text{E.6})$$

Model 3

In model 3, a Holling type II predator response with a constant $v = 0.3$ and an oxygen loss term due to sedimentation is chosen.

$$\frac{dc}{dt} = A\left(1 - \frac{c}{c+1}\right)u - mc - uc, \quad (\text{E.7})$$

$$\frac{du}{dt} = \left(\frac{Bc}{c+c_1} - u\right)\gamma u - \frac{uv}{u+h} - \sigma u. \quad (\text{E.8})$$

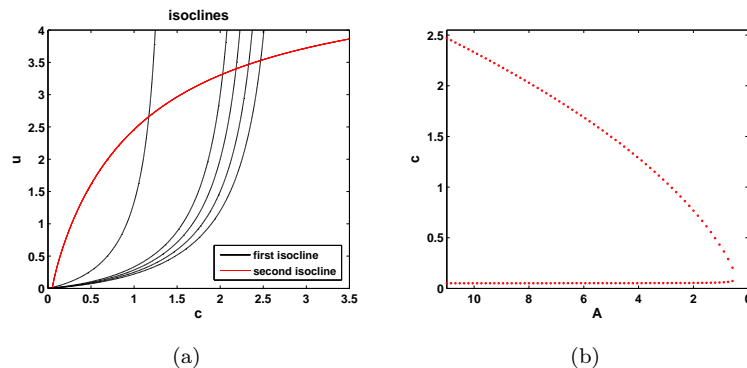


FIGURE E.2: The (null)-isoclines of the oxygen-phytoplankton system for Model 2. Black curves show the oxygen isocline for $A = 3.5, 8, 9, 10, 11$ from left to right; while red curve shows the phytoplankton isocline. (b) Intersection points of two (red-black curves) isoclines are shown by A vs. phytoplankton steady states for various A values and the other parameters are $c_1 = 1$, $B = 5$, $\gamma_1 = 2.5$, $m = 1$, $\sigma = 0.1$, $h = 0.5$, $v = 0.3$.

The system (E.7–E.8) isoclines are as follows:

$$u = \frac{c(c+1)}{A - c(c+1)} \quad (I), \quad c = \frac{c_1 \left(\frac{v}{u+h} + \sigma + u\gamma \right)}{B\gamma - \left(\frac{v}{u+h} + \sigma + u\gamma \right)} \quad (II). \quad (E.9)$$

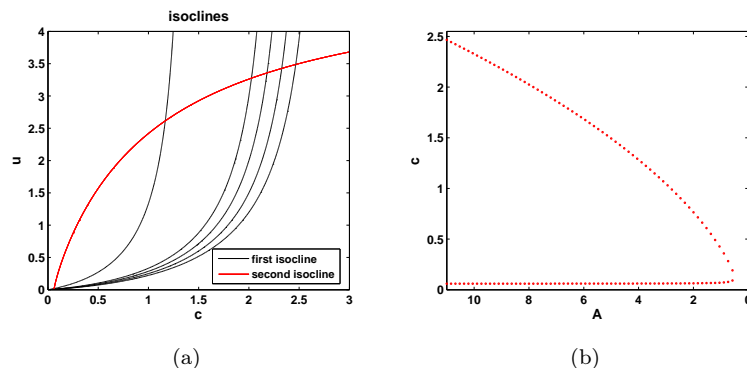


FIGURE E.3: The (null)-isoclines of the oxygen-phytoplankton system for Model 3. Black curves show the oxygen isocline for $A = 3.5, 8, 9, 10, 11$ from left to right; while red curve shows the phytoplankton isocline. (b) Intersection points of two (red-black curves) isoclines are shown by A vs. phytoplankton steady states for various A values and the other parameters are given in the text.

Model 4

In model 4, the consumption term of oxygen comes from the respiration term of phytoplankton. For more details see Chapter 4 for model formulation.

$$\frac{dc}{dt} = A\left(1 - \frac{c}{c+1}\right)u - mc - \frac{uc}{c+c_2}, \quad (\text{E.10})$$

$$\frac{du}{dt} = \left(\frac{Bc}{c+c_1} - u\right)\gamma u - \frac{uv}{u+h}. \quad (\text{E.11})$$

The system (E.10–E.11) isoclines are as follows:

$$u = \frac{c(c+1)(c+c_2)}{A(c+c_2) - c(c+1)} \quad (I) \quad c = \frac{c_1\left(\frac{v}{(u+h)\gamma} + u\right)}{B - \left(\frac{v}{(u+h)\gamma} + u\right)} \quad (II) \quad (\text{E.12})$$

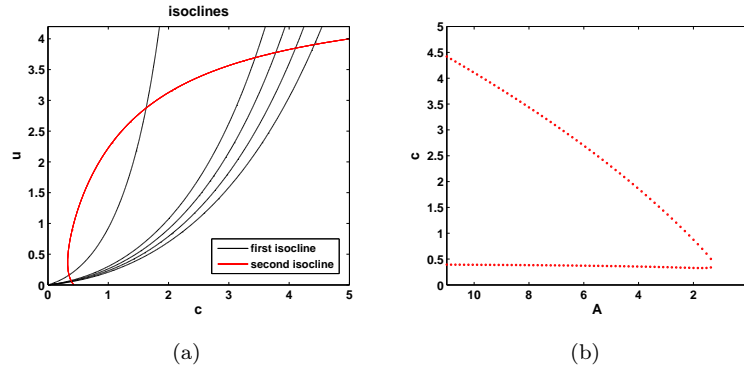


FIGURE E.4: The (null)-isoclines of the oxygen-phytoplankton system for Model 4. Black curves show the oxygen isocline for $A = \{3.5, 8, 9, 10, 11\}$ from left to right; while red curve shows the phytoplankton isocline. (b) Intersection points of two (red-black curves) isoclines are shown by A vs. phytoplankton steady states for various A values and the other parameters are given in the text.

Model 5

In model 5, the phytoplankton respiration term is considered in terms of oxygen consumption, while the Holling type II predation response assumes the zooplankton density as a constant.

$$\frac{dc}{dt} = A\left(1 - \frac{c}{c+1}\right)u - mc - \frac{uc}{c+c_2}, \quad (\text{E.13})$$

$$\frac{du}{dt} = \left(\frac{Bc}{c+c_1} - u\right)\gamma u - \frac{uv}{u+h} - \sigma u. \quad (\text{E.14})$$

The system (E.13–E.14) isoclines are as follows:

$$u = \frac{c(c+1)(c+c_2)}{A(c+c_2) - c(c+1)} \quad (I), \quad c = \frac{c_1\left(\frac{v}{u+h} + \sigma + u\gamma\right)}{B\gamma - \left(\frac{v}{u+h} + \sigma + u\gamma\right)} \quad (II). \quad (\text{E.15})$$

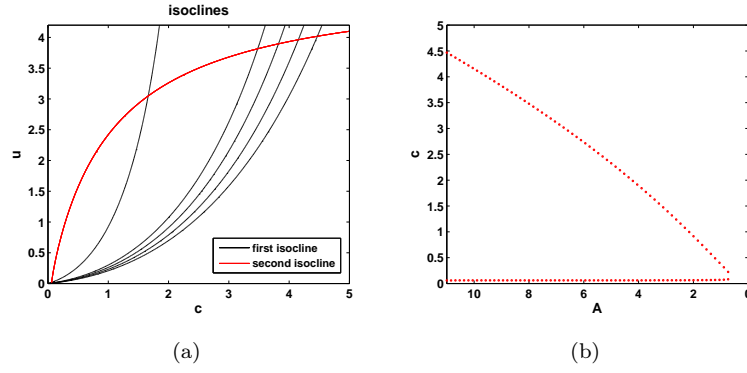


FIGURE E.5: The (null)-isoclines of the oxygen-phytoplankton system for Model 5. Black curves show the oxygen isocline for $A = 3.5, 8, 9, 10, 11$ from left to right; while red curve shows the phytoplankton isocline. (b) Intersection points of two (red-black curves) isoclines are shown by A vs. phytoplankton steady states for various A values and the other parameters are given in the text.

Model 6

In model 6, phytoplankton respiration is considered oxygen consumption.

$$\frac{dc}{dt} = A\left(1 - \frac{c}{c+1}\right)u - mc - \frac{uc}{c+c_2}, \quad (\text{E.16})$$

$$\frac{du}{dt} = \left(\frac{Bc}{c+c_1} - u\right)\gamma u - \sigma u. \quad (\text{E.17})$$

The system (E.16–E.17) isoclines are as follows:

$$u = \frac{c(c+1)(c+c_2)}{A(c+c_2) - c(c+1)} \quad (I), \quad u = \frac{Bc\gamma - \sigma(c+c_1)}{\gamma(c+c_1)} \quad (II). \quad (\text{E.18})$$

Model 7

Model 7 is the improved version of our baseline model system with the addition of plankton respiration terms accounting for loss of oxygen and a Holling type predatory response accounting for phytoplankton loss. For detailed model formulation see Chapter 4.

$$\frac{dc}{dt} = A\left(1 - \frac{c}{c+1}\right)u - mc - \frac{uc}{c+c_2} - \frac{\nu cv}{c+c_3}, \quad (\text{E.19})$$

$$\frac{du}{dt} = \left(\frac{Bc}{c+c_1} - u\right)\gamma u - \frac{uv}{u+h} - \sigma u. \quad (\text{E.20})$$

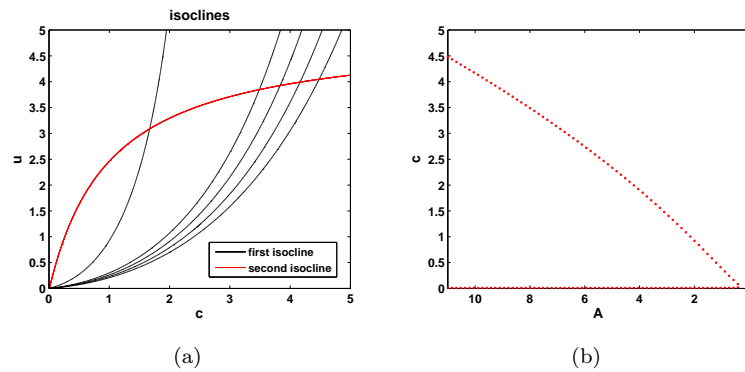


FIGURE E.6: The (null)-isoclines of the oxygen-phytoplankton system for Model 6. Black curves show the oxygen isocline for $A = 3.5, 8, 9, 10, 11$ from left to right; while red curve shows the phytoplankton isocline. (b) Intersection points of two (red-black curves) isoclines are shown by A vs. phytoplankton steady states for various A values and the other parameters are given in the text.

The system (E.19–E.20) isoclines are as follows:

$$u = \frac{c + \frac{\nu cv}{c+c_3}}{\frac{A}{c+1} - \frac{c}{c+c_2}} \quad (I), \quad c = \frac{c_1 \left(\frac{v}{u+h} + \sigma + u\gamma \right)}{B\gamma - \left(\frac{v}{u+h} + \sigma + u\gamma \right)} \quad (II). \quad (\text{E.21})$$

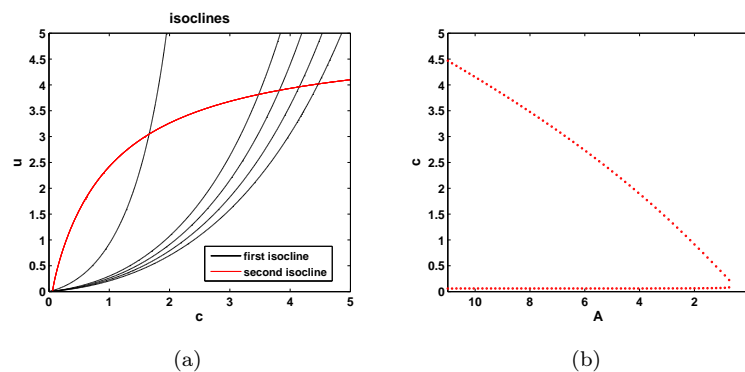


FIGURE E.7: The (null)-isoclines of the oxygen-phytoplankton system for Model 7. Black curves show the oxygen isocline for $A = 3.5, 8, 9, 10, 11$ from left to right; while red curve shows the phytoplankton isocline. (b) Intersection points of two (red-black curves) isoclines are shown by A vs. phytoplankton steady states for various A values and the other parameters are given in the text with $c_3 = 1, v = 0.01$.

It should be emphasized that the behavior of the system steady states are qualitatively similar, regardless of the choice of different model formulations.

Bibliography

- [1] (2001). *Climate change 2001: Synthesis report. A contribution of working groups, I, II and III to the to the third assessment report of the Intergovernmental Panel on Climate Change*. Cambridge University Press.
- [2] Abbott, M. R. (1993). Phytoplankton patchiness: Ecological implications and observation methods. *Patch Dynamics*, 96:37–49.
- [3] Addy, K. and Green, L. (1996). Algae in aquatic ecosystem. *University of Rhode Island, College of Resources Department of Natural Resources Science, Natural Resources Fact Sheet*, No.96-4.
- [4] Addy, K. and Green, L. (1997). Dissolved oxygen and temperature. *Natural Resources Fact Sheet*, No.96-3.
- [5] Allegretto, W., Mocenni, C., and Vicino, A. (2005). Periodic solutions in modelling lagoon ecological interactions. *Journal of Mathematical Biology*, 51(4):367–388.
- [6] Anderson, T. R. (1992). Modelling the influence of food c: N ratio, and respiration on growth and nitrogen excretion in marine zooplankton and bacteria. *Journal of Plankton Research*, 14(12):1645–1671.
- [7] Andersson, A., Haecky, P., and Hagström, Å. (1994). Effect of temperature and light on the growth of micro-nano-and pico-plankton: impact on algal succession. *Marine Biology*, 120(4):511–520.
- [8] Andrew, T., Cabrera, S., and Montecino, V. (1989). Diurnal changes in zooplankton respiration rates and the phytoplankton activity in two chilean lakes. *Hydrobiologia*, 175(2):121–135.
- [9] Apel, J. R. (1983). Remote measurement of the ocean - an overview. *Remote Sensing Applications in Marine Science and Technology*, pages 1–16.
- [10] Bain, R. C. (1968). Predicting do variations caused by algae. *Journal of the Sanitary Engineering Division*, 94(5):867–882.

- [11] Banerjee, M. and Petrovskii, S. (2011). Self-organised spatial patterns and chaos in a ratio-dependent predator–prey system. *Theoretical Ecology*, 4(1):37–53.
- [12] Baretta-Bekker, J. G., Duursma, E. K., and Kuipers, B. R. (1998). *Encyclopedia of marine sciences*. Springer Science & Business Media.
- [13] Barnes, R. S. K. and Mann, K. H. (2009). *Fundamentals of Aquatic Ecology*. John Wiley & Sons.
- [14] Bauernschmitt, R. and Ahlrichs, R. (1996). Treatment of electronic excitations within the adiabatic approximation of time dependent density functional theory. *Chemical Physics Letters*, 256(4):454–464.
- [15] Behrenfeld, M. J. and Falkowski, P. G. (1997). Photosynthetic rates derived from satellite-based chlorophyll concentration. *Limnology and Oceanography*, 42(1):1–20.
- [16] Berges, J. A., Varela, D. E., and Harrison, P. J. (2002). Effects of temperature on growth rate, cell composition and nitrogen metabolism in the marine diatom *Thalassiosira pseudonana* (Bacillariophyceae). *Marine Ecology Progress Series*, 225:139–146.
- [17] Blackman, R. B. and Tukey, J. W. (1958). The measurement of power spectra from the point of view of communications engineering - part II. pages 485–569.
- [18] Boano, F., Revelli, R., and Ridolfi, L. (2006). Stochastic modelling of DO and BOD components in a stream with random inputs. *Advances in Water Resources*, 29(9):1341–1350.
- [19] Boney, A. (1975). *Phytoplankton*. Edward Arnold Press.
- [20] Bopp, L., Le Quéré, C., Heimann, M., Manning, A. C., and Monfray, P. (2002). Climate-induced oceanic oxygen fluxes: Implications for the contemporary carbon budget. *Global Biogeochemical Cycles*, 16(2):6–1.
- [21] Breitburg, D. L., Loher, T., Pacey, C. A., and Gerstein, A. (1997). Varying effects of low dissolved oxygen on trophic interactions in an estuarine food web. *Ecological Monographs*, 67(4):489–507.
- [22] Brown, J. H., Gillooly, J. F., Allen, A. P., Savage, V. M., and West, G. B. (2004). Toward a metabolic theory of ecology. *Ecology*, 85(7):1771–1789.
- [23] Caduto, M. J. (1985). *Pond and brook: a guide to nature in freshwater environments*. University Press of New England.
- [24] Cantrell, R. S. and Cosner, C. (2004). *Spatial ecology via reaction-diffusion equations*. John Wiley & Sons.

- [25] Carpenter, J. H. (1966). New measurements of oxygen solubility in pure and natural water. *Limnology and Oceanography*, 11(2):264–277.
- [26] Carr, J. (2012). *Applications of centre manifold theory*, volume 35. Springer Science & Business Media.
- [27] Cassie, R. M. et al. (1963). Microdistribution of plankton. *Oceanography and marine biology: an annual review*, 1:223–252.
- [28] Chapelle, A. and et al. (2000). Modelling nitrogen, primary production and oxygen in a mediterranean lagoon. impact of oysters farming and inputs from the watershed. *Ecological Modelling*, 127(2):161–181.
- [29] Charlson, R. J., Lovelock, J. E., Andreae, M. O., Warren, S. G., et al. (1987). Oceanic phytoplankton, atmospheric sulphur, cloud albedo and climate. *Nature*, 326(6114):655–661.
- [30] Chattopadhyay, J. and Pal, S. (2002). Viral infection on phytoplankton–zooplankton system - a mathematical model. *Ecological Modelling*, 151(1):15–28.
- [31] Childress, J. J. (1975). The respiratory rates of midwater crustaceans as a function of depth of occurrence and relation to the oxygen minimum layer off southern california. *Comparative Biochemistry and Physiology Part A: Physiology*, 50(4):787–799.
- [32] Childress, J. J. (1976). Effects of pressure, temperature and oxygen on the oxygen consumption rate of the midwater copepod *gaussia princeps*. *Marine Biology*, 39(1):19–24.
- [33] Clark, R. A. and et al. (2003). North sea cod and climate change—modelling the effects of temperature on population dynamics. *Global Change Biology*, 9(11):1669–1680.
- [34] Collins, C. D. (1980). Formulation and validation of a mathematical model of phytoplankton growth. *Ecology*, 61(3):639–649.
- [35] Conover, R. J. (1968). Zooplankton-life in a nutritionally dilute environment. *American Zoologist*, 8(1):107–118.
- [36] Conte, F. and Cabbage, J. (2001). Phytoplankton and recreational ponds. *Western Regional Aquaculture Center*, 5(105):1–6.
- [37] Cossellu, M. and Nordberg, K. (2010). Recent environmental changes and filamentous algal mats in shallow bays on the swedish west coast—A result of climate change? *Journal of Sea Research*, 63(3):202–212.

- [38] Costanza, R., d'Arge, R., Groot, R. d., Farber, S., Grasso, M., Hannon, B., Limburg, K., Naeem, S., O'Neill, R. V., Paruelo, J., et al. (1998). The value of the world's ecosystem services and natural capital. *Ecological Economics*, 25(1):3–15.
- [39] Crank, J. (1975). *The Mathematics of Diffusion*. Clarendon Press.
- [40] Cushing, D. H. (1975). *Marine ecology and fisheries*. Cambridge University Press.
- [41] Dachs, J., Eisenreich, S. J., and Hoff, R. M. (2000). Influence of eutrophication on air-water exchange, vertical fluxes, and phytoplankton concentrations of persistent organic pollutants. *Environmental Science & Technology*, 34(6):1095–1102.
- [42] Dai, M., Guo, X., Zhai, W., Yuan, L., Wang, B., Wang, L., Cai, P., Tang, T., and Cai, W.-J. (2006). Oxygen depletion in the upper reach of the pearl river estuary during a winter drought. *Marine Chemistry*, 102(1):159–169.
- [43] Davenport, J. and Trueman, E. R. (1985). Oxygen uptake and buoyancy in zooplanktonic organisms from the tropical eastern atlantic. *Comparative Biochemistry and Physiology Part A: Physiology*, 81(4):857–863.
- [44] De Vries, I. d., Duin, R., Peeters, J., Los, F., Bokhorst, M., and Laane, R. (1998). Patterns and trends in nutrients and phytoplankton in dutch coastal waters: comparison of time-series analysis, ecological model simulation, and mesocosm experiments. *ICES Journal of Marine Science: Journal du Conseil*, 55(4):620–634.
- [45] Decker, M. B., Breitburg, D. L., and Purcell, J. E. (2004). Effects of low dissolved oxygen on zooplankton predation by the ctenophore *mnemiopsis leidyi*. *Marine Ecology Progress Series*, 280:163–172.
- [46] Del Giorgio, P. A. and Duarte, C. M. (2002). Respiration in the open ocean. *Nature*, 420(6914):379–384.
- [47] Denman, K., Hofmann, E., and Marchant, H. (1996). Marine biotic responses to environmental change and feedbacks to climate. In: *Climate Change 1995*, Houghton, J. T., Meira Filho, L. G., Callander, B. A., Harris, N., Kattenberg, A., and Maskell, K. (eds.), *Intergovernmental Panel on Climate Change*, pages 483–516.
- [48] Denman, K. L. (1976). Covariability of chlorophyll and temperature in the sea. *Deep Sea Research and Oceanographic Abstracts*, Elsevier, 23(6):539–550.
- [49] Denman, K. L. and Dower, J. F. (2001). Patch dynamics. In: *Steele, J. H., Thorpe, S. A., and Turekian, K. K. (eds.). Encyclopedia of Ocean Sciences*, pages 2107–2114.
- [50] Devol, A. H. (1981). Vertical distribution of zooplankton respiration in relation to the intense oxygen minimum zones in two british columbia fjords. *Journal of Plankton Research*, 3(4):593–602.

- [51] Diaz, R. J. and Rosenberg, R. (1995). Marine benthic hypoxia: a review of its ecological effects and the behavioural responses of benthic macrofauna. *Oceanography and Marine Biology: An Annual Review*, 33:245–03.
- [52] Diaz, R. J. and Rosenberg, R. (2008). Spreading dead zones and consequences for marine ecosystems. *Science*, 321(5891):926–929.
- [53] Droop, M. (1983). 25 years of algal growth kinetics a personal view. *Botanica Marina*, 26(3):99–112.
- [54] Dubois, D. M. (1975). A model of patchiness for prey - predator plankton populations. *Ecological Modelling*, 1(1):67–80.
- [55] Dugdale, R. (1967). Nutrient limitation in the sea: Dynamics, identification, and significance 1. *Limnology and Oceanography*, 12(4):685–695.
- [56] Edelstein-Keshet, L. (1988). *Mathematical Models in Biology*, volume 46. SIAM Classics in Applied Mathematics.
- [57] Edwards, A. M. and Brindley, J. (1999). Zooplankton mortality and the dynamical behaviour of plankton population models. *Bulletin of Mathematical Biology*, 61(2):303–339.
- [58] Elton, C. S. (1924). Periodic fluctuations in the numbers of animals: Their causes and effects. *Journal of Experimental Biology*, 2(1):119–163.
- [59] Enquist, B. J. and et al. (2003). Scaling metabolism from organisms to ecosystems. *Nature*, 423(6940):639–642.
- [60] Eppley, R. W. (1972). Temperature and phytoplankton growth in the sea. *Fishery Bulletin*, 70(4):1063–1085.
- [61] Falkowski, P. G., Greene, R. M., and Geider, R. J. (1992). Physiological limitations on phytoplankton productivity in the ocean. *Oceanography*, 5(2):84–91.
- [62] Falkowski, P. G. and Owens, T. G. (1978). Effects of light intensity on photosynthesis and dark respiration in six species of marine phytoplankton. *Marine Biology*, 45(4):289–295.
- [63] Fallesen, G., Andersen, F., and Larsen, B. (2000). Life, death and revival of the hypertrophic mariager fjord, denmark. *Journal of Marine Systems*, 25(3):313–321.
- [64] Fasham, M. (1978). The statistical and mathematical analysis of plankton patchiness. *Oceanography Marine Biology: An Annual Review*, 16:43–79.

- [65] Fasham, M., Ducklow, H., and McKelvie, S. (1990). A nitrogen-based model of plankton dynamics in the oceanic mixed layer. *Journal of Marine Research*, 48(3):591–639.
- [66] Feltham, D. and Chaplain, M. A. (2000). Travelling waves in a model of species migration. *Applied Mathematics Letters*, 13(7):67–73.
- [67] Fisher, R. A. (1937). The wave of advance of advantageous genes. *Annals of Eugenics*, 7(4):355–369.
- [68] Fleming, R. H. (1939). The control of diatom populations by grazing. *Journal du Conseil*, 14(2):210–227.
- [69] Franke, U., Hutter, K., and Jöhnk, K. (1999). A physical-biological coupled model for algal dynamics in lakes. *Bulletin of Mathematical Biology*, 61(2):239–272.
- [70] Franks, P. J. S. and Walstad, L. J. (1997). Phytoplankton patches at fronts: a model of formation and response to wind events. *Journal of Marine Research*, 55(1):1–29.
- [71] Fukasawa, M. and et al. (2004). Bottom water warming in the north pacific ocean. *Nature*, 427(6977):825–827.
- [72] Gaarder, T. and Gran, H. H. (1927). Investigations of the production of plankton in the Oslo Fjord. *Conseil Permanent International l’exploration de le mer*, 42:3–48.
- [73] Ganf, G. G. (1974). Rates of oxygen uptake by the planktonic community of a shallow equatorial lake (Lake George, Uganda). *Oecologia*, 15(1):17–32.
- [74] Garcia, H. E. and Gordon, L. I. (1992). Oxygen solubility in seawater: Better fitting equations. *Limnology and Oceanography*, 37(6):1307–1312.
- [75] Gerdol, R., Bonora, A., Marchesini, R., Gualandri, R., and Pancaldi, S. (1998). Growth response of sphagnum capillifolium to nighttime temperature and nutrient level: mechanisms and implications for global change. *Arctic and Alpine Research*, 30(4):388–395.
- [76] Gibson, C. (1975). A field and laboratory study of oxygen uptake by planktonic blue-green algae. *The Journal of Ecology*, 63(3):867–879.
- [77] Gilbert, D., Rabalais, N., Diaz, R., and Zhang, J. (2010). Evidence for greater oxygen decline rates in the coastal ocean than in the open ocean. *Biogeosciences*, 7(7):2283–2296.
- [78] Glime, J. (2007). *Bryophyte Ecology. Physiological Ecology, vol. 1. Ebook Sponsored by Michigan Technological University and the International Association of Bryologists.*

- [79] Gliwicz, Z. M., Kinne, O., and Lampert, W. (2003). *Between hazards of starvation and risk of predation: the ecology of offshore animals*, volume 12. Excellence of Ecology.
- [80] Gray, J. S., Shiu-sun Wu, R., and Ying, Y. O. (2002). Effects of hypoxia and organic enrichment on the coastal marine environment. *Marine Ecology Progress Series*, 238:249–279.
- [81] Greene, C. H., Widder, E. A., Youngbluth, M. J., Tamse, A., and Johnson, G. E. (1992). The migration behavior, fine structure, and bioluminescent activity of krill sound-scattering layers. *Limnology and Oceanography*, 37(3):650–658.
- [82] Gulland, J. A. (1978). *Fish Population Dynamics*. Wiley-Interscience Publication.
- [83] Hallegraeff, G. M. (1988). *Plankton: A Microscopic World*. Brill Archive, London.
- [84] Hamme, R. C. and Keeling, R. F. (2008). Ocean ventilation as a driver of interannual variability in atmospheric potential oxygen. *Tellus B*, 60(5):706–717.
- [85] Hancke, K. and Glud, R. N. (2004). Temperature effects on respiration and photosynthesis in three diatom-dominated benthic communities. *Aquatic Microbial Ecology*, 37:265–281.
- [86] Haney, J. D. and et al. (1996). Modeling phytoplankton growth rates. *Journal of Plankton Research*, 18(1):63–85.
- [87] Harbison, G., Madin, L., and Swanberg, N. (1978). On the natural history and distribution of oceanic ctenophores. *Deep Sea Research*, 25(3):233–256.
- [88] Hardy, A. (1936). The continuous plankton recorder. *Discovery Rep.*, 11:457–510.
- [89] Harley, C. D. G. and et al. (2006). The impacts of climate change in coastal marine systems. *Ecology Letters*, 9(2):228–241.
- [90] Harris, G. P. (1980). Temporal and spatial scales in phytoplankton ecology. mechanisms, methods, models, and management. *Canadian Journal of Fisheries and Aquatic Sciences*, 37(5):877–900.
- [91] Harris, G. P. (1986). *Phytoplankton ecology: structure, function and fluctuation*. Springer.
- [92] Harris, L. A., Duarte, C. M., and Nixon, S. W. (2006). Allometric laws and prediction in estuarine and coastal ecology. *Estuaries and Coasts*, 29(2):340–344.
- [93] Hartnett, H. E., Keil, R. G., Hedges, J. I., and Devol, A. H. (1998). Influence of oxygen exposure time on organic carbon preservation in continental margin sediments. *Nature*, 391(6667):572–575.

- [94] Haury, L., McGowan, J., and Wiebe, P. (1978). Patterns and processes in the time-space scales of plankton distributions. *Spatial pattern in plankton communities*, 3:277–327.
- [95] Hein, B., Viergutz, C., Wyrwa, J., Kirchesch, V., and Schöl, A. (2014). Modelling the impact of climate change on phytoplankton dynamics and the oxygen budget of the elbe river and estuary (germany). *ICHE 2014. Hamburg-Lehfeldt and Kopmann (eds)*, pages 1035–1042.
- [96] Hensen, V. (1887). *Über die Bestimmung des Planktons oder des im Meere treibenden Materials an Pflanzen und Tieren*. Schmidt & Klaunig.
- [97] Hernández-León, S. and Ikeda, T. (2005). Zooplankton respiration. *Respiration in Aquatic Systems. Oxford University Press, New York*, pages 57–82.
- [98] Hessler, R. R. and Lonsdale, P. F. (1991). Biogeography of mariana trough hydrothermal vent communities. *Deep Sea Research Part A. Oceanographic Research Papers*, 38(2):185–199.
- [99] Hinrichsen, H.-H., von Dewitz, B., Dierking, J., Haslob, H., Makarchouk, A., Peterreit, C., and Voss, R. (2016). Oxygen depletion in coastal seas and the effective spawning stock biomass of an exploited fish species. *Royal Society Open Science*, 3(1):150338.
- [100] Hope Jahren, A. (2002). The biogeochemical consequences of the mid-cretaceous superplume. *Journal of Geodynamics*, 34(2):177–191.
- [101] Hoppe, H.-G., Gocke, K., Koppe, R., and Begler, C. (2002). Bacterial growth and primary production along a north–south transect of the atlantic ocean. *Nature*, 416(6877):168–171.
- [102] Houghton, J. T., Ding, Y., Griggs, D. J., Noguer, M., van der Linden, P. J., Dai, X., Maskell, K., and Johnson, C. (2001). *Climate change 2001: the scientific basis*, volume 881. Cambridge University Press.
- [103] Houghton, J. T. and et al. (1996). *Climate change 1995: The science of climate change: contribution of working group I to the second assessment report of the Intergovernmental Panel on Climate Change*, volume 2. Cambridge University Press.
- [104] Hughes, L. (2000). Biological consequences of global warming: is the signal already apparent? *Trends in Ecology & Evolution*, 15(2):56–61.
- [105] Hull, V., Mocenni, C., Falcucci, M., and Marchettini, N. (2000). A trophodynamic model for the lagoon of fogliano (italy) with ecological dependent modifying parameters. *Ecological Modelling*, 134(2):153–167.

- [106] Hull, V., Parrella, L., and Falcucci, M. (2008). Modelling dissolved oxygen dynamics in coastal lagoons. *Ecological Modelling*, 211(3):468–480.
- [107] Hutchinson, G. (1975). A treatise on limnology, vol. 2, introduction to lake biology and the limnoplankton. *Niche: Theory and Application*, 3:185.
- [108] Hutchinson, G. E. (1941). Limnological studies in connecticut IV. The mechanisms of intermediary metabolism in stratified lakes. *Ecological Monographs*, 11(1):21–60.
- [109] Ikeda, T. (1977). Feeding rates of planktonic copepods from a tropical sea. *Journal of Experimental Marine Biology and Ecology*, 29(3):263–277.
- [110] Ishikawa, M. and Takai, Y. (2012). Simulation analysis of spatio-temporal patterns in stochastic plankton-fish systems. *International Journal of Innovative Computing, Information and Control*, 8(3):2183–2191.
- [111] Itsumi, C. (2007). Increasing dissolved oxygen concentration and temperature causes an increase in plankton density and increasing salinity causes a decrease in plankton density. <http://www.learningace.com/doc/2753778/73364e20ed623bbc56e49ac9a8efc161/itsumi-bio-470-ecology-independent-project-paper-2>. [Online; accessed 07-September-2014].
- [112] Ivlev, V. (1945). Biologicheskaya produktivnost vodoemov. *Uspekhi Sovremennoi Biologii*, 19(1):98–120.
- [113] Jankovic, M. and Petrovskii, S. (2013). Gypsy moth invasion in north america: A simulation study of the spatial pattern and the rate of spread. *Ecological Complexity*, 14:132–144.
- [114] Jiang, H. and Strickler, J. R. (2005). Mass density contrast in relation to the feeding currents in calanoid copepods. *Journal of plankton research*, 27(10):1003–1012.
- [115] Jin, Z., Charlock, T. P., Smith, W. L., and Rutledge, K. A parameterization of ocean surface albedo. *Geophysical Research Letters*, 31(22):13–15.
- [116] Jolliffe, P. A. and Tregunna, E. B. (1968). Effect of temperature, co₂ concentration, and light intensity on oxygen inhibition of photosynthesis in wheat leaves. *Plant Physiology*, 43(6):902–906.
- [117] Jones, R. I. (1977). The importance of temperature conditioning to the respiration of natural phytoplankton communities. *British Phycological Journal*, 12(3):277–285.
- [118] Joos, F., Plattner, G.-K., Stocker, T. F., Körtzinger, A., and Wallace, D. W. (2003). Trends in marine dissolved oxygen: Implications for ocean circulation changes and the carbon budget. *EOS*, 84(21):197–201.

- [119] Justic, D., Rabalais, N. N., and Turner, R. E. (1996). Effects of climate change on hypoxia in coastal waters: A doubled CO_2 scenario for the northern Gulf of Mexico. *Limnology and Oceanography*, 41:992–1003.
- [120] Kareiva, P. and Odell, G. (1987). Swarms of predators exhibit "preytaxis" if individual predators use area-restricted search. *American Naturalist*, 130(2):233–270.
- [121] Keeling, R. F., Körtzinger, A., and Gruber, N. (2010). Ocean deoxygenation in a warming world. *Annual Review of Marine Science*, 2:199–229.
- [122] Keller, K., Slater, R. D., Bender, M., and Key, R. M. (2001). Possible biological or physical explanations for decadal scale trends in north pacific nutrient concentrations and oxygen utilization. *Deep Sea Research Part II: Topical Studies in Oceanography*, 49(1):345–362.
- [123] Kemp, W. M. and et al. (2005). Eutrophication of chesapeake bay: historical trends and ecological interactions. *Marine Ecology Progress Series*, 303(21):1–29.
- [124] Klausmeier, C. A. (1999). Regular and irregular patterns in semiarid vegetation. *Science*, 284(5421):1826–1828.
- [125] Kremer, J. and Nixon, S. W. (1978). *A coastal marine ecosystem: simulation and analysis*. Springer, Berlin.
- [126] Ku, S.-B. and Edwards, G. E. (1977). Oxygen inhibition of photosynthesis I. temperature dependence and relation to O_2/CO_2 solubility ratio. *Plant Physiology*, 59(5):986–990.
- [127] Kutzelnigg, W. (1997). The adiabatic approximation I. the physical background of the born-handly ansatz. *Molecular Physics*, 90(6):909–916.
- [128] Kuypers, M. M., Blokker, P., Erbacher, J., Kinkel, H., Pancost, R. D., Schouten, S., and Damsté, J. S. S. (2001). Massive expansion of marine archaea during a mid-cretaceous oceanic anoxic event. *Science*, 293(5527):92–95.
- [129] Lalli, C. and Parsons, T. R. (1997). *Biological Oceanography: An Introduction: An Introduction*. Butterworth-Heinemann.
- [130] Leen, T. K. (1993). A coordinate independent center manifold reduction. *Physics Letters, A-174*, pages 89–93.
- [131] Leising, A. W., Pierson, J. J., Cary, S., and Frost, B. W. (2005). Copepod foraging and predation risk within the surface layer during night-time feeding forays. *Journal of Plankton Research*, 27(10):987–1001.

- [132] Levin, S. A. and Segel, L. A. (1976). Hypothesis for origin of planktonic patchiness. *Nature*, 259(5545):659–659.
- [133] Levitus, S., Antonov, J., and Boyer, T. (2005). Warming of the world ocean, 1955–2003. *Geophysical Research Letters*, 32, L02604, DOI:10.1029/2004GL021592.
- [134] Levitus, S., Antonov, J. I., Boyer, T. P., and Stephens, C. (2000). Warming of the world ocean. *Science*, 287(5461):2225–2229.
- [135] Lewis, M. A., Petrovskii, S. V., and Potts, J. R. (2016). *The Mathematics Behind Biological Invasions*. Springer.
- [136] Li, W., Smith, J., and Platt, T. (1984). Temperature response of photosynthetic capacity and carboxylase activity in arctic marine phytoplankton. *Marine Ecology Progress Series*, 17:237–243.
- [137] Loehle, C. (2004). Challenges of ecological complexity. *Ecological Complexity*, 1(1):3–6.
- [138] Lomas, M. W., Glibert, P. M., Shiah, F. K., and Smith, E. M. (2002). Microbial processes and temperature in chesapeake bay: current relationships and potential impacts of regional warming. *Global Change Biology*, 8(1):51–70.
- [139] Lotka, A. J. (1925). *Elements of physical biology*. Williams & Wilkins Company.
- [140] Lu, Z., Hoogakker, B. A., Hillenbrand, C.-D., Zhou, X., Thomas, E., Gutchess, K. M., Lu, W., Jones, L., and Rickaby, R. E. (2016). Oxygen depletion recorded in upper waters of the glacial southern ocean. *Nature communications*, 7.
- [141] Macfadyen, W. (1950a). Soil and vegetation in British Somaliland. *Nature*, 165:121–121.
- [142] Macfadyen, W. (1950b). Vegetation patterns in the semi-desert plains of british somaliland. *Geographical Journal*, 116(4-6):199–211.
- [143] Mackas, D. L. and Boyd, C. M. (1979). Spectral analysis of zooplankton spatial heterogeneity. *Science*, 204(4388):62–64.
- [144] Malchow, H. (1993). Spatio-temporal pattern formation in nonlinear non-equilibrium plankton dynamics. *Proceedings of the Royal Society of London B: Biological Sciences*, 251(1331):103–109.
- [145] Malchow, H. and Petrovskii, S. (2002). Dynamical stabilization of an unstable equilibrium in chemical and biological systems. *Mathematical and Computer Modelling*, 36(3):307–319.

- [146] Malchow, H., Petrovskii, S. V., and Hilker, F. M. (2003). Models of spatiotemporal pattern formation in plankton dynamics. *Nova Acta Leopoldina NF*, 88(332):325–340.
- [147] Malchow, H., Petrovskii, S. V., and Venturino, E. (2008). *Spatiotemporal patterns in ecology and epidemiology: theory, models, and simulation*. Chapman & Hall/CRC Press London.
- [148] Mann, M. E., Bradley, R. S., and Hughes, M. K. (1999). Northern hemisphere temperatures during the past millennium: inferences, uncertainties, and limitations. *Geophysical Research Letters*, 26(6):759–762.
- [149] Marba, N. and Duarte, C. M. (2010). Mediterranean warming triggers seagrass (*Posidonia oceanica*) shoot mortality. *Global Change Biology*, 16(8):2366–2375.
- [150] Marchettini, N., Mocenni, C., and Vicino, A. (1999). Integrating slow and fast dynamics in a shallow water coastal lagoon. *Annali Di Chimica*, 89(7-8):505–514.
- [151] Marcus, N. H. (2001). Zooplankton: responses to and consequences of hypoxia. *Coastal hypoxia: consequences for living resources and ecosystems*, 58:49–60.
- [152] Masuda, S. and et al. (2010). Simulated rapid warming of abyssal north pacific waters. *Science*, 329(5989):319–322.
- [153] Matear, R., Hirst, A., and McNeil, B. (2000). Changes in dissolved oxygen in the southern ocean with climate change. *Geochemistry, Geophysics, Geosystems*, 1, 1050, DOI:10.1029/2000GC000086.
- [154] Matear, Y. O. and Hirst, A. C. (2003). Long-term changes in dissolved oxygen concentrations in the ocean caused by protracted global warming. *Global Biogeochemical Cycles*, 17, 1125, DOI:10.1029/2002GB001997.
- [155] May, R. M. (2001). *Stability and complexity in model ecosystems*, volume 6. Princeton University Press.
- [156] Medvinsky, A. B., Petrovskii, S. V., Tikhonova, I. A., Malchow, H., and Li, B.-L. (2002). Spatiotemporal complexity of plankton and fish dynamics. *SIAM Review*, 44(3):311–370.
- [157] Meehl, G. A., Stocker, T. F., Collins, W. D., and et al. (2007). Global climate projections. In *climate change 2007: Physical science basis. Contribution of working group I to the fourth assessment report of the intergovernmental panel on climate change*. *Climate Change*, 3495:747–845.
- [158] Middelburg, J. and Levin, L. (2009). Coastal hypoxia and sediment biogeochemistry. *Biogeosciences Discussions*, 6(2):3655–3706.

- [159] Mimura, M. and Murray, J. (1978). On a diffusive prey-predator model which exhibits patchiness. *Journal of Theoretical Biology*, 75(3):249–262.
- [160] Misra, A. (2010). Modeling the depletion of dissolved oxygen in a lake due to submerged macrophytes. *Nonlinear Analalysis: Modelling and Control*, 15(2):185–198.
- [161] Misra, A. K. (2007). Mathematical modeling and analysis of eutrophication of water bodies caused by nutrients. *Nonlinear Analysis: Modelling and Control*, 12(4):511–524.
- [162] Misra, A. K., Chandra, P., and Raghavendra, V. (2011). Modeling the depletion of dissolved oxygen in a lake due to algal bloom: Effect of time delay. *Advances in Water Resources*, 34(10):1232–1238.
- [163] Mocenni, C. (2006). Mathematical modelling of coastal systems: engineering approaches for parameter identification, validation and analysis of the models. http://web.univ-ubs.fr/lmam/frenod/SiteGdmEtGdm2/GGDDMM/03D22BA4-6225-46CC-8968-D8621FBFD967_files/confMocenni.pdf. [Online; accessed 11-August-2011].
- [164] Moloney, C. L., Bergh, M. O., Field, J. G., and Newell, R. C. (1986). The effect of sedimentation and microbial nitrogen regeneration in a plankton community: a simulation investigation. *Journal of Plankton Research*, 8(3):427–445.
- [165] Monin, A. S., Lumley, J. L., and IAglom, A. M. (1971). *Statistical Fluid Mechanics: Mechanics of Turbulence. Vol. 1*. MIT press.
- [166] Morozov, A. and Petrovskii, S. (2009). Excitable population dynamics, biological control failure, and spatiotemporal pattern formation in a model ecosystem. *Bulletin of Mathematical Biology*, 71(4):863–887.
- [167] Morozov, A. and Petrovskii, S. (2013). Feeding on multiple sources: towards a universal parameterization of the functional response of a generalist predator allowing for switching. *Plos One*, 8(9):e74586.DOI:10.1371/journal.pone.0074586.
- [168] Morozov, A., Petrovskii, S., and Li, B.-L. (2006). Spatiotemporal complexity of patchy invasion in a predator-prey system with the allee effect. *Journal of Theoretical Biology*, 238(1):18–35.
- [169] Moss, B. R. (2009). *Ecology of fresh waters: man and medium, past to future*. John Wiley & Sons.

- [170] Müren, U., Berglund, J., Samuelsson, K., and Andersson, A. (2005). Potential effects of elevated sea-water temperature on pelagic food webs. *Hydrobiologia*, 545(1):153–166.
- [171] Murray, J. D. (2002). *Mathematical biology i: An introduction*, vol. 17 of *Interdisciplinary Applied Mathematics*.
- [172] Murray, L. and Wetzel, R. L. (1987). Oxygen production and consumption associated with the major autotrophic components in two temperate seagrass communities. *Marine Ecology Progress Series*, 38(1):231–239.
- [173] Murrell, M. C., Stanley, R. S., Lehrter, J. C., and Hagy III, J. D. (2013). Plankton community respiration, net ecosystem metabolism, and oxygen dynamics on the louisiana continental shelf: Implications for hypoxia. *Continental Shelf Research*, 52:27–38.
- [174] Najjar, R. G. and et al. (2010). Potential climate-change impacts on the chesapeake bay. *Estuarine, Coastal and Shelf Science*, 86(1):1–20.
- [175] Najjar, R. G., Walker, H. A., Anderson, P. J., Barron, E. J., Bord, R. J., Gibson, J. R., Kennedy, V. S., Knight, C. G., Megonigal, J. P., O'Connor, R. E., et al. (2000). The potential impacts of climate change on the mid-atlantic coastal region. *Climate Research*, 14(3):219–233.
- [176] Nestlerode, J. A. and Diaz, R. J. (1998). Effects of periodic environmental hypoxia on predation of a tethered polychaete, *glycera americana*: implications for trophic dynamics. *Marine Ecology Progress Series*, 172:185–195.
- [177] Nicholson, A. J. (1957). The self-adjustment of populations to change. 22:153–173.
- [178] Nielsen, E. S. (1952). The use of radio-active carbon (C14) for measuring organic production in the sea. *Journal du Conseil*, 18(2):117–140.
- [179] Nielsen, S. L., Sand-Jensen, K., Borum, K., and Geertz-Hansen, O. (2002). Phytoplankton, nutrients, and transparency in danish coastal waters. *Estuaries*, 25(5):930–937.
- [180] Nisbet, R. M. and Gurney, W. (1982). *Modelling fluctuating populations*. John Wiley and Sons Limited.
- [181] Nixon, S. W., Granger, S., Buckley, B. A., Lamont, M., and Rowell, B. (2004). A one hundred and seventeen year coastal water temperature record from woods hole, massachusetts. *Estuaries*, 27(3):397–404.

- [182] Odum, H. T. (1956). Primary production in flowing waters 1. *Limnology and Oceanography*, 1(2):102–117.
- [183] Okubo, A. (1980). *Diffusion and ecological problems: Mathematical models. Biomathematics*, volume 10. Springer - Verlag Berlin.
- [184] Okubo, A. (1984). Critical patch size for plankton and patchiness. *Lecture Notes in Biomathematics*, 54:456–477.
- [185] Okubo, A. and Levin, S. A. (2001). *Diffusion and Ecological Problems: Modern Perspectives. Interdisciplinary Applied Mathematics*, volume 14. Springer, NewYork.
- [186] Paasche, E. (1988). Pelagic primary production in nearshore waters. blackburn, t. h., sorenson j. (eds). *Nitrogen cycling in coastal marine environments*, pages 33–65.
- [187] Palmer, M. A., Lettenmaier, D. P., Poff, N. L., Postel, S. L., Richter, B., and Warner, R. (2009). Climate change and river ecosystems: protection and adaptation options. *Environmental Management*, 44(6):1053–1068.
- [188] Parry, M. L. (2007). *Climate Change 2007: Impacts, adaptation and vulnerability: Contribution of Working Group II to the fourth assessment report of the Intergovernmental Panel on Climate Change*, volume 4. Cambridge University Press.
- [189] Parsons, T. R. and Seki, H. (1995). A historical perspective of biological studies in the ocean. *Aquatic Living Resources*, 8:113–113.
- [190] Pascual, M. and Caswell, H. (1997). Environmental heterogeneity and biological pattern in a chaotic predator–prey system. *Journal of Theoretical Biology*, 185(1):1–13.
- [191] Paul, A. and Peters, R. H. (1994). Patterns in planktonic p: R ratios in lakes: Influence of lake trophy and dissolved organic carbon. *Limnology and Oceanography*, 39(4):772–787.
- [192] Petrovskii, S. (1999). On the plankton front waves accelerated by marine turbulence. *Journal of Marine Systems*, 21(1):179–188.
- [193] Petrovskii, S., Kawasaki, K., Takasu, F., and Shigesada, N. (2001). Diffusive waves, dynamical stabilization and spatio-temporal chaos in a community of three competitive species. *Japan Journal of Industrial and Applied Mathematics*, 18(2):459–481.
- [194] Petrovskii, S., Li, B.-L., and Malchow, H. (2004). Transition to spatiotemporal chaos can resolve the paradox of enrichment. *Ecological Complexity*, 1(1):37–47.
- [195] Petrovskii, S. V. and Li, B.-L. (2005). *Exactly solvable models of biological invasion*. CRC Press.

- [196] Petrovskii, S. V. and Malchow, H. (2000). Critical phenomena in plankton communities: Kiss model revisited. *Nonlinear Analysis: Real World Applications*, 1(1):37–51.
- [197] Petrovskii, S. V. and Malchow, H. (2004). *Mathematical models of marine ecosystems*. In: Filar, J. (Ed), *Mathematical Models*. In: *The Encyclopedia of Life Support Systems (EOLSS)*. EOLSS Publisher.
- [198] Petrovskii, S. V., Malchow, H., Hilker, F. M., and Venturino, E. (2005). Patterns of patchy spread in deterministic and stochastic models of biological invasion and biological control. *Biological Invasions*, 7(5):771–793.
- [199] Petrovskii, S. V., Morozov, A. Y., and Venturino, E. (2002). Allee effect makes possible patchy invasion in a predator–prey system. *Ecology Letters*, 5(3):345–352.
- [200] Platt, T. (1972). Local phytoplankton abundance and turbulence. *Deep Sea Research and Oceanographic Abstracts*, 19(3):183–187.
- [201] Plattner, G.-K., Joos, F., Stocker, T., and Marchal, O. (2001). Feedback mechanisms and sensitivities of ocean carbon uptake under global warming. *Tellus B*, 53(5):564–592.
- [202] Powell, T. M. and Okubo, A. (1994). Turbulence, diffusion and patchiness in the sea. *Philosophical Transactions of the Royal Society B: Biological Sciences*, 343(1303):11–18.
- [203] Prosser, C. (1973). Oxygen: respiration and metabolism. *Comparative Animal Physiology*, 3rd ed. Ed. Prosser, C. L. Philadelphia: Saunders:165–211.
- [204] Rabalais, N. N., Harper, D. E., and Turner, R. E. (2001a). Responses of nekton and demersal and benthic fauna to decreasing oxygen concentrations. *Coastal hypoxia: consequences for living resources and ecosystems*. In: Rabalais, N. N. and Turner, R. E. (eds.). *Coastal and Estuarine Studies 58*, American Geophysical Union, Washington, DC, pages 115–128.
- [205] Rabalais, N. N., Smith, L. E., Harper, D. E., and Justic, D. (2001b). Effects of seasonal hypoxia on continental shelf benthos. *Coastal hypoxia: consequences for living resources and ecosystems*. In: Rabalais, N. N. and Turner, R. E. (eds.). *Coastal Hypoxia: Consequences for Living Resources and Ecosystems*. *Coastal and Estuarine Studies 58*, American Geophysical Union, Washington, DC, pages 211–240.
- [206] Rabalais, N. N., Turner, R. E., J., D. R., and Justić, D. (2009). Global change and eutrophication of coastal waters. *ICES Journal of Marine Science: Journal du Conseil*, 66(7):1528–1537.

- [207] Raven, J. A. and Geider, R. J. (1988). Temperature and algal growth. *New Phytologist*, 110(4):441–461.
- [208] Raymont, J. E. (1980). *Plankton & Productivity in the Oceans: Volume 2: Phytoplankton*. Pergamon Press.
- [209] Raymont, J. E. (1983). *Plankton & Productivity in the Oceans: Volume 2: Zooplankton*. Pergamon Press, Oxford.
- [210] Reigada, R., Hillary, R., Bees, M., Sancho, J., and Sagués, F. (2003). Plankton blooms induced by turbulent flows. *Proceedings of the Royal Society of London B: Biological Sciences*, 270(1517):875–880.
- [211] Reynolds, C. S. (1984). The ecology of freshwater phytoplankton.
- [212] Reynolds, C. S. (2006). *The ecology of phytoplankton*. Cambridge University Press.
- [213] Riley, G. A. (1946). Factors controlling phytoplankton populations on Georges Bank. *Journal of Marine Research*, 6(1):54–73.
- [214] Riley, G. A., Stommel, H., and Burdus, D. P. (1949). Qualitative ecology of the plankton of the western north atlantic. *Bulletin of Bingham Oceanographic*, 12:1–169.
- [215] Rinaldi, S., Soncini-Sessa, R., Stehfest, H., and Tamura, H. (1979). *Modeling and control of river quality*. McGraw-Hill New York.
- [216] Ritschard, R. (1992). Marine algae as a CO_2 sink. In: *Natural Sinks of CO_2* . Springer, 64:289–303.
- [217] Robinson, C. (2000). Plankton gross production and respiration in the shallow water hydrothermal systems of milos, aegean sea. *Journal of Plankton Research*, 22(5):887–906.
- [218] Ruttner, F. (1937). Limnologische studien an einigen seen der ostalpen:(seen des salzkammergutes, des ötscher-und hochschwabgebietes). *Archiv für Hydrobiologie*, 32:167–319.
- [219] Sage, R. F. and Sharkey, T. D. (1987). The effect of temperature on the occurrence of O_2 and CO_2 insensitive photosynthesis in field grown plants. *Plant Physiology*, 84(3):658–664.
- [220] Schaffer, G., Leth, O., Ulloa, O., Bendtsen, J., Daneri, G., Dellarossa, V., Hormazabal, S., and Sehlstedt, P.-I. (2000). Warming and circulation change in the eastern south pacific ocean. *Geophysical Research Letters*, 27(9):1247–1250.

- [221] Scheffer, M., Bascompte, J., Brock, W. A., Brovkin, V., Carpenter, S. R., Dakos, V., Held, H., van Nes, E. H., Rietkerk, M., and Sugihara, G. (2009). Early-warning signals for critical transitions. *Nature*, 461(7260):53–59.
- [222] Scheffer, M., Straile, D., van Nes, E. H., and Hosper, H. (2001). Climatic warming causes regime shifts in lake food webs. *Limnology and Oceanography*, 46(7):1780–1783.
- [223] Schiel, D. R., Steinbeck, J. R., and Foster, M. S. (2004). Ten years of induced ocean warming causes comprehensive changes in marine benthic communities. *Ecology*, 85(7):1833–1839.
- [224] Segel, L. A. and Jackson, J. L. (1972). Dissipative structure: an explanation and an ecological example. *Journal of Theoretical Biology*, 37(3):545–559.
- [225] Sekerci, Y. and Petrovskii, S. Path to global warming. *In preparation*.
- [226] Sekerci, Y. and Petrovskii, S. (2015a). Mathematical modelling of plankton–oxygen dynamics under the climate change. *Bulletin of Mathematical Biology*, 77(12):2325–2353.
- [227] Sekerci, Y. and Petrovskii, S. (2015b). Mathematical modelling of spatiotemporal dynamics of oxygen in a plankton system. *Mathematical Modelling of Natural Phenomena*, 10(2):96–114.
- [228] Sherratt, J. A., Lewis, M. A., and Fowler, A. C. (1995). Ecological chaos in the wake of invasion. *Proceedings of the National Academy of Sciences*, 92(7):2524–2528.
- [229] Shigesada, N. and Kawasaki, K. (1997). *Biological Invasions: Theory and Practice*. Oxford University Press.
- [230] Shimps, E. L., Rice, J. A., and Osborne, J. A. (2005). Hypoxia tolerance in two juvenile estuary-dependent fishes. *Journal of Experimental Marine Biology and Ecology*, 325(2):146–162.
- [231] Shukla, J. B., Misra, A. K., and Chandra, P. (2008). Modeling and analysis of the algal bloom in a lake caused by discharge of nutrients. *Applied Mathematics and Computation*, 196(2):782–790.
- [232] Sieburth, J. M., Smetacek, V., and Lenz, J. (1978). Pelagic ecosystem structure: Heterotrophic compartments of the plankton and their relationship to plankton size fractions 1. *Limnology and Oceanography*, 23(6):1256–1263.
- [233] Simpson, J. T. (1991). Volunteer lake monitoring: a methods manual. EPA 440/4-91-002.

- [234] Skellam, J. G. (1951). Random dispersal in theoretical populations. *Biometrika*, 38(1-2):196–218.
- [235] Smetacek, V., Montresor, M., and Verity, P. (2002). *Marine productivity: footprints in the past and steps into the future*. Blackwell Science, Ltd., Oxford.
- [236] Smith, D. W. and Piedrahita, R. H. (1988). The relation between phytoplankton and dissolved oxygen in fish ponds. *Aquaculture*, 68(3):249–265.
- [237] Smith, I. (1982). A simple theory of algal deposition. *Freshwater Biology*, 12(5):445–449.
- [238] Sommer, U. (1994). *Planktologie*. Springer-Verlag.
- [239] Steele, J. (1976). Patchiness. In: *Functioning of Freshwater Ecosystems*, Cambridge University Press, pages 98–115.
- [240] Steele, J. (1977). *Fisheries mathematics*. Marine Laboratory. Aberdeen, Scotland.
- [241] Steele, J. and Henderson, E. (1977). Plankton patches in the northern North Sea. In: *Fisheries mathematics*, Steele, J. H. (eds.), pages 1–19.
- [242] Steele, J. A. (1980). Phytoplankton models. In: *Functioning of Freshwater Ecosystems*, Cambridge University Press, Cambridge, pages 220–227.
- [243] Steele, J. H. (1962). Environmental control of photosynthesis in the sea. *Limnology and Oceanography*, 7(2):137–150.
- [244] Steele, J. H. (1978a). Some comments on plankton patches. In *Spatial pattern in plankton communities*, volume 3, pages 1–20. NATO Conference Series.
- [245] Steele, J. H. (1978b). *Spatial pattern in plankton communities*, volume 3. NATO Conference Series.
- [246] Steele, J. H. and Henderson, E. W. (1992). The role of predation in plankton models. *Journal of Plankton Research*, 14(1):157–172.
- [247] Stramma, L., Johnson, G. C., Sprintall, J., and Mohrholz, V. (2008). Expanding oxygen-minimum zones in the tropical oceans. *Science*, 320(5876):655–658.
- [248] Svensson, C. J., Jenkins, S. R., Hawkins, S. J., and Åberg, P. (2005). Population resistance to climate change: modelling the effects of low recruitment in open populations. *Oecologia*, 142(1):117–126.
- [249] Sverdrup, H. (1953). On conditions for the vernal blooming of phytoplankton. *Journal du Conseil*, 18(3):287–295.

- [250] Tian, Y., Akamine, T., and Suda, M. (2004). Modeling the influence of oceanic-climatic changes on the dynamics of pacific saury in the northwestern pacific using a life cycle model. *Fisheries Oceanography*, 13(s1):125–137.
- [251] Tonolli, V. and Tonolli, L. (1960). Irregularities of distribution of plankton communities: Considerations and models. *Perspective in Marine Biology*, Buzzati-Traverso, A. A. (ed.), pages 137–143.
- [252] Torres, J. J. and Childress, J. J. (1983). Relationship of oxygen consumption to swimming speed in euphausia pacifica. *Marine Biology*, 74(1):79–86.
- [253] Turchin, P. (2003). *Complex population dynamics: a theoretical/empirical synthesis*. Princeton University Press.
- [254] Turing, A. M. (1952). The chemical basis of morphogenesis. *Philosophical Transactions of the Royal Society of London B: Biological Sciences*, 237(641):37–72.
- [255] Turner, R. E., Rabalais, N. N., and Justic, D. (2008). Gulf of mexico hypoxia: Alternate states and a legacy. *Environmental Science & Technology*, 42(7):2323–2327.
- [256] Valiela, I. (2013). *Marine ecological processes*. Springer.
- [257] Vaquer-Sunyer, R. and Duarte, C. M. (2011). Temperature effects on oxygen thresholds for hypoxia in marine benthic organisms. *Global Change Biology*, 17(5):1788–1797.
- [258] Vargas-Yáñez, M. and et al. (2005). Trends and time variability in the northern continental shelf of the western mediterranean. *Journal of Geophysical Research: Oceans (1978–2012)*, 110(C10).
- [259] Villarante-Tonido, K. (2012). Atmospheric oxygen decline due to fossil fuel combustion. <http://www.curezone.org/forums/am.asp?i=2155071>. [Online: accessed 22 January 2014].
- [260] Voinov, A. and Tonkikh, A. (1987). Qualitative model of eutrophication in macrophyte lakes. *Ecological Modelling*, 35(3):211–226.
- [261] Volpert, V. and Petrovskii, S. (2009). Reaction–diffusion waves in biology. *Physics of Life Reviews*, 6(4):267–310.
- [262] Volterra, V. (1926). Fluctuations in the abundance of a species considered mathematically. *Nature*, 118:558–560.
- [263] Von Victon Hensen, H. (1892). Ergebnisse der in dem Atlantischen Ocean von Mitte Jul: bis Anfang November 1889 ausgeführten Plankton Expedition der Humboldt-Stiftung. *Lipsus & Tischer, Kiel and Leipzig*.

- [264] Walther, G. R. and et al. (2002). Ecological responses to recent climate change. *Nature*, 416(6879):389–395.
- [265] Warkentin, M., Freese, H. M., Karsten, U., and Schumann, R. (2007). New and fast method to quantify respiration rates of bacterial and plankton communities in freshwater ecosystems by using optical oxygen sensor spots. *Applied and Environmental Microbiology*, 73(21):6722–6729.
- [266] Wiggert, J., Haskell, A., Paffenhöfer, G.-A., Hofmann, E., and Klinck, J. (2005). The role of feeding behavior in sustaining copepod populations in the tropical ocean. *Journal of Plankton Research*, 27(10):1013–1031.
- [267] Wignall, P. B. and Twitchett, R. J. (1996). Oceanic anoxia and the end permian mass extinction. *Science*, 272(5265):1155–1158.
- [268] Williamson, P. and Gribbin, J. (1991). How plankton change the climate(jgofs). *New Scientist*, 129(1760):48–52.
- [269] Wyatt, T. (1973). The biology of oikopleura dioica and fritillaria borealis in the southern bight. *Marine Biology*, 22(2):137–158.
- [270] Yacobi, Y. Z., Kalikhman, I., Gophen, M., and Walline, P. (1993). The spatial distribution of temperature, oxygen, plankton and fish determined simultaneously in lake kinneret, israel. *Journal of Plankton Research*, 15(6):589–601.